



HAL
open science

Etude et Modélisation de la rhéologie des polymères au cours du procédé FDM (Fabrication additive)

Hamidreza Vanaei

► **To cite this version:**

Hamidreza Vanaei. Etude et Modélisation de la rhéologie des polymères au cours du procédé FDM (Fabrication additive). Mécanique des matériaux [physics.class-ph]. HESAM Université, 2021. Français. NNT : 2021HESAE047 . tel-03682154

HAL Id: tel-03682154

<https://pastel.hal.science/tel-03682154>

Submitted on 30 May 2022

HAL is a multi-disciplinary open access archive for the deposit and dissemination of scientific research documents, whether they are published or not. The documents may come from teaching and research institutions in France or abroad, or from public or private research centers.

L'archive ouverte pluridisciplinaire **HAL**, est destinée au dépôt et à la diffusion de documents scientifiques de niveau recherche, publiés ou non, émanant des établissements d'enseignement et de recherche français ou étrangers, des laboratoires publics ou privés.

ÉCOLE DOCTORALE SCIENCES DES MÉTIERS DE L'INGÉNIEUR

LIFSE - Laboratoire d'Ingénierie des Fluides et des Systèmes Énergétiques
PIMM - Procédés et Ingénierie en Mécanique et Matériaux
– Campus de Paris–

THÈSE

présentée par : **Hamidreza VANAEI**

soutenue le : **04 Octobre 2021**

pour obtenir le grade de : **Docteur d'HESAM Université**

préparée à : **École Nationale Supérieure d'Arts et Métiers**

Spécialité : **Mécanique des matériaux**

Étude et Modélisation de la Rhéologie des Polymères au cours du Procédé FDM (Fabrication Additive)

THÈSE dirigée par :

M. Sofiane KHELLADI, Professeur, École Nationale Supérieure d'Arts et Métiers

et co-encadrée par :

M. Abbas TCHARKHTCHI, Professeur, École Nationale Supérieure d'Arts Métiers

M. Mohammadali SHIRINBAYAN, Docteur, École Nationale Supérieure d'Arts et Métiers

M. Ivan IORDANOFF	Professeur	I2M, Arts et Métiers ParisTech	Président
Mme. Marie-France LACRAMPE	Professeur	École des Mines de Douai	Rapporteuse
M. Mario Domingo MONZÓN	Professeur	Universidad de Las Palmas	Rapporteur
M. Jose Antonio COVAS	Professeur	University of Minho	Examineur
M. Reza FARSANI	Professeur	KNT University of Technology	Examineur
M. Sofiane KHELLADI	Professeur	LIFSE, Arts et Métiers ParisTech	Examineur
M. Abbas TCHARKHTCHI	Professeur	PIMM, Arts et Métiers ParisTech	Examineur
M. Mohammadali SHIRINBAYAN	Docteur	PIMM, Arts et Métiers ParisTech	Examineur
M. Michael DELIGANT	MCF(HDR)	LIFSE, Arts et Métiers ParisTech	Invité

**Je dédie cette thèse à mes parents,
Sans qui rien n'aurait été possible...**

Acknowledgements

My first and foremost acknowledgments are made to my supervisor, Professor Sofiane KHELLADI, for all the support, guidance and encouragement during these past years. He has always been available and spent much time helping me overall in modeling approaches and defining the experimental approaches. His undeniable patience and outstanding ability in transmitting his knowledge were fundamental for the improvement of this work. I have learned a lot during my thesis and I truly appreciate this.

To Professor Abbas TCHARKHTCHI, my co-supervisor, for his knowledge, effectiveness and careful supervision. He always showed an incredible scientific view and gave me essential advice and ideas that contributed to the improvement of my work. Meetings with him always gave me a significant refresh and better thinking of the objectives during my thesis.

I also would like to express my sincere thanks to Dr. Mohammadali SHIRINBAYAN, my co-supervisor, for his great support and supervision during my thesis. Without his assistance and dedicated involvement in every step throughout the process, this thesis would not have been progressed as it did.

I thank the Jury members for agreeing to review my work.

I am also sincerely grateful to Dr. Michael DELIGANT for his help and great collaboration during my thesis. Without his support, the familiarization with the performed approaches would have been complicated.

To Doctor Kaddour RAISSI, for his great point of view both in a scientific manner and industrial application of the approaches that were defined during my thesis. His great supports and ideas were fundamental in the accomplishment of this study.

I also would like to acknowledge Dr. Joseph FITOUSSI significantly for his kind help in developing the different manners of this thesis.

By last, I'd like to give special thanks to LIFSE and PIMM laboratories of Ecole Nationale Supérieure des Arts et Métiers. Finally, I would like to thank my family who endured this long process with me, always offering support and love.

Résumé

L'étude a pour objet de modéliser les caractéristiques rhéologiques des pièces imprimées en 3D. Pour atteindre cet objectif, une étude bibliographique a été réalisée sur les effets des principales variables du processus de l'évolution de la température et leur impact sur les caractéristiques rhéologiques. Puisque les caractéristiques rhéologiques telles que la viscosité dépendent de la température, elles pourraient être corrélées à l'évolution de la température des filaments déposés. Par ailleurs, pour reconnaître la liaison des filaments adjacents, il est important de prendre en considération l'évolution de la température à leurs interfaces. Au début, le rôle de la température du la buse, la température du plateau et la vitesse d'impression sur la résistance mécanique et la qualité de la pièce finale a été discuté. Il a été constaté que l'interaction des paramètres joue un rôle important en ce qui concerne la caractérisation mécanique des pièces imprimées et le module de Young. De plus la déformation à la rupture pourraient être un indicateur pour évaluer les performances mécaniques des pièces imprimées. Ensuite, la méthode des volumes finis a été appliquée pour modéliser le transfert de chaleur des filaments déposés puis a été validé par une nouvelle approche expérimentale dans laquelle de très petits thermocouples de type K ont été utilisés pour surveiller la température du profil à l'interface des filaments déposés. L'évolution de la température a été prédite en concordance avec les résultats expérimentaux enregistrés. Les résultats obtenus ont ensuite été intégrés dans la caractéristique rhéologique des filaments en modélisant l'évolution de leur viscosité et l'effet des principales variables du processus. De plus, un diagramme « Temps-Température-Transformation » (TTT) des filaments pendant le dépôt qui permet d'évaluer simultanément la température et la viscosité a été mis en place. Cette étude a permis d'aboutir à un code informatique regroupant les résultats obtenus qui peut permettre aux chercheurs d'optimiser le processus d'obtention de pièces possédant un bon état de surface.

Mots clés: Impression 3D, Rhéologie, Évolution de la température, Liaison des couches, Résistance mécanique.

Résumé en anglais

The aim of this study is to model the rheological characteristics of 3D-printed parts. To achieve this goal, a bibliographic study was carried out on the effects of major process variables on temperature evolution and their impact on rheological characteristics. Since the rheological characteristics such as viscosity are a function of temperature, they could be correlated to the temperature evolution of deposited filaments. Besides, to acknowledge the bonding of adjacent filaments, it is important to consider the temperature evolution at their interfaces. At the early stage, the role of three parameters, liquefier temperature, platform temperature, and print speed on the mechanical strength and the quality of final part has been discussed. It was found that interaction of parameters plays the most important role in consideration of mechanical characterization of printed parts and also Young's modulus and failure strain could be an indicator to evaluate the mechanical performance of printed parts. Then, finite volume method was applied to model the heat transfer of deposited filaments and then was validated by a novel experimental approach in which very small K-type thermocouples were employed to perform the in-process monitoring of temperature profile at the interface of deposited filaments. The temperature evolution was predicted in good agreement with the recorded experimental results. The obtained results were then embedded into the rheological characteristic of filaments by modeling the viscosity evolution of filaments and the effect of major process variables on them. Moreover, efforts have been made to propose a 'Time-Temperature-Transformation' (TTT) diagram of filaments during deposition that enables the evaluation of temperature and viscosity simultaneously. The consequence of this study is then a computer code that considers the obtained results and predictions, with the potential of letting researchers in optimizing the process to obtain good final parts.

Keywords: 3D printing, Rheology, Temperature evolution, Inter-layer bonding, Mechanical strength.

Contents

Table des figures	ix
Liste des tableaux	xvi
Introduction Générale	1
1 Literature review	5
1.1 Additive Manufacturing/Rapid Prototyping overview	5
1.2 Fused Deposition Modeling (FDM)	8
1.3 Applicable materials in FDM/FFF	9
1.4 FDM/FFF parameters and their impact on part quality	15
1.5 Role of process parameters on part quality	20
1.5.1 Liquefier temperature	23
1.5.2 Platform temperature	24
1.5.3 Print speed	25
1.6 Role of heat transfer on part quality	26
1.7 Role of viscosity evolution and coalescence on part quality	29
1.8 Conclusion	32
2 Material and experimental procedure	35
2.1 Material	35
2.2 Methodology	36
2.2.1 Definition of the case study	36
2.2.2 Characterization methods and equipment layout	38
2.2.3 <i>in situ</i> monitoring of temperature profile of filaments	40
3 Influence of process parameters	47
3.1 Initial characterization and definition of conditions	47
3.2 Liquefier temperature	49
3.2.1 Physico-chemical and mechanical characterizations	49
3.2.2 Thermal characterization: <i>in situ</i> monitoring of temperature profile	56

3.3	Platform temperature	57
3.3.1	Physico-chemical and mechanical characterizations	57
3.3.2	Thermal characterization: <i>in situ</i> monitoring of temperature profile	59
3.4	Print speed	59
3.4.1	Physico-chemical and mechanical characterizations	59
3.4.2	Thermal characterization: <i>in situ</i> monitoring of temperature profile	61
3.5	Microstructure characterization: deposition sequence of filaments	62
3.6	Conclusion	64
4	Heat transfer modeling of FDM/FFF	65
4.1	Modeling of filament cooling: validation of the measurement methodology	65
4.1.1	Deposition of a single filament	66
4.1.2	Deposition of the vertical wall	68
4.1.3	Influence of process parameters	71
4.2	Modeling of filament cooling: Development of a numerical approach	74
4.2.1	Conservation equation	75
4.2.2	Numerical method	75
4.2.3	Convection with the environment	79
4.2.4	Experimental validation of the obtained results	82
4.2.5	Parametric study: influence of process parameters on temperature variation	84
4.2.6	Optimization exploration with the developed code	87
5	Time-Temperature-Transformation diagram of filaments	90
5.1	case studies: influence of process parameters	94
5.2	Correction to the viscosity evolution	95
	Conclusion	99
	Bibliographie	102
	Appendix : Résumé en français	113
A	Introduction générale	114
B	Étude bibliographique	118
B.1.	Fabrication Additive/Prototypage rapide	118

B.2.	Fused Deposition Modeling (FDM)	120
B.3.	Rôle des paramètres du processus sur la qualité des pièces	122
B.4.	Rôle du transfert de chaleur sur la qualité des pièces	123
B.5.	Rôle de l'évolution de la viscosité et de la coalescence sur la qualité des pièces	123
B.6.	Conclusion	124
C	Procédure expérimentale	125
C.1.	Matériaux	125
C.2.	Méthodologie	125
C.2.1.	Définition de l'étude	125
C.2.2.	Méthodes de caractérisation et disposition des équipements	127
C.2.3.	<i>in situ</i> surveillance du profil de température des filaments	128
D	Influence des paramètres du processus	134
D.1.	Influence de la température de la plate-forme sur le profil de température	135
D.2.	Influence de la vitesse d'impression sur le profil de température	136
D.3.	Conclusion	137
E	Modélisation du transfert thermique du FDM/FFF	138
E.1.	Équation de conservation	138
E.2.	Méthode numérique	139
E.2.1.	Méthode des volumes finis	139
E.2.2.	Formulation du problème	139
E.2.3.	Génération du grid	140
E.2.4.	Discretisations	141
E.2.5.	Conditions aux limites	142
E.3.	Convection avec l'environnement	142
E.4.	Validation expérimentale des résultats obtenus	144
E.5.	Optimisation avec le code développé	146
F	Diagramme temps-température-transformation des filaments	148
F.1.	études de cas : influence des paramètres du processus	152
F.2.	Correction de l'évolution de la viscosité	153
G	Conclusion et perspectives	157

List of Figures

- 1 Schematic of AM techniques (Reprinted with permission from [1]) 2
- 2 Roadmap and the main elements/challenges exist in this process 3
- 1.1 The Rapid Prototyping/Additive Manufacturing flow (Reprinted with permission from [12]) 6
- 1.2 Schematic of RP/AM techniques (Reprinted with permission from [12]) 7
- 1.3 Evolution of 3D printers. 8
- 1.4 Schematic of FDM/FFF process 9
- 1.5 Representation of the characteristics of applicable materials in FDM/FFF process 11
- 1.6 Synthesis of PLA from L- and D-lactic acids (reprinted with permission from [20]). 12
- 1.7 Comparison of glass transition and melting temperatures of PLA with other thermoplastics. 13
- 1.8 DSC thermograms of water quenched, air-annealed (cooled from 220 °C to ambient temperature in 5 min), and full-annealed (cooled from 220 °C to ambient temperature in 105 min) PLLA samples. DSC scans were performed at a heating rate of 10 °C/min (Reprinted with permission from [22]). 14
- 1.9 DSC scans for 1.5% D-lactide PLA samples cooled from the melt at 10 K/min and then reheated at different heating rates from 30 to 0.3 K/min (Reprinted with permission from [30]). 14
- 1.10 Poly lactic Acid (PLA) and its characteristics 15
- 1.11 Scanning electron microscope images of fracture surface morphology of printed sample parts according to various printing layer thicknesses of: (A) 0.1, (B) 0.15, and (C) 0.20 mm [30]. 18
- 1.12 Representation of FDM/FFF process parameters [48–52]. 21

1.13	Cross section of PEEK samples at different printing speed. (a–c) PEEK samples printed considering of extrusion control algorithm and (d–f) PEEK samples printed disregarding the swelling of molten polymer die.	25
1.14	SEM micrographs of tensile-fracture surfaces of PEEK samples printed under different speeds (a) at 17 mm/s and (b) at 26 mm/s [37].	26
1.15	Temperature history of filaments during extrusion as a function of print speed (90–270 mm/min) at TLiq=325 °C (Reprinted with permission from [85]).	28
1.16	Sketch (left) and picture (right) of the measurement setup. (1) Liquefier Bondtech QR, (2) E3D v6 or volcano hot-end with variable nozzle liquefier, (3) PTFE Bowden tube, (4) 3D printer controller RAMPS v1.4, (5) 20 kg load cell with the interface HX711, (6) Data acquisition device (Arduino Mega board), (7) 12 V power supply (Reprinted with permission from [86]).	28
1.17	Possible contact areas of one filament. A_1, A_3, A_4, A_5 , areas of contacts 1,3,4,5 with adjacent filaments; A_2 area of contact 2 with the supporting table (Reprinted with permission from [78] [78])	29
1.18	Coalescence of two particles at the moment of contact and after bridge formation (neck-growth)	31
2.1	Top view of layer with different fullfills and raster angles	36
2.2	Different configuration for unidirectional filaments	37
2.3	Schematic of the designed test case of the present thesis	37
2.4	An overview on the experimental characterization methods	40
2.5	General view of the employment of <i>Datapaq</i> [®] Telemetry Tracking system from Rotational Molding to FDM/FFF process.	41
2.6	Set-up of in situ monitoring of temperature profile during the deposition stage.	42
2.7	Temperature evolution of second layer (at a specific location) during deposition of the vertical wall consisting of single filaments deposited on top of each other.	44
2.8	Representation of local and global in situ measurement of temperature profile using K-type thermocouples and IR-camera simultaneously	45
3.1	Initial characterization of the PLA spool materials: a) DSC results, b) Tensile behavior.	49
3.2	DSC results for samples printed at various liquefier temperatures.	50
3.3	Tensile behavior for samples printed at various liquefier temperatures.	50

3.4	Tensile behavior for the set of five sample according to the condition No. 1 at $T_{Liq}= 210\text{ }^{\circ}\text{C}$	51
3.5	Tensile behavior of printed PLA samples from condition No. 1 at different liquefier temperature.	52
3.6	Damage mechanisms under quasi-static loading for the samples printed at $T_{Liq}= 220\text{ }^{\circ}\text{C}$	53
3.7	a) Applied stress for PLA printed from condition No. 2 and b) macroscopic damage evolution.	54
3.8	Wöhler curves for PLA printed at the three conditions mentioned in table 2 at 1 Hz	55
3.9	Evolutions of the relative Young's modulus (E/E_0) during fatigue tests of three conditions: (a) $\sigma_{max}= 18\text{ MPa}$ and (b) $\sigma_{max}= 46\text{ MPa}$	56
3.10	Temperature evolution during FFF process ($T_{Liq}= 210^{\circ}\text{C}$, $T_{Platform}= 50^{\circ}\text{C}$, $V = 20\text{ mm/s}$, $h = 0.2\text{ mm}$).	57
3.11	DSC results for samples printed at various platform temperatures.	58
3.12	Tensile behavior for samples printed at various platform temperatures.	58
3.13	Temperature evolution for samples printed at various platform temperatures.	59
3.14	DSC results for samples printed at various print speed.	60
3.15	Tensile behavior for samples printed at various print speed.	60
3.16	Temperature evolution for samples printed at various print speed.	61
3.17	Analysis of the length of contact between two adjacent filaments (the reference sample).	62
3.18	Consequence of deposited filaments in condition No. 1 ($T_{Liq}= 230^{\circ}\text{C}$) for (a) layers 1-8 and (b) layers 9-17, condition No. 2 ($T_{Platform}= 70^{\circ}\text{C}$) for (c) layers 1-12 and (d) layers 13-26, No. 3 ($V= 60\text{ mm/s}$) for (e) layers 1-11 and (f) layers 12-24	63
3.19	Analysis of the length of contact between two adjacent filaments.	64
4.1	Temperatures of the ten first layers of the vertical wall at some instants of the deposition process.	66
4.2	Experimental ($\pm 2\text{ }^{\circ}\text{C}$) and theoretical temperature evolution during the deposition of a single filament (at $x = 5\text{ mm}$).	68

4.3	Temperature evolution at six locations during the deposition of a vertical wall consisting of single filaments deposited on top of each other. Point 1-6 correspond to the 5 th , 20 th , 37 th , 54 th , 63 rd and 88 th while indicating 30 mm, 20 mm, 35 mm, 40 mm, 25 mm and 40 mm from start of deposition, respectively.	69
4.4	Temperature contour at six locations during the deposition of a vertical wall consisting of single filaments deposited on top of each other. Point 1-6 correspond to the 5 th , 20 th , 37 th , 54 th , 63 rd and 88 th while indicating 30 mm, 20 mm, 35 mm, 40 mm, 25 mm and 40 mm from start of deposition, respectively.	70
4.5	Experimental (± 2 °C) and theoretical temperature evolution during the deposition of a single filament (at x = 5 mm).	71
4.6	Temperature profile (± 2 °C) of vertical wall at x = 5 mm from the start of deposition at different platform temperatures.	72
4.7	Representation of a) schematic of the test case, b) nodes for finite difference method, c) obtained results at steady state.	73
4.8	Temperature profile (± 2 °C) of vertical wall at (x = 5 mm) from the start of deposition at different print speed.	74
4.9	Schematic of the object in finite volume (T_{Liq} : Liquefier temperature, $T_{Platform}$: Platform temperature, T_a : Ambient temperature, N: North, S: South, W: West, E:East).	77
4.10	Temperature evolution of layer 5 (at x=30 mm) during the deposition of the vertical wall consisting of single filaments deposited on top of each other: Peaks 1, 2, 3, 4 are re-heating of 5 th filament (layer 5) by deposition of 6 th , 7 th , 8 th , 9 th , respectively.	80
4.11	The effect of h_{conv} on filament cooling: temperature evolution for $h_{conv}=5, 10, 30, 50, 70, 88$ W/m ² .°C for (a) Layer 5, (b) Layer 20, (c) Layer 88.	81
4.12	Temperature at some instances of the deposition process for the vertical wall: (a) general view, (b) layers 5, 10, 43 as well as the presentation of CVs, (c) layer 15 with high resolution of CVs.	82
4.13	Comparison of temperature evolution at different locations during the deposition of a vertical wall consisting of single filaments deposited on top of each other with prediction from theoretical model for various layer with specific locations.	84

4.14	Influence of liquefier temperature on temperature evolution during the deposition of a vertical wall consisting of single filaments deposited on top of each other with prediction obtained from theoretical model.	85
4.15	Influence of platform temperature on temperature evolution during the deposition of a vertical wall consisting of single filaments deposited on top of each other with (a) prediction obtained from theoretical model and (b) experimental validation.	86
4.16	Influence of print speed on temperature evolution during the deposition of a vertical wall consisting of single filaments deposited on top of each other with prediction obtained from theoretical model.	87
4.17	Temperature evolution during the deposition of a vertical wall consisting of single filaments deposited on top of each other with prediction obtained from theoretical model for (a) Layers 1-4, (b) optimized value for layers 1-4, (c) Layers 20-23, and (d) Optimized value for layers 20-23.	89
5.1	Dynamic viscosity evolution in different temperature	92
5.2	TTT diagram of a single filament deposition	93
5.3	TTT diagram of a single filament deposition	93
5.4	Viscosity evolution of the first layer during deposition of a vertical wall consisting of single filaments on top of each other versus the temperature evolution of the deposited filament	95
5.5	DMTA test result for PLA	96
5.6	Linear regression of WLF equation	97
5.7	TTT diagram of a single filament deposition using WLF prediction	98
A.1	Schéma des techniques AM [1]	116
A.2	Principaux éléments/défis existant dans ce processus	116
B.1	Prototypage rapide et fabrication additive [12]	119
B.2	Évolution des imprimantes 3D	120
B.3	Schéma du processus FDM/FFF	121
B.4	Représentation des paramètres du processus FDM/FFF [48-52].	123
C.1	Vue de dessus de la couche avec différents remplissages et angles de trame . .	126
C.2	Différentes configurations de filaments unidirectionnels	126
C.3	Schéma du cas d'essai conçu dans le cadre de la présente thèse	127

C.4	Un aperçu des méthodes de caractérisation expérimentales	128
C.5	Vue générale de l'utilisation du système de suivi télémétrique <i>Datapaq</i> [®] du moulage par rotation au processus FDM/FFF	129
C.6	Mise en place de l'in situ surveillance du profil de température pendant l'étape de dépôt	130
C.7	Évolution de la température de la deuxième couche (à un endroit spécifique) pendant le dépôt de la paroi verticale constituée de filaments uniques déposés les uns sur les autres.	132
C.8	Représentation de la mesure in situ locale et globale du profil de température en utilisant simultanément des thermocouples de type K et une caméra IR.	133
D.1	Évolution de la température pendant le processus FFF ($T_{Liq} = 210^{\circ}\text{C}$, $T_{Platform} = 50^{\circ}\text{C}$, $V = 20 \text{ mm/s}$, $h = 0.2 \text{ mm}$).	135
D.2	Évolution de la température des échantillons imprimés à différentes températures de la plate-forme.	136
D.3	Évolution de la température pour les échantillons imprimés à différentes vitesses d'impression.	137
E.1	Schématisation de l'objet en volume fini (T_{Liq} : Température du liquéfacteur, $T_{Platform}$: Température de la plate-forme, T_a : Température ambiante, N: Nord, S: Sud, W: Ouest, E:Est).	141
E.2	L'effet de h_{conv} sur le refroidissement des filaments: évolution de la température pour $h_{conv} = 5, 10, 30, 50, 70, 88 \text{ W/m}^2 \cdot ^{\circ}\text{C}$ pour (a) La couche 5, (b) La couche 20, (c) La couche 88.	143
E.3	Température à certains moments du processus de déposition pour la paroi verticale : (a) vue générale, (b) couches 5, 10, 43 ainsi que la présentation des CVs, (c) couche 15 avec haute résolution des CVs.	144
E.4	Comparaison de l'évolution de la température à différents endroits pendant le dépôt d'une paroi verticale constituée de filaments uniques déposés les uns sur les autres avec la prédiction du modèle théorique pour différentes couches avec des emplacements spécifiques.	145

E.5	Évolution de la température pendant le dépôt d'une paroi verticale constituée de filaments uniques déposés les uns sur les autres avec la prédiction obtenue à partir du modèle théorique pour (a) les couches 1-4, (b) la valeur optimisée pour les couches 1-4, (c) les couches 20-23, et (d) la valeur optimisée pour les couches 20-23.	147
F.1	Évolution de la viscosité dynamique à différentes températures	150
F.2	Diagramme TTT d'un dépôt d'un seul filament	151
F.3	Diagramme TTT d'un dépôt d'un seul filament	151
F.4	Évolution de la viscosité de la première couche pendant le dépôt d'une paroi verticale constituée de filaments uniques superposés en fonction de l'évolution de la température du filament déposé.	153
F.5	Résultat du test DMTA pour le PLA	154
F.6	Régression linéaire de l'équation WLF	155
F.7	Diagramme TTT d'un dépôt à filament unique utilisant la prédiction WLF .	156

List of Tables

- 1.1 Summary of the literature review done on the influence of process parameters on strength of FDM/FFF parts [38, 50, 53–62]. 22
- 2.1 Technical data sheet for the purchased PLA filaments (Adapted from manufacturer). 35
- 2.2 Technical data of Optris PI 450 Camera. 46
- 3.1 Representation of the groups of process parameters. 48
- 3.2 Values of different properties obtained from DSC, DMA and tensile results for samples printed at various liquefier temperature. 50
- 3.3 Results of tensile behavior of printed PLA samples from condition No. 1 to 3. 52
- 3.4 Value of different properties obtained from DSC, DMA and tensile results for samples printed at various platform temperatures. 59
- 3.5 Value of different properties obtained from DSC, DMA and tensile results for samples printed at various printed speed. 61
- 4.1 Technical data of Optris PI 450 Camera. 68
- 4.2 Data collected from the difference in peak values (Calculated using ‘ $\Delta T = T_{IR-camera} - T_{Thermocouple}$ ’ at each peak). 70

Introduction general

The problems of effective bonding, reduced strength and mechanical performance of fused filament fabrication (FFF)-printed 3D models are still major concerns in 3D-printed structures. Fused filament fabrication – also known as 3D printing – is extensively used to produce prototypes for applications in, e. g., the aerospace, medical, and automotive industries. In this process, a thermoplastic polymer is fed into a liquefier that extrudes a filament while moving in successive X-Y planes along the Z direction, to fabricate a 3D part in a layer-by-layer process. Consequently, as the deposition progresses, the hot filament is deposited onto filaments that were previously deposited and that are now in the process of cooling. This causes their re-heating, defining a time during which the interfaces of contacting filaments are above the glass transition temperature (T_g), in the case of amorphous material, or of the crystallization temperature (T_c) for semi-crystalline materials, which is necessary for proper bonding to take place. Therefore, each filament should be sufficiently hot during deposition, but not too hot, to avert deformation due to gravity and the weight of the filaments deposited in subsequent layers.

Accordingly, several parameters affect the manufactured part quality, like the temperature profile of the polymer and thus the inter-layer bonding. It is therefore important to understand how the process parameters affect the evolution of filaments temperature as mentioned. Moreover, since the rheological characteristic such as viscosity are a function of temperature, believably this dependence could be correlated to the temperature evolution of deposited filaments. This is an idea to create a dependent relationship between viscosity and temperature simultaneously. Hence, this leads to a concept name as TTT (Time, Temperature, Transformation) diagram of material to investigate the temperature and temperature dependence viscosity at once. Despite the advantages of FDM/FFF, it needs to be improved and optimized to reach the industry requirements. This optimization could be obtained by maximization of mechanical characteristics and bonding quality (objective: part quality), and by minimization of part cost and build time (objective: process optimization).

Given the above-mentioned statements, the temperature evolution during FDM/FFF process thoroughly specified the quality and mechanical strength of fabricated structures. Experimental monitoring and analytical investigations are still challenging in FFF and lack of practical knowledge corresponds to the problem of bonding in this process. Since the rheological characteristics are a function of temperature, together with the mentioned process variables, are widely affected by temperature evolution of filaments while printing. To sum up, investigation on temperature and temperature dependence viscosity of FFF materials while printing is still in its early stage and it governs the bonding quality itself.

The present thesis focuses on the most important variables that play an important role and control the bonding quality of the final product as i) temperature profile, and ii) temperature dependence viscosity variation of filaments. Bonding quality is mainly controlled by the temperature evolution that manage the viscosity evolution of filaments, and altogether affect the quality of final part.

Therefore, two inter-dependent phenomena will be considered during FDM/FFF process: temperature profile of filaments and temperature dependence viscosity. Furthermore, the process variables will also be considered during each stage of study (Figure 1). The objective is to investigate the rheological characteristics both experimentally and numerically, where these three phenomena as well as the process variables are taken into account and inter-related, to evaluate the influence of process parameters or define a proper condition to optimize the bonding and the quality of final product.

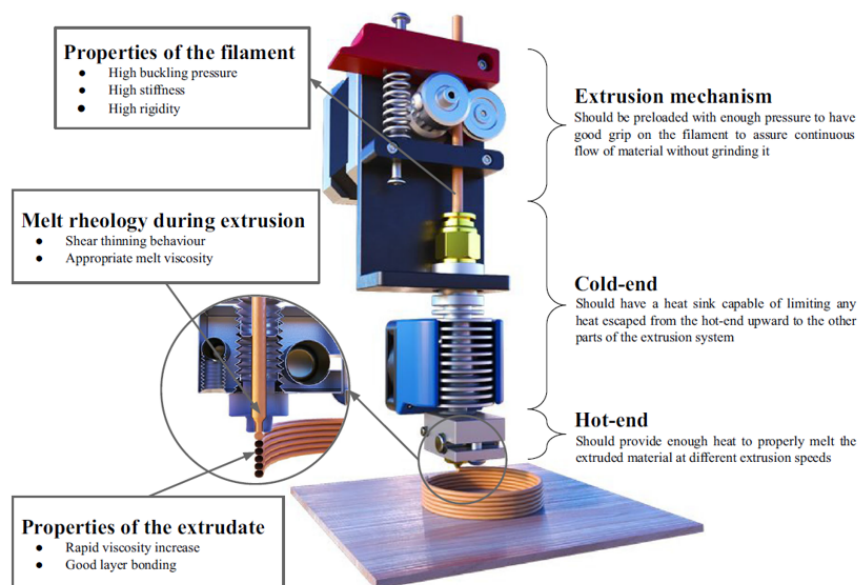


Figure 1: Schematic of AM techniques (Reprinted with permission from [1])

The main objective of this research is to study the rheological characteristics of materials during FDM/FFF process. To reach this goal (see Figure 2), temperature profile of filaments and temperature dependence viscosity must be introduced and inter-related to be implemented. The sub-objective is to optimize the FDM/FFF using the interaction of process variables further with the mentioned phenomena. This gives the opportunity of performing a parametric study of the process.

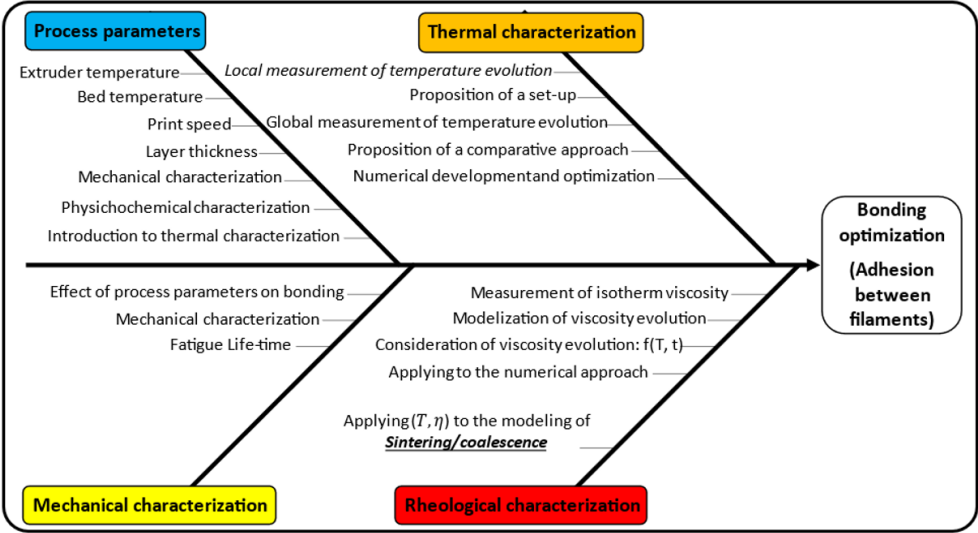


Figure 2: Roadmap and the main elements/challenges exist in this process

This thesis comprises 5 chapters excluding this introduction. A brief explanation of each has been gathered as follows:

- Chapter 1:** Literature review
- Chapter 2:** Experimental assessment of the main process variables
- Chapter 3:** Influence of process variables: Initial characterizations
- Chapter 4:** Heat transfer modeling of FDM/FFF
- Chapter 5:** Time-Temperature-Transformation diagram of filaments

Also, the published papers of the present thesis are listed as follows which are cited in the text with the label of “**Article No.–**”.

Article No. 1: HR Vanaei, M Shirinbayan, M Deligant, K Raissi, S Khelladi, A Tcharkhtchi; Influence of process parameters on thermal and mechanical properties of PLA fabricated by Fused Filament Fabrication; Polymer Engineering and Science Journal, 60:1822–1831 (2020). DOI: 10.1002/pen.25419.

Article No. 2: HR Vanaei, K Raissi, M Deligant, M Shirinbayan, J Fitoussi, S Khelladi, A Tcharkhtchi; Towards the Understanding of Temperature Effect on Bonding Strength, Dimensions and Geometry of 3D-printed Parts; J. of Mat. Sci., 55:14677–14689 (2020). DOI: 10.1007/s10853-020-05057-9.

Article No. 3: HR Vanaei, M Shirinbayan, SF Costa, FM Duarte, JA Covas, M Deligant, S Khelladi, A Tcharkhtchi; Experimental study of PLA Thermal Behavior during Fused Filament Fabrication (FFF); Journal of Applied Polymer Science, 138(4): 1-7 (2021). DOI: 10.1002/app.49747.

Article No. 4: HR Vanaei, M Deligant, M Shirinbayan, K Raissi, J Fitoussi, S Khelladi, A Tcharkhtchi; A comparative in-process monitoring of temperature profile in fused filament fabrication; Polymer Engineering and Science Journal, 61(1): 68-76 (2021). DOI: 10.1002/pen.25555.

Article No. 5: HR Vanaei, M Shirinbayan, S Vanaei, J Fitoussi, S Khelladi, A Tcharkhtchi; Multi-scale damage analysis and fatigue behavior of PLA manufactured by Fused Deposition Modeling (FDM); Rapid prototyping Journal, 27(2): 371-378 (2021). DOI: 10.1108/RPJ-11-2019-0300.

Article No. 6: HR Vanaei, S Khelladi, M Deligant, M Shirinbayan, A Tcharkhtchi; Numerical prediction for temperature profile of parts manufactured using fused filament fabrication; Submitted.

Article No. 7: HR Vanaei, M Shirinbayan, M Deligant, S Khelladi, A Tcharkhtchi; In-process monitoring of temperature evolution during Fused Filament Fabrication: A journey from numerical to experimental approaches; Accepted for publication in 2021.

Article No. 8: HR Vanaei, M Shirinbayan, S Khelladi, A Tcharkhtchi; Roadmap: Numerical and experimental characterization toward optimizing the 3D-printed parts – A review; Submitted.

Chapter 1

Literature review

1.1 Additive Manufacturing/Rapid Prototyping overview

With the fast development of technology, the role of manufacturing techniques is more obvious and industries are focusing more to find faster techniques [2, 3]. In 19th century, the existence of several challenges of producing the complex structures forced researchers to focus more on the manufacturing techniques which led to the appearance of new technology named Rapid Prototyping (RP) [4]. In comparison to traditional techniques such as machining, drilling, and milling, RP refers to the quick fabrication of models (more precisely: 3D models) that is capable of manufacturing complex geometries using CAD (Computer Aided Design) model without any tooling or machining during the process [5–7]. The main mechanism of the process is based on 3D design of a thin layer from liquid polymer by using laser beam and the final product is based on a layer of hardened resin having the same shape and dimension, which has been already generated by computer-generated slice. The production of this kind of shape was then named as Additive Manufacturing (AM) [8–10].

RP/AM is a generic term for a number of techniques in which components are fabricated without the requirement for conventional tooling. The use of these techniques allows the automatic construction of physical objects from computer geometric models and permits quick production of prototypes, and thus substantially reduces product development time [11]. As shown in Figure 1.1, the general RP/AM process flow comprises the following steps from the beginning to the final product: 1) CAD-based 3D model, 2) STL file, 3) Sliced layers, 4) RP/AM system, 5) End part finishing. Basically, the process starts by using a CAD software to draw a 3D CAD model. Then, the model is saved as a STL file format.

Using the software of 3D printer machines, the STL file model is sliced into individual layers. Finally, by sending the sliced file to the machine, it starts printing layers beside/on top of each other to form the final product. Notably, the final part may be under some post processing depending on the desired property and application of the printed part.

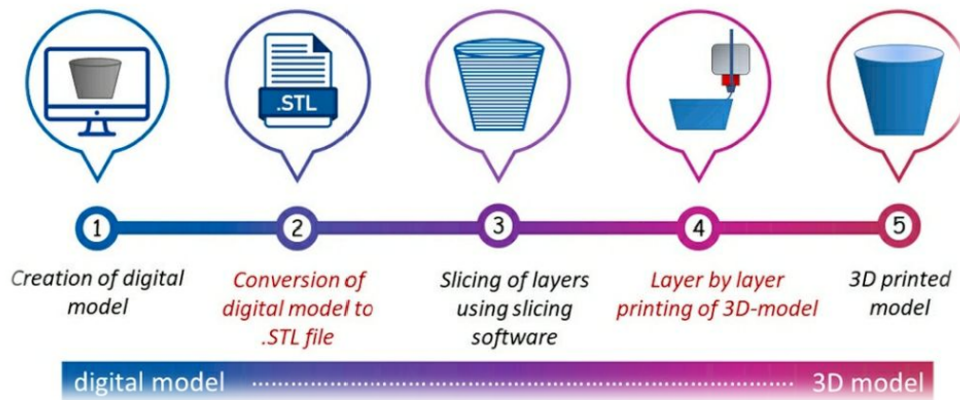


Figure 1.1: The Rapid Prototyping/Additive Manufacturing flow (Reprinted with permission from [12])

Nowadays, AM is becoming increasingly popular and its application has been expanded in a wide range of industries such as automotive, aerospace, and medicine. AM industry revenues grew 33.5% reaching \$ 9.795 billion in 2018. As explained, its advantages over conventional manufacturing techniques primarily include flexibility in design, reduced need for tooling, and product customization. These allow utilization of advanced computational techniques such as topology optimization in accomplishing the advantages of AM. Moreover, lattice metamaterials, minimal surface geometries, and functional grading have been recently become possible in manufacturing practices, lately. Combining these advantages of AM with low cost of 3D printers and availability of CAD geometries allowed almost everyone to 3D print needed parts. However, different AM processes have their own advantages, and disadvantages. Therefore, AM technologies can be classified into several categories. Accordingly, some of the main AM processes are classified as follows:

- **Fused Deposition Modeling (FDM)**

In general, it is also known as Fused Filament Fabrication (FFF). In this process, the thermoplastic filament is molten inside the extrusion head (known as liquefier or extruder) and deposited onto a build plate (known as platform/envelope/support). Materials such as reinforced thermoplastics and flexible filaments can also be used instead of thermoplastics.

- **Power Bed Fusion (PBF)**

This process mainly uses a binder or laser beam to fuse powder together forming a functional part. Successive layers of powder are then rolled on the previous layer and the process repeats itself. Finally, parts are post-processed if required. The most popular PBF systems are Selective Laser Sintering (SLS) and Selective Laser Melting (SLM).

- **Stereolithography (SLA)**

Being one of the first AM methods, SLA uses ultraviolet (UV) light to polymerize liquid resin that solidifies and, eventually, shapes the part. Unsolidified resin is removed after the printing process. While SLA can print with low resolution, it has a limited choice of materials, longer printing time as well as high material costs.

- **Laminated Object Manufacturing (LOM)**

is based on layer-by-layer cutting and, eventually, laminating sheets of different materials. Sheets are cut with high precision and then bonded together or vice versa. Uncut material is used as support and can be recycled after the printing process.

Regarding the presented category in Figure 1.2, the main factors in classification of RP/AM technologies refer to as the fabrication mechanisms and also the applicable materials. In addition, the number of different materials that can be employed in each process has increased significantly, improving the precision and functionality of the end products. Therefore, RP/AM techniques are now worthy of consideration as alternative methods of the direct production of parts, components or models for use in manufacturing processes.

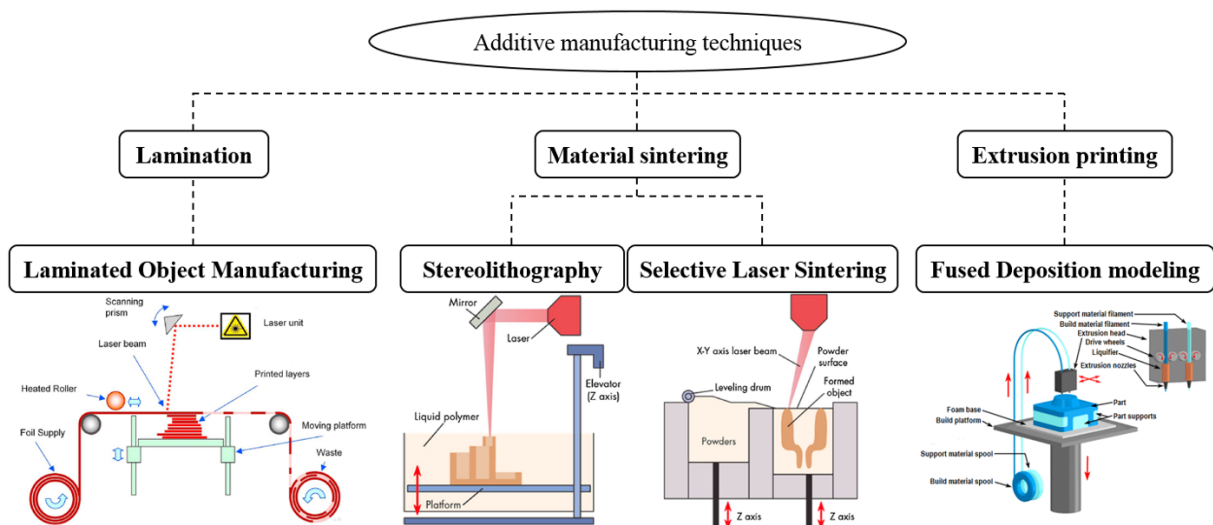


Figure 1.2: Schematic of RP/AM techniques (Reprinted with permission from [12])

1.2 Fused Deposition Modeling (FDM)

Fused deposition modeling (FDM), also known as fused filament fabrication (FFF), was first developed in 1988 by Scott Crump who co-founded Stratasys Inc, USA and was then commercialized in 1992 [13]. It is a solid free-form fabrication and forms three-dimensional objects from computer generated solid or surface models. The evolution and development of 3D printers are shown in Figure 1.3.

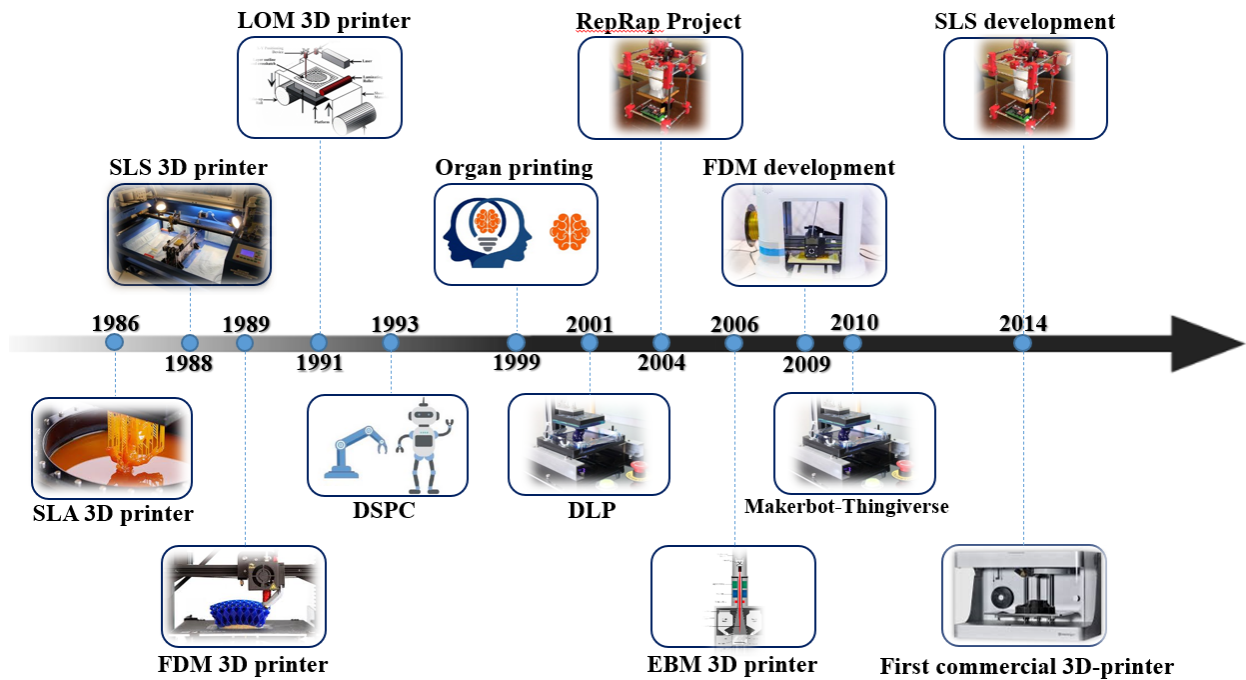


Figure 1.3: Evolution of 3D printers.

The desired part is initially modeled in CAD and is converted into an STL file (Stereolithography file format). During the build process and layer deposition, filament is heated to its melting temperature to be extruded layer by layer from a nozzle tip in an extrusion head which moves along the X-Y direction. The head, controlled by a motor, lays thin beads of material onto the surface of the platform to form the first layer which solidifies quickly due to the low temperature of the platform [14]. The base plate is maintained at a lower temperature to aid the material cool down in a controlled temperature environment when laid on it.

The platform then lowers by a specified distance, i.e., for the liquefier/nozzle to lay the second layer onto it. This process continues until the part is built based on the dimensions given in the design input. Along with the part, build supports are built to support the weaker sections and hanging structures of the part. A schematic diagram of the FDM/FFF process is provided in Figure 1.4.

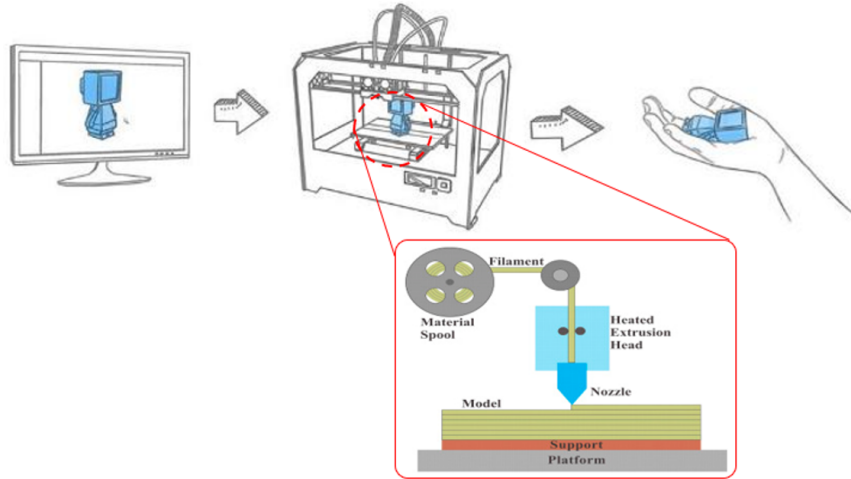


Figure 1.4: Schematic of FDM/FFF process

Comparing the FDM/FFF process to other AM processes, there are several advantages such as lower initial machine purchase costs, minimal wastage of build material, easy removal of support material, ease of use, and reduced risk of material contamination and safety of users [15]. Some of the disadvantages include poor dimensional accuracy, low strength of the parts, and higher build time. The build time and cost of an FDM/FFF part are influenced by the process parameters used to build the parts. Hence, it is very crucial to make the correct choice of parameters as the part quality including strength, accuracy and surface roughness mainly depend on the process parameters [16]. This issue will be discussed in the next section.

1.3 Applicable materials in FDM/FFF

The most common materials employed in FDM/FFF process could be classified as follows:

- **Poly lactic acid (PLA)**
- **Investment casing wax**
- **Acrylonitrile butadiene styrene (ABS)**
- **Polycarbonate (PC)**
- **Polyphenylsulfone (PPSF)**

The materials are selected based on their thermo-physical and mechanical characteristics. Key mechanical properties of a FDM/FFF material include strength, stiffness, ductility, and

flexibility. The other requirements on thermo-physical properties include low coefficient of thermal expansion, minimal shrinkage, high heat resistance, no/few volatile molecules, and no phase transformation in the solid state. A lower thermal expansion is essential to achieving the part dimensional accuracy. The amount of linear shrinkage in a part between the building temperature and the end-use temperature should be less than 1%.

Rheological and thermal properties are also taken into consideration in the material formulation and selection. A relatively low melt viscosity is required for the material to flow through the liquefier. The deposited material must be capable of solidifying in a relatively short time in order to achieve a good build speed. However, a sufficient amount of time is needed to allow a solidifying layer to well adhere to a previously deposited layer. Most commercial materials for FDM/FFF are amorphous thermoplastics. The solid to liquid transformation of the amorphous polymer is a gradual process characterized by a transition temperature commonly referred to as glass transition temperature (T_g). The glass transition temperature is interpreted in terms of molecular behavior as the temperature above the polymer chains has acquired sufficient thermal energy for an isomeric rotational motion to occur in most of bonds in the main chain, while below T_g , the polymer is in a glassy state. When the filament is deposited and it is in contact with the surrounding material, the interface's temperature is well above the material's glass transition temperature. This condition favors the rapid development of adhesive bonds.

In Figure 1.5, the most important characteristics of the applicable polymers in FDM/FFF have been classified using a classification from lower to higher of each characteristic. This diagram shows that every material has its own characteristic. As an example, for PLA, it has been mentioned that it has a better layer adhesion during FDM/FFF process and is categorized as the easy-printable material compares with others.

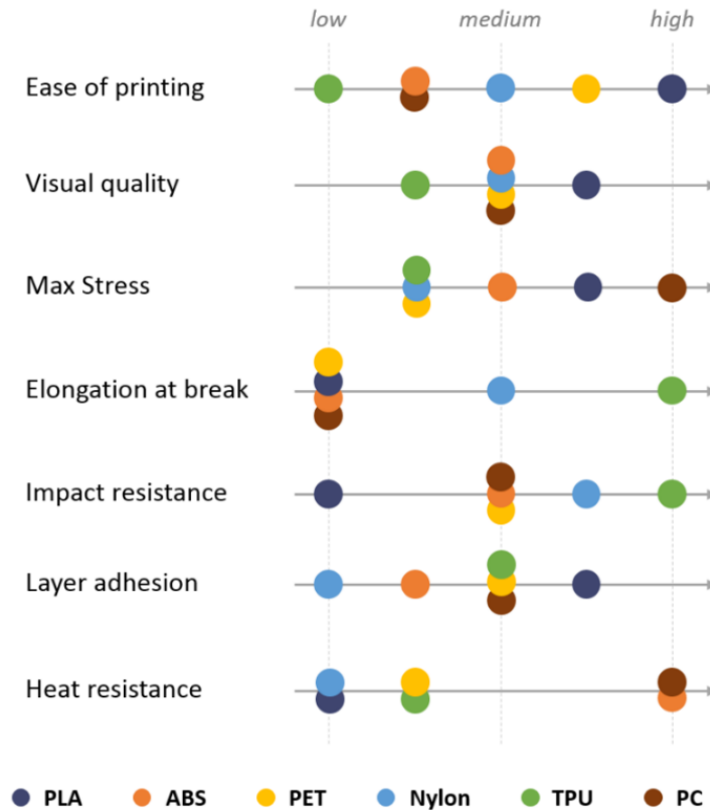


Figure 1.5: Representation of the characteristics of applicable materials in FDM/FFF process

Polylactic acid (PLA) is a biodegradable polymer made of renewable raw material (such as corn and sugar beets) and it is an alternative to petrochemical plastics. PLA is colorless, semi-crystalline, glossy, aliphatic (non-aromatic compound), rigid thermoplastic and it has got similar properties to polyethylene (PET). Several applications of this polymer include biomedicine, pharmaceutical solutions, fibers, paper coating and conventional large-scale polymer uses. Physico-chemical and mechanical properties of PLA depend on purity and molecular weight. Pure PLA is semi-crystalline with glass transition temperature (T_g) of about 55-65 °C. At the temperatures more than T_g , polymer becomes softer, decreases density, toughness and rigidity and gets to be state between the molten and rigid states. PLA monomers and molecular weight affects the glass transition temperatures and whit increase molecular weight; value of glass transition of temperature increase until 60 °C. In addition, Melting point of pure PLA is about 150-170 °C and over this temperature the polymer becomes a viscous liquid. T_g and T_m fix the working range temperature for PLA. By knowing T_g and T_m , it is possible to classify the optimal application of each type of PLA. Thermal degradation happens over 200 °C due to hydrolysis, oxidative, intermolecular and intramolecular transesterification at the high temperatures. The structure of PLA with

diffusion water molecules is swelled and hydrogen bonds are broken. Rheological properties of this polymer depends on temperature, molecular weight and shear rate. The viscosity is about 500-1000 Pa.S to high molecular weight PLA, and it has a non-Newtonian behavior (pseudoplastic). PLA denotes the family of aliphatic polyesters that has been derived from α -hydroxy acids. Its reasonable mechanical, physical, and optical properties compared to existing petroleum-based polymers, make it an important material in polymer studying [17]. Today, the main fabrication technique for thermoplastic polymers such as PLA is based on melt processing, and thus, understanding the rheological characteristics as well as its thermal and crystallization behavior, is an important criterion in optimization purposes and enhancement of parts quality. As the basic building block of PLA, lactic acid can be produced by chemical synthesis (specifically carbohydrate fermentation), most of the lactic acid production is based on the fermentation route. Various purification techniques for lactic acid and lactide can be found in a recent review by Datta and Henry [18]. These polymers can be produced using several techniques, including azeotropic dehydrative condensation, direct condensation polymerization, and/or polymerization through lactide formation (Figure 1.6) [19, 20].

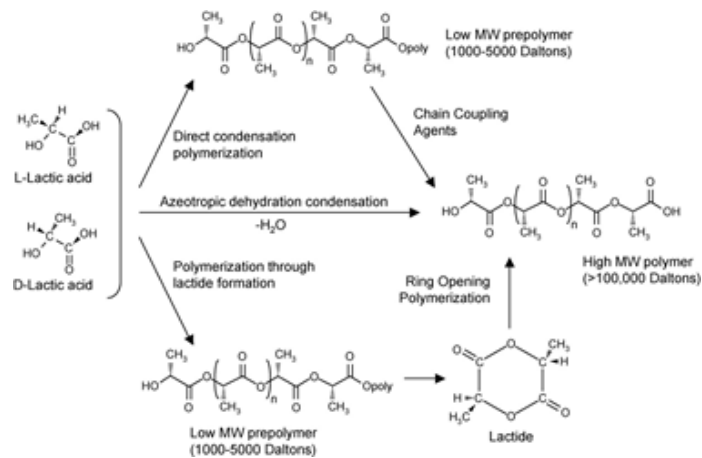


Figure 1.6: Synthesis of PLA from L- and D-lactic acids (reprinted with permission from [20]).

Commercial PLA are classified as copolymers of poly(L-lactic acid) (PLLA) and poly(D,L-lactic acid) (PDLLA), which are produced from L-lactides and D,L-lactides, respectively [20]. The L-isomer constitutes the main fraction of PLA derived from renewable sources since the majority of lactic acid from biological sources exists in this form. Depending on the composition of the optically active L- and D,L-enantiomers, PLA can crystallize in three forms (α , β and γ). The α - structure is more stable and has a melting temperature of 185 °C compared to the β -structure, with a $T_m=175$ °C [3]. The optical purity of PLA has many profound

effects on the structural, thermal, barrier and mechanical properties of the polymer [21–23].

PLA faces with thermal degradation when elevated temperature is implemented. It has been suggested that this property may be leveraged for the feedstock recycling of PLA [24]. However, the propensity for the lactide monomer to undergo racemization to form meso-lactide can impact the optical purity and thus the material properties of the resulting PLA polymer [25]. PLA exhibits a glass transition, above T_g (~ 58 °C) PLA is rubbery, while below T_g , it becomes a glass which is still capable to creep until it is cooled to its β transition temperature at approximately -45 °C, below which it behaves as a brittle polymer [26]. Figure 1.7 compares glass transition and melting temperature of PLA with other polymers. As shown, PLA has relatively high T_g and low T_m as compared to other thermoplastics. The T_g of PLA is dependent on both the molecular weight and the optical purity of the polymer.

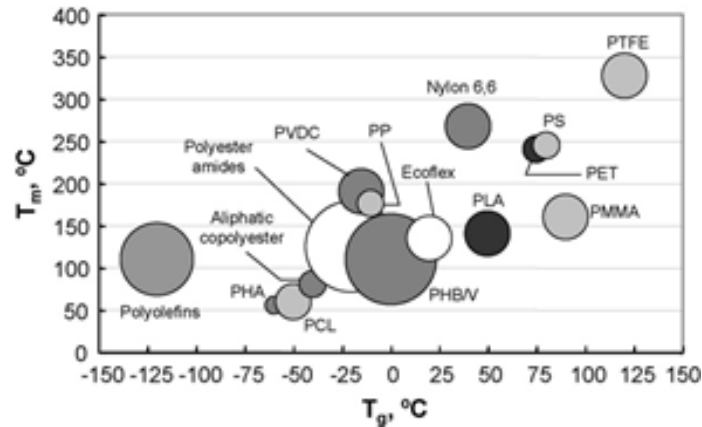


Figure 1.7: Comparison of glass transition and melting temperatures of PLA with other thermoplastics.

PLA can be either amorphous or semicrystalline, depending on its stereochemistry and thermal history. The crystallinity of PLA is most determined using the differential scanning calorimetry (DSC) technique. By measuring the heat of fusion ΔH_m and heat of crystallization ΔH_c , the crystallinity can be determined based on the following equation:

$$X_c = \frac{(\Delta H_c - \Delta H_m)}{\Delta H_m^\circ} \quad (1.1)$$

where ΔH_m and ΔH_c are the melting crystallization and cold crystallization enthalpies, respectively (obtaining by the curve extracted from Differential Scanning Calorimetry (DSC) test). Also, ΔH_m° is the melting enthalpy of 100% crystalline PLA, which is considered to be equal to 93.7 j/gr [27–29].

On quenching the optically pure PLA polymer from the melt phase (e.g., during injection molding process), the resulting polymer will become quite amorphous. As shown in Figure 1.8, quenching the polymer from melt at a high cooling rate resulted in an exothermic crystallization peak on the DSC thermogram during the subsequent reheat, while slow cooling produced a polymer with higher crystallinity with much lower enthalpy of crystallization. The tendency for PLA to crystallize upon reheat also depended on the heating rate (Figure 1.9).

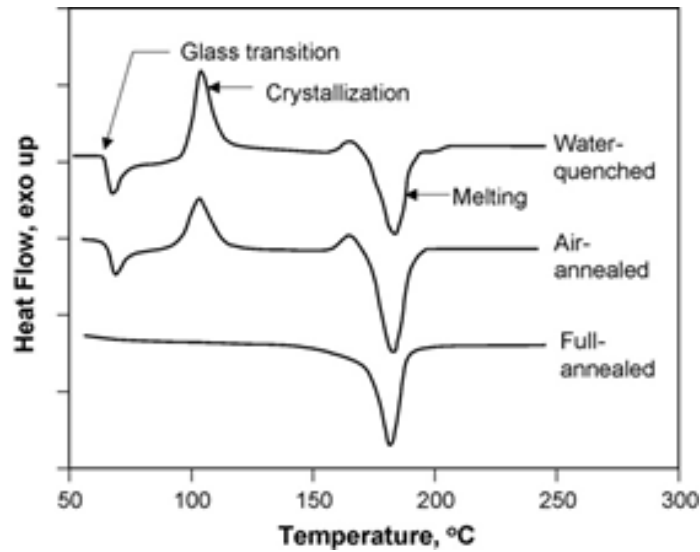


Figure 1.8: DSC thermograms of water quenched, air-annealed (cooled from 220 °C to ambient temperature in 5 min), and full-annealed (cooled from 220 °C to ambient temperature in 105 min) PLLA samples. DSC scans were performed at a heating rate of 10 °C/min (Reprinted with permission from [22]).

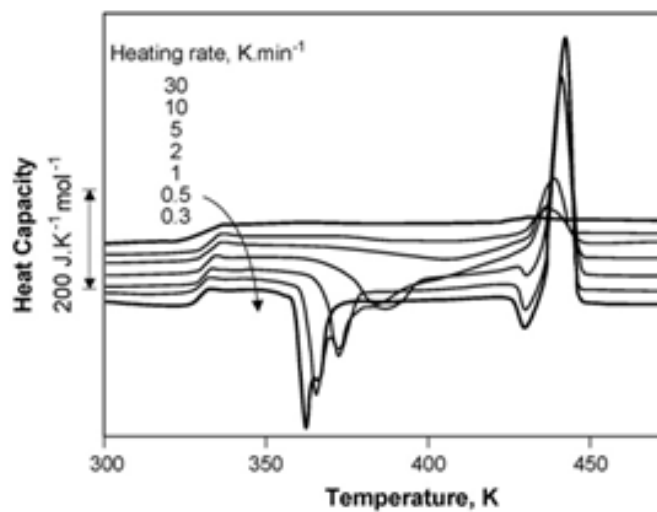


Figure 1.9: DSC scans for 1.5% D-lactide PLA samples cooled from the melt at 10 K/min and then reheated at different heating rates from 30 to 0.3 K/min (Reprinted with permission from [30]).

Commonly, PLA polymers are prepared using thermal processes, such as injection molding and extrusion. As other plastic polymers, the PLA melt is viscoelastic in nature. Therefore, it exhibits a flow behavior that is a combination of irreversible viscous flow due to the polymer chain slippage as well as a reversible elastic deformation due to molecular predica- ment (Figure 1.10).

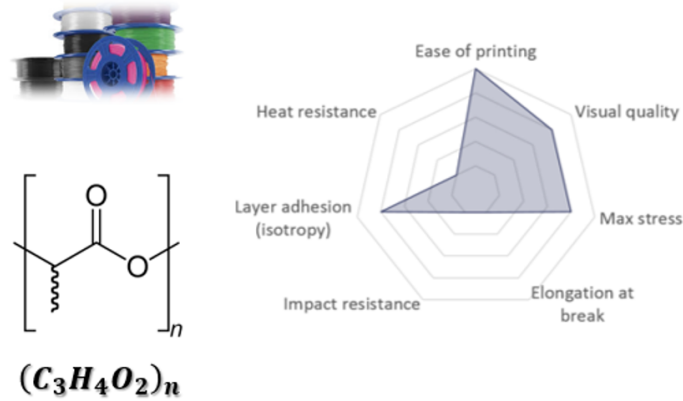


Figure 1.10: Poly lactic Acid (PLA) and its characteristics

1.4 FDM/FFF parameters and their impact on part quality

Literature on additive technologies shows that much work has been done on various RP/AM methods such as SLS, LOM, SLA, etc. but the likelihood of improvement in FDM/FFF has not been properly addressed. In general, FDM/FFF is considered to be a slower process when compared to the other RP techniques such as SLS because of its inherent layer-by-layer method of fabrication. This layer-based fabrication produces parts with anisotropic properties and residual stresses which directly affects the mechanical strength of the parts [31]. FDM/FFF parts are fabricated by stacking the layers upon each other to build the part geometry. This holds true for geometries such as cubes but for a geometry with curved surfaces and inclined surfaces, the accurate dimensions cannot be achieved. A work done by Chennakesava et al. [32] have shown orientation to be the main parameter affecting the dimensional accuracy of the 3D printed parts. They have concluded that the lower the value of orientations, the higher the accuracy and thus lower angle for layer deposition should be taken into account. Various studies have focused on improving the dimensional and surface roughness aspect of FDM/FFF parts quality. However, for the purpose of increasing the application of FDM/FFF process, the strength and mechanical performances of the final parts need to be focused.

The strength of FDM/FFF fabricated parts is usually less when compared to that of parts obtained from traditional manufacturing processes. Though a portion of this drawback is due to the principle involved in the manufacturing of the part in this process, a major portion is due to the inappropriate choice of the process parameters. As stated in the work of Chennakesava et al. [32], The print quality of an FDM/FFF prototype is greatly influenced by the choice of process parameters used in the part fabrication. As the FDM/FFF parameters set at the time of fabricating the part determine the build cost and time, it is very crucial for developers and designers to understand the influence of process parameters to enhance the parts quality [33]. Furthermore, an optimal parameter for one material may not be the same for a different material. So, it is important to investigate the link between the properties of materials and their dependence on the process parameters. In what follows, a review on the literature has been performed in order to realize the studies that have been done in this direction.

As an important indicator, the mechanical performance of the fabricated parts has been argued to be taken into account during the AM/RP manufacturing process. More precisely, in the case of FDM/FFF process, the part quality mainly depends on the process parameters that were presented in the machine during the part production. Unsuitable choice of the process parameters in the FDM/FFF technique can be a crucial reason for the poor mechanical properties of the fabricated parts. Controlling and optimizing the process parameters on the part quality, the strength of FDM/FFF parts could be improved and thus it is essential to understand the importance of them [33].

Górski et al. (2015) studied the influence of part orientation by performing the mechanical tests such as bending and tensile tests on the parts produced in different orientations [34]. Changing the build orientation varied the strength index of ABS samples. Their results showed that orientation of the part during manufacturing has a strong impact on the tensile and bending strength of the part. The study also designated supposed ranges of critical orientations where the transition from ‘yield point’ to ‘brittle’ happens for different loads and provided a supposed range of orientation for various loads. In another work, Lee et al. [35] studied the effect of build orientation on the compressive strength of parts produced by three different additive methods namely FDM, 3D printer and Nano-composite deposition (NCDS). Axially printed FDM parts showed higher compressive strength than the transversely printed FDM parts by almost 11.6%. Whereas, 3D printing diagonally printed

specimens were found to have a much higher compressive strength in comparison to the axially printed specimens. NCDS specimens which were printed axially had 23.6% higher compressive strength than the transversely printed specimens. Similarly, the impact of part orientation has been investigated considering the tensile strength, flexural strength and impact resistance of ABS solid models [36]. It was found that parts printed by laying the layers along the direction of the length exhibited higher strength over other orientations. It was then reported that the anisotropic property in FDM/FFF parts is due to the weak interlayer bonding caused by the volume shrinkage during solidification of the semi-molten filament from the liquefier in the chamber.

Another parameter that has an impact on the mechanical behavior and quality of final parts is layer thickness. Depending on the type of the machine, layer thickness varies between 0.1 and 0.4 mm. Several works have noted the influence of this parameter on the mechanical properties of the 3D-printed parts. Ahn et al. [31] evaluated the effect of layer thickness of ABS and they found that there is not significant change in mechanical properties of fabricated parts, whereas another work on PLA showed that the increase in layer thickness, results in higher strength of 3D-printed parts. Approximately, in all researches on PLA and ABS, it has been tried to consider the effect of layer thickness by investigation of the variation of mechanical properties. However, researchers have widely focused on other thermoplastic polymers such as PEEK. El Magri et al. [30] investigated the influence of layer thickness on the mechanical and thermal properties of 3D-printed PEEK, both as-produced and annealed parts. They found that layer thickness has a considerable impact, however, without any specific order. As shown in Figure 1.11, this issue has been compared with the SEM images of fractured surfaces: the higher the layer thickness, the higher the number of voids and poor adhesion will be obtained.

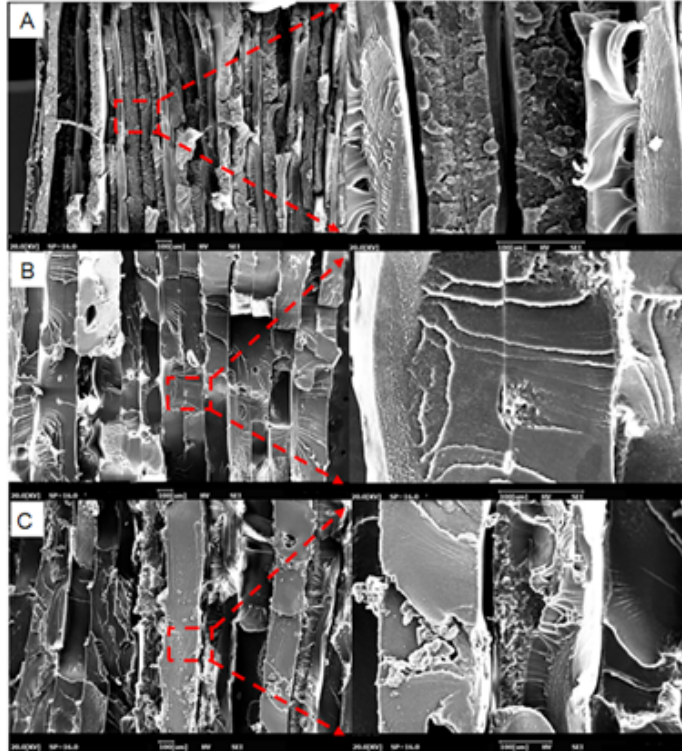


Figure 1.11: Scanning electron microscope images of fracture surface morphology of printed sample parts according to various printing layer thicknesses of: (A) 0.1, (B) 0.15, and (C) 0.20 mm [30].

Another interesting work by Wang et al. [37] compared the effect of layer thickness as a function of the liquefier diameter. They stated when the layer thickness surpasses 1.5 times higher than the nozzle diameter; surface quality deteriorates as well as the gap between layers. Layer angle between deposited filaments also acts as an important parameter in determination of the mechanical properties of the printed parts. Several works studied how the layer angle affects the mechanical properties of the fabricated parts [15, 38–40]. They all have reported that the mechanical characteristics changed by variation of this parameter. Smith et al studied the influence of build orientation on the mechanical strength of polycarbonate samples [41]. They found that repeatable measurements can be made of the ultimate tensile strength in FDM/FFF printed PLA samples. In the work of Schöppner et al. [42], the influence of build direction and toolpath generation have been studied and its impact on the mechanical properties of Polyetherimide (PEI) parts printed by FDM/FFF has been taken into consideration. It was reported that parts built in horizontal direction had higher yield strength and compressive modulus when compared to the parts that were built in a vertical direction.

Although most studies concentrated on individual contribution of process parameters, very few works have focused on the simultaneous effect of parameters. Masood et al. [43]

studied the influence of process parameters such as air gap, raster width, and raster angle on the tensile strength of 3D printed polycarbonate parts. In another similar work, Motaparti et al. [44] investigated the influence of air gap along with build orientation and raster angle on the compressive strength of ULTEM 9085 samples. They observed that the interaction between raster angle and build direction affected the compressive strength of the ULTEM samples and air gap had the least effect. It was also found that horizontal built parts had a higher compressive strength in comparison to the vertical built for both solid and sparse specimens.

More broadly, Khan et al. performed Taguchi analysis to find the optimal set of process parameters such as layer thickness and air gap that affect the elastic performance of ABS prototypes [45]. Air gap was found to be the maximum contributor for lower angles of displacement, whereas layer thickness was found to be the maximum contributor for higher angle of catapult displacement. The influence of raster angle on the resulted residual stress due to rapid heating and cooling of the parts has also been studied [46]. They found parts built with a raster angle of ± 30 had the higher residual stress and the ones built with ± 45 had the least residual stress.

Apart from the mechanical strength, the process parameters also have a strong impact on the build time and consequently the cost of final product. Very few studies have been done in this direction. Rathee et al. [47] studied the influence of spatial orientation on the build time of FDM/FFF parts. They have used Response Surface Methodology (RSM) to design the experiments. It was found that orientations had a major impact on build time and individual process parameter contribution varied based on the spatial orientation.

Given the above-mentioned studies, a thorough investigation of the literature shows the following limitations:

- An overview performed on the influence of process parameters through the part quality fabricated by FDM/FFF process appears to have conflict in their obtained results. As an example, a study in 2002 concluded that layer thickness has less significant influence on the tensile strength, while after 3 years other researchers found that tensile strength of an FDM/FFF part first decreased and then increased as layer thickness increased. A few years later, in 2010, another research proposed that layer thickness has low impact on the tensile strength. These consequences call for an overall investigation through the FDM/FFF parameters.
- FDM/FFF parameters not only affect the part quality but also greatly influence the

build time involved. However, studies found in the literature did not focus on the influence of process parameters on the build time.

- Almost all researches have focused on the investigation of one material at a time or even one parameter at a time, whereas there are numbers of parameters in reality that play an important role during production. Furthermore, based on the various researches exist in literature, it is required to investigate the simultaneous effect of important parameters to get a better understanding of the FDM/FFF parameters.
- A thorough investigation on the combined effect of FDM/FFF parameters is required which helps understanding the influence of each parameter further with their interaction on the bond quality. This point of view helps optimizing the FDM/FFF process to reach the final goal which is the improvement of bond quality.

As discussed, the quality of a final object fabricated by FDM/FFF process mainly relies on applied parameters. The main issues and areas of concern of any FDM/FFF user with respect to the quality are the build time and build cost. Even though studies have focused on identifying the optimal parameters for improving the quality of the parts, there is still no optimal set of parameters for all types of materials and parts. The lower mechanical properties of parts fabricated by FDM/FFF in comparison with traditional manufacturing processes shows that the final parts are highly affected by various parameters. To improve the part quality, it is important to consider the main parameters and their impact on the final part.

1.5 Role of process parameters on part quality

The design for FDM/FFF demands high attention as it is necessary to well predict the various characteristics of the final product, e.g. mechanical properties. Hence, the influence of process parameters on the mechanical characteristics and consequently the bonding between deposited layers should be taken into account. FDM/FFF parameters could be mainly categorized in 3 different groups: material parameters, process parameters, and machine parameters (Figure 1.12).

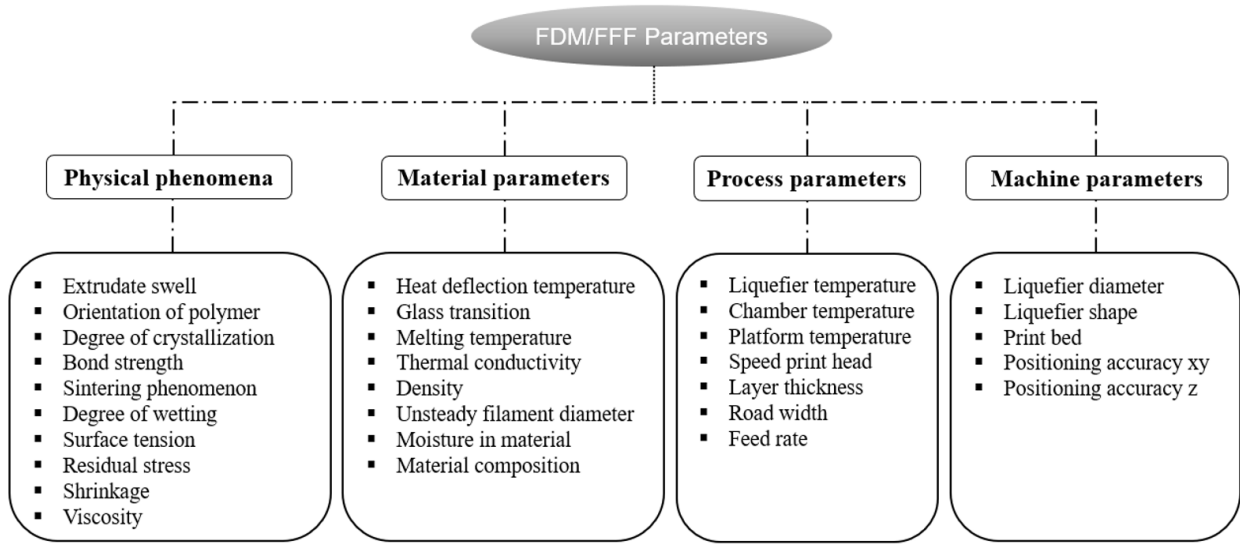


Figure 1.12: Representation of FDM/FFF process parameters [48–52].

Due to the nature of FDM/FFF, almost all the 3D-printing machines comprise various parameters. The temperature of liquefier and chamber, path width, print speed, layer thickness, air pocket, and frame angle could be considered in the characterizations of fabricated parts. Almost all of them affect the filament bonding and consequently the mechanical behavior of 3D-printed parts. However, researchers tried to focus on some key parameters to get the combination of them and optimize the quality of the final parts. Various researches considered the influence of material, process, or machine parameters on the bonding and its quality in FDM/FFF. Although the effect of build orientation and frame angle on the mechanical properties of 3D-printed parts have been consequently studied, raster angle was found to have an impact by consideration of infill patterns [38, 50].

In addition, the effect of in-process and post-process on thermal global state during parts 3D-printing have been investigated by taking into consideration the importance of environment and platform temperatures. Diffusion and neck-growth between two adjacent filaments would be affected by changing of environment or platform temperatures, which confirm the significance of heat transfer in this process. Regarding the applied material and studied parameters, it was found that almost all researchers tried to consider the influence of parameters by different methods of characterization (e.g. tensile or bending) with using a unique parameter at different values. A brief representation of researches on various materials has been performed in Table 1.1.

Table 1.1: Summary of the literature review done on the influence of process parameters on strength of FDM/FFF parts [38, 50, 53–62].

Material	Variable parameters	Mechanical properties
PLA	Layer thickness	Shear stress
	infill density	
	Post-processing heat treatment at T=100 °C	
ABS/PC	Raster angle	Tensile strength
	Build orientation	Failure strength Young's modulus
ABS	Building orientation	Tensile strength
	Infill Density	
PLA	Temperature	Tensile strength
	Infill direction	
	Layer thickness	
ABS	Thickness and infill density	Tensile strength
PLA	Building orientation	Tensile strength
	Layer thickness	Flexural strength
ABS	Raster orientation	Tensile strength
	Number of layers (1-35)	Elastic modulus
PLA	Process parameters effect on mechanical properties	Tensile strength
		Flexural strength
		Impact strength
PEEK	Bed temperature	Tensile strength
	Environment temperature	
PLA	Deposition orientation	Tensile strength
	Layer thickness	Flexural strength
	Raster variation	Impact strength
ABS	Temperature profile	3-point bending test
	Temperature variation with part building	Thermal analysis

According to the large number of studies performed by several researchers, following

parameters found to have more impact on the part quality and mechanical strength of final parts: liquefier temperature, platform temperature and ambient temperature, print speed, layer thickness, and layer angle. Interaction of mentioned parameters plays an important role on determination of the mechanical properties of the printed parts. In what follows, a brief explanation on the influence of the mentioned parameters on mechanical behavior of the printed parts has been taken into consideration.

1.5.1 Liquefier temperature

The liquefier temperature can have a positive influence on the part quality and its strength. The inter-diffusion between the new layer and the existing layers takes place before the extruded filament cools down below its glass transition temperature in the case of an amorphous material or crystallization temperature in the case of a crystalline material. The longer the material stays at a higher temperature than its glass transition level, the better the bond becomes. This is the reason why the mechanical performance of materials like PLA parts are greater than that of ABS [63]. The study performed by Coogan et al. [64] illustrated that the increase in the liquefier temperature yields stronger adhesion between the filaments. Similarly, in the work of Jatti et al., it has been shown that high liquefier temperature has positive effect on the adhesion and mechanical performance of the parts. In another study, the influence of liquefier temperature has been experimentally studied using ABS reinforced with carbon fiber [65]. Analyzing the fracture surface, it was found that by increasing the liquefier temperature, the parts become stronger but until a specific value of temperature ($T_{Liq}=220$ °C). A further rise of temperature increased the fluidity of molten plastic, due to which the filaments lose their viscosity and void were constantly produced reducing the mechanical properties of the part. These observations were then confirmed by another work that considered the effect of the liquefier temperature on the PLA-PHA [66]. Their results showed that with the increase of the temperature up to $T_{Liq}=240$ °C, the tensile strength increased. However, as the temperature increased to $T_{Liq}=250$ °C, the mechanical properties started to become lower.

A work done by Jiang et al. [67] on the construction of PEI parts, illustrates the influence of high liquefier temperature on the mobility of the macromolecular chains of the extruded filaments. They found that a value of liquefier temperature $T_{Liq}=370$ °C contributes to the highest tensile strength and Young's modulus. The flowability of the extruded filament and

inter-layer bonding strength of adjacent layers are affected by the liquefier temperature. Yang et al. [68] investigated the influence of this parameter on the mechanical properties and the crystallinity of PEEK. A period of $360 < T_{Liq} < 380$ °C demonstrates 3% variation in its crystallinity. However, further increase of the liquefier temperature indicates about 21% increase in the crystallinity. At this point, the increase of mechanical properties and Young's modulus was observed, the same as those observed by Jing et al. [67] on PEI. These findings could be distinguished by the energy supplies to the material due to the enhancement of the liquefier temperature, providing better crystallization during deposition of the material. Considering both PEEK and PEI, Ding et al. [69] evaluated the influence of liquefier temperature on mechanical properties and also the microstructural behavior. They found that the increase in temperature gradually improves the flexural strength. Regardless of the consideration of the amount of mechanical improvement on each material, they concluded that an optimized value for liquefier temperature should be obtained. Furthermore, by paying attention to the fabrication of composite materials, Berretta et al. [70] investigated the effect of liquefier temperature on the surface quality of the PEEK reinforced with carbon nanotubes (CNTs). By choosing some values of T_{Liq} , different morphologies were obtained, but no significant variations were observed. Using a fine liquefier diameter, Monzon et al. [71] considered an experimental approach and an analytical model to analyze the temperature variation along the liquefier. They found that both liquefier and platform temperatures play an important role in 3D printing.

1.5.2 Platform temperature

The impact of platform temperature has also been reported in several studies. Xiaoyong et al. [53] investigated that the mechanical properties of the 3D printed parts are affected by the platform and the variation of its temperature. They noted that variation of its temperature causes an increase in the tensile strength of the 3D printed parts, whereas Ahn et al. [31] mentioned that platform temperature has no effect on the mechanical properties of the 3D printed parts. This statement was then confirmed by another work [72]. Consequently, Sun et al. [73] stated that the filament bonding and consequently the mechanical behavior of the material are affected by the variation of platform temperature.

1.5.3 Print speed

There are several studies that have investigated the effect of print speed. Christiyan et al. [74] considered experimentally the effect of print speed on the mechanical behavior of ABS composite, and they found that the increase in print speed decreases the tensile and flexural behavior of the materials. In another work, it was shown that print speed plays an important role in controlling material solidification [75]. The higher the print speed, the lower the cooling rate and thus better bonding at the interface of deposited filaments. Geng et al. [76] have also considered the effect of print speed through the microstructure of PEEK filaments. They found that the surface morphology and dimensional stability of printed parts were improved by controlling the print speed (Figure 1.13).

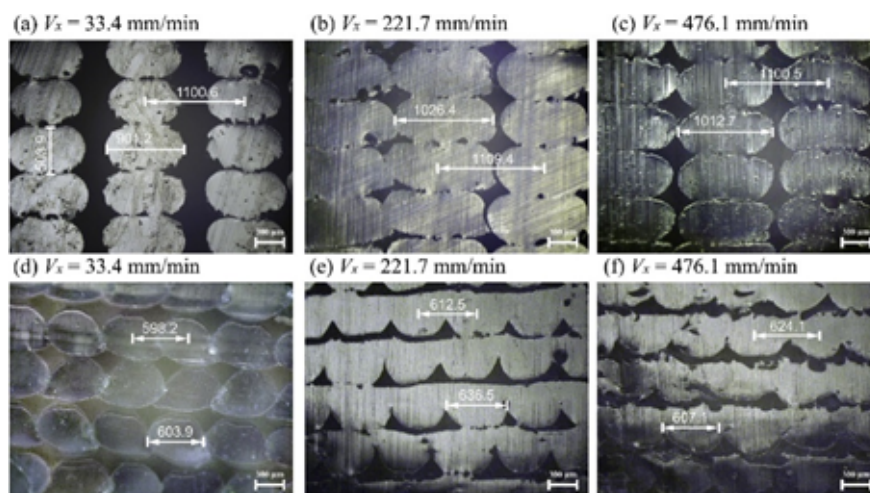


Figure 1.13: Cross section of PEEK samples at different printing speed. (a–c) PEEK samples printed considering of extrusion control algorithm and (d–f) PEEK samples printed disregarding the swelling of molten polymer die.

Despite the mentioned works, another research demonstrated that rising the print speed decreases the mechanical strength of PEEK that is related to the crystallinity of the material. As the fracture surface of the PEEK tensile samples is observed in Figure 1.14, the samples printed at higher print speed comprise a consequence of voids [37].

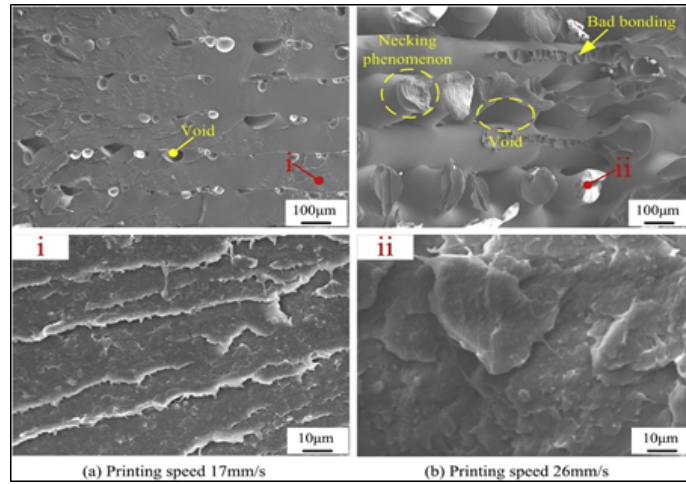


Figure 1.14: SEM micrographs of tensile-fracture surfaces of PEEK samples printed under different speeds (a) at 17 mm/s and (b) at 26 mm/s [37].

A review through literature indicates that the influence of FDM/FFF parameters has not been studied much; almost all studies have focused on the investigation of individual parameters. So, considerable work remains to be done for process optimization by taking into account the interaction of parameters.

1.6 Role of heat transfer on part quality

In FDM/FFF process, a thermoplastic polymer is fed into a liquefier that extrudes a filament while moving in successive X-Y planes along the Z direction, to fabricate a 3D part in a layer-by-layer process. Consequently, as the deposition progresses, the hot filament is deposited onto the filaments that were previously deposited and that are now in the process of cooling. This causes their re-heating, defining a time during which the interfaces of contacting filaments are above the glass transition temperature (T_g) in the case of amorphous materials, or of the crystallization temperature (T_c) for semi-crystalline materials, which is necessary for proper bonding to take place. Therefore, each filament should be sufficiently hot during deposition, but not too hot to avert deformation due to the gravity and the weight of the filaments deposited in subsequent layers.

Several researches were performed on thermal history prediction of filaments while deposited. Bellehumeur et al. [77] proposed the Lumped capacity model by assuming a uniform temperature profile of filament's cross-section. This 2D analysis was then simplified to a 1D transient heat transfer model, so the cooling process was simplified into a 1D heat transfer model. Despite the simplification proposed in this approach, the simulation does not

contribute to the complex geometries. Taking into account the contacts between filaments, Costa et al. [78] suggested an analytical solution for the transient heat transfer during the deposition of filaments. Although they have neglected the axial and radial heat conductions, they have recently distinguished the contribution of various thermal phenomena engaged in the process [79]. The main disadvantage of their approaches is the limitation of experimental validations and the distance that exists between the obtained results with reality. Thomas and Rodriguez [80] have also presented a 2D thermal model in a specific shape of deposition. In this work, the conduction and any contact resistance of filaments have been neglected. Moreover, Yardimici et al. [81, 82] proposed a 1D thermal model in their works by taking into account the thermal interaction with the environment and between the deposited filaments. Zhang et al. [83] developed a FEM, applying element activation, to simulate the thermomechanical characterization in FDM/FFF. A 3D transient thermal FEM developed by Ji et al. [84] considering the thermal conduction and heat capacity. The weakness of all analytic approaches is that simplified closed-form solutions are limited to simple geometry and could not be applied to realistic parts and manufacturing processes.

After a decade and by expiration of the Stratasys FDM^{TM} in 2010, the number of works on 3D printing has progressively raised up. The main reason relies on the emersion of open-source 3D printers and thus the possibility of working on different possible aspects of optimization purposes. Peng et al. [85] used a temperature sensor to study the temperature variation during the extrusion process. As shown in Figure 1.15, by raising the print speed, there is a deviation from the isothermal flow. Taking into account the experimental validation that they implemented for their approach, the extrusion process during the filament deposition acts as a non-isothermal process. So, temperature variation plays an important role and should be controlled for optimization purposes.

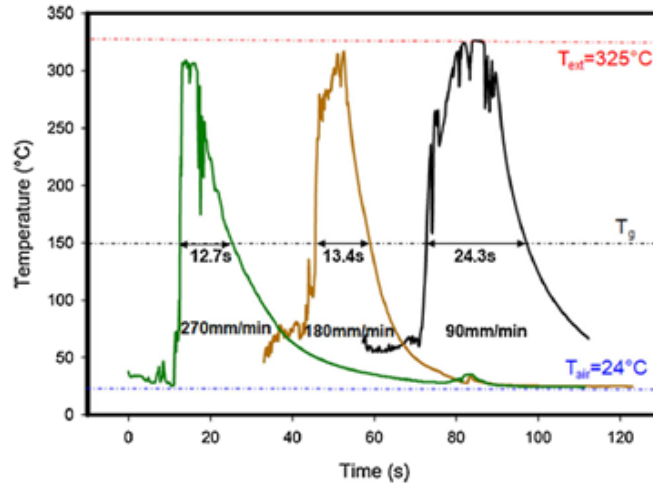


Figure 1.15: Temperature history of filaments during extrusion as a function of print speed (90–270 mm/min) at $T_{Liq}=325\text{ }^{\circ}\text{C}$ (Reprinted with permission from [85]).

Similarly, another work considered an experimental set-up to investigate the relationship between the input filament speed and feeding force at different liquefier temperatures (See Figure 1.16 for the measurement set-up) [86]. They found that liquefier temperature acts as a limitation criterion. Also, Vaes et al. [87] applied an IR sensor to investigate the temperature variation parallel to the filament deposition. Cattenone et al. [28] predicted the distortion of 3D printed parts using a finite element analysis. By implementing an experimental validation to the obtained results, the authors show that the mechanical properties of 3D printed parts are highly affected by the local temperature distribution.

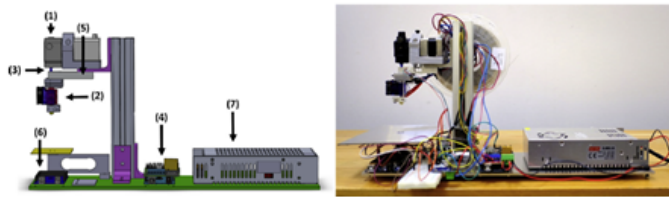


Figure 1.16: Sketch (left) and picture (right) of the measurement setup. (1) Liquefier Bondtech QR, (2) E3D v6 or volcano hot-end with variable nozzle liquefier, (3) PTFE Bowden tube, (4) 3D printer controller RAMPS v1.4, (5) 20 kg load cell with the interface HX711, (6) Data acquisition device (Arduino Mega board), (7) 12 V power supply (Reprinted with permission from [86]).

In addition, Seppala and Migler [88] used an IR-camera to study the temperature distribution around the active printing area. In other similar work, D’Amico and Peterson [89] applied a finite element analysis for simulation of the heat transfer during FDM/FFF process. In both works, using an IR-camera, they contributed a temperature profile of the external surface of the printed objects and thus the simulations were validated based on the

mentioned results. More recently, Costa et al. Developed a heat transfer model including the transient heat conduction between the filament and/or the built platform [78, 90]. As illustrated in Figure 1.17, they found that the temperature profile of filaments is highly affected by the physical contact that existed between the filaments. Accordingly, they considered the involved parameters during their experimental validation and the results, however, obtained by implementing an IR-camera, show that the contacts between filaments play a crucial role and should be considered in heat transfer investigations.

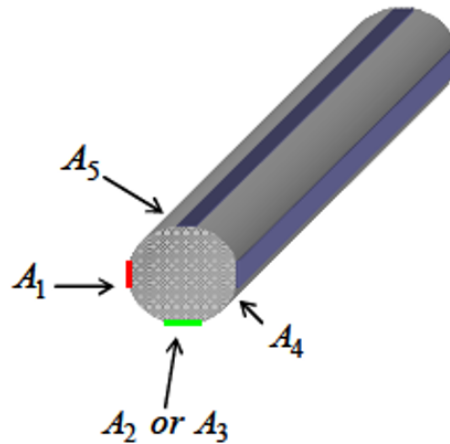


Figure 1.17: Possible contact areas of one filament. A_1 , A_3 , A_4 , A_5 , areas of contacts 1,3,4,5 with adjacent filaments; A_2 area of contact 2 with the supporting table (Reprinted with permission from [78] [78])

1.7 Role of viscosity evolution and coalescence on part quality

In FFF/FDM, based on the matter of heating the material during printing, the selection of liquefier temperature is an important issue. The point is to prevent overheating or even low flowability of material during deposition. Therefore, the realization of the rheological characteristics is determinant. Certifying optimum material feeding as well as rapid changing in the viscosity, printed material should show sufficient increase in its viscosity while extruding to avert instability of geometry of the 3D printed final parts.

So, this is the reason why thermoplastic polymers are being used with an outstanding viscoelastic behavior while encountered with cyclic temperature profile during 3D printing [67]. To describe shear-thinning, rheological characteristics such as viscosity should be taken into consideration. Besides, there are two main parameters, storage modulus and loss modulus, determining the viscoelastic behavior of the material. The appropriate relative balance

between these two important factors specifies the solidity or liquidity of the material during the process. Despite the fact that the viscosity decreases drastically while melted and the material subjects to a high shear rate (depending on the liquefier diameter), even a greater decrease in the material viscosity is afforded [91]. Conversely, after extrusion of the material, the sudden drop in temperature results in a massive increase in the material viscosity [94]. These variations and transformations play an important role during FDM/FFF process. Given the above-mentioned explanations and the statements described in the previous section, controlling the viscosity variation further with the temperature profile between the deposited and previously deposited layer is an important issue to give sufficient time for proper diffusion and bonding. These are key factors to retain the temperature in a specified zone based on the type of material [88]. They thus imitate the material diffusion and welding process between two adjacent layers and are categorized as a thermally driven phenomenon named ‘Coalescence’.

Coalescence is a phenomenon by which several individual bodies merge to form an integrated mass [92, 93]. Various mechanisms such as capillary-induced flow, mass diffusion, or crystallization could occur to facilitate it. According to literature, a large curvature could be created on the surface of two bodies when they became in contact (see Figure 2.18). Hence, the flowability of the bodies is crucial which helps the surface tension force to implement a flow through the particles. (or filaments/cylinders in the case of FDM/FFF process) [94]. Then, it gradually grows while the completion of the mentioned integration, however, it could be limited by external forces. Coalescence at its early stage (particle-particle attachment) is considered as a micro-scale approach, which is then applicable in macro-scale for bulk materials. The most important criterion in this approach is the bridge growth kinetic, which is also referred to as neck-growth [95]. Firstly, a mathematical modeling was implemented by Frenkel [96] to investigate the dynamic formation of neck-growth of two spheres under viscous flow mechanism. Although the model considered the constant radius for the spheres, it was not true as the mass conservation law was not satisfied. Regarding the usefulness of the model, Eshelby modified the model considering variable radius of spheres and presented it as the Frenkel-Eshelby relation. The modified Frenkel’s model was limited to the early stage of the neck-growth based on the small amount for the θ angle was assured in this approach.

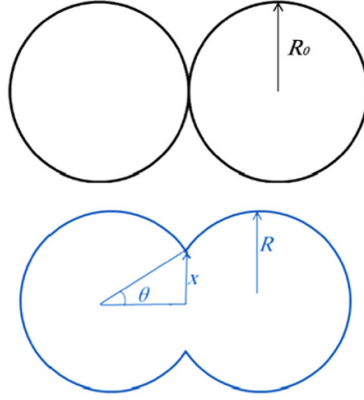


Figure 1.18: Coalescence of two particles at the moment of contact and after bridge formation (neck-growth)

Enlarging the range of neck-growth validity, Pokluda et al. [97] modified the Frankel-Eshelby relation. It was then validated experimentally by the work of Bellehumeur et al. [98]. These models have all considered the Newtonian flow and isothermal condition in the coalescence phenomenon (even for the model proposed by Hopper [99] that considered the coalescence of two cylinders) so far. There is still a lack of studies that consider the non-isothermal conditions, using both experimental and numerical approaches. Tarafdar and Bergman [100] tried to investigate the influence of temperature on particle coalescence by combining the heat conduction equation and Pokluda model. They assumed that the densification and porosity of the sintered material are strongly affected by the temperature. Seemingly, the influence of temperature was found to be an effective criterion under non-isotherm conditions. In almost all approaches, viscosity was assumed constant for both isothermal and non-isothermal conditions. Wadsworth et al.[101] have recently applied a constant heating rate to assume the viscosity temperature dependence criteria.

With reference to the above-mentioned explanations, one of the main problems that have an impact on the bonding and mechanical strength of parts manufactured by FDM/FFF, is the coalescence of filaments (simple word: coalescence of cylinders) which itself is influenced by several factors. Prediction and measurement of neck-growth help optimizing the process variables to reach the main goal which is the improved-quality of final parts. Sun et al. [73] introduced the adhesion and bonding quality in the FDM/FFF process as the succession of the following steps: intimate contact, coalescence, and healing with a random distribution of polymer chains.

Furthermore, neck-growth was predicted from various point of view. Bhalodi et al. [102]

tried to investigate the effect of temperature and time on neck-growth by considering the heat transfer of filaments. Although they have concluded that, there is a good agreement between experimental and theoretical results, there is still a missing point in consideration of temperature evolution and temperature dependent viscosity. Another work was also concentrated on the effect of heating and cooling on viscous sintering of cylinders during FDM/FFF process. Although they predicted the sintering time as well as the neck-growth, there is still a missing point regarding the consideration of cyclic evolution of temperature in FDM/FFF process [103].

Regardless of study on the influence of parameters on neck-growth or neck-growth prediction by viscoelastic models, there is still a lack of practical knowledge on consideration of temperature dependent viscosity and its influence on the coalescence of two adjacent filaments. To eliminate the mentioned missing spot, a thermo-mechanical approach is an essential manner by applying the results of temperature evolution of filaments at their interface.

1.8 Conclusion

Accordingly, from the very beginning of the application of FDM/FFF process, numerous studies have been performed for the development of this process. Proposing various analytical models, a better description of the rheological characteristics such as material flow and mechanical strength allowed researchers for a better point of view of the challenges. Seemingly, the availability of released open-source software and hardware after the time in which Stratasys FDM/FFF patent was expired, shows the development of the researches. Besides the mentioned explanations, there are still many challenges in consideration of the role of optimization by taking into account the rheological characteristics in the matter of process optimizations. This approach along with in-process monitoring of various parameters, will help to reach the final goal which is the production of optimum-quality final parts. Considering the above-mentioned explanations, the following statements as prerequisites for optimization purposes could be highlighted:

- Interaction of parameters and their influences on temperature evolution of filaments.
- Temperature profile of filaments is an important matter and influences the bonding.
- Temperature dependence viscosity must be included.

In this study, based on the review of the literature, distinctive parameters that affect the part quality were chosen. The selected process parameters are the liquefier temperature, platform temperature, and print speed. This study differs from previous studies in the following ways:

- The interaction of crucial parameters such as liquefier temperature, platform temperature, and print speed (identified from the literature) on the mechanical properties have been considered.
- The heat transfer and temperature evolution of filaments during FDM/FFF process by proposing a new in-process monitoring of temperature measurement at the interface of adjacent filaments has been considered.
- A numerical approach using Finite Volume Method (FVM) has been employed for heat transfer modeling of temperature profile of filaments.
- Moreover, using the recorded temperature value, this study investigates the non-isotherm viscosity evolution of filaments.

This chapter talked about the FDM/FFF process with a brief introduction to the AM/RP technologies. For simplicity and a better understanding of the different existence features, it has been divided into sections and sub-sections. Section 1.1 presented an overview of AM processes, including the mechanisms involved in them. Section 1.2 gives a summary of FDM/FFF process by providing a brief history of developing 3D printing machines. Section 1.3 also gives a summary of applicable and the most common materials in FDM/FFF process with paying much attention to the PLA as the main material utilized in this study. Section 1.4 gives out the studies done so far toward investigating the influence of FDM/FFF parameters on mechanical performance and part quality. In detail, the complexity of this process and the involvement of various parameters have been indicated. The variety and a large number of parameters have made it difficult to understand the influence of mentioned parameters on the mechanical strength and particularly the adhesion of deposited filaments. An overview of the literature demonstrated that some of them play an important role in comparison with others, and thus the investigation and the role of those parameters on the mechanical strength are inevitable. The influence of three process parameters, liquefier temperature, platform temperature, and print speed, on the part quality during FDM/FFF process has been presented in section 1.5. It is believed that temperature plays an important

role in determination of the final characteristic of the 3D-printed parts in which the liquefier temperature and platform temperature have been selected to be considered separately. The print speed is also capable of controlling the cooling rate of the deposited layers and itself acts as a temperature controller. So, attempts have been made to understand the influence of process parameters on part quality. However, an overview of the literature indicates that the overall conclusions in each study differ from one another. This issue calls for a thorough investigation of the interaction of the process parameters. Section 1.6 highlights the heat transfer phenomenon and the influence of temperature evolution on the part quality which is the basis for the consideration of viscosity evolution and adhesion of filaments during deposition. In section 1.6 and 1.7, the overall researches performed during FDM/FFF process have been briefly presented by considering the experimental and numerical efforts.

This study focuses on the temperature evolution of filaments during deposition which acts as the main characteristic through the adhesion and bonding of adjacent filaments. It aims at considering the temperature profile of filaments and its effect on the part quality with consideration of the main process parameters as mentioned in previous sections. Moreover, this study takes into account the non-isotherm viscosity using the recorded temperature profile obtained by the proposed approach.

Chapter 2

Material and experimental procedure

2.1 Material

Commercially PLA filament, purchased from Fillamentum, with a diameter of 1.75 ± 1 mm has been implemented. By applying this filament and for various objectives classified in this study, different characterization methods have been used in order to correct the existed features in this process. Technical data sheet for this PLA filament is presented in Table 2.1 which has been adapted from the manufacturer datasheet.

Table 2.1: Technical data sheet for the purchased PLA filaments (Adapted from manufacturer).

Characteristics	Typical value	Test method	Test condition
Material density	1.24 g/cm ³		
Melt flow index	3 g/10 min	ISO 1133-A	190 °C, 2.16 Kg
Diameter tolerance	8 g/10 min	ISO 1133-A	210 °C, 2.16 Kg
Weight	750 g of filament		
Tensile strength	50 MPa	ISO 527-1	
Elongation at break	≤ 5%	ISO 527-1	
Tensile modulus	3500 MPa	ISO 527-1	
Glass transition temperature	55-60 °C	DSC	
Heat deflection temperature	55-60 °C	ISO 75-1	Amorphous
	100-110 °C	ISO 75-1	Crystalline
Print temperature	210-230 °C	Recommended settings	
Hot pad	50-60 °C		
Bed adhesive	Magigoo		

2.2 Methodology

2.2.1 Definition of the case study

According to the nature of FDM/FFF process, each deposition strongly has its own influence on different aspects of the constructed parts. This issue clearly means that the thermal, mechanical, and rheological characteristics of the final parts would be affected by different deposition mechanisms. As explained in section 1, there are various mechanisms of deposition based on the filling of layers namely counter fill, raster fill, counter and raster fill.

As stated by Agarwala et al. [104] from the very beginning, raster fill is the most useful deposition mechanism since it offers better movement in adjacent layers. However, deposited layers could be laid in different directions and consider this direction based on different raster angles (α) [105]. Figure 2.1 schematically indicates the various fulfill forms and possible mechanisms of deposition.

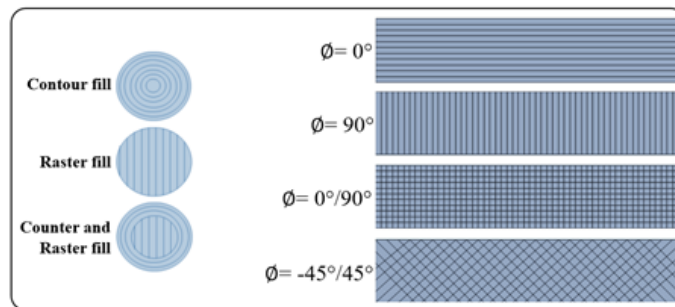


Figure 2.1: Top view of layer with different fullfills and raster angles

By defining the raster angle, as it is relative to the moving direction, it can vary layer by layer. So, filaments could be perpendicular to each other or having a unidirectional direction in which for the unidirectional mode, they could be deposited as skewed or aligned filaments (Figure 2.2). As the deposition mechanisms strongly affect the:

- Interdiffusion of adjacent filaments and thus bonding
- Quality and finish surface of the final part
- Mechanical strength of the final part,

It should be taken into account in different ways of analysis and characterization [106].

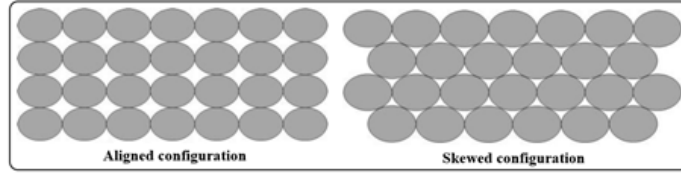


Figure 2.2: Different configuration for unidirectional filaments

In this study, an attempt has been made to design a test case that permits us to meet the requirements. As stated in section 1, a is filament faced with various heat transfer mechanisms due to the different heat sources during the construction. Consequently, the physical contacts resulting from the deposition mechanisms also play an important role in the way of characterization and analysis. So, a single deposition road has been modeled including the following characteristics (Figure 2.3):

- Homogeneous deposition of filaments on top of each other
- Unidirectional deposition of filaments (Consideration the time of deposition for each filament)
- Same convection of layers with the environment
- Same conduction between layers
- 1st layer: conduction with support (and with 2nd layer) simultaneously (for thermal characterization)
- 2nd, 3rd, ..., n^{th} layers: same conduction with each other's
- Symmetric effect of environment and platform temperature on the solidification of material while cooling down.

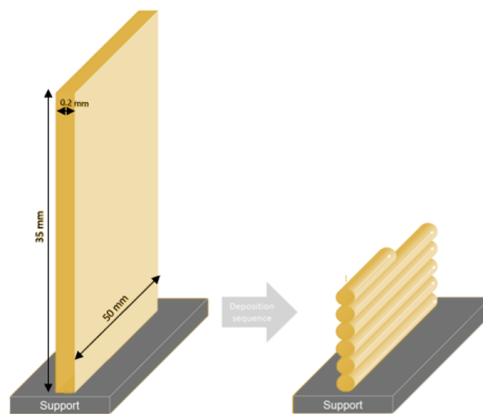


Figure 2.3: Schematic of the designed test case of the present thesis

2.2.2 Characterization methods and equipment layout

According to the objective of this study, several characterization methods should be considered and the effect of their interaction is inevitable. Given the common means of characterization, the implemented procedures have been classified into the following groups which have all been briefly presented in Figure 2.4.

Microstructure observation

A Scanning Electron Microscope (HITACHI4800 SEM) is used to qualitatively investigate the material structure and particularly the bonding of filaments, existence of voids in between the filaments/layers, and the dimensional accuracy of the fabricated parts. To evaluate the dimension variation, ImageJ software is also utilized on the recorded SEM images.

Thermal analysis

To measure the physicochemical characteristics of the employed material (spool material) and the material after printing, DSC was used. TA instrument Q1000 (New Castle, USA) is employed. Samples are cut from different parts of the printed material to be sealed in aluminum pans and heated from ambient temperature to a temperature 50 °C higher than the melting temperature of the material (as mentioned in the datasheet of the material with the heating rate of 10 °C/min. The aim is to determine the glass transition temperature, crystallization temperature, and melting temperature further with the crystallinity of the PLA. Following the explanation in the literature review section, the crystallinity of PLA is calculated using Equation 1.1 as explained in section 1.2.

Viscosity measurements

A rheometer MCR502 from Anton paar is used to determine the rheological characterization of the PLA filament. The experiments were operated under Nitrogen flow implementing a 25 mm diameter parallel plate configuration with PLA disks of approximately 1 mm thickness. Viscoelastic functions were determined in both Newtonian and Non-Newtonian zones at varying temperatures between 170°C to 240°C (Common temperature range in FDM/FFF).

To measure the main transition temperatures and the viscoelastic characteristics of the applied polymeric filaments, Dynamic Mechanical Analysis tests were performed using DMA

Q800 (from TA Company) under flexion mode from 30 °C to 120 °C at a temperature rate of 2 °C/min and frequencies of 0.1, 1, 5, 10, and 30 Hz. The rectangular sample with a dimension of 60*12 mm^2 was used.

Mechanical characterizations

- Quasi-static tensile test

Tensile test until failure is implemented using a INSTRON4301 machine. The specimen geometry used to cut samples from the printed vertical wall is based on the ISO-37 Sta. The loading velocity is fixed at 1 mm/min.

Also, to employ the explained procedure (using ISO-37 mold to cut samples from the vertical wall) the dog bone specimen based on ASTM D638 Type IV printed in specific conditions (based on the preliminary observations) to consider the effect of the most important parameters in the specimens directly by the 3D printing machine. This approach could be a confirmation to the underlying assumption that in the additively manufactured polymer being tested, the mechanical behavior in the incipient failure condition was markedly affected by the mechanism of layer-by-layer deposition.

- Fatigue test

Tension-tension fatigue test was carried out at different applied maximum stress on MTS830 Hydraulic fatigue machine using the same standard (ASTM D638 Type IV) on the printed dog bone samples. The minimum applied stress was chosen to be equal to 10% of the maximum applied stress, and the tests were conducted on different frequencies of 1, 10, and 80 Hz.

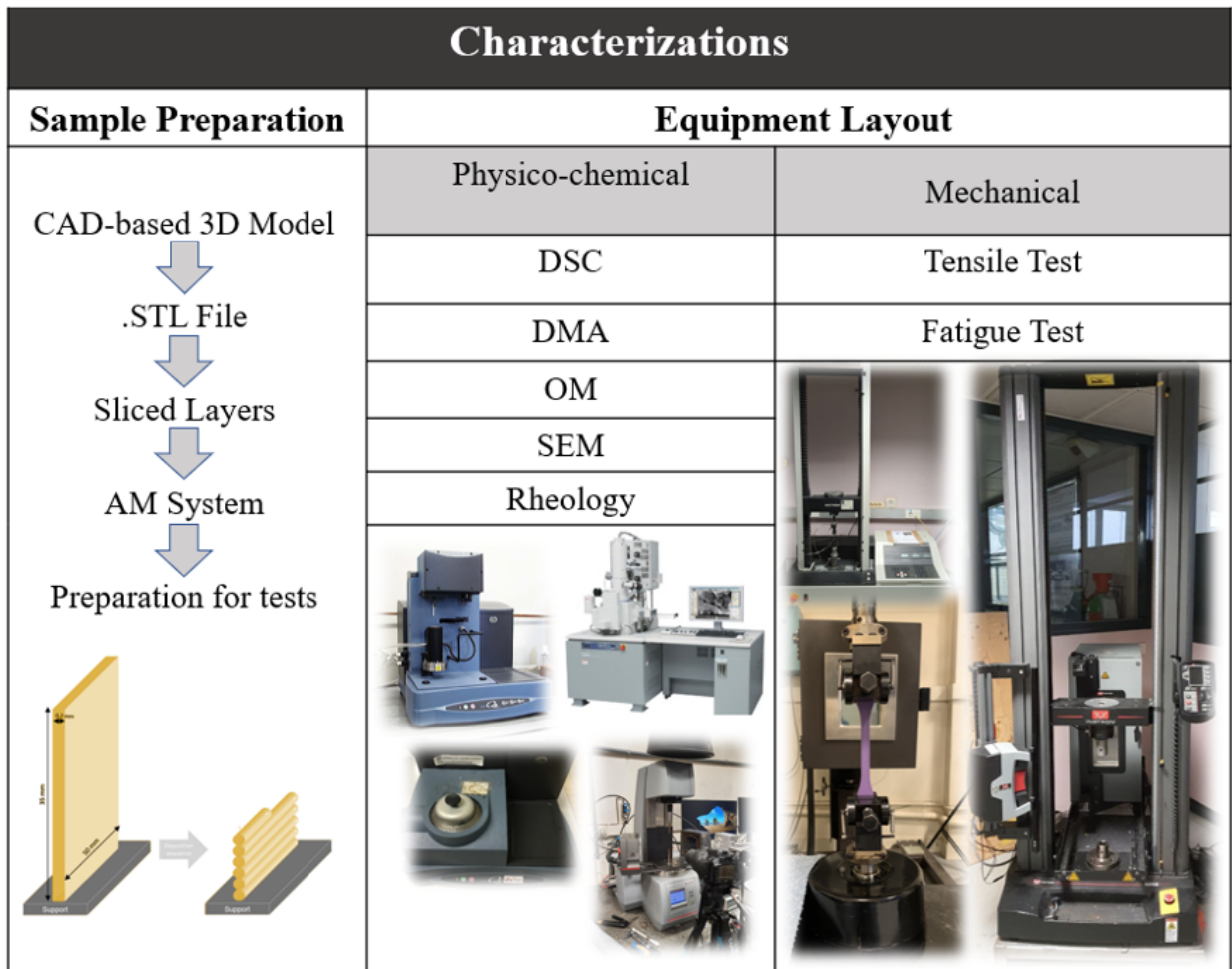


Figure 2.4: An overview on the experimental characterization methods

2.2.3 *in situ* monitoring of temperature profile of filaments

In FDM/FFF, the temperature evolution of deposited layers plays an important role in the mechanical performance and thus the quality of the final part. More precisely, the cooling and re-heating peaks that occur during the deposition of layers, are the critical points during fabrication of 3D-printed parts. The temperature history of the FDM/FFF parts is very important for understanding the adhesion between adjacent filaments [107, 108]. Furthermore, the thermal residual stress induced within the fabricated parts could affect their dimensional accuracy. Other issues such as distortion or part failure could also be resulted and affect the inter/intra layer delamination [109, 110].

Toward the scope of optimizing the FDM/FFF process, *in situ* monitoring (or real-time monitoring) of temperature evolution of filaments during deposition is an important issue for quality control purposes. Nevertheless, in the manner of experimental investigation, the circumstances that exist in this process make the integration of *in situ* recording tools a challenging issue for researchers. As regards the experimental implementation of *in situ*

temperature monitoring, In-situ temperature monitoring should be sufficiently precise and quick to track filament cooling and the re-heating peaks arising from contact between freshly and previously deposited filaments. In addition, it should be possible to apply the sensor locally without the requirement to pause the process. Despite the variety of works done by researchers all over the world, at present, the absence of a precise and quick technique is still a missing spot.

For that reason, an experimental set-up was used to perform the in situ and in real-time the temperature profiles during the filament deposition of a part. To record the temperature distribution of filaments during deposition, very small K-type thermocouples with a diameter of $d=80 \mu\text{m}$ were employed. Consequently, for temperature recording using the K-type thermocouples, a device was employed names *Datapaq* Tracker Telemetry System'. Indeed, this device uses as a temperature recorder during a fabrication technique: Rotational Molding process. Rotational molding is a process that involves a heated hollow mold filling with a charge or shot weight of material (normally in powder).

As shown in Figure 2.5, the *Datapaq* Tracker Telemetry System, connects remotely to the Rotational Molding machine (the LAB40 of shuttle type built by STP is available at PIMM laboratory), which includes several ports for adding K-type thermocouples and they are operated by its software.

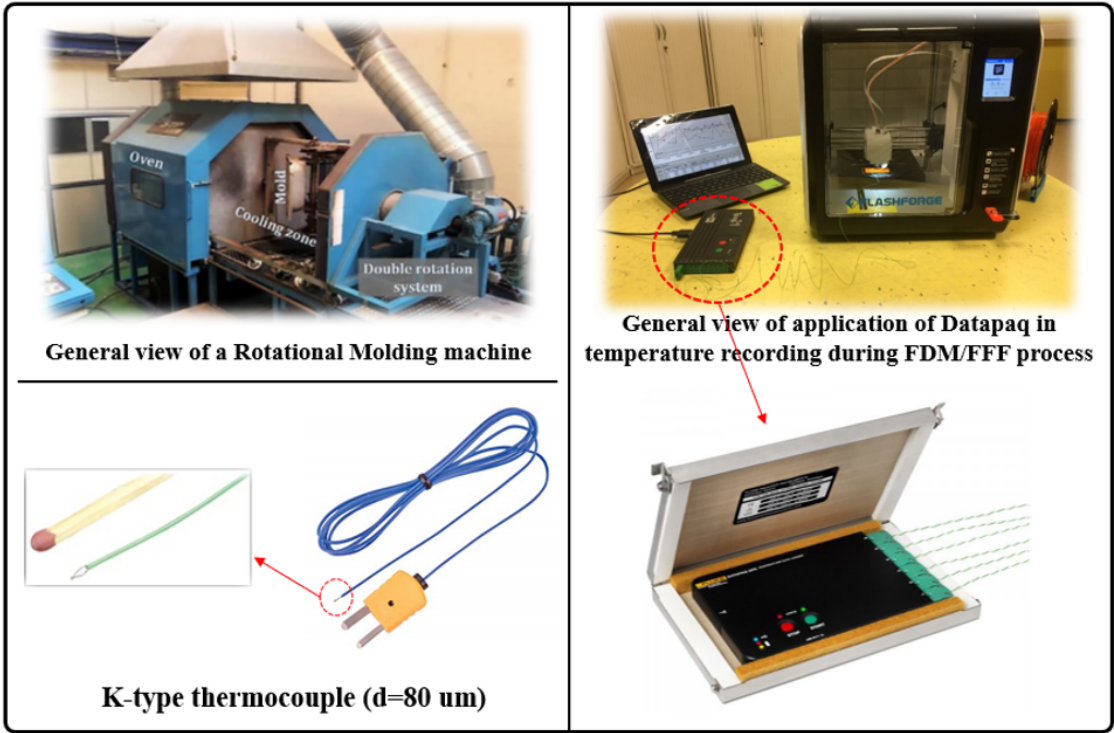


Figure 2.5: General view of the employment of *Datapaq*[®] Telemetry Tracking system from Rotational Molding to FDM/FFF process.

To reach our objective, the *Datapaq*[®] has been employed to perform the in situ temperature monitoring of filaments during deposition. Hence, the K-type thermocouples have been connected to *Datapaq*[®] to proceed with the temperature recording during filament deposition. Figure 2.6 illustrates schematically the employment of the mentioned device for conducting the proposed approach through the temperature recording of filaments during deposition. Using the designed test case, several efforts have been taken into account to place the thermocouples in different locations.

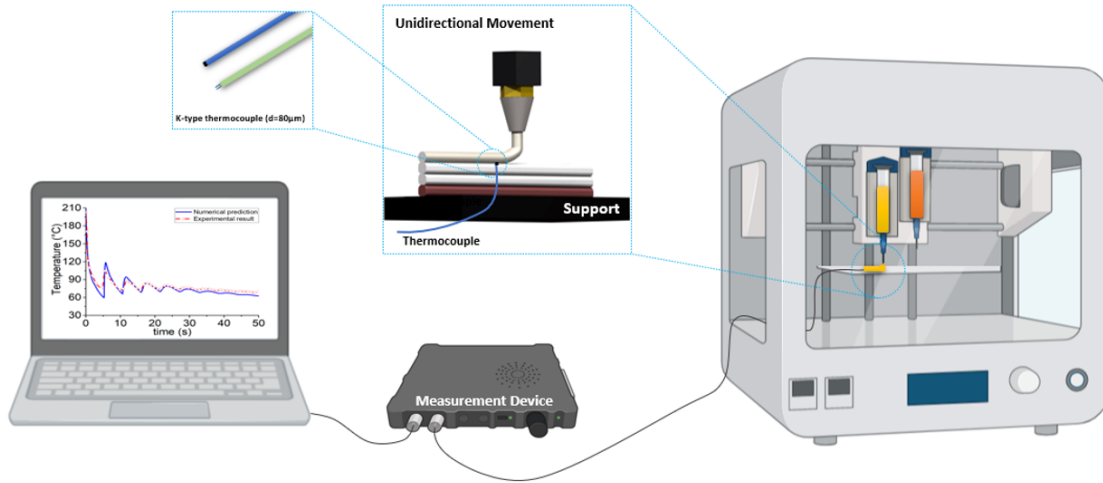


Figure 2.6: Set-up of in situ monitoring of temperature profile during the deposition stage.

By taking the advantage of the size of thermocouples, it is important to fix the head tip of them precisely at the interface of deposited layers. Due to the following reasons and statements:

- The movement of the liquefier and its distance from the previously deposited filament.
- The layer height of the deposited layer is too small (about 200 µm)
- The start of temperature recording is so important to be able to evaluate the first cooling curve and thus the successive cooling and re-heating curves.

the mentioned issue is crucial and it is necessary to be included in the in situ monitoring/recording of the temperature profile.

With refer to Figure 2.7, one can notice that the local temperature recording at the interface of adjacent filaments without pausing the process is a promising technique. As an example, the point number 1 shows the location of a thermocouple at the interface of layers

1 and 2 at a specific location. By placing the thermocouples, the software shows an increase in the temperature recording which refers to the temperature of the first layer. This means the thermocouple is under recording the temperature variation of the first layer that has already been deposited and that is under cooling (zone I). The sudden increase represents the temperature at the instance by which the second layer is deposited. It then starts cooling down representing the cooling of the second layer (zone II). It is noticeable that by assuming the same temperature gradient, the recorded temperature at the interface of both first and second layers represents their temperature variation as well. Before the deposition of the third layer, the same re-heating and sudden increase appear and then start cooling down and so on. Worth mentioning to say that the above explanations correspond to the recorded temperature evolution of the second layer by deposition of 3rd, 4th, 5th,

The presented curve (in Figure 2.7) not only shows the adhesion of filaments, but also represents the successive decrease in the temperature evolution of a layer even by deposition of younger filaments. The presence of peaks obviously indicates the adhesion of layers and their successive decrease shows that the successive layers (layers 3, 4, 5, 6, ...) are not sufficient to keep the temperature of the previously deposited layer (layer 1) hot enough.

This statement is the pre-requisite of the optimization purposes and adhesion improvement of successive layers by recognizing the temperature evolution at the interface of deposited layers. For this reason, efforts have been taken into account by considering the influence of the main process variables on the temperature evolution of filaments. Also, by implementing several thermocouples at the same time, the temperature evolution has been recorded at different locations from the start of deposition.

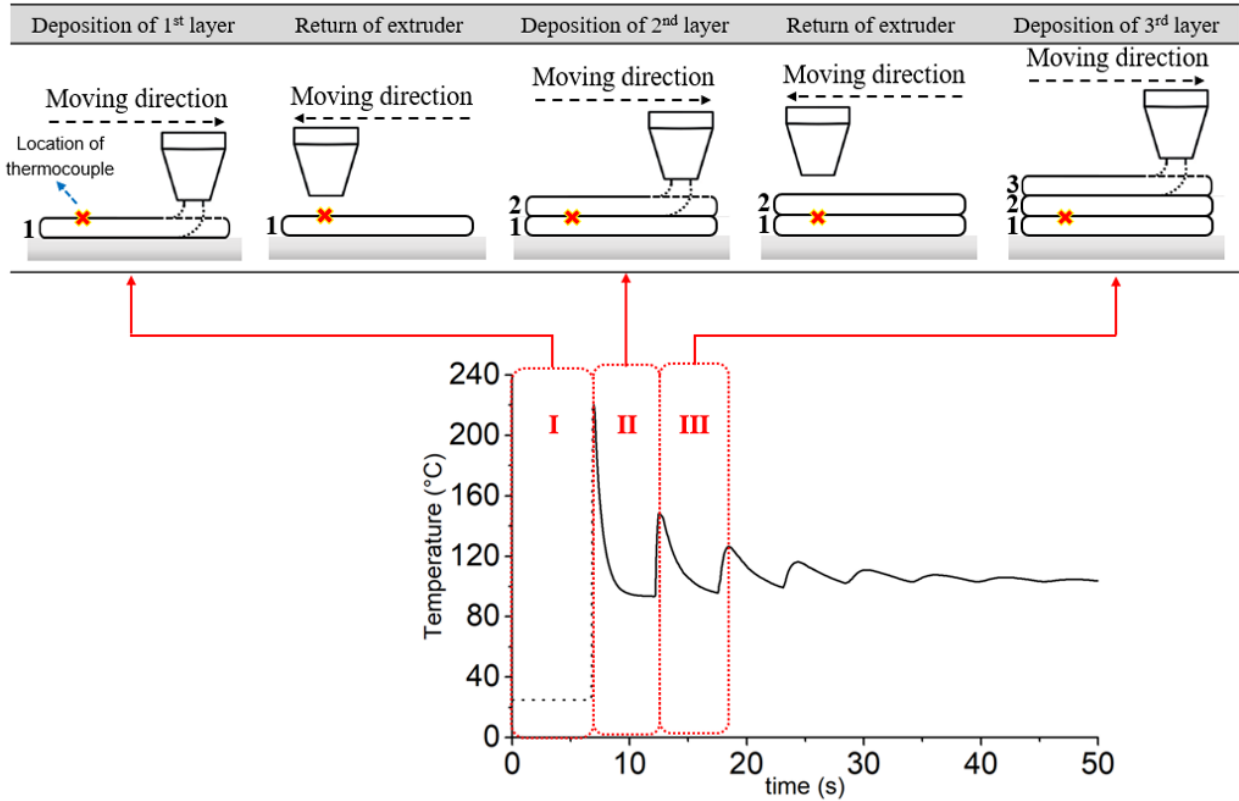


Figure 2.7: Temperature evolution of second layer (at a specific location) during deposition of the vertical wall consisting of single filaments deposited on top of each other.

The first step of this approach was resulted in a paper that has been published by Kallel et al in 2017 [111]. Adding thermocouples to the build simultaneously with the fabrication, they indicated that it is possible to measure locally the temperature variation without damaging or pausing the process. Although a drop of approximately 50 °C was observed on the recorded experimental data, the preliminary results open a new way and let us to continue the work to have more precise and considerable results.

Furthermore, parallel to the main objective of the work on local in situ recording of temperature profile, efforts have been made to employ global in situ recording of the temperature profile. The aim is to show the usefulness of the proposed approach (employing K-type thermocouples) and the importance of the temperature evolution at the interface of adjacent filaments. As discussed in previous sections, almost all researchers have focused on using IR-camera. Although it seems it is an easier approach, due to the following reasons and statements, it is not as useful as employing the thermocouples:

- Recording the temperature on the external surfaces of the deposited layers.
- Depending on the type of the camera, the precision varies.

- The influence of other phenomena such as radiation distributed from the platform or other layers is inevitable.

Hence, an Optris IR-camera was employed to show the difference between the proposed approach and common techniques (in this case: the IR-camera) that are popular. However, it is noticeable that both approaches, local and global in situ temperature recording during filament deposition, have been applied simultaneously. This means that at the same location that thermocouples are placed, the data have been extracted from the recorded temperature profile by IR-camera. As shown in Figure 2.8, the presented schematic contains the set-up for in situ monitoring of temperature profile and the assembly of two methods together with the following details: the thermogram of the printed wall with corresponding layers and locations highlighted for temperature profile.

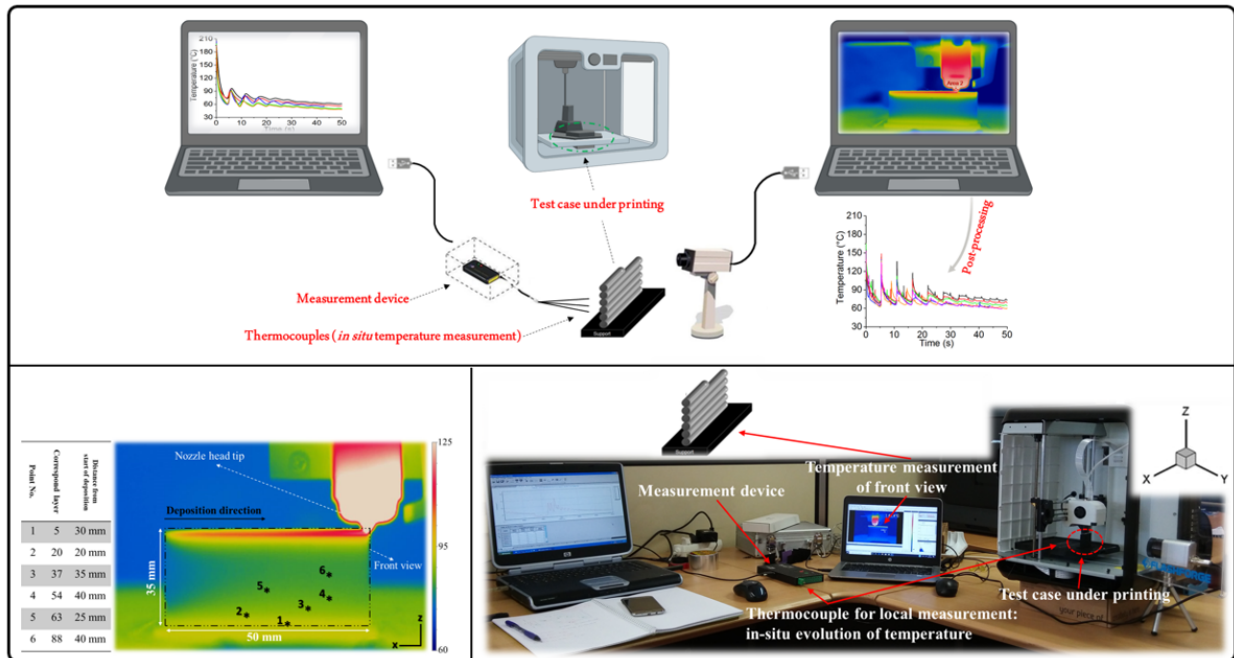


Figure 2.8: Representation of local and global in situ measurement of temperature profile using K-type thermocouples and IR-camera simultaneously

In parallel to the deposition and temperature recording using K-type thermocouples, an Optris PI450 infrared camera was used with the technical data presented in Table 2.2. Material emissivity (ϵ) is obtained by calibrating the absolute difference of the tracks obtained by IR-Camera and a thermocouple. The camera is placed at a specific distance from the liquefier to have the plain field of view (FOV) of all the deposited layers while the camera is inspecting x-z planes. So, the IR-Camera records the temporal temperature variations in the object front plane.

Table 2.2: Technical data of Optris PI 450 Camera.

Technical data	Value
Wavelength range (μm)	8-14
Frequency (Hz)	32
Frame rate (Hz)	80
Optical resolution (pixels)	382*288
Material emissivity	0.89
Accuracy (%)	± 2

Chapter 3

Influence of process parameters

3.1 Initial characterization and definition of conditions

This section presents the results and discussion of the experiments implemented in this study considering the influence of the major process parameters. Influence of variation of the main process parameters has been experimentally investigated to recognize the various characteristics of 3D-printed parts as a function of process parameters. Furthermore, to be capable of reaching the analytical modeling of temperature profile, the influence of process parameters has been experimentally recorded to observe their impact on the cooling stage and temperature evolution of filaments. The influence of liquefier temperature, platform temperature, and print speed has been taken into account by defining three conditions. The detail of each as well as the chosen value have been presented in Table 3.1. Worth mentioning to say that the named values have been considered based on the researches performed in literature. Also, to perform a comparison between the microstructure and deposition of filaments in different conditions, one has been marked as the reference.

Table 3.1: Representation of the groups of process parameters.

Condition No.	Liquefier Temperature (°C)	Support Temperature (°C)	Speed (mm/s)	Layer Height (mm)
1	200	50	20	0.2
	210			
	220			
	230			
2	210	50	20	0.2
		70		
		100		
3	210	50	20	0.2
			40	
			60	

Prior to the main objective of this step, initial characterizations consisting of thermal analysis of the spool material (using DSC test) and its mechanical behavior (using tensile test) have been performed. Figure 3.1 shows the DSC curve and tensile behavior of the as-received PLA filaments. From Figure 3.1(a), it has been observed that the crystallization temperature and melting temperatures are $T_c=99$ °C and $T_m=153$ °C, respectively. Recognizing these values is crucial and it is important to be taken into account for studying the heat transfer of the filament during deposition. As a crystalline material, a strategic zone for PLA is the zone between material crystallization and its melting point and it is important to recognize their variation. Besides, the tensile test performed on the as-received (spool material) PLA filament shows a ductile behavior with a failure strain around 9.5% and ultimate strength around 40 MPa (See Figure 3.1(b)).

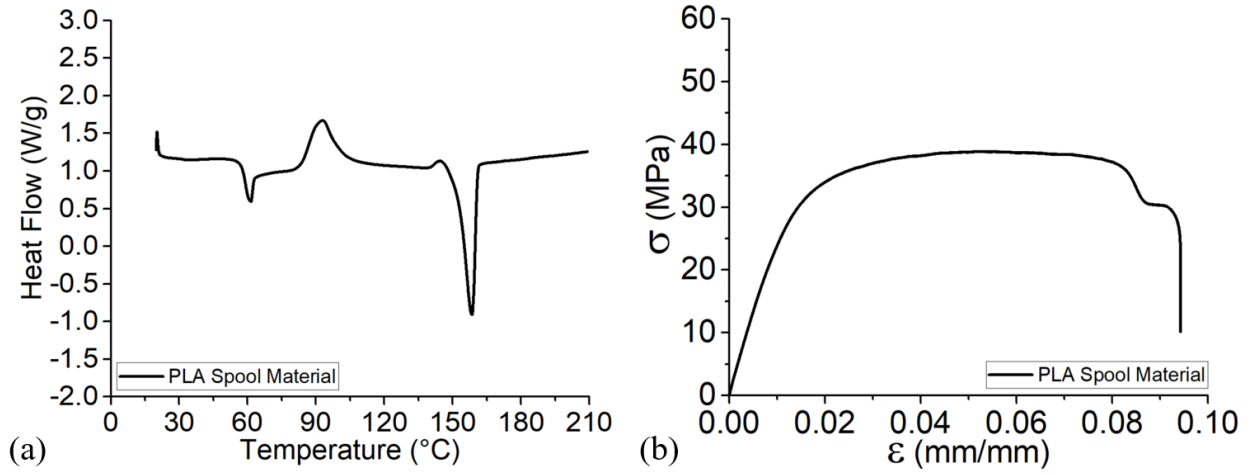


Figure 3.1: Initial characterization of the PLA spool materials: a) DSC results, b) Tensile behavior.

3.2 Liquefier temperature

3.2.1 Physico-chemical and mechanical characterizations

The influence of liquefier temperature (T_{Liq}) was investigated assuming four values, $T_{Liq}=200\text{ }^{\circ}\text{C}$, $T_{Liq}=210\text{ }^{\circ}\text{C}$, $T_{Liq}=220\text{ }^{\circ}\text{C}$, and $T_{Liq}=230\text{ }^{\circ}\text{C}$, corresponding to approximately a difference of 5% between them. In Figure 3.2 and 3.3, the DSC results and stress-strain curve are shown, respectively. The obtained curve from DSC test of the printed samples at different liquefier temperature obviously presents the variation of heat flow and thus the different characteristics of the material (Figure 3.2). Despite the negligible variation of glass transition temperature (T_g), there is almost $\pm 1\text{ }^{\circ}\text{C}$ variation in crystallization temperature (T_c). The data collected in Table 3.2 show the crystallinity in each condition obtained by Equation 2.1 Concerning the degree of crystallinity of PLA from literature, 2% variation in different conditions indicates that the liquefier temperature has an effective impact on the degree of crystallinity and thus the bonding of adjacent filaments. This issue could be correlated to the mechanical behavior of the samples cut from the printed vertical wall as described in previous section.

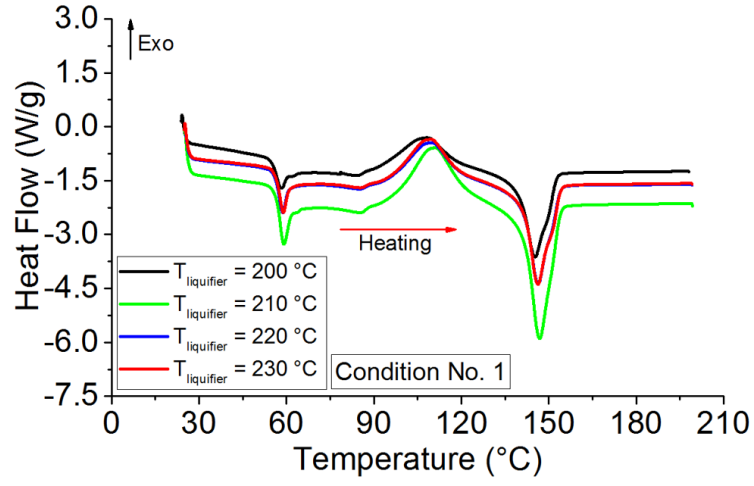


Figure 3.2: DSC results for samples printed at various liquefier temperatures.

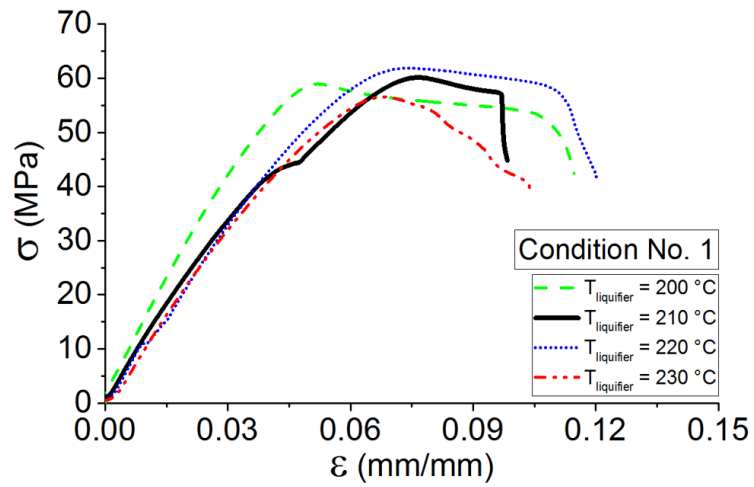


Figure 3.3: Tensile behavior for samples printed at various liquefier temperatures.

The accompanying graphs in Figure 3.3 show that the ultimate strength slightly increased as the crystallinity enhanced, whereas the ductility decreased. One can note that $T_{Liq} = 220$ °C is the best temperature value for liquefier, however, Young's modulus and its periodic variation demonstrates that there is not a specific direct relation between them.

Table 3.2: Values of different properties obtained from DSC, DMA and tensile results for samples printed at various liquefier temperature.

Conditions	T_g (°C)	T_c (°C)	T_m (°C)	%crystallinity	σ_{max} (MPa)	E (GPa)
TLiquefier = 200 °C	62.3	108.4	140.5	6.72	59 ± 2	1.8 ± 0.1
TLiquefier = 210 °C	62.2	109.7	146.9	5.12	60 ± 1.5	1.2 ± 0.1
TLiquefier = 220 °C	62	108.4	146.3	7.25	62 ± 2	1.4 ± 0.1
TLiquefier = 230 °C	62	107.8	146.4	6.83	57 ± 1.5	1.1 ± 0.1

Given the above-mentioned results and following the performed discussion on the mechanical behavior of the printed samples, the overall conclusion could be taken into account

so far as:

- Influence of liquefier temperature on Young's modulus is limited. It roughly changed from 1.8 GPa to 1.1 GPa (by increasing the T_{Liq} from 200 °C to 230 °C), while it abruptly increases ($E= 1.4$ GPa) at $T_{Liq}= 220$ °C.
- Similarly, ultimate strength varies as Young's modulus.
- Failure strain periodically changes by the increase in T_{Liq} .

In addition, efforts have been taken into account to investigate the influence of liquefier temperature (condition No. 1 for $T_{Liq}= 210, 220,$ and 230 °C) on the tensile behavior and life cycle of the 3D-printed samples by performing fatigue test as well as analyzing the accumulated damage on them. According to the defined condition on the samples cut from the vertical wall printed at different liquefier temperatures, samples were printed directly using ASTM D638 type IV standard. To have a clearer precision on the characterization of the printed samples, tensile tests were applied at least 5 times on the samples per each condition. Figure 3.4 presents the tensile behavior for the set of five specimens assessed according to condition No.1 ($T_{Liq}= 210$ °C). One explanation might be the fact that rupture occurred at the center of the specimens (activate zone of tensile loading). Another convincing point was the repeatability of the set of specimens by the occurrence of rupture at the center of them as well as the fact that the failure mode was due to the material departure in a plane almost normal to the tensile stress (**Article No. 1**).

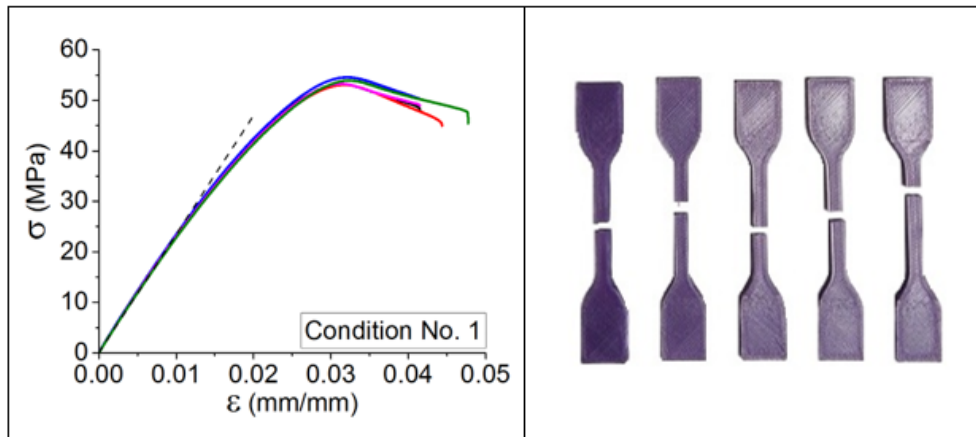


Figure 3.4: Tensile behavior for the set of five sample according to the condition No. 1 at $T_{Liq}= 210$ °C.

Given the above-mentioned results and following the discussion performed on the mechanical behavior, tensile tests have been realized to illustrate the influence of liquefier tem-

perature on the tensile behavior. The graph presented in Figure 3.5 and data collected in Table 3.3, clearly display and compare the overall results as follows:

- Influence of the liquefier temperature on Young's modulus is limited. It roughly changed from 2.3 GPa to 2.5 GPa as it increased from 210 °C to 220 °C.
- By variation of T_{Liq} from 220 °C to 230 °C, a sudden drop observed below that of the $T_{Liq}= 210$ °C.
- Failure stress changed periodically from 52 MPa to 53 MPa and then 47 MPa by the increase in T_{Liq} .
- Failure strain stayed around 3.5% as the T_{Liq} decreased from 230 °C to 220 °C, at $T_{Liq}= 210$ °C.

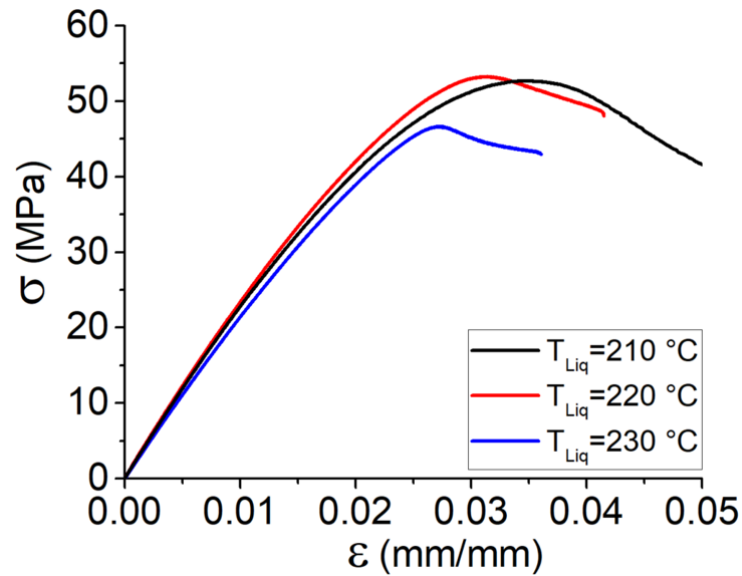


Figure 3.5: Tensile behavior of printed PLA samples from condition No. 1 at different liquefier temperature.

Table 3.3: Results of tensile behavior of printed PLA samples from condition No. 1 to 3.

Samples	E (GPa)	σ_{max} (MPa)	ϵ at σ_{max} (%)
Condition No. 1 (TLiq = 210 °C)	2.3 ± 0.1	52 ± 2	3.5 ± 0.3
Condition No. 1 (TLiq = 220 °C)	2.5 ± 0.1	53 ± 1.5	3.5 ± 0.2
Condition No. 1 (TLiq = 230 °C)	2.2 ± 0.1	47 ± 2	2.7 ± 0.2

Experimental stress-strain curves for quasi-static tensile tests coupled with microstructure observations are shown in Figure 3.6. The same representative observation zone was microscopically analyzed at consecutive increasing value of applied stress level. The local

investigation was assumed as a statistical representation of the damage accumulation in the studied material. Furthermore, microscopic observations have confirmed that this zone is statistically representative of the damage accumulation. The first observed damage phenomenon corresponds to the inter-layer failure of the filament interface at the stress value of 40 MPa. This phenomenon is the predominant damage mechanism for quasi-static loading.

Filaments oriented perpendicularly to the principal stress direction are submitted to a high local normal stress at the interface.

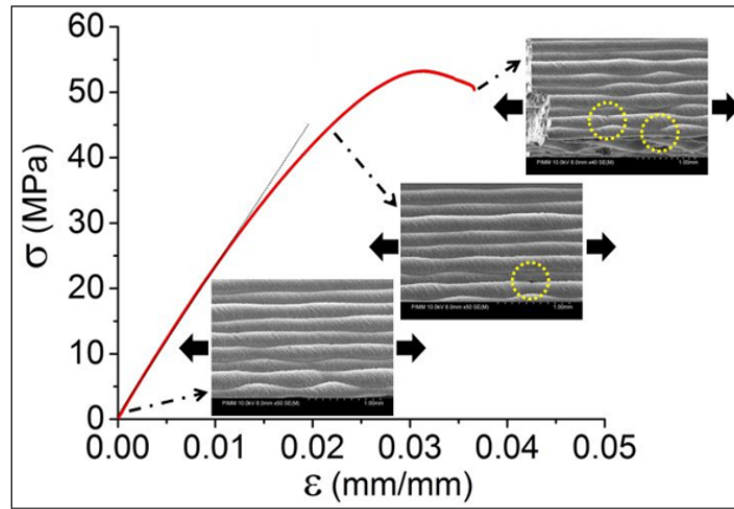


Figure 3.6: Damage mechanisms under quasi-static loading for the samples printed at $T_{Liq}=220\text{ }^{\circ}\text{C}$

To clarify the mentioned issue, a ‘quantitative multi-scale analysis’ of damage effect was performed in this section. At the macroscopic scale, the evolution of stiffness reduction is determined for PLA samples printed from condition No. 1 ($T_{Liq}=220\text{ }^{\circ}\text{C}$) under quasi-static loading. Stiffness reduction is an appropriate macroscopic damage indicator to express the damage development in materials. In the case of tensile loading, one can define a macroscopic damage variable as:

$$D = 1 - \frac{E_D}{E_0} \quad (3.1)$$

where E_0 and E_D are Young’s modulus of virgin and the damaged material, respectively. The graph shown in Figure 3.7(a) provides the evolution of the macroscopic damage parameter, D , under quasi-static loading-unloading tensile test as a function of applied stress. It should be indicated that for each microstructure, several tests (at least 3) were performed

and the results have been reported in this figure in such a way that at least 15 points have been measured until the very last stages just before failure. Figure 3.7(b) shows the damage threshold in the term of stress is almost about 35 MPa. Seemingly, an altered slope of the curve (from $D = 0.12$) signifies the saturation of the filaments interface failure occurring together, with the beginning of the propagation of transverse cracks.

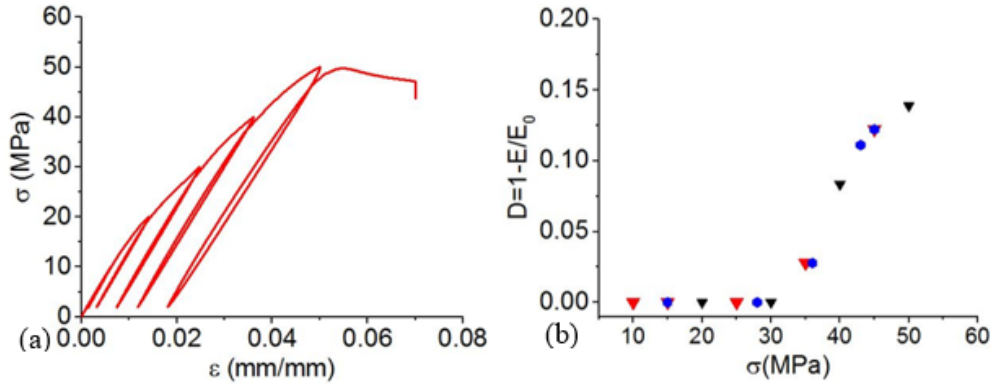


Figure 3.7: a) Applied stress for PLA printed from condition No. 2 and b) macroscopic damage evolution.

Figure 3.8 shows the Wöhler curve obtained in tension-tension fatigue tests for a frequency of 1 Hz. The diagram shows that for the three cases at high applied stresses, the same fatigue lifetime was observed. However, at low amplitudes, there is a significant difference in fatigue lifetime. In the case of samples printed at $T_{Liq} = 230$ °C, the fatigue lifetime is about 7×10^3 cycles for applied stress (30 MPa), while the fatigue lifetime is about 2×10^4 cycles for sample printed according to the condition with $T_{Liq} = 220$ °C. So, a variation of 10 °C on liquefier temperature leads to a fatigue lifetime three times greater. Figure 3.7 confirms that the samples printed according to the condition with $T_{Liq} = 220$ °C represented acceptable fatigue properties.

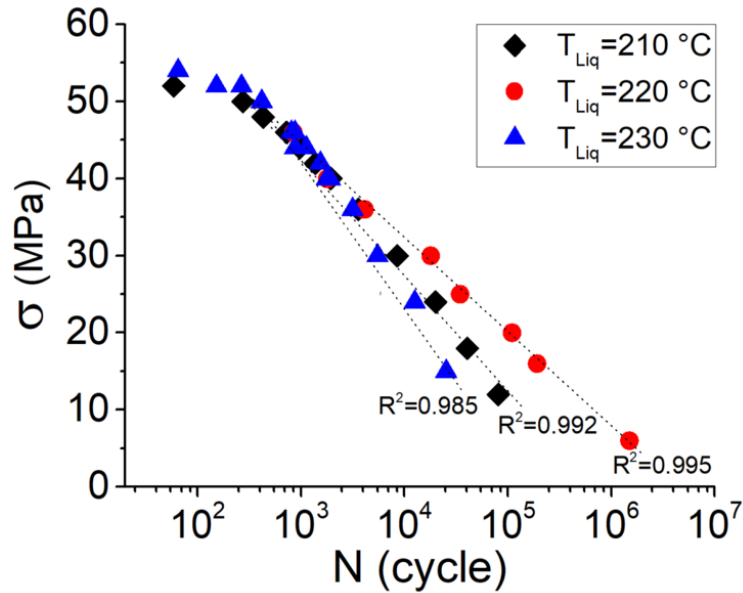


Figure 3.8: Wöhler curves for PLA printed at the three conditions mentioned in table 2 at 1 Hz

The evolution of the relative Young's modulus is followed to describe quantitatively the degree of fatigue damage. It may be used in a stiffness-based fatigue failure criterion. Figure 3.9 shows the evolution of the relative Young's modulus for two applied maximum stresses equal to 18 MPa and 46 MPa corresponding to low and high amplitudes, respectively. These results confirm that for three values of liquefier temperature, the same evolution of relative Young's modulus could be observed at high amplitudes (Figure 3.9(b)). It can confirm the same damage mechanism. Believable, the extruder temperature has no effect on the relative Young's modulus evolution while it can affect the fatigue lifetime (Figure 3.9(a)). In addition, the graph highlighted the fact that there is no significant damage at low amplitudes just before the failure of the samples while it is more significant at high fatigue amplitudes (**Article No. 5**).

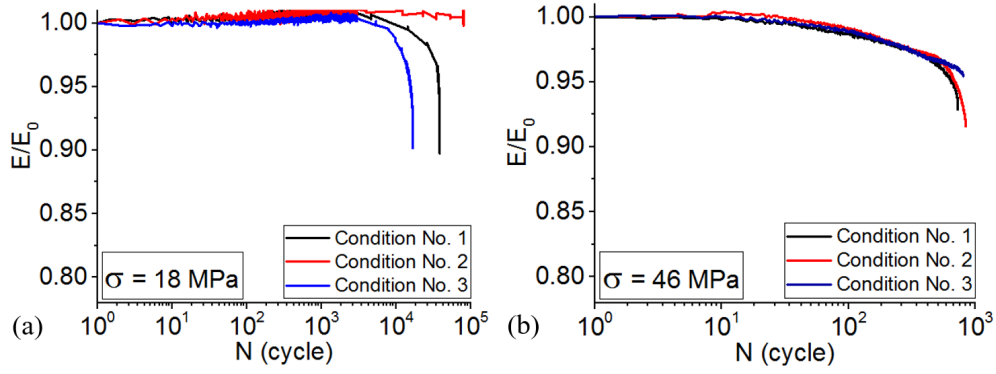


Figure 3.9: Evolutions of the relative Young's modulus (E/E_0) during fatigue tests of three conditions: (a) $\sigma_{max} = 18$ MPa and (b) $\sigma_{max} = 46$ MPa

3.2.2 Thermal characterization: *in situ* monitoring of temperature profile

Using local measurement, several experiments have been accomplished in order to record the filaments' temperature profile in different locations. The recorded temperature profile for the first filament in a sequence of deposition at a location of $x = 5$ mm from the start of deposition is indicated in Figure 3.10.

The test case was built considering the values for the processing variables as T_{Liq} : 210 °C, $T_{Platform} = 50$ °C, $V = 20$ mm/s, and $h = 0.2$ mm that are commonly used in the desktop 3D printer to ensure a good quality part in terms of mechanical strength according to literature. Points A, B, C, D, and E correspond to the deposition of the 2nd, 3rd, 4th, 5th and 6th filaments, respectively. These temperature peaks recorded by k-type thermocouple are described as following:

- **Peak 1:** re-heating of the first filament by deposition of 2nd filament
- **Peak 2:** re-heating of the first filament by deposition of 3rd filament
- **Peak 3:** re-heating of the first filament by deposition of 4th filament
- **Peak 4:** re-heating of the first filament by deposition of 5th filament
- **Peak 5:** re-heating of the first filament by deposition of 6th filament

Owing to the nature of the measurement approach and after the contact (by new deposition), the temperature of filament increases due to the heating provided by the contact (at the location of which the thermocouple was placed) with a hotter filament. From the presented curve in Figure 3.10, the following observations could be concluded so far:

- As a general observation, each filament faces a cyclic temperature evolution during its deposition
- At least, the first peak has a considerable impact on the temperature enhancement equal/above the crystallization temperature, T_c in the case of semi-crystalline material.
- Recognizing the temperature profile at the interface of adjacent filaments during the deposition stage is inevitable.

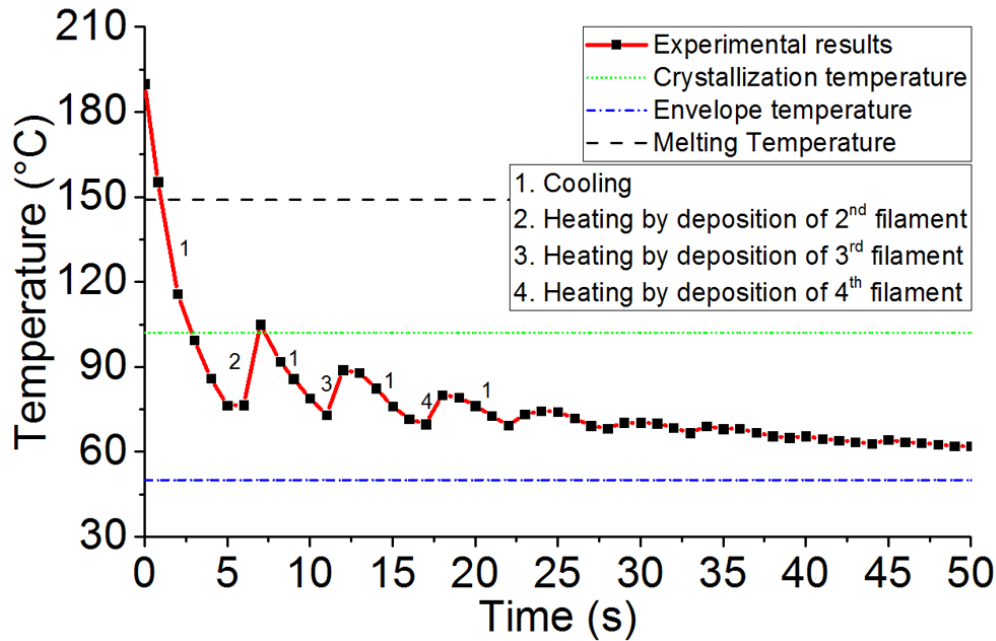


Figure 3.10: Temperature evolution during FFF process ($T_{Liq}= 210^{\circ}\text{C}$, $T_{Platform}= 50^{\circ}\text{C}$, $V = 20 \text{ mm/s}$, $h = 0.2 \text{ mm}$).

3.3 Platform temperature

3.3.1 Physico-chemical and mechanical characterizations

Studying the influence of platform temperature (also mentioning as support temperature), three values as $T_{Platform}= 50^{\circ}\text{C}$, $T_{Platform}= 70^{\circ}\text{C}$, and $T_{Platform}= 100^{\circ}\text{C}$ with a difference of approximately 40% between them. The DSC results and stress-strain curve are depicted in Figure 3.11 and Figure 3.12, respectively. Notably, the condition with $T_{Platform}= 100^{\circ}\text{C}$ resulted with the vertical wall printed in a deformed situation and thus it was not included in the analysis of results. Contrary to the previous condition (various liquefier temperatures), there is no obvious changing in the value of degree of crystallinity despite the

enormous variation of platform temperature (40%). However, the results from tensile test indicate an important issue.

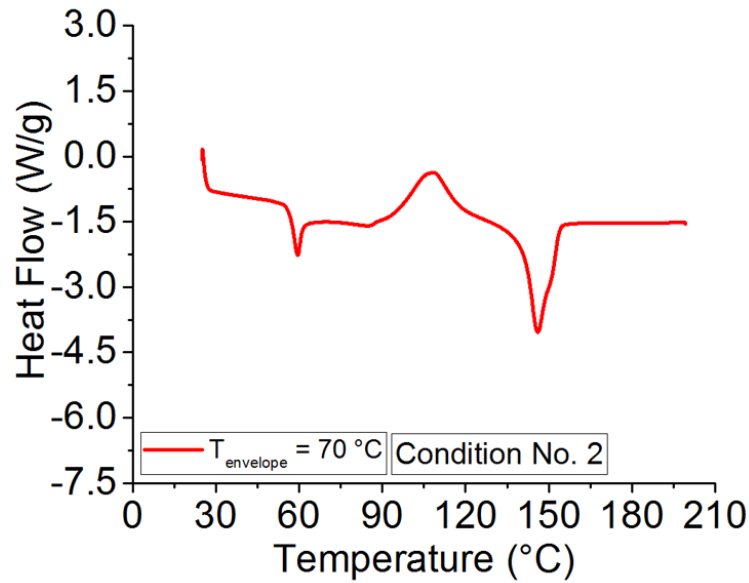


Figure 3.11: DSC results for samples printed at various platform temperatures.

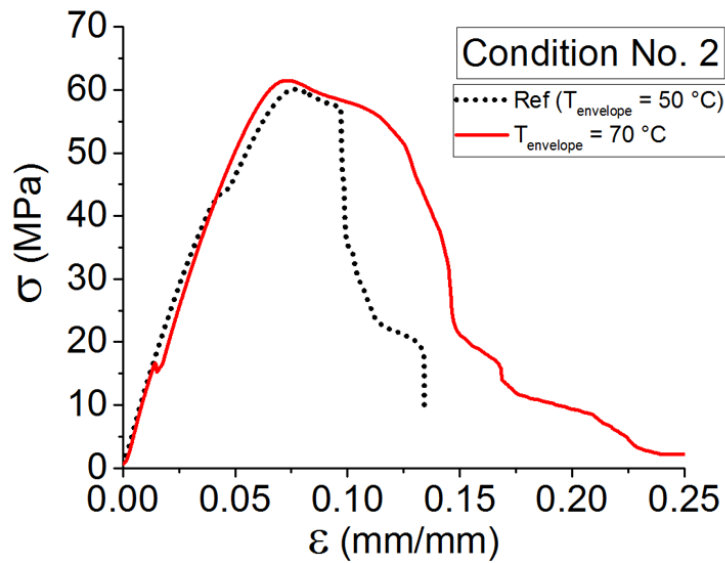


Figure 3.12: Tensile behavior for samples printed at various platform temperatures.

Although the data collected in Table 3.4 report a small change in Young's modulus as well as the ultimate strength, the failure strain shows that the increase in the platform temperature corresponds to a lower cooling rate that keeps the whole temperature higher than other conditions and this fact could let the material to have better bonding and increase the ductility of the printed samples.

Table 3.4: Value of different properties obtained from DSC, DMA and tensile results for samples printed at various platform temperatures.

Conditions	T _g (°C)	T _c (°C)	T _m (°C)	%crystallinity	σ_{max} (MPa)	E (GPa)
T _{supp} = 50 °C	62.2	109.7	146.9	5.12	60 ± 1.5	1.2 ± 0.1
T _{supp} = 70 °C	62	107.8	146.4	6.83	61.5 ± 2	1.3 ± 0.1

3.3.2 Thermal characterization: *in situ* monitoring of temperature profile

The study about the influence of platform temperature on the temperature evolution of filaments was performed at the same location and conditions of printing based on the previous condition. As expected, the lower the platform temperature the faster the cooling (Figure 3.13). For re-heating peaks, they have identical onsets, but the magnitude tends to decrease with increasing platform temperature. When it sets to 100 °C, the filament being monitored reheats repeatedly above its crystallization temperature (T_c), favoring bonding (**Article No. 3**).

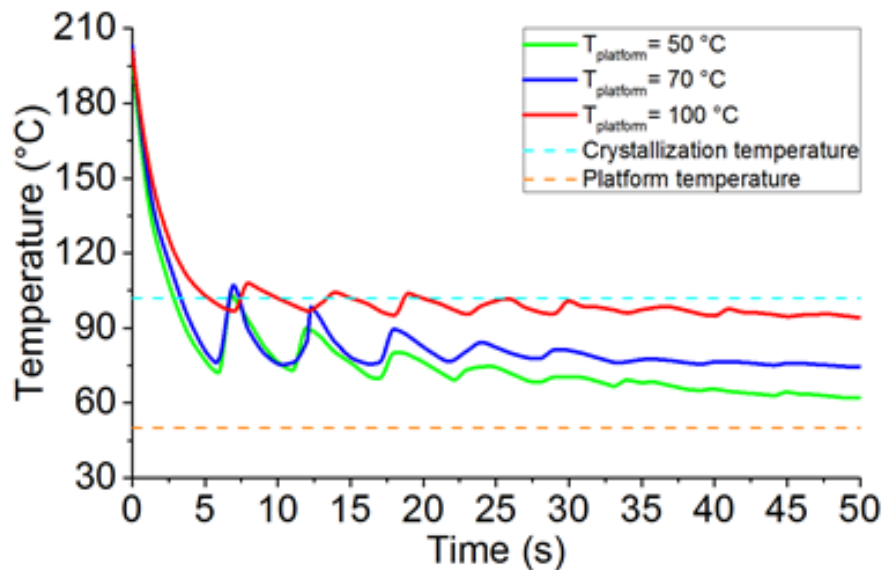


Figure 3.13: Temperature evolution for samples printed at various platform temperatures.

3.4 Print speed

3.4.1 Physico-chemical and mechanical characterizations

Three values were used to evaluate the influence of print speed: $V_{Liq} = 20$ mm/s, $V_{Liq} = 40$ mm/s, and $V_{Liq} = 60$ mm/s. The DSC results, stress-strain curve, and data collected from both characterizations have been presented in Figure 3.14, Figure 3.15, and Table 3.5, respectively. Seemingly, the higher the print speed the higher the degree of crystallinity. As discussed and due to the nature of PLA, almost 2% variation in degree of crystallinity should be taken into account.

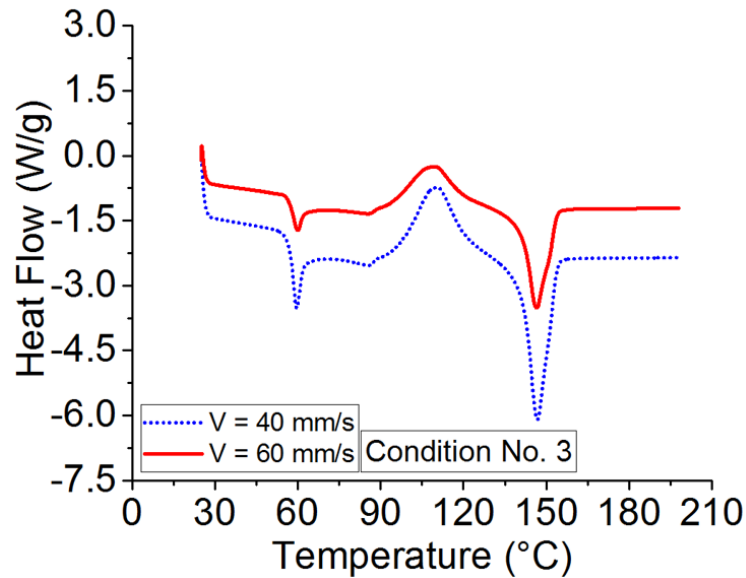


Figure 3.14: DSC results for samples printed at various print speed.

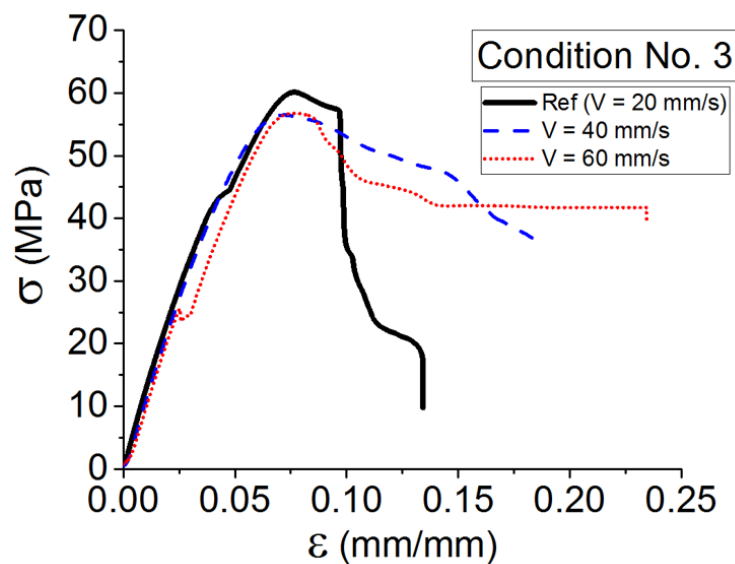


Figure 3.15: Tensile behavior for samples printed at various print speed.

Comparing the obtained degree of crystallinity with mechanical behavior of the printed

samples in different printing speeds, the higher crystallinity corresponds to the higher ductility, the lower Young's modulus, and ultimate strength.

Table 3.5: Value of different properties obtained from DSC, DMA and tensile results for samples printed at various printed speed.

Conditions	T _g (°C)	T _c (°C)	T _m (°C)	%crystallinity	σ_{max} (MPa)	E (GPa)
V = 20 mm/s	62.2	109.7	146.9	5.12	60 ± 1.5	1.2 ± 0.1
V = 40 mm/s	62	108.4	146.3	6.83	56.5 ± 2	1.1 ± 0.1
V = 60 mm/s	62	107.8	146.4	7.25	56.5 ± 2	1 ± 0.1

3.4.2 Thermal characterization: *in situ* monitoring of temperature profile

Considering the influence of print speed, Figure 3.16 shows the temperature profile of the filament at the same location and conditions of printing at three print speeds as stated. When the print speed increases, the rate of cooling decreases. As expected, the onset of the peaks occurs at different times and their breath is also altered. Finally, the magnitude of the peaks for the lowest print speed is higher, probably due to the higher difference between the temperatures of adjacent filaments.

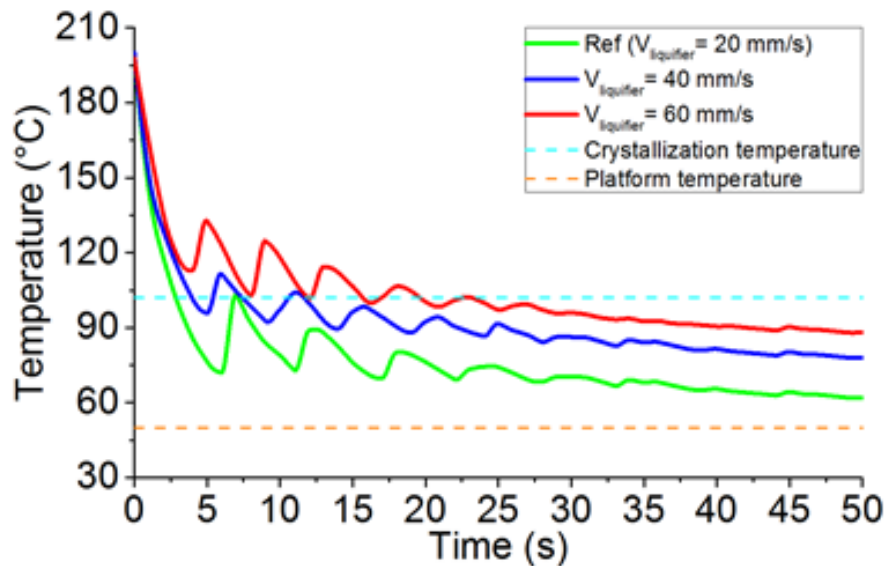


Figure 3.16: Temperature evolution for samples printed at various print speed.

3.5 Microstructure characterization: deposition sequence of filaments

Figure 3.17 shows the microstructure analysis of the printed part (10 deposited filaments) for this condition: $T_{Liq} = 210^{\circ}\text{C}$, $T_{Platform} = 50^{\circ}\text{C}$, $V = 20\text{ mm/s}$, and $h = 0.2\text{ mm}$. The aim is to show the contact surface of two adjacent filaments. Results show that as much as the distance from platform increases, the contact surface of two adjacent filaments decreases. Also based on the temperature evolution of filaments, one can observe that after two or three sequences of deposition, the temperature decreases below crystallization temperature. This fact contributes to the speed of cooling, solidification of material, lower material diffusion, and then decrease in the contact surface between two adjacent filaments.

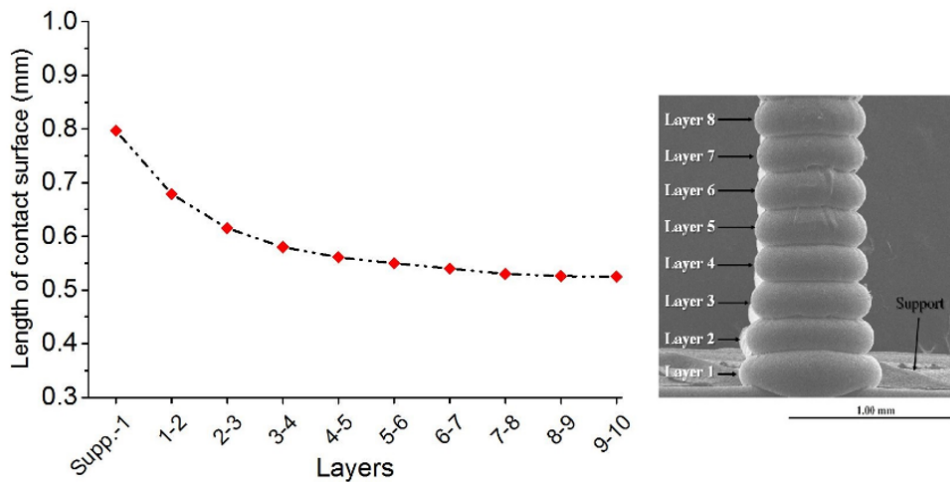


Figure 3.17: Analysis of the length of contact between two adjacent filaments (the reference sample).

This analysis was performed on the samples by applying the process parameters. Figure 3.18 indicates the microstructure analysis of condition No. 1 ($T_{Liq} = 230^{\circ}\text{C}$), condition No. 2 ($T_{Platform} = 70^{\circ}\text{C}$), and condition No. 3 ($V = 60\text{ mm/s}$). Each condition has its own influence on the quality and microstructure of the printed parts. One can note that in condition No. 2 ($T_{Platform} = 70^{\circ}\text{C}$) after almost 10 deposited layers, perhaps due to high temperature, layers slide on each other. However, in condition No. 1 ($T_{Liq} = 230^{\circ}\text{C}$) after 20 deposited layers, filaments remain in a good quality of printing as well as condition No. 3 ($V = 60\text{ mm/s}$).

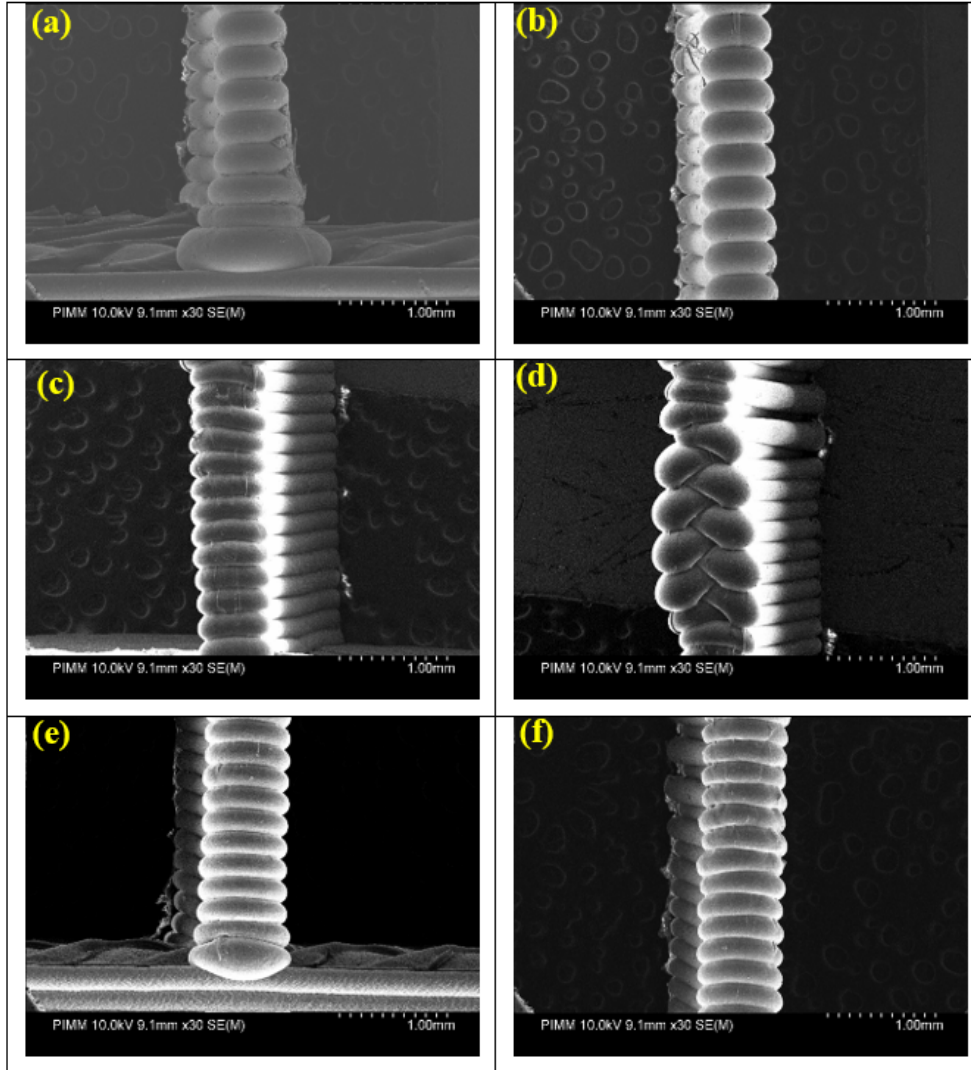


Figure 3.18: Consequence of deposited filaments in condition No. 1 ($T_{Liq} = 230^{\circ}\text{C}$) for (a) layers 1-8 and (b) layers 9-17, condition No. 2 ($T_{Platform} = 70^{\circ}\text{C}$) for (c) layers 1-12 and (d) layers 13-26, No. 3 ($V = 60 \text{ mm/s}$) for (e) layers 1-11 and (f) layers 12-24

Based on the SEM observations, the same analysis was performed on the deposit layers (Figure 4.19) and the percentages of the contact surface of each two adjacent filaments have been compared. This analysis is a useful summary of the influence of each process parameter. One can note that the influence of increasing the liquefier temperature is more significant in comparison with other process parameters. As seen, the higher liquefier temperature causes a higher contact surface between two adjacent filaments. However, the influence of print speed is more discussable based on the SEM micrograph performed on the sequence of layers. One can notice that the value of contact length between adjacent filaments is almost constant with increasing the print speed. Moreover, the quality of the printed part is better.

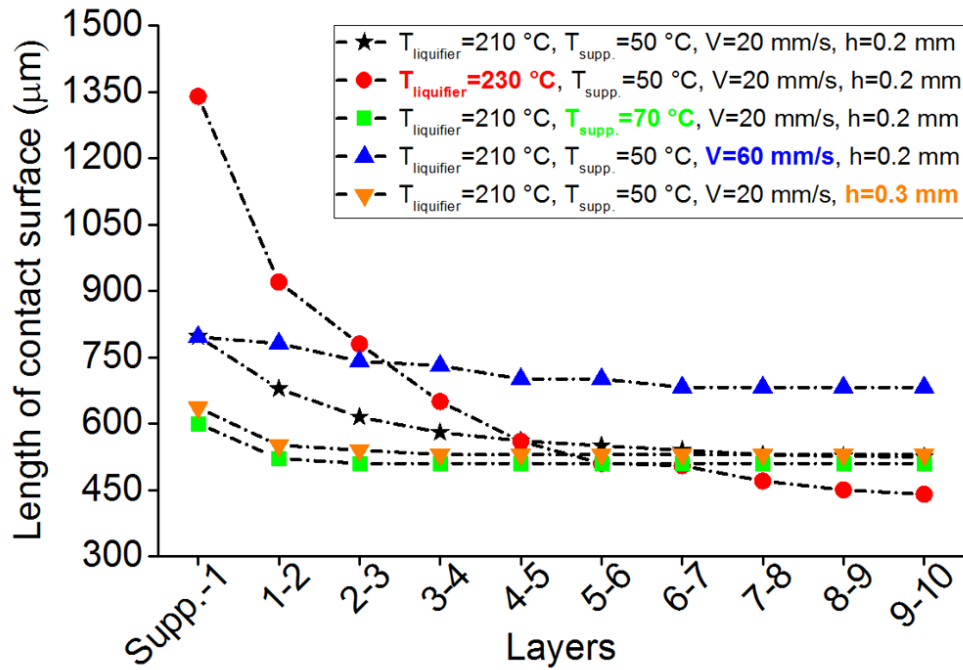


Figure 3.19: Analysis of the length of contact between two adjacent filaments.

3.6 Conclusion

This study allowed us to perform many conclusions so far:

- Interaction of parameters plays the most important role in consideration of mechanical characterization of printed parts.
- Young's modulus and failure strain could be an indicator to evaluate the mechanical performance of printed parts.
- Temperature of filaments plays an important role in the characteristics of printed parts.
- The consequence of deposition in different conditions shows that increasing the liquefier temperature is more significant on the contact of filaments, however, the impact of print speed is more considerable.
- The liquefier temperature and print speed have higher impact on the temperature evolution of filaments.

Chapter 4

Heat transfer modeling of FDM/FFF

Quality improvement of FDM/FFF parts demands significant research. In order to enhance the dimensional stability and mechanical properties of the final product, numerous studies with respect to analytical modeling and experimental assessments have been proposed and investigated. In this study, we have focused on two aspects: heat transfer and flowability; which altogether have to be taken into account for optimization purposes.

4.1 Modeling of filament cooling: validation of the measurement methodology

Heat transfer during deposition is complex, with contributions from radiation, convection, and conduction. However, it has been demonstrated that I) the heat losses by convection with the environment II) the thermal contacts with the support and with adjacent filaments are the main contributors to the filament temperature evolution [112]. A computer code that has been already developed, was applied assuming the gradual deposition of small axial filament segments, an analytical solution for the energy equation [79] whilst updating the local thermal conditions, and a healing criterion proposed by Yang & Pitchumani [113]. This gave rise to a useful tool that allows us to predict the temperature evolution and the degree of bonding between filaments for 3D parts including the usage of two distinct materials (e.g., the material of the part plus support material).

Figure 4.1 shows the evolution of the temperature of the filaments at specific instants upon building the first ten layers of a vertical wall. As in the experiments reported in this work, the liquefier deposits one filament, then stops and returns to the initial point to deposit

the next filament. Under these printing conditions, when a new filament is deposited, the previous one has already significantly cooled down. Nevertheless, the deposition of a new hot filament prompts the re-heating of filaments of the previous layers (as seen at 32.5 and 41.5 seconds), thus demonstrating the importance of considering the thermal contacts in the calculations (**Article No. 3**).

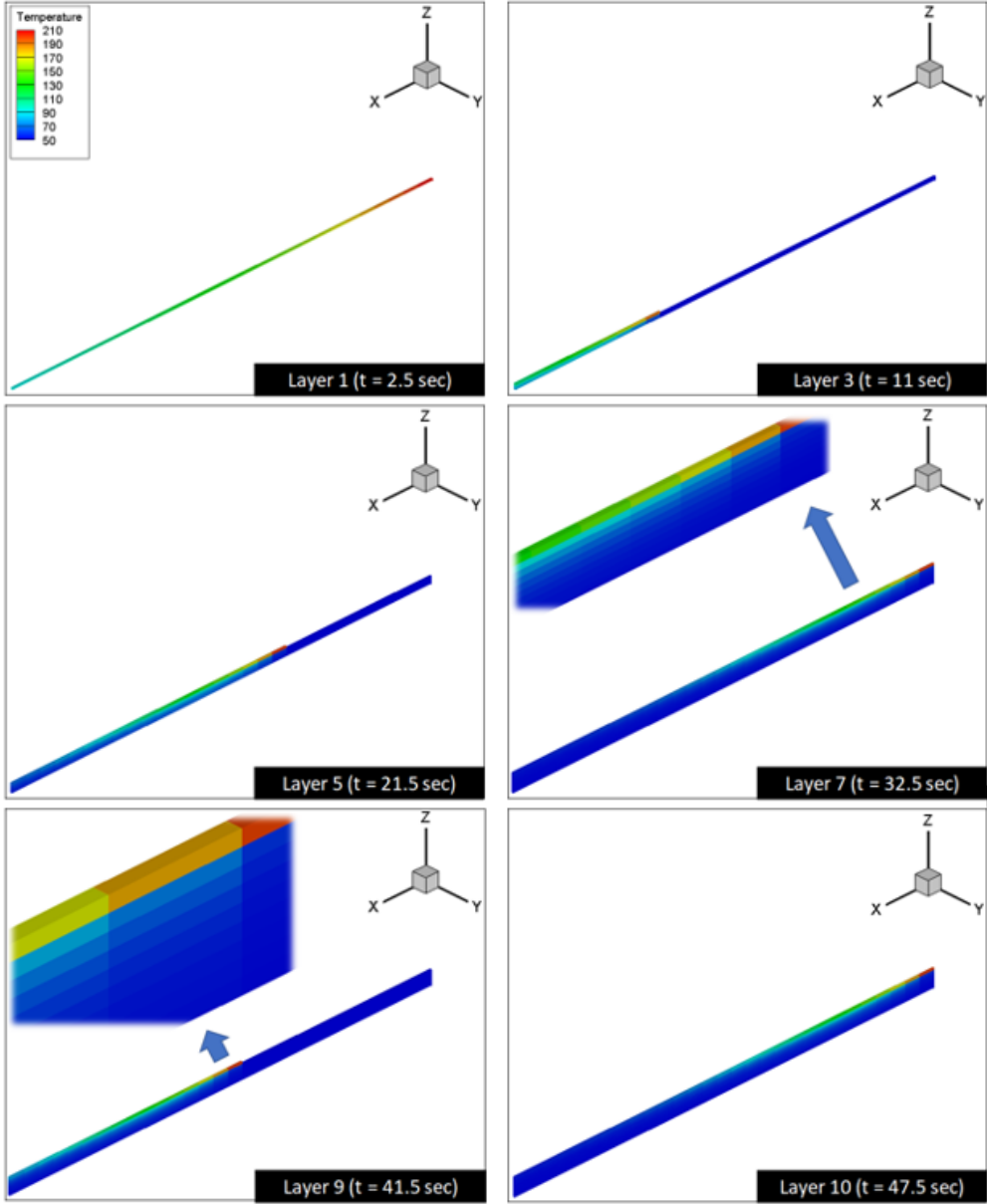


Figure 4.1: Temperatures of the ten first layers of the vertical wall at some instants of the deposition process.

4.1.1 Deposition of a single filament

The temperature evolution during the deposition of a single filament is presented in Figure 4.2 for the first deposited filament. Both experimental measurements and theoretical curves for

two values of the heat transfer coefficient are shown. Practice revealed that opening/closing the door of the environmental chamber to add/remove thermocouples would slightly disturb the platform temperature. This is why an interval in the range 50-60 °C (approximated using thermocouples to see the temperature variation of the platform) and not the value of 60 °C is shown in the mentioned figure (Figure 4.2). The value of 70 W/m².°C for the heat transfer coefficient (h_{conv}) is commonly used (for example, [114]). A value of 88 W/m².°C is obtained when using the Churchill correlation for the cooling down of a cylinder by natural convection [115]:

$$h_{conv} = \frac{Nu_d \cdot k}{d} \quad (4.1)$$

where d is the diameter (m), k is the thermal conductivity (W/m.°C), and Nu_d is the Nusselt number defined by:

$$Nu_d = \left\{ 0.6 + \frac{0.387 Ra_d^{1/6}}{\left[1 + \left(\frac{0.559}{Pr} \right)^{9/16} \right]^{8/27}} \right\}^2 \quad (4.2)$$

where the Rayleigh Rad number and Pr are expressed as:

$$\begin{cases} Ra_d = Gr_d Pr \\ Pr = \frac{v_k}{\alpha} \end{cases} \quad (4.3)$$

In the above expressions, v_k is the kinematic viscosity (m²/s), α is the thermal diffusivity (m²/s) and Gr_d is the Grashof number:

$$Gr_d = \frac{g \beta (T_s - T_E) d^3}{v_k^2} \quad (4.4)$$

Here g is the gravity acceleration (9.8 m/s²), β is the volumetric thermal expansion coefficient, T_s is the cylinder temperature (°C) and T_E is the environment temperature (°C).

Figure 4.2 shows a good agreement between the theoretical and the experimental values. The difference between the two sets of data occurs mostly between 3 and 8 s, when the predicted cooling rate is higher than the one measured. This is probably due to the fact that the theoretical model does not consider the change in state and crystalline growth, and thus forecasts faster cooling.

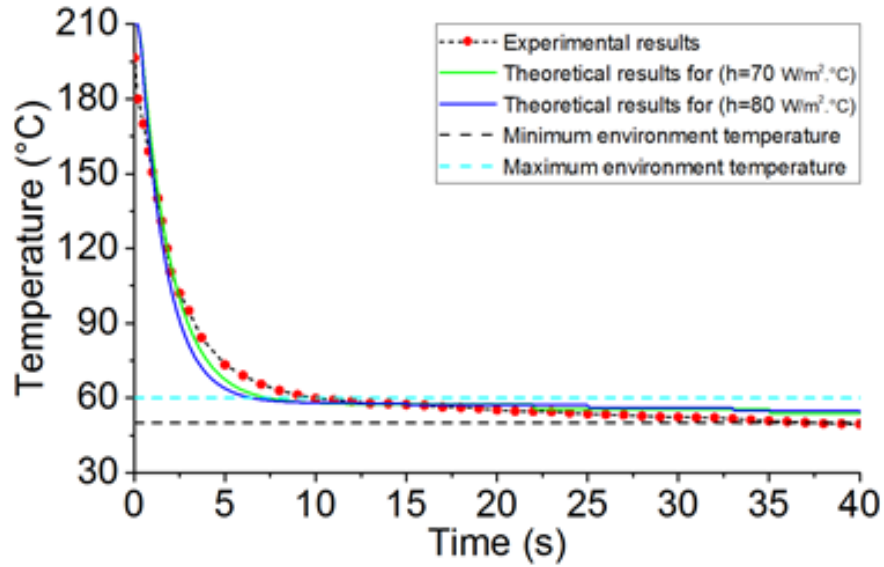


Figure 4.2: Experimental (± 2 °C) and theoretical temperature evolution during the deposition of a single filament (at $x = 5$ mm).

4.1.2 Deposition of the vertical wall

To show the usefulness of the applied experimental approach in temperature recording using K-type thermocouples, in parallel to the deposition and temperature recording, an Optris PI450 infrared camera was used (at the same points 1-6) with the technical data presented in Table 4.1. Material emissivity (ϵ) was obtained by calibrating the absolute difference of the tracks obtained by IR-camera and a thermocouple.

Table 4.1: Technical data of Optris PI 450 Camera.

Technical data	Value
Wavelength range (μm)	8-14
Frequency (Hz)	32
Frame rate (Hz)	80
Optical resolution (pixels)	382*288
Material emissivity	0.89
Accuracy (%)	± 2

The accompanying graphs presented in Figure 4.3 provide the experimental results (temperature profile) of both IR-camera and K-type thermocouple. They comprise six points in different locations (in different layers) of the sample. As described, the reported experiments are based on the layer-by-layer deposition of filaments. Under the 3D printing conditions, when a new filament is deposited, the previous one has significantly cooled down. Although there is a notable variance in starting point (when the filament exists from the Liquefier)

of deposition for each layer, the temperature evolves in the same cooling rate. For post processing, the two signals are synchronized at $t=0$, based on the instant of the first peak of temperature (the highest measured value considered as a value at $t=0$).

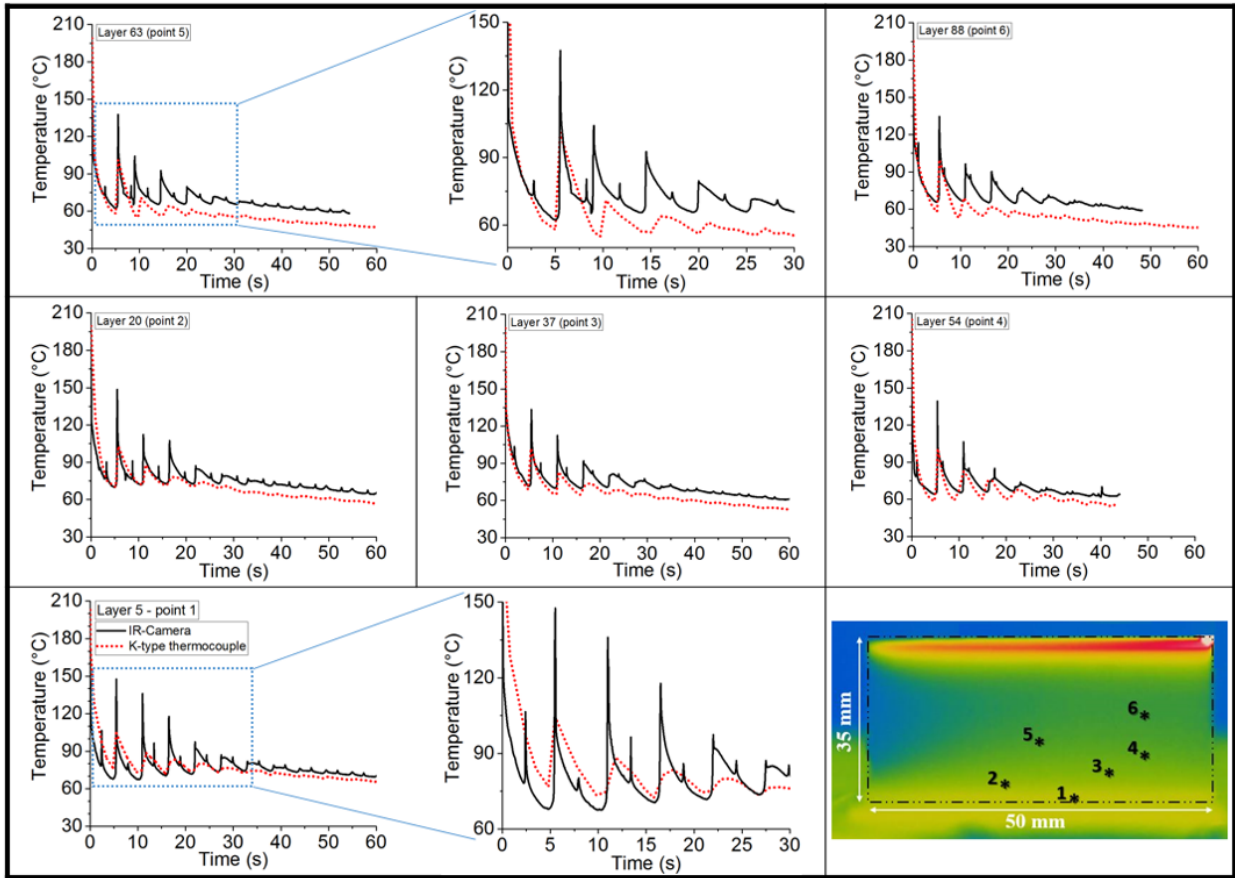


Figure 4.3: Temperature evolution at six locations during the deposition of a vertical wall consisting of single filaments deposited on top of each other. Point 1-6 correspond to the 5th, 20th, 37th, 54th, 63rd and 88th while indicating 30 mm, 20 mm, 35 mm, 40 mm, 25 mm and 40 mm from start of deposition, respectively.

Table 4.2 shows the ' $\Delta T = T_{IR-camera} - T_{Thermocouple}$ ' at each peak. Worth mentioning that based on described features such as support radiation, there is a small difference in correspond peaks at layers far from the Platform.

Table 4.2: Data collected from the difference in peak values (Calculated using ' $\Delta T = T_{IR-camera} - T_{Thermocouple}$ ' at each peak).

Layer	$\Delta T = T_{IR-camera} - T_{Thermocouple}$				
	1	2	3	4	5
5	44.9	31.5	34.2	21	18.4
20	43	29	26.8	18	15.1
37	37.3	27	21.2	15.8	13.2
54	36.5	25.3	13.7	12.1	9.9
63	33.5	24.3	11.1	10.8	9.6
88	33.2	21	8.1	5.8	3.6

The graphs in Figure 4.4 reveal the difference of upper-limit obtained by both methods as a function of building time. The specified contour for each layer expresses the nature of each measurement method. Apparently, temperature varies between T_c and T_m in first layers, whereas the contour drops below T_c as the distance from the platform is increasing. Their relative change is an important concern in the problem of inter-layers bonding and it should be taken into consideration (**Article No. 4**).

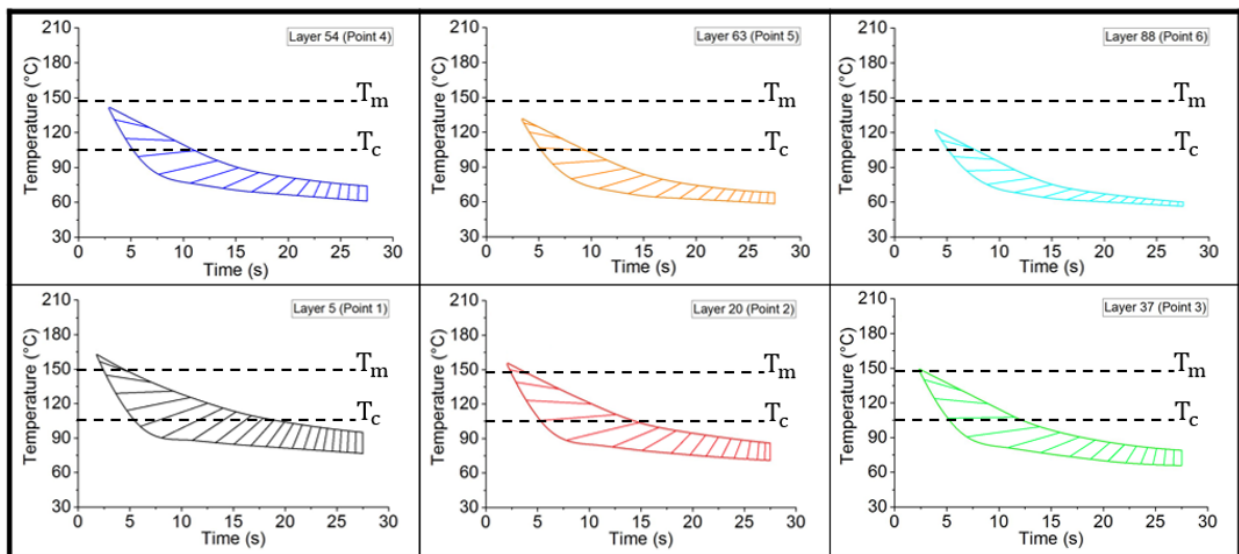


Figure 4.4: Temperature contour at six locations during the deposition of a vertical wall consisting of single filaments deposited on top of each other. Point 1-6 correspond to the 5th, 20th, 37th, 54th, 63rd and 88th while indicating 30 mm, 20 mm, 35 mm, 40 mm, 25 mm and 40 mm from start of deposition, respectively.

Figure 4.5 depicts the evolution of the temperature of the first filament (at a location distant 5 mm from the edge) during the building of a vertical wall consisting of single filaments deposited on top of each other. It is clear that the cooling of this first filament is significantly affected by the successive deposition of younger filaments, which may cause important re-heating. The numbers identify regions of the data (1: cooling of the first filament;

2-4: re-heating of the filament due to the deposition of filaments 2 to 4). The crystallization and platform temperatures are also identified.

For computational purposes, it is important to define the thermal contact conductance (h) between adjacent filaments. This is difficult, as it depends on pressure, surface roughness, and other conditions that are difficult to quantify. Apparently, there are no theoretical or empirical correlations providing an exact value for h . Using a value of $h = 800 \text{ W}/m^2 \cdot ^\circ\text{C}$, the magnitude of the experimental and theoretical re-heating peaks became virtually coincident.

Regardless of this approximation, the onset, relative magnitude, and breadth of the various temperature peaks are similarly captured by the two approaches. As expected, the peaks become gradually smaller with time, as the new filament being deposited is separated from the first filament by more filaments. As before, the predictions seem to overestimate the cooling rate, as no phase change and crystallization were built in the model. On the other hand, a delay in receiving the experimental data can exist and contribute to the differences.

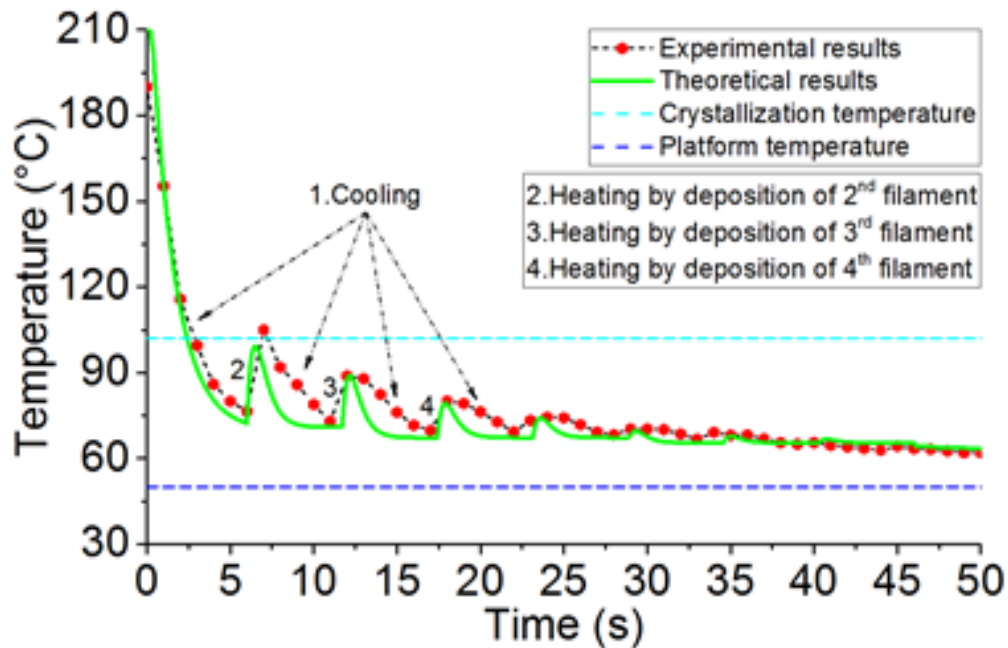


Figure 4.5: Experimental ($\pm 2 \text{ }^\circ\text{C}$) and theoretical temperature evolution during the deposition of a single filament (at $x = 5 \text{ mm}$).

4.1.3 Influence of process parameters

This section demonstrates the usefulness of the proposed in situ temperature measurement technique, by studying the influence of the platform temperature and deposition velocity on

the heat transfer during cooling (Figure 4.6). As expected, the lower the platform temperature the faster the cooling. As for the re-heating peaks, they have identical onsets, but the magnitude tends to decrease with increasing platform temperature. When the platform temperature is set to 100 °C, the filament being monitored re-heats repeatedly above its crystallization temperature, favoring bonding.

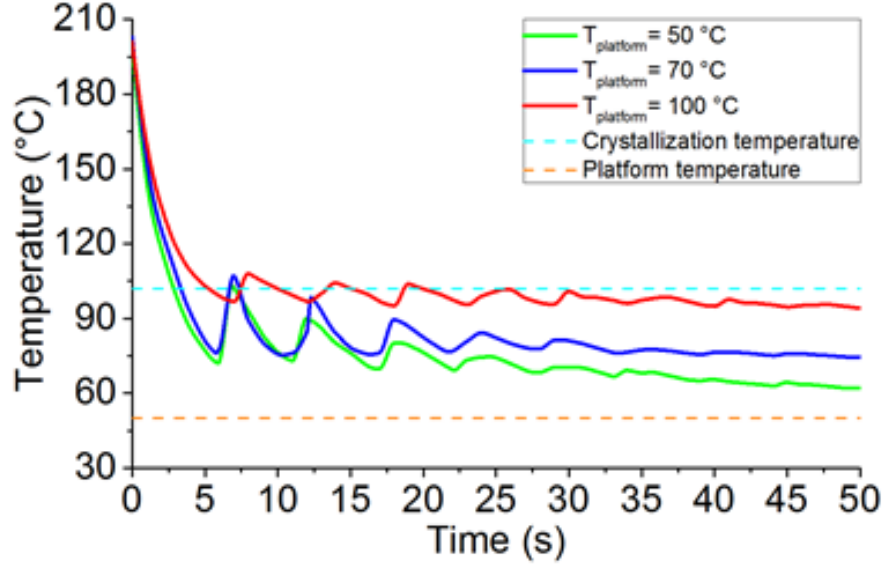


Figure 4.6: Temperature profile (± 2 °C) of vertical wall at $x = 5$ mm from the start of deposition at different platform temperatures.

As previously explained, in addition to the heat transfer from the liquefier, these filaments also undergo heat transfer originated by the platform. This heat transfer from the heating bed to the filaments will increase the anisotropy of the sample. Heat diffusion equation was applied by replacing the objective to a set of nodes at steady state. Then, the derivative of temperature with respect to X and Y direction was calculated using the following equation and taking into account the grid generation (**Article No. 2**):

$$\frac{\partial^2 T}{\partial x^2} + \frac{\partial^2 T}{\partial y^2} = 0 \quad (4.5)$$

$$\left[\left(\frac{T_{i-1,j}^k - 2T_{i,j}^k + T_{i+1,j}^k}{\Delta x^2} \right) + \left(\frac{T_{i,j-1}^k - 2T_{i,j}^k + T_{i,j+1}^k}{\Delta y^2} \right) \right] = 0 \quad (4.6)$$

The temperature of node (i,j) was obtained as follows:

$$T_{i,j} = \frac{1}{4}(T_{i,j-1} + T_{i-1,j} + T_{i+1,j} + T_{i,j+1}) \quad (4.7)$$

Concerning the dimensions of the object (Figure 4.7 (a-b)), these are applied to a source of heat and injected in *MATLAB* based on the following boundary conditions:

- $\Delta x = \Delta y$ (Consideration of Gauss-Seidel iterative)
- $dt=0$ (Consideration of steady state)

Based on the obtained results in Figure 4.7 (c), it is observable that the source of heat contributes to the anisotropy of the fabricated parts and demonstrates the effect of the heating bed on the temperature distribution in the printed part.

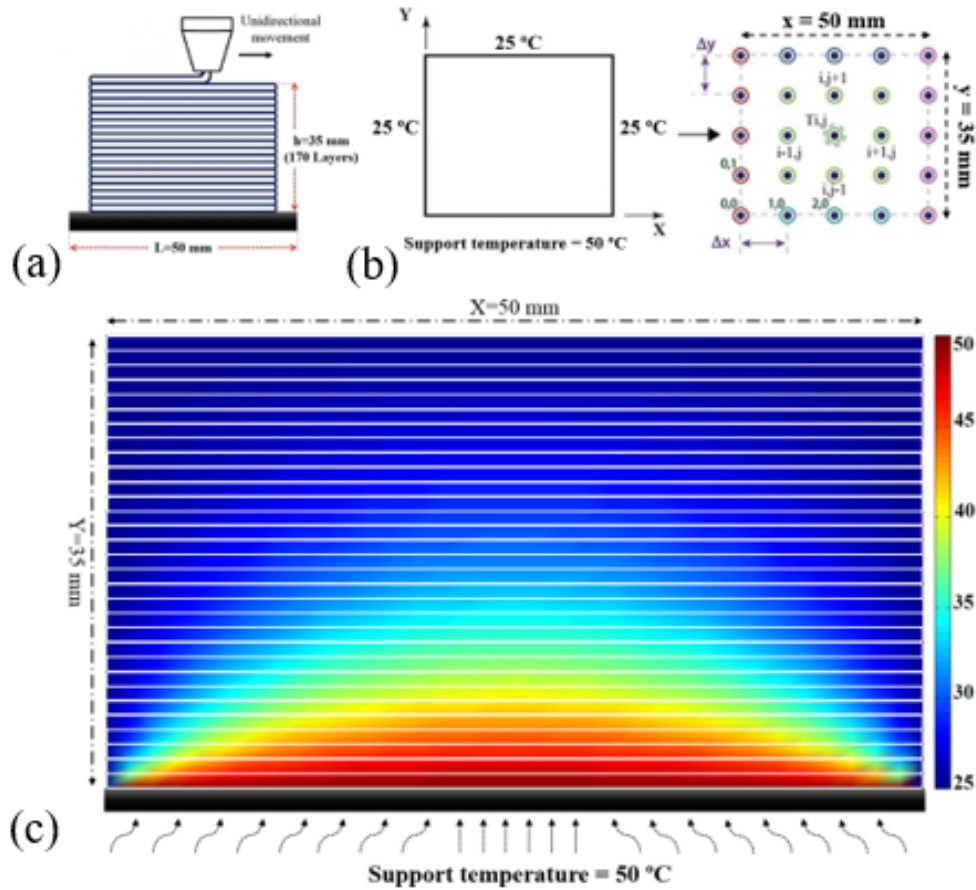


Figure 4.7: Representation of a) schematic of the test case, b) nodes for finite difference method, c) obtained results at steady state.

When the deposition velocity increases (Figure 4.8), the rate of cooling decreases. Also, and as expected, the onset of the peaks occurs at different times and their breadth is also altered. Finally, the magnitude of the peaks for the lowest deposition velocity is higher, probably due to the higher difference between the temperatures of adjacent filaments.

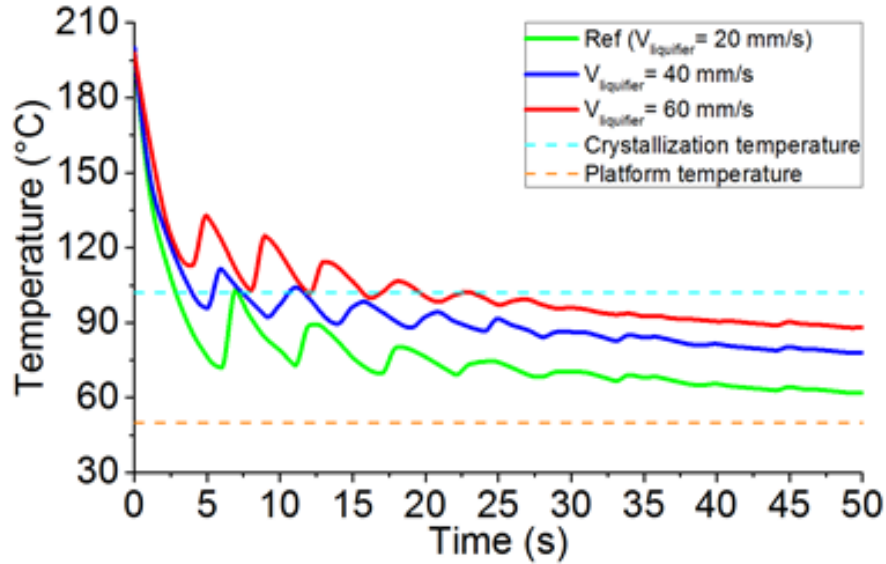


Figure 4.8: Temperature profile (± 2 °C) of vertical wall at ($x = 5$ mm) from the start of deposition at different print speed.

4.2 Modeling of filament cooling: Development of a numerical approach

As mentioned in section 1, most of the experimental and modeling approaches toward the heat transfer of the filaments are only valid for specific conditions. They are not considered for all geometries, and do not consider all the possible phenomena in this process. Additionally, in almost all experimental approaches, heat transfer has been recorded using global approaches such as implementing an IR-camera. Following our explanations in section 2, a novel approach has been proposed enabling the local in-process monitoring of temperature profile at the interface of adjacent filaments. To develop the proposed approach, obtaining a predictive approach based on the performed efforts is inevitable. A numerical study was performed using Finite Volume Method (FVM) with the following characteristics:

- Simple, prompt, generic, and applicable to complex geometries
- Include all possible mechanisms that exist in FDM/FFF
- Possible to be considered as the basis of optimization objectives
- To be validated by experimental results

When a filament is deposited, its accompanying temperature is higher than that of environment and heat transfer occurs by one/all of the following mechanisms: conduction with

platform, convection with the environment, and radiation with the environment. They appear by deposition of other filaments of the same or further layers. Worth mentioning to say that heat fluxes are negligible due to the small amount of polymer's thermal conductivity according to the small dimensions of filament's cross-section.

4.2.1 Conservation equation

The conservation equation governing the heat transfer in FDM/FFF-3D printing is given by:

$$\frac{\partial}{\partial t}(\rho T) + \text{div}(\rho u T) = \text{div}(\Gamma \text{grad} T) + S_T \quad (4.8)$$

where Γ is diffusion coefficient and S is the source term. Finite volume method (FVM) [116] is a good candidate to solve numerically Equation 4.8. Below is presented the overall FVM formulation used for this problem. In this work, a FVM heat transfer code is applied in order to perform the temperature evolution of deposited filaments in FDM/FFF process.

4.2.2 Numerical method

Finite Volume Method

In our case, FVM consists of performing a heat transfer balance over a given an infinitesimal volume. Using the divergence theorem, volume integrals of a partial differential equation are converted to the full surface. So, in finite volume approach, the governing equations under their conservative form are widely used and the aim is to ensure that all characteristics remain similar in each cell/volume control. The main features of FVM could be mentioned as follows:

- Subdivision of the problem extent into non-overlapping control volumes (CVs).
- Consolidation of the governing equations (in our case: heat equation) over the CVs.
- Evaluation of the integrals using the temperature variation between the grid points.
- Representation of the conservation principle for the finite control volume using the obtained discretized equation.

Problem formulation

We consider solving two-dimensional unsteady heat conduction problem on a vertical wall of rectangular shape with the dimension of 50*35*0.2 mm as described in section 2. This test

case was designed to predict the heat transfer during deposition of filaments based on the following assumptions: Same physical contact between filaments and filament/support, and convection between filament and air at the same time; thickness assumed to be as a diameter of a filament; a unidirectional moving of the liquefier; consisting of more homogeneity in temperature distribution.

Maintaining the first term of Equation 4.8 in the discretization process, the finite volume integration of this equation over the CV by replacing the convective and diffusive terms with surface integrals obtained as follows:

$$\int_{CV} \frac{\partial(\rho T)}{\partial t} dV + \int_{CV} div(\rho T u) dV = \int_{CV} div(\Gamma grad T) dV + \int_{CV} S_T dV \quad (4.9)$$

By using Gauss divergence theorem, we obtain:

$$\int_{\Delta t} \frac{\partial}{\partial t} \left(\int_{CV} (\rho T) dV \right) dt + \int_{\Delta t} \int_A n(\rho T u) dA dt = \int_{\Delta t} \int_A n(\Gamma_T grad T) dA dt + \int_{\Delta t} \int_{CV} S_T dV dt \quad (4.10)$$

Grid generation

The first step in launching FVM refers to the generation of grids by the means of dividing the applicable area into the small discrete CVs. The borders of CVs are positioned halfway in between the adjacent nodes which itself is surrounded by control volume/cell. Figure 4.9 indicates a rectangular domain divided into non-overlapping CVs.

They are divided by dashed-lines introducing the boundaries of the individual CVs. These patterns that are created by the mentioned dashed-lines are called the computational grids. A general nodal point 'P' is specified by its neighbors, in a 2D geometry, nodes on north, south, west, and east; N, S, W, and E, respectively. As shown in Figure 4.9, two sets of grid lines could be defined as follows: the grid lines defining the location of nodes, and those defining the CV faces. So, the nodal point P is always placed in the geometric center of its CV with the following destinations:

$$y_P - y_s = y_n - y_P = \frac{\Delta y}{2} \quad (4.11)$$

$$x_P - x_w = x_e - x_P = \frac{\Delta x}{2} \quad (4.12)$$

Notably, lower case subscripts refer to the locations of the CV faces; whereas the upper case subscripts refer to the locations of the nodes. So, it is important to distinguish between upper and lower letters.

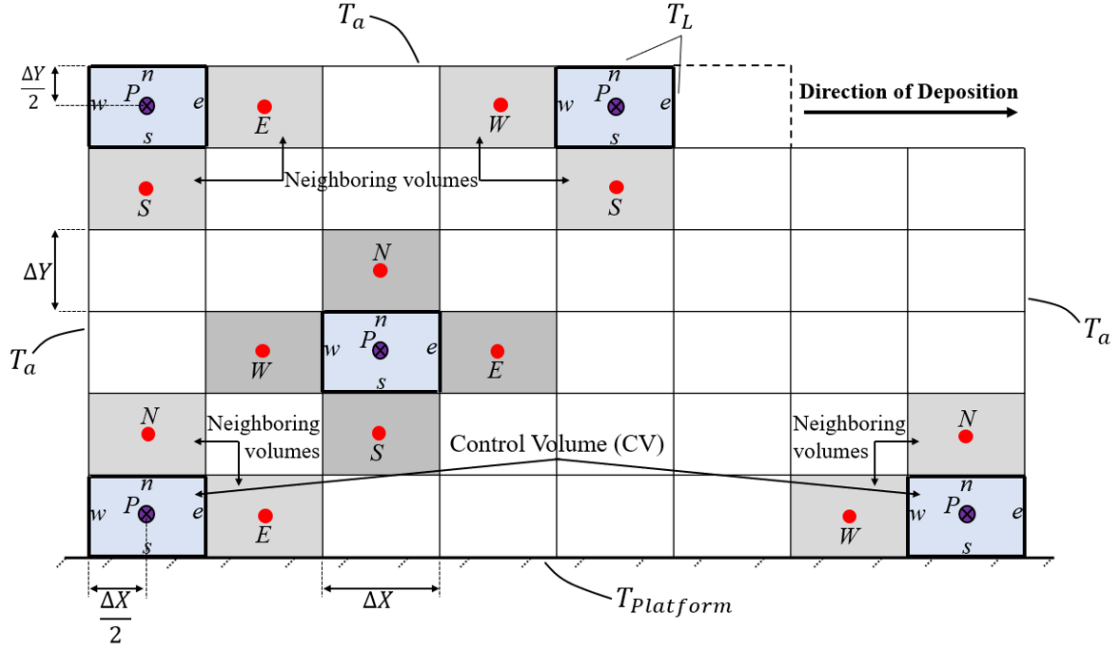


Figure 4.9: Schematic of the object in finite volume (T_{Liq} : Liquefier temperature, $T_{Platform}$: Platform temperature, T_a : Ambient temperature, N: North, S: South, W: West, E: East).

Discretization

Integration of governing equation on a CV is the most important characteristic of the FVM. The idea is to obtain a discretized equation to its nodal point P. The unsteady two-dimensional diffusion equation is as follows:

$$\rho C \frac{\partial T}{\partial t} = \frac{\partial}{\partial X} \left(K \frac{\partial T}{\partial X} \right) + \frac{\partial}{\partial Y} \left(K \frac{\partial T}{\partial Y} \right) + S \quad (4.13)$$

By integrating Equation 4.13 over the CV and a time interval from t to $t+\Delta t$, we have:

$$\int_t^{t+\Delta t} \int_{CV} \rho C \frac{\partial T}{\partial t} dV dt = \int_t^{t+\Delta t} \int_{CV} \frac{\partial}{\partial X} \left(K \frac{\partial T}{\partial X} \right) dV dt + \int_t^{t+\Delta t} \int_{CV} \frac{\partial}{\partial Y} \left(K \frac{\partial T}{\partial Y} \right) dV dt + \int_t^{t+\Delta t} \int_{CV} S dV dt \quad (4.14)$$

This may be written as:

$$\int_t^{t+\Delta t} \int_{CV} \rho C \frac{\partial T}{\partial t} dV dt = \int_t^{t+\Delta t} \int_{CV} \left[\left(KA \frac{\partial T}{\partial X} \right)_e - \left(KA \frac{\partial T}{\partial X} \right)_w \right] + \int_t^{t+\Delta t} \int_{CV} \left[\left(KA \frac{\partial T}{\partial Y} \right)_n - \left(KA \frac{\partial T}{\partial Y} \right)_s \right] + \int_t^{t+\Delta t} \bar{S} dV dt \quad (4.15)$$

where A is the face area of the control volume, ΔV is its volume ($\Delta V = A \Delta X = A \Delta Y$), and \bar{S} is the average source strength. By considering the following statements: (1) temperature at node P is implemented to the CV, (2) temperature at time t is assumed as T_p^0 , (3) substituting $(T_p - T_p^0) / \Delta t$ for $\partial T / \partial t$, (4) assuming the two-dimensional CV for discretization; the resulting equation is:

$$a_P T_P = a_W T_W + a_E T_E + a_S T_S + a_N T_N + a_P^0 T_P^0 + S_u \quad (4.16)$$

where

$$a_P = a_W + a_E + a_S + a_N + a_P^0 - S_P$$

$$a_P^0 = \rho c \frac{\Delta V}{\Delta t}$$

$$a_N = \frac{\Gamma_n A_n}{\delta y_{PN}}$$

$$a_S = \frac{\Gamma_s A_s}{\delta y_{SP}}$$

$$a_W = \frac{\Gamma_w A_w}{\delta x_{WP}}$$

$$a_E = \frac{\Gamma_e A_e}{\delta x_{PE}}$$

Boundary condition

Alongside with the parameters related to the implemented material, the boundary conditions defined as follows:

- North boundary: fixed temperature equal to the liquefier temperature.
 - Cell in front of the liquefier: fixed temperature equal to liquefier temperature.

- Other cells: fixed temperature equal to the ambient temperature.
- South boundary: fixed temperature equal to the platform temperature.
- West boundary: fixed temperature equal to the ambient temperature.
- East boundary: fixed temperature equal to the ambient temperature.

As the code is in 2D, particular attention has been taken into account in definition of the boundary conditions. Accordingly, a thermal source has been added through the front and back boundaries to be implemented to the conservation equation that let us considering of convection with environment. This make it possible to have 3D implicit scheme for our modeling.

4.2.3 Convection with the environment

The graph presented in Figure 4.10 provides the experimental results of the recorded temperature profile by implementing K-type thermocouples at the interface of adjacent filaments. As previously explained, the recorded experiment is based on the layer-by-layer filament deposition. Under the defined 3D printing condition, the previously deposited filament(s) has sufficiently cooled down. As an example (according to Figure 5.10), the first cooling curve corresponds to the cooling of layer 5 (at the specific location) by deposition of younger filaments, a cyclic cooling and re-heating evolution appears to layer 5 which could be described as follows:

- First re-heating: re-heating of layer 5 by deposition of layer 6.
- Second cooling: cooling of layer 5 after deposition of layer 6.
- Second re-heating: re-heating of layer 5 by deposition of layer 7.
- Third cooling: cooling of layer 5 after deposition of layer 7.
- Third re-heating: re-heating of layer 5 by deposition of layer 8.
- Peaks 1, 2, 3, 4, etc.: re-heating peaks at the instant of deposition of layers 6, 7, 8, and 9, respectively.

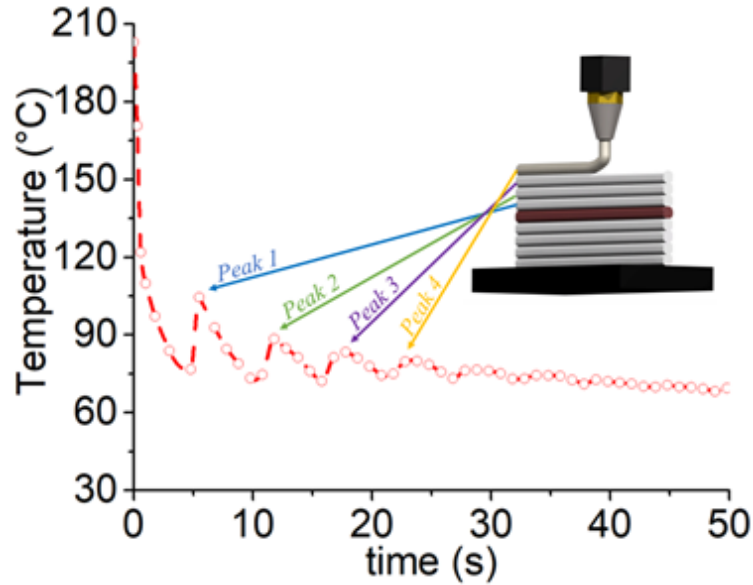


Figure 4.10: Temperature evolution of layer 5 (at $x=30$ mm) during the deposition of the vertical wall consisting of single filaments deposited on top of each other: Peaks 1, 2, 3, 4 are re-heating of 5th filament (layer 5) by deposition of 6th, 7th, 8th, 9th, respectively.

Convective heat transfer that exists in FDM/FFF process has been investigated in literature to a good extent. According to the developed numerical code and to evaluate its functionality, the temperature evolution during 50 seconds of cooling the vertical wall deposition at different locations has been presented. For post-processing, all signals are synchronized at $t=0$ s based on the instant of the first recorded temperature (the highest measured value considered as a value at $t=0$ s).

The obtained results regarding the heat exchanges by convection for $h=5, 10, 30, 50, 70,$ and $88 \text{ W/m}^2\cdot\text{C}$ has shown that the effect of this coefficient is evident, particularly on the cooling rate and temperature peaks. It could be clearly seen in Figure 4.11 for random locations (as highlighted for layers 5, 20, and 88). A value of $h_{conv}=70 \text{ W/m}^2\cdot\text{C}$ is normally used and as it increased from 5 to $70 \text{ W/m}^2\cdot\text{C}$, the cooling rate increased and its effect is remarkable on the re-heating peaks. Besides, using the Churchill correlation for cooling of a cylinder by natural convection, $h_{conv}=88 \text{ W/m}^2\cdot\text{C}$ was obtained which has been taken into account for the computation [115].

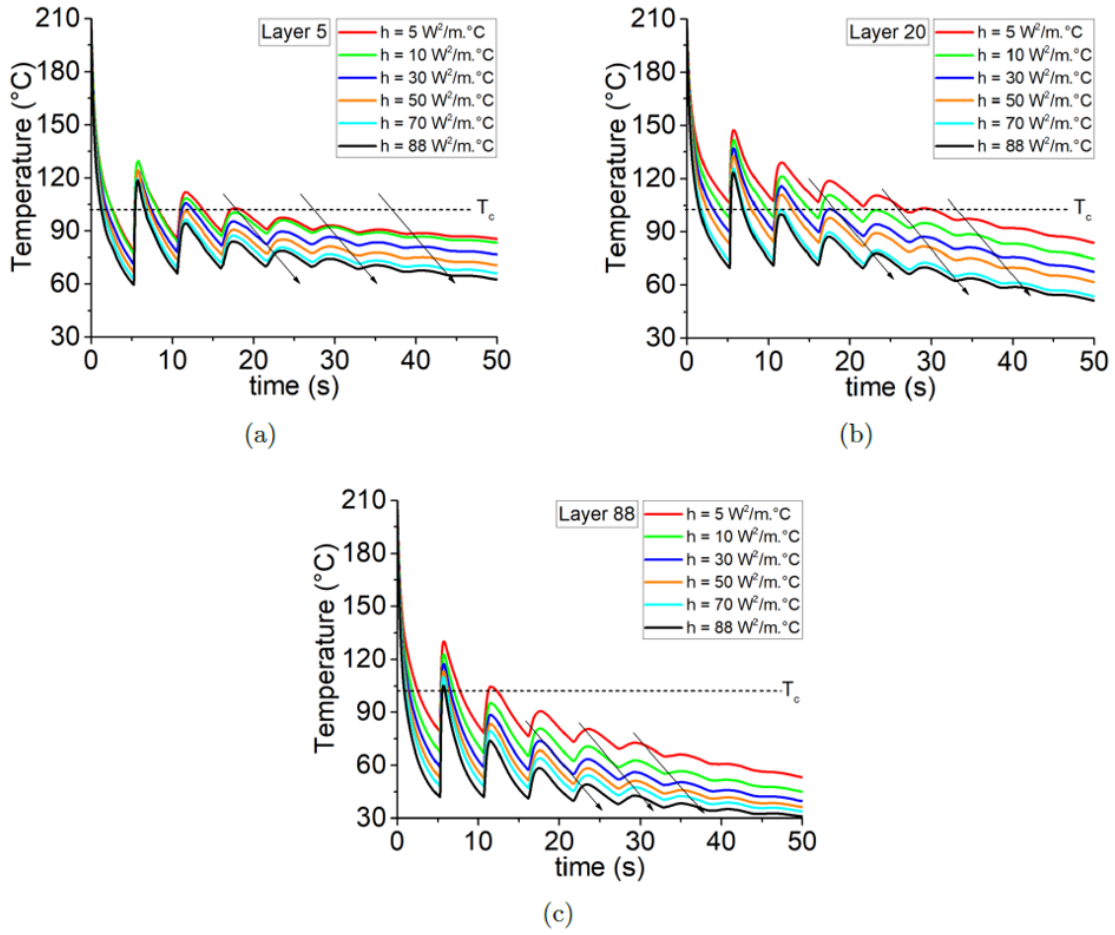


Figure 4.11: The effect of h_{conv} on filament cooling: temperature evolution for $h_{conv}=5, 10, 30, 50, 70, 88 W/m^2 \cdot ^\circ C$ for (a) Layer 5, (b) Layer 20, (c) Layer 88.

Figure 4.12 shows the temperature evolution of filaments at specific instants upon constructing the vertical wall. Following the results reported above, under these printing conditions, deposition of a new filament causes the re-heating of those that have already been cooled down. Presenting a general overview in Figure 4.12(a), the temperature evolution over the CVs has been recorded for layers 5, 10, and 43, respectively (Figure 4.12(b)).

From these thermograms, the re-heating of previously deposited filaments is obviously depending on their location. As an example, deposition of the 43rd layer raises the temperature of approximately 4-5 layers, which is about 8-9 layers when the 10th layer is deposited; this is more obvious in Figure 5.12(c) for the deposition of the 15th layer (**Article No. 6**).

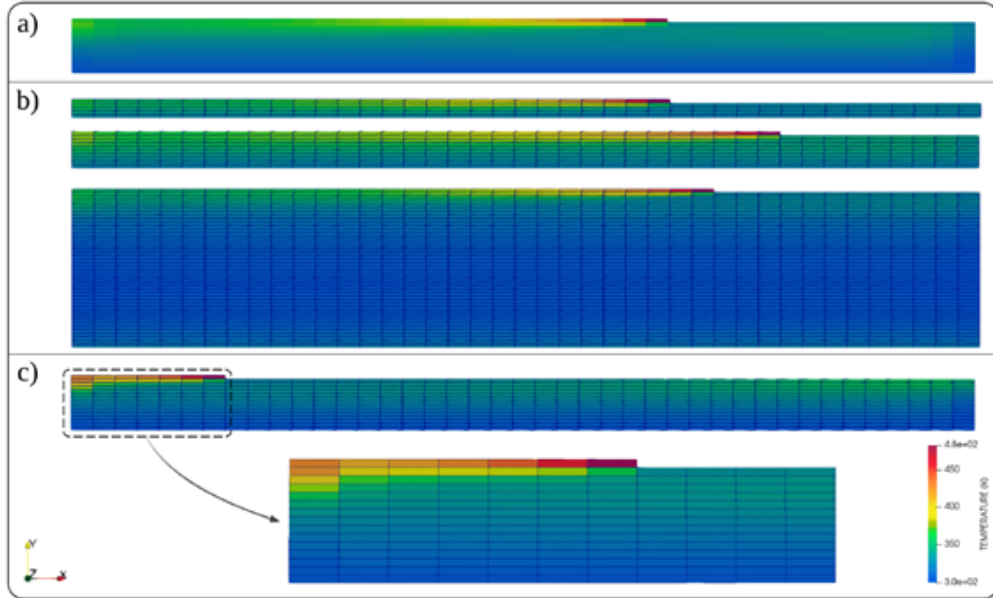


Figure 4.12: Temperature at some instances of the deposition process for the vertical wall: (a) general view, (b) layers 5, 10, 43 as well as the presentation of CVs, (c) layer 15 with high resolution of CVs.

4.2.4 Experimental validation of the obtained results

In-process monitoring of temperature profile enables local measurement of temperature distribution along with the consequence of deposition. This is carried out for a defined condition alongside with different locations of the proposed vertical wall.

In this set of experiments, the filament temperature profile is randomly recorded at some instants: Layer 5 ($x=30$ mm, $y=1$ mm), layer 20 ($x= 20$ mm, $y=4$ mm), layer 37 ($x= 35$ mm, $y= 7.4$ mm), layer 54 ($x= 40$ mm, $y= 10.8$ mm), layer 63 ($x= 25$ mm, $y= 12.6$ mm), and layer 88 ($x= 40$ mm, $y= 17.6$ mm). The liquefier temperature was maintained at 210 °C as well as the platform temperature at 50 °C. Figure 4.13 summarizes the recorded data by plotting the recorded temperature evolution as a function of time. In each case, as mentioned in the previous section, the cyclic temperature evolution of filaments varies based on their location. One key parameter to the cooling curve of all extracted data is that the influence of temperature radiation of the support/platform is observable, which is expected due to the nature of the means of measurement. Figure 4.13 also plots the temperature distribution obtained by the prediction of the analytical model. Over a broad range of layers and various locations, there is a good agreement between the analytical model and the experimental data.

Regardless of cooling curves, the breath of temperature peaks is recorded and predicted

by both approaches. However, the difference between the onset and relative magnitude of the peaks could be correlated to the nature of measurement approach. Further, the peaks that they themselves represent the existence of adhesion and contact of adjacent layers, become gradually smaller with time. On the other hand, as no phase changes were taken into account in the model, the released energy could be referred to as the difference of captured peaks. Overall, based on the obtained prediction and recorded data, one can note that the cooling rate of previously deposited filament won't be affected after 4-5 deposition sequence; the higher the distance from platform/support, the higher the cooling rate predicted by the analytical approach. However, the recorded data represent a lower cooling rate in comparison with the obtained prediction. The main reasons could be listed as follows:

- The influence of the released energy due to phase change (both at melting and crystallization points) has an impact on the temperature profile of filaments.
- The platform plays an important role in the cooling stage of filaments (As of layer 5, in which there is a very good agreement between the two approaches).

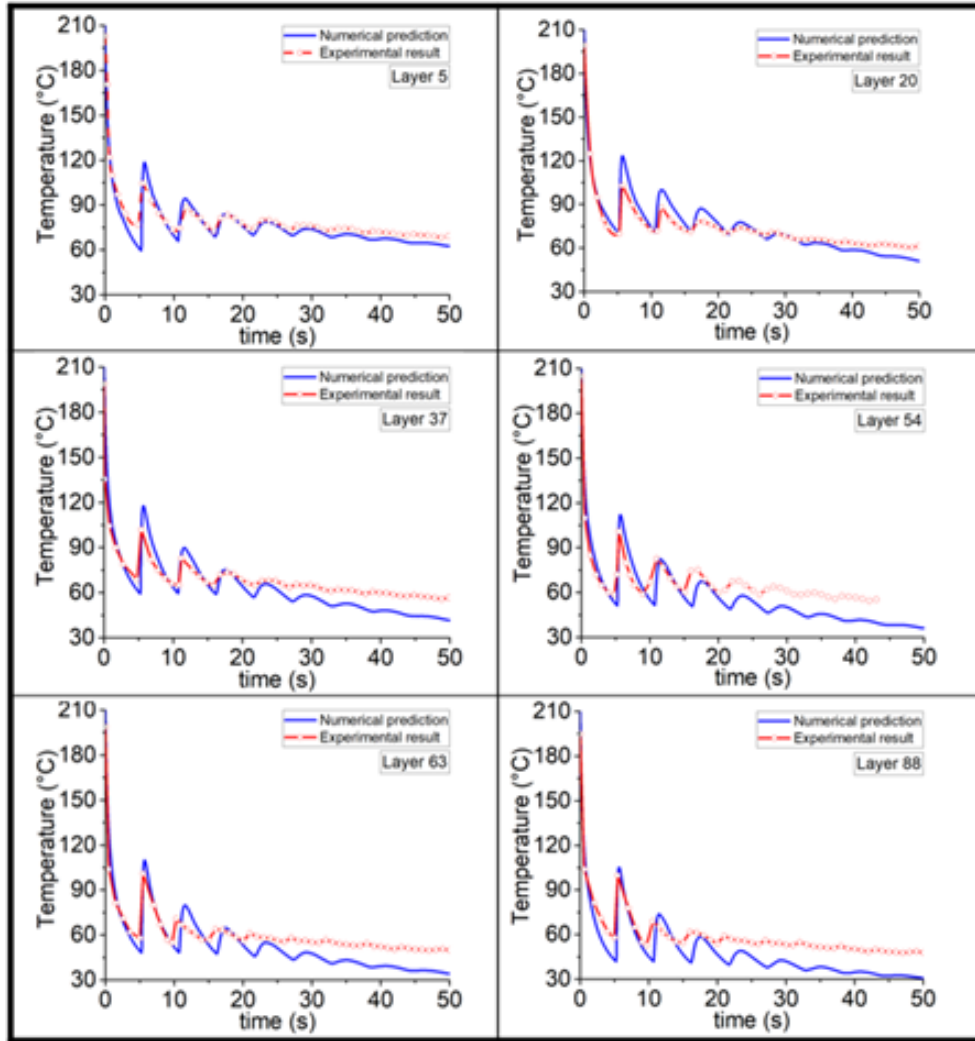


Figure 4.13: Comparison of temperature evolution at different locations during the deposition of a vertical wall consisting of single filaments deposited on top of each other with prediction from theoretical model for various layer with specific locations.

4.2.5 Parametric study: influence of process parameters on temperature variation

Liquefier temperature

The influence of liquefier temperature during layer deposition is considered first. A set of predictions is carried out where the filament is cooled at different liquefier temperatures. As it varies from $T_{Liq} = 200$ to 230 °C, greater values for the re-heating peaks are anticipated to shift the filament temperature profile around T_c . The predicted results indicate the same breadth, whereas, the variation of cooling rates is negligible. Clearly, as indicated in Figure 4.14, the temperature profile of the first deposited layer ($x=30$ mm) at different liquefier temperatures are so close to each other, which obviously represents the ineffectiveness of this

parameter.

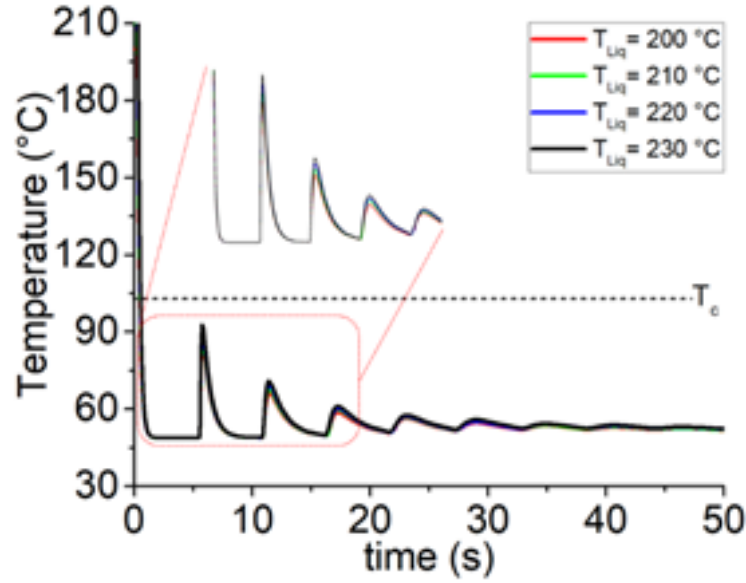


Figure 4.14: Influence of liquefier temperature on temperature evolution during the deposition of a vertical wall consisting of single filaments deposited on top of each other with prediction obtained from theoretical model.

Platform temperature

Furthermore, efforts are taken into account to consider the effect of platform temperature on temperature profile during deposition of the vertical wall (with the same condition as explained in the previous section). Figure 4.15(a) demonstrates the temperature profile by changing the platform temperature. As expected for the re-heating peaks, they all have identical onsets besides the great shift that occurs by enhancing the platform temperature. Worth mentioning to say that the higher the platform, the lower the cooling rate. Accordingly, and unlike the observation was taken into account by changing the liquefier temperature, platform plays an important role in temperature evolution of filaments. In this case, the temperature profile is recorded experimentally at $T_{Platform} = 100\text{ °C}$ and compared with the results predicted by the analytical model (Figure 4.15(b)). Presumably, the temperature varies around T_c , favorable adhesion of filaments. However, deformation and low quality of the printed part is an important issue.

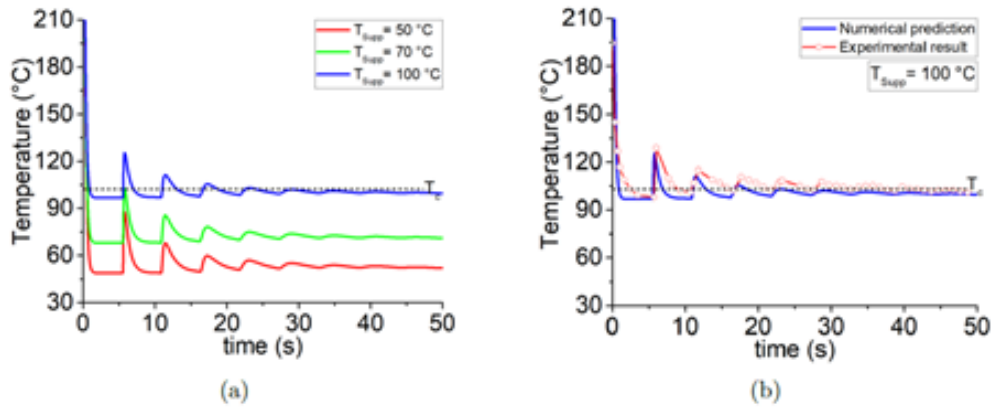


Figure 4.15: Influence of platform temperature on temperature evolution during the deposition of a vertical wall consisting of single filaments deposited on top of each other with (a) prediction obtained from theoretical model and (b) experimental validation.

Print speed

The effect of print speed during filament deposition is evaluated next. Prediction is carried out where the filaments are printed at various speeds of deposition $V=20, 40, 60$ mm/s. Similar to the predictions observed for variation of liquefier temperature, onsets of the peaks are approximately similar, whereas the cooling rate almost decreased by increasing the print speed (Figure 4.16). The main characteristic of this parameter is that it helps raising the temperature profile of filaments and keeps them hot enough during the deposition sequences. Following previous studies, enhancing the print speed acts as a manner of a heating source by which it does not let the filament cool down quickly. Also, worth mentioning to say that the onset of the peaks is found to arise at a different time and thus their breadth is also decreased.

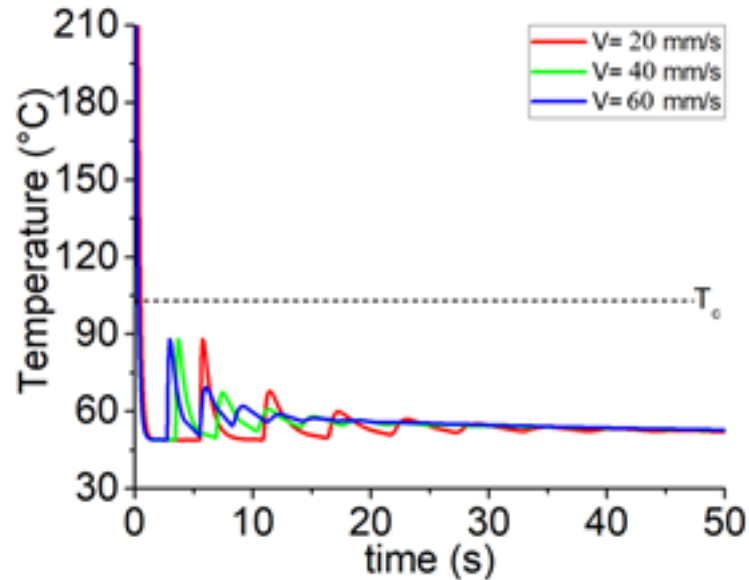


Figure 4.16: Influence of print speed on temperature evolution during the deposition of a vertical wall consisting of single filaments deposited on top of each other with prediction obtained from theoretical model.

4.2.6 Optimization exploration with the developed code

The introduced analytical heat transfer model can be implemented for optimization purposes. The main advantage of the proposed model is that it is general and it could be implemented for various groups of materials, whether amorphous or semi-crystalline polymers, by considering complex geometry. Specifically, the role of various process parameters can be taken into account based on the experimentally validated model.

In the case of a semi-crystalline material (in our study: PLA), it is broadly believed that the defined time due to the cooling and re-heating of filaments is crucial for proper bonding to take place. So, filaments must be hot enough, but not too hot, to avoid the deformation and reduced quality of the final part. Furthermore, the key assumption of the proposed analytical model is that the dynamic mesh is considered by the implementation of the finite volume method. This issue corresponds to the unsteady state heat transfer that exists in FDM/FFF.

To have a better understanding, extracted data from the prediction of analytical code is presented at real time of deposition (without synchronization of time at $t=0$). Figure 4.17(a, c) shows the temperature profile of layers 1-4, and layers 20-23. Parameter optimization using the values $T_{Liq}= 220$ °C, $T_{Platform}= 70$ °C, $T_{amb}= 30$ °C, $V= 20$ mm/s) is demonstrated in Figure 4.17(b, d) for the same layers as shown in Figure 4.17(a, c). Figure 4.17(b) shows

that temperature varies around T_c by implementing the mentioned values. This leads to the better crystallization of the printed layers and thus better adhesion, favorable bonding. Unlikely, Figure 4.17(d) indicates that temperature varies for a period of time (about 20 seconds for each filament) around T_c and it drops again below T_c and hence cooling of material does not give sufficient time for crystallization and better adhesion of layers. Seemingly, these differences can be resulted into the in-homogeneity of the printed structures and affect their strength through different layers.

Designed curves (Figure 4.17(b, d)) demonstrate the capability of the analytical code presented here for accurate thermal analysis and further objectives. This could be used for optimization purposes by implementing all engaged parameters to have the possibility of improving the process to be resulted in bonding and adhesion enhancements. These results can also be used for consideration of temperature dependence viscosity and coalescence of filaments in rheological objectives.

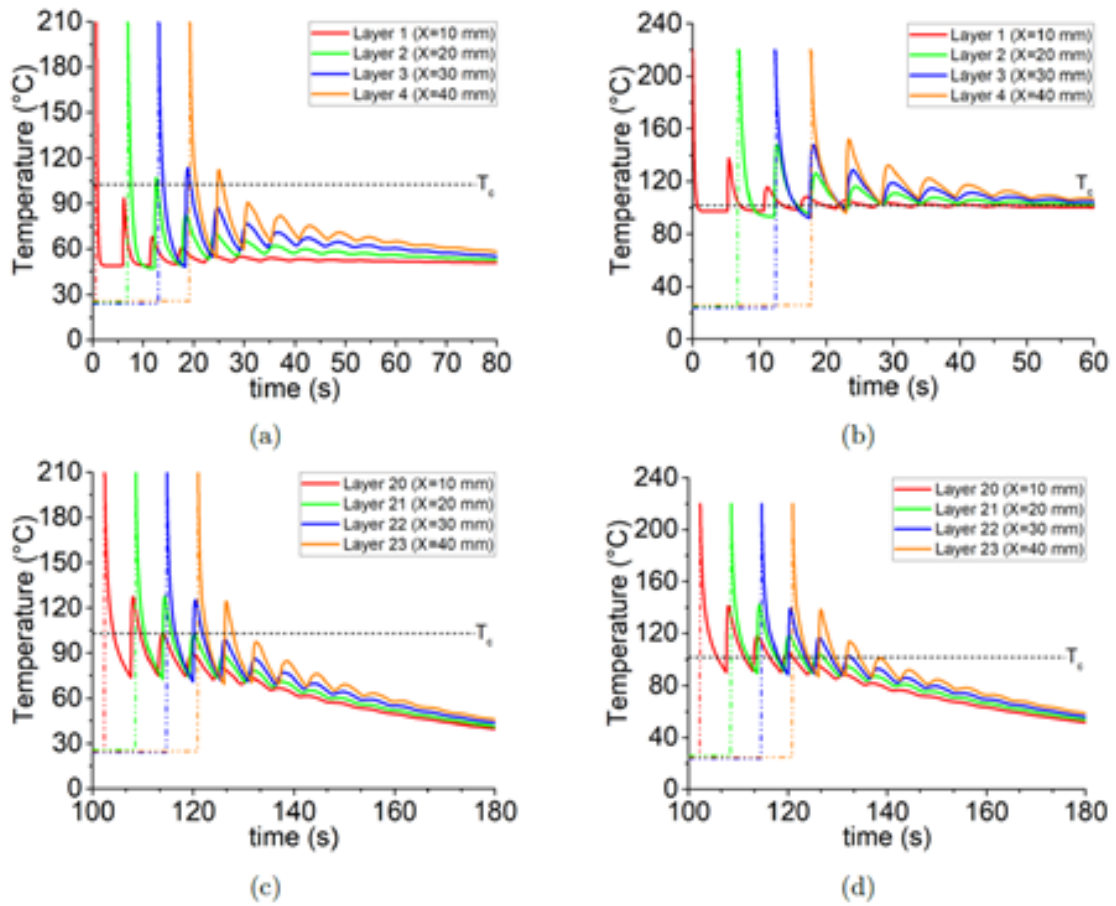


Figure 4.17: Temperature evolution during the deposition of a vertical wall consisting of single filaments deposited on top of each other with prediction obtained from theoretical model for (a) Layers 1-4, (b) optimized value for layers 1-4, (c) Layers 20-23, and (d) Optimized value for layers 20-23.

Chapter 5

Time-Temperature-Transformation diagram of filaments

Recognizing the temperature evolution of thermoplastic polymers is a crucial issue in 3D printing and the enhancement of final characteristics of fabricated parts. During the solidification process of thermoplastics, various modes of heat transfer (e.g. convection, conduction, and radiation) are engaged. This heat transfer has been explained in the previous section with the obtained results so far. In fact, those results help in understanding the temperature profile at the filament-filament interfaces versus time of deposition. By simplifying the general Lumped parameter model for a pair of cylinders (or even a pair of spheres) and according to Holman estimation, we will have:

$$\rho C_P V \frac{dT(t)}{dt} = Q + hA [T(t) - T_\infty(t)] \quad (5.1)$$

where h considers both convective and radiative heat transfer coefficient, Q the heat generation, C_p the specific heat, ρ the density, A the surface area, V the volume, and k the thermal conductivity.

In addition, temperature dependence viscosity for molten polymers relies on temperature giving by an Arrhenius expression in an exponential form [103]:

$$\eta = \eta_0 e^{\left[\frac{E}{R} \left(\frac{1}{T} - \frac{1}{T_0}\right)\right]} \quad (5.2)$$

where E is the activation energy and R is the gas constant. Since the rheological properties such as viscosity are a function of temperature, believably this dependence could be correlated to the temperature evolution of deposited filaments. This is an idea to create a relationship between viscosity as a criterion for ‘Transformation’ and the ‘Temperature’

of filaments during process versus ‘Time’ of deposition to have the TTT (Transformation-Temperature-Time) diagram. TTT diagram helps to understand at which zone of temperature and/or viscosity, the process should be performed. In the case of FDM/FFF, better adhesion could be resulted by knowing the viscosity. Although the reduction in viscosity causes better flow, it should be obtained by increasing the temperature that itself results in degradation. Hence, the TTT diagram helps to optimize the required viscosity with respect to the temperature in a given deposition time.

Accordingly and due to the cyclic cooling and re-heating evolution of temperature during FDM/FFF, by considering the following boundary conditions:

$$T = T_0 \text{ at } x = 0 \text{ (nozzle head) and } t \geq 0$$

$$T = T_\infty \text{ at } x = \infty \text{ and } t \geq 0$$

And by solving the Equation 5.1 using the above boundary conditions and taking into account the Lumped Capacity for modeling the cooling process of the cylindrical filament, we will have:

$$T = T_\infty + (T_0 - T_\infty) \exp\left(-\frac{2h}{\rho C_p a_0} t\right) \quad (5.3)$$

where T_0 refers to the liquefier temperature. Substitution of Equation 5.3 in Equation 5.2 results in the following relation:

$$\eta = \eta_0 e^{\left[\frac{E}{R} \left(\frac{1}{T_\infty + (T_0 - T_\infty) \exp(-2ht/\rho C_p a_0)} - \frac{1}{T_0}\right)\right]} \quad (5.4)$$

Equation 5.4 is the temperature dependence of viscosity for a cylindrical filament during its cooling and consequently the re-heating/cooling by deposition of younger filaments.

The viscosity variation in melt state as a function of temperature obeys Arrhenius law (Equation 5.2). To show the validity of this law for the PLA in the molten state, we determined the Newtonian viscosity of PLA at different temperatures by performing isothermal tests. According to this equation, by plotting $\ln \eta$ as a function of $1/T$, we will obtain the following equation that is a linear function:

$$\ln \eta = \ln \eta_0 + \left(\frac{E}{R}\right) \times \frac{1}{T} \quad (5.5)$$

Figure 5.1 clearly demonstrates the measured value for viscosity at different temperatures and isotherm states. The values could be fit to the mentioned equation and the related curve,

which means that the constants of this law, E and η_0 , are 26045 J and 1.7 Pa.S, respectively.

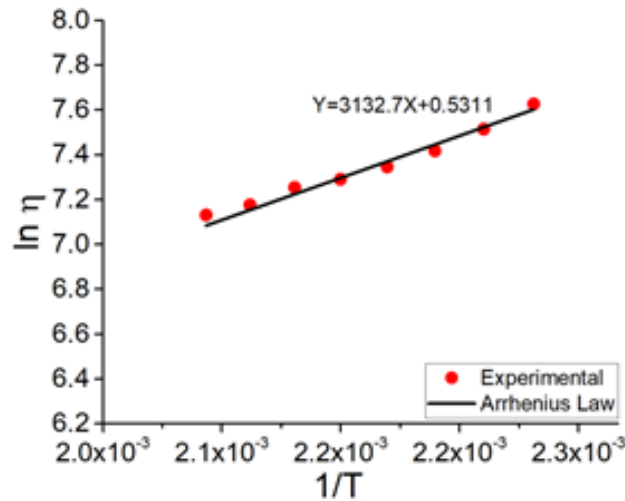


Figure 5.1: Dynamic viscosity evolution in different temperature

As can be seen in Figure 5.2, viscosity varies during the cooling stage of a single filament from $T=210$ °C to ambient temperature in a specific time. While cooling, the viscosity increases rapidly in a non-linear regime until the time ($t=3.5$ s), follows by a linear one, and return again to a non-linear regime (with a lower rate) while reaching the ambient temperature. Seemingly, the $t=2$ s corresponds to the $T=120$ °C, the temperature at which crystallization begins. On the other hand, the strategic zone is in between crystallization and melting points ($1s < t < 2s$). Hereupon, it is required to keep the temperature around or above crystallization temperature for further purposes such as strength improvement as explained in previous sections.

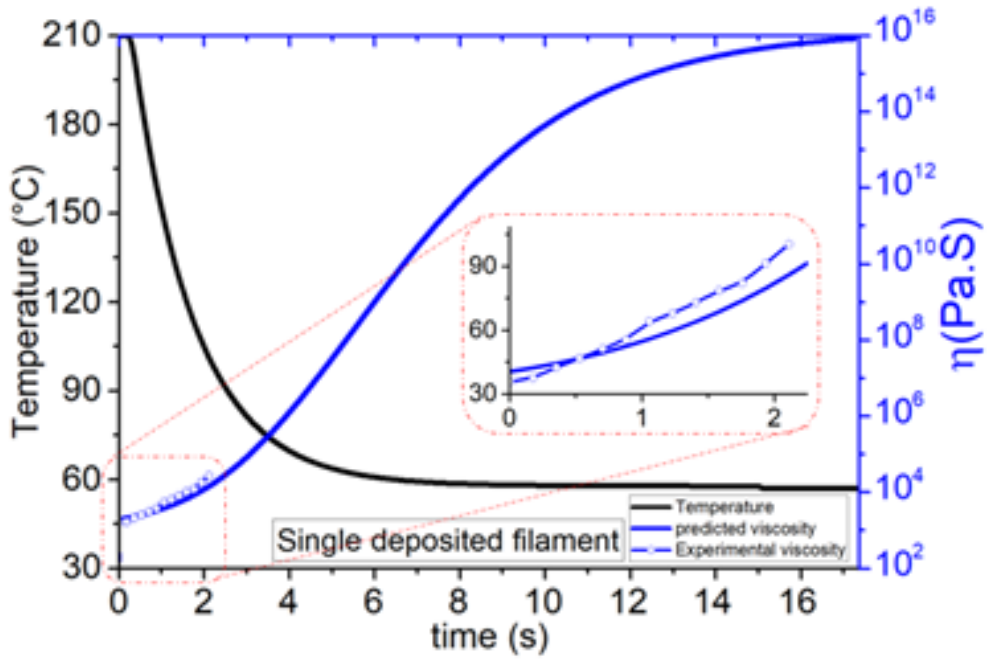


Figure 5.2: TTT diagram of a single filament deposition

Furthermore, to have a better vision of correlating the three mentioned parameters (Time-Temperature-Transformation), their variation has been presented in a 3D curve as shown in Figure 5.3.

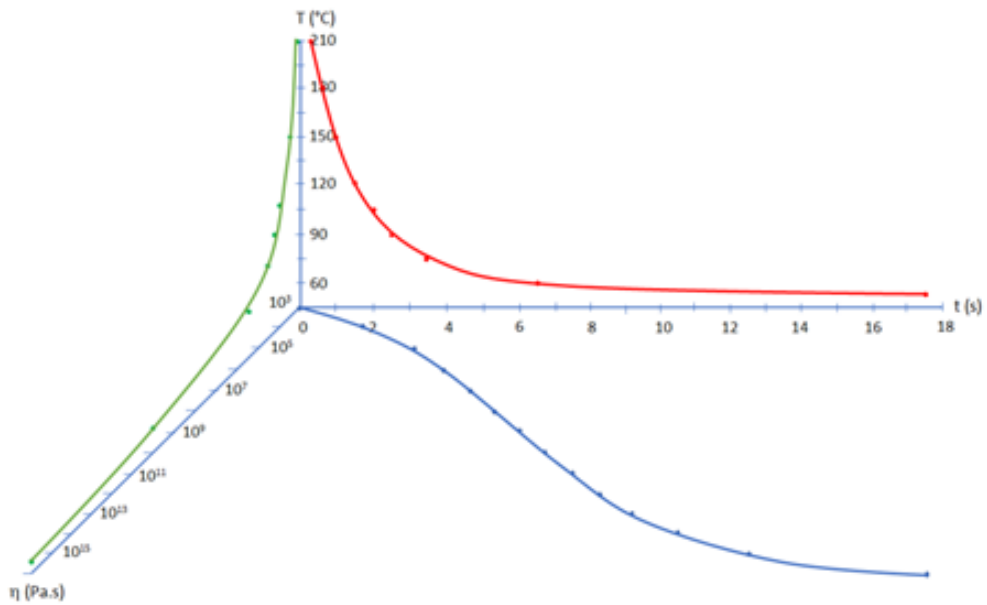


Figure 5.3: TTT diagram of a single filament deposition

As the temperature evolution during the cooling stage (and thus the re-heating peaks) of filaments plays an important role in determination of the filament bonding while depositing, the correlation of rheological characteristics along with the mechanical properties is a spot

point. So, simultaneous characterization of thermal and rheological properties is inevitable. Regarding the mechanism of deposition and temperature profile of each layer, viscosity varies accordingly. In general, the following observations could be concluded:

- The lower the cooling rate, the higher the viscosity.
- Lower cooling rate limits the viscosity enhancement; favorable flowability of the material.
- By cooling the deposited filament from the temperature of the liquefier to the ambient temperature, the viscosity varies depending on the deposition conditions.
- Viscosity tends to unlimited values depending on the filament's temperature evolution.

One benefit of temperature dependence viscosity consideration over FDM/FFF process is that it enables us to have more precise investigations of rheological characteristics. This issue could be more highlighted while considering the interaction of engaged parameters through them. This is a potential concern that engaged researchers in the study of bonding and mechanical strength; it has been briefly presented in the next section.

5.1 case studies: influence of process parameters

Despite a large variety of studies trying to optimize the bonding of deposited filaments and consequently the strength of final parts [117–119], there is still a lack of researches in this regard. Therefore, it is required to consider both the interaction of parameters and thermo-rheological characteristics of the applied materials during FDM/FFF process. This section demonstrates the usefulness of the proposed approach by studying the influence of process parameters on viscosity evolution. So far, we have shown the importance of investigating viscosity and temperature at the same time and how they vary in the given parameters in FDM/FFF.

Temperature evolution at different print speeds and platform temperatures, the same as previous explanations, has been taken into account as discussed in previous sections. The higher the print speed, the lower the cooling rate and thus the re-heating peaks occur at different times. Seemingly, the higher the platform temperature, the slower the cooling rate and decreases the period of viscosity variation. The evolution of viscosity versus temperature

is shown in Figure 5.4. As discussed, the viscosity increases gradually at the print speed of ($V_{Liq}=60$ mm/s) in comparison with the reference condition ($V_{Liq}= 60$ mm/s, $T_{Platform}= 50$ °C). By linking the observations from the presented graphs in Figure 5.4, it could be concluded that print speed plays an important role in viscosity evolution rather than platform temperature.

To finalize, optimizing the rheological characteristic and thus the bonding of final parts required interaction of parameters to be taken into account.

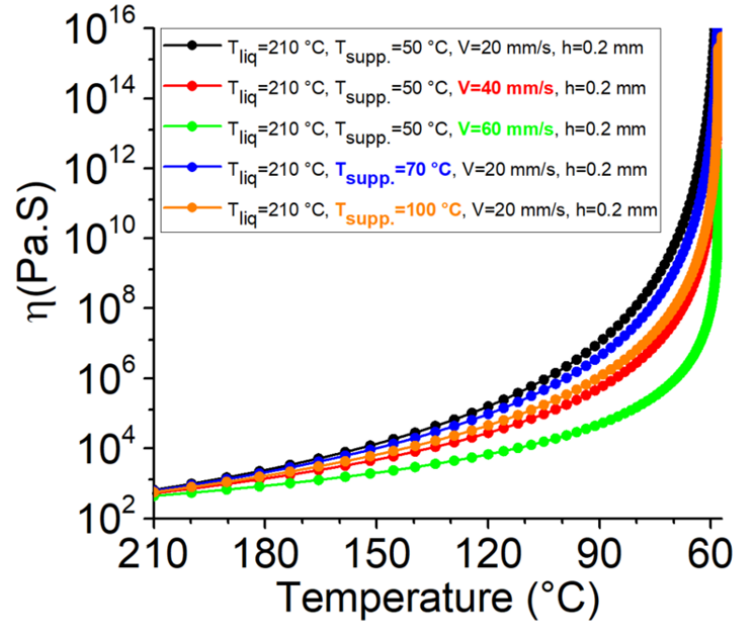


Figure 5.4: Viscosity evolution of the first layer during deposition of a vertical wall consisting of single filaments on top of each other versus the temperature evolution of the deposited filament

5.2 Correction to the viscosity evolution

So far, we have considered the evolution of viscosity and temperature simultaneously, so far. The temperature dependence viscosity is considered to vary from the liquefier temperature to the ambient temperature using the Arrhenius equation by implementing the temperature evolution to it. However, since the thermomechanical behavior of the polymer determines the diverse transitions and change of physical state of polymer, DMTA test is implemented using the alternating bending configuration (with the frequency of 1 Hz). The obtained result is shown in Figure 5.5 including three physical states: glassy state, glass transition zone, and rubbery state. As can be seen in Figure 5.5, the material shows a glassy state up

to $\sim 55^\circ\text{C}$ in which there is no significant change E' , E'' , and $\tan \delta$. In glassy state, E' is relatively high (>16 GPa). The second zone ($55^\circ\text{C} < T < 85^\circ\text{C}$) corresponds to α -transition zone that glass transition phenomenon has taken place. E' decreases drastically from 16 GPa to a value lower than 2 GPa. E'' increases first and then decreases; representing a peak at $\sim 70.2^\circ\text{C}$ call as glass transition temperature of the material. $\tan \delta$ (E'/E'') indicates the same tendency as E'' . The rubbery state of the material is then in the zone of temperature higher than 85°C . Presumably, the value of E' is low and the sample is relatively soft.

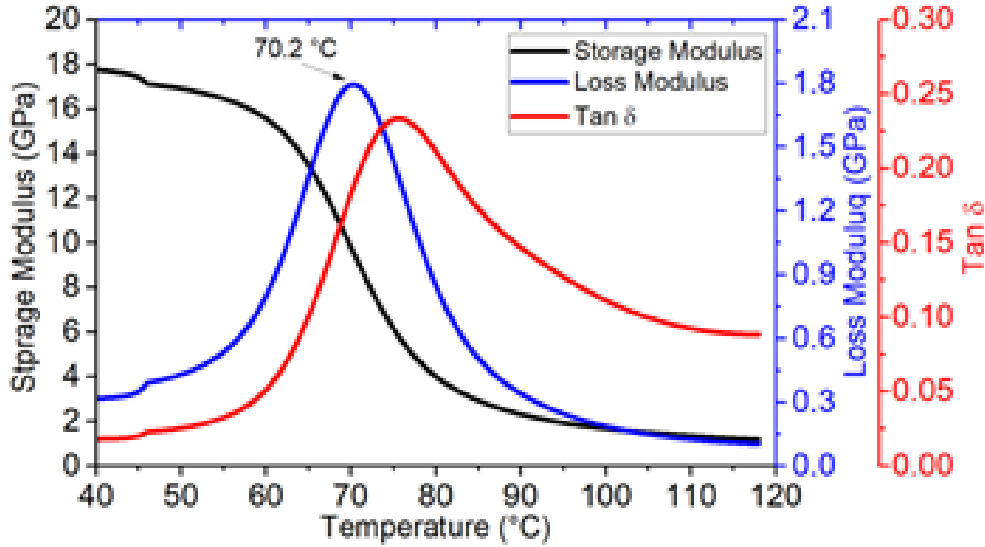


Figure 5.5: DMTA test result for PLA

Consequently, to explore the influence of temperature on viscoelastic properties of PLA, multi-frequencies DMA test was implemented in flexural bending mode. The evolution of viscosity could be calculated using Williams-Landel-Ferry (WLF) equation:

$$\text{Log } a_T = \frac{-C_1(T - T_r)}{C_2 + (T - T_r)} \quad (5.6)$$

where a_T is WLF shift factor, C_1 and C_2 are empirical constants adjusted to fit the values of superposition parameter a_T , T is the temperature, and T_r is the reference temperature at the reference frequency.

Using linear regression method, WLF equation could be transformed to the following equation:

$$\frac{1}{\log a_T} = \frac{-C_2}{C_1} \frac{1}{T - T_r} + \frac{1}{C_1} \quad (5.7)$$

Then, $\frac{1}{\log a_T}$ was plotted versus $\frac{1}{T - T_r}$. The fitted curve is shown in Figure 5.6 ($R^2=0.9993$). The value of C_1 and C_2 are then calculated using the obtained results.

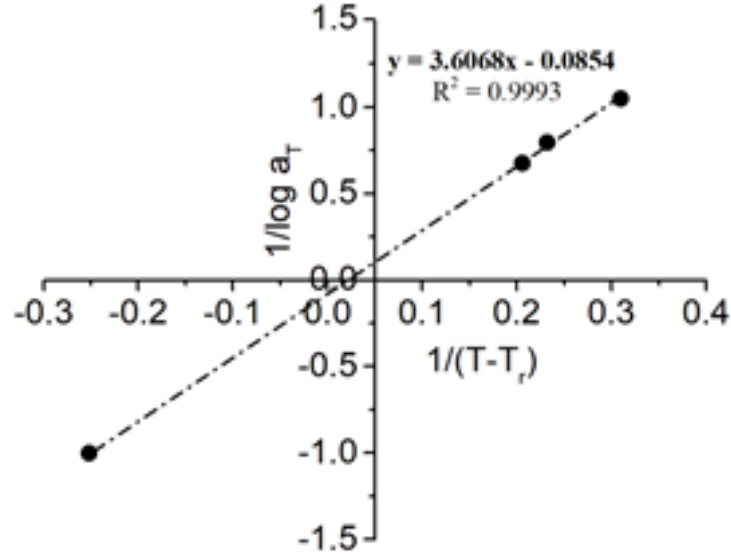


Figure 5.6: Linear regression of WLF equation

Also, the shift factor, a_T , is defined as $\frac{\eta}{\eta_0}$ resulting in the following equation:

$$\eta = \eta_0 \left[10^{\frac{11.7(T-70.2)}{T-28}} \right] \quad (5.8)$$

Substituting Equation 5.3 in Equation 5.8, we obtain:

$$\eta = \eta_0 \left[10^{\frac{11.7(T=T_\infty+(T_0-T_\infty)e^{-\frac{2h}{\rho C_p a_0 t}-70.2}}{T=T_\infty+(T_0-T_\infty)e^{-\frac{2h}{\rho C_p a_0 t}-28}} \right]} \quad (5.9)$$

Equation 5.9 is the temperature dependent viscosity of the polymer at solid state (commonly for $T_{amb} < T < T_g + 50$ °C). Following the presented results in section 5.1, the TTT diagram of a single filament during its deposition at a specific amount of time has been presented indicating the corrected viscosity obtained by WLF equation. From the beginning of the deposition ($T = 210$ °C), temperature dependence viscosity (Arrhenius equation) until $t = 1.8$ s ($T = 110$ °C) has been presented. Then, from $t = 1.8$ s ($T = 110$ °C) until $t = 17.4$ s ($T = 57$ °C), temperature dependence viscosity obtained by WLF equation has been plotted. The considerable shift between two curves clearly shows the viscoelastic behavior of the material.

As highlighted in Figure 5.7, zone 1-3 correspond to the rubbery state, glass transition zone, and glassy state, respectively. In the rubbery state, there is a gradual increase in viscosity by entering the zone in which glass transition occurs, whereas the viscosity evolution remains almost constant in glassy state. Although the viscoelastic behavior of the mate-

material has been taken into consideration using WLF equation, believably an abrupt increase must occur as a result of two phase changes, in melting zone and crystallization zone, respectively. In the proposed approach, this term is not included as it should separately be studied.

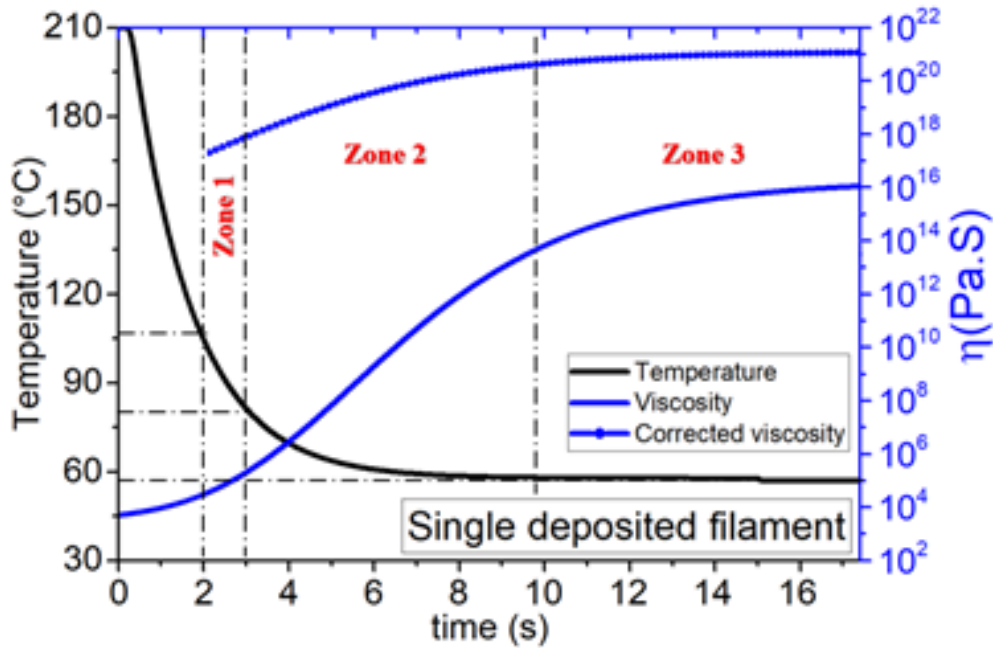


Figure 5.7: TTT diagram of a single filament deposition using WLF prediction

The main characteristic of the presented approach is the possibility of obtaining the Time-Temperature-Transformation diagram of material during deposition and apply the findings in optimization procedures. It has been shown that viscosity that is affected by the cyclic temperature profile could determine the characteristic of final products. Its variation through the consequence of layers has been presented. Furthermore, a parametric study on the influence of process parameters upon viscosity evolution has also been performed. The influence of print speed and platform temperature on the evolution of viscosity indicates that the effect of process parameters is inevitable and interaction of parameters should be taken into account.

Also, the influence of cyclic temperature profile on the viscoelastic behavior of the material using WLF equation indicated that the viscosity variation in solid state plays an important role in the rheological characteristic of the material. The results presented here may help researchers to improve the quality of constructed parts in FDM/FFF and consequently ameliorate their strength.

Conclusion and perspectives

This thesis was carried out between two laboratories, LIFSE and PIMM, at Arts et Métiers institute of Technology. It aims to study the rheological characteristics of materials during FDM/FFF process by performing experimental and numerical approaches. In addition, an in situ technique for measurement of temperature evolution of deposited layers at their interfaces has been proposed.

This work is the resumption of the experimental results obtained using a local recording of temperature profile (A. Kallel et al. [111]). Their results relate to adding thermocouples to the build simultaneously with the fabrication and they indicated that it is possible to measure locally the temperature variation locally without damaging or pausing the process. Although a drop of approximately 50 °C was observed on the recorded experimental data, the preliminary results open a new way and let us to continue the work to have more precise and considerable results.

At the early stage, a bibliographic study was carried out on the role of process variables and heat transfer as well as the variation of viscosity on the part quality. Regarding the process parameters, the role of three parameters as Liquefier temperature, Platform temperature, and Print speed on the mechanical strength and quality of the final part has been discussed. Then, the influence of these parameters on temperature variation of filaments during deposition was experimentally discussed. To do this, a local measurement technique using K-type thermocouples ($d=80\ \mu\text{m}$) was employed letting us to recognize the temperature variation of each layer during the deposition stage. Our observations allow us to have a set of conclusions through the influence of the mentioned process parameters:

- Interaction of parameters plays the most important role in consideration of mechanical characterization of printed parts.
- Young's modulus and failure strain could be an indicator to evaluate the mechanical

performance of printed parts.

- Temperature of filaments plays an important role in the characteristics of printed parts.
- The consequence of deposition in different conditions shows that increasing the liquefier temperature is more significant on the contact of filaments, however, the impact of print speed is more considerable.
- The liquefier temperature and print speed have higher impact on the temperature evolution of filaments.

The recorded temperature profile was then compared with the results obtained by employing IR-camera as a global approach letting us record the temperature variation at the external surface of deposited layers. In these two approaches, despite the advantages and limitations of each, the obtained results showed that there is a remarkable difference between the cooling rate and re-heating peaks. This outcome makes it possible to consider the proposed technique as a promising approach for further steps (**Article No. 7**).

Finite volume method was applied to model the heat transfer of deposited filaments and then was validated by the mentioned technique for in situ temperature measurement. The temperature evolution was predicted in good agreement with the recorded experimental results. To show the usefulness of the developed code, efforts have been taken into account, for optimization purposes, to consider the influence of major process variables on the temperature variation of the filaments while depositing. Conventionally, the parameters are determined based on the fact that by decreasing the cooling rate of the material, it keeps its temperature high enough for having better adhesion with the previously deposited filament or the one that is under deposition.

The obtained results were then embedded into the rheological characteristic of filaments by modeling the viscosity evolution of filaments and the effect of major process variables on them. The idea, therefore, is to evaluate together the influence of process variables and temperature evolution of filaments simultaneously to be implemented into the evolution of non-isotherm viscosity of filament during deposition. So, efforts have been made to propose a ‘Time-Temperature-Transformation’ (TTT) diagram of filaments during deposition enabling the evaluation of temperature and viscosity simultaneously. The consequence of this study is then a computer code that considers the obtained results and predictions, with the potential

of letting researchers in optimizing the process to obtain good final parts.

In summary, this work has contributed to the development of a code allowing the prediction of the temperature evolution of filaments. It is based on the modeling of heat transfer and related engaged phenomena. The next step would be the implementation of rheological parameters together with the related parameters for optimization purposes (**Article No. 8**).

Bibliography

- [1] Bahaa Shaqour et al. “Gaining a better understanding of the extrusion process in fused filament fabrication 3D printing: a review”. In: *The International Journal of Advanced Manufacturing Technology* (2021), pp. 1–13.
- [2] Rafiq Noorani. *Rapid prototyping: principles and applications*. John Wiley & Sons Incorporated, 2006.
- [3] Kaufui V Wong and Aldo Hernandez. “A review of additive manufacturing”. In: *International scholarly research notices 2012* (2012).
- [4] Steven Ashley. “Rapid prototyping systems”. In: *Mechanical engineering* 113.4 (1991), p. 34.
- [5] Jeffrey W Stansbury and Mike J Idacavage. “3D printing with polymers: Challenges among expanding options and opportunities”. In: *Dental materials* 32.1 (2016), pp. 54–64.
- [6] Terry Wohlers and Tim Gornet. “History of additive manufacturing”. In: *Wohlers report* 24.2014 (2014), p. 118.
- [7] Daniel P Cole et al. “Interfacial mechanical behavior of 3D printed ABS”. In: *Journal of Applied Polymer Science* 133.30 (2016).
- [8] Prashant Kulkarni, Anne Marsan, and Debasish Dutta. “A review of process planning techniques in layered manufacturing”. In: *Rapid prototyping journal* (2000).
- [9] Edson Costa Santos et al. “Rapid manufacturing of metal components by laser forming”. In: *International Journal of Machine Tools and Manufacture* 46.12-13 (2006), pp. 1459–1468.
- [10] Shan-Shan Yao et al. “Recent advances in carbon-fiber-reinforced thermoplastic composites: A review”. In: *Composites Part B: Engineering* 142 (2018), pp. 241–250.

- [11] Jan Holmström et al. “Rapid manufacturing in the spare parts supply chain: Alternative approaches to capacity deployment”. In: *Journal of Manufacturing Technology Management* (2010).
- [12] Mark Vitale, Mark Cotteleer, and Jonathan Holdowsky. “An Overview of Additive Manufacturing”. In: *Defense AT&L, November-December* (2016).
- [13] Andreas Gebhardt. “Rapid Prototyping–Rapid Tooling–Rapid Manufacturing”. In: *Carl Hanser, München* (2007).
- [14] ML Shofner et al. “Nanofiber-reinforced polymers prepared by fused deposition modeling”. In: *Journal of applied polymer science* 89.11 (2003), pp. 3081–3090.
- [15] Kazi Moshir Rahman, Todd Letcher, and Riley Reese. “Mechanical properties of additively manufactured PEEK components using fused filament fabrication”. In: *ASME International Mechanical Engineering Congress and Exposition*. Vol. 57359. American Society of Mechanical Engineers. 2015, V02AT02A009.
- [16] Anoop K Sood, Raj K Ohdar, and Siba S Mahapatra. “Experimental investigation and empirical modelling of FDM process for compressive strength improvement”. In: *Journal of Advanced Research* 3.1 (2012), pp. 81–90.
- [17] Rafael A Auras et al. “Mechanical, physical, and barrier properties of poly (lactide) films”. In: *Journal of plastic film & sheeting* 19.2 (2003), pp. 123–135.
- [18] Rathin Datta and Michael Henry. “Lactic acid: recent advances in products, processes and technologies—a review”. In: *Journal of Chemical Technology & Biotechnology: International Research in Process, Environmental & Clean Technology* 81.7 (2006), pp. 1119–1129.
- [19] Yoshito Ikada and Hideto Tsuji. “Biodegradable polyesters for medical and ecological applications”. In: *Macromolecular rapid communications* 21.3 (2000), pp. 117–132.
- [20] Rafael Auras, Bruce Harte, and Susan Selke. “An overview of polylactides as packaging materials”. In: *Macromolecular bioscience* 4.9 (2004), pp. 835–864.
- [21] Matthew H Hutchinson et al. “Optical properties of polylactides”. In: *Journal of Polymers and the Environment* 14.2 (2006), pp. 119–124.
- [22] JR Sarasua et al. “Crystallinity and mechanical properties of optically pure polylactides and their blends”. In: *Polymer Engineering & Science* 45.5 (2005), pp. 745–753.

- [23] Marek Pyda, RC Bopp, and B Wunderlich. “Heat capacity of poly (lactic acid)”. In: *The Journal of Chemical Thermodynamics* 36.9 (2004), pp. 731–742.
- [24] Takayuki Tsukegi et al. “Racemization behavior of l, l-lactide during heating”. In: *Polymer degradation and stability* 92.4 (2007), pp. 552–559.
- [25] Yujiang Fan et al. “Control of racemization for feedstock recycling of PLLA”. In: *Green Chemistry* 5.5 (2003), pp. 575–579.
- [26] Amar K Mohanty, Manjusri Misra, and Lawrence T Drzal. *Natural fibers, biopolymers, and biocomposites*. CRC press, 2005.
- [27] Ryan Vadori, Amar K Mohanty, and Manju Misra. “The Effect of Mold Temperature on the Performance of Injection Molded Poly (Lactic Acid)-Based Bioplastic”. In: *Macromolecular Materials and Engineering* 298.9 (2013), pp. 981–990.
- [28] Alberto Cattenone et al. “Finite element analysis of additive manufacturing based on fused deposition modeling: distortions prediction and comparison with experimental data”. In: *Journal of Manufacturing Science and Engineering* 141.1 (2019), p. 011010.
- [29] Shady Farah, Daniel G Anderson, and Robert Langer. “Physical and mechanical properties of PLA, and their functions in widespread applications—A comprehensive review”. In: *Advanced drug delivery reviews* 107 (2016), pp. 367–392.
- [30] Anouar El Magri et al. “Optimization of printing parameters for improvement of mechanical and thermal performances of 3D printed poly (ether ether ketone) parts”. In: *Journal of Applied Polymer Science* 137.37 (2020), p. 49087.
- [31] Sung-Hoon Ahn et al. “Anisotropic material properties of fused deposition modeling ABS”. In: *Rapid prototyping journal* (2002).
- [32] P Chennakesava and Y Shivraj Narayan. “Fused deposition modeling-insights”. In: *Proceedings of the international conference on advances in design and manufacturing ICAD&M*. Vol. 14. 2014, pp. 1345–1350.
- [33] DR Katti, A Sharma, and KS Katti. “Predictive methodologies for design of bone tissue engineering scaffolds”. In: *Materials for bone disorders*. Elsevier, 2017, pp. 453–492.
- [34] Filip Górski et al. “Strength of ABS parts produced by Fused Deposition Modelling technology—a critical orientation problem”. In: *Advances in Science and Technology Research Journal* 9.26 (2015), pp. 12–19.

- [35] CS Lee et al. “Measurement of anisotropic compressive strength of rapid prototyping parts”. In: *Journal of materials processing technology* 187 (2007), pp. 627–630.
- [36] OS Es-Said et al. “Effect of layer orientation on mechanical properties of rapid prototyped samples”. In: *Materials and Manufacturing Processes* 15.1 (2000), pp. 107–122.
- [37] Peng Wang et al. “Effects of printing parameters of fused deposition modeling on mechanical properties, surface quality, and microstructure of PEEK”. In: *Journal of Materials Processing Technology* 271 (2019), pp. 62–74.
- [38] Wenzheng Wu et al. “Influence of layer thickness and raster angle on the mechanical properties of 3D-printed PEEK and a comparative mechanical study between PEEK and ABS”. In: *Materials* 8.9 (2015), pp. 5834–5846.
- [39] Kate Iren Byberg, Aboma Wagari Gebisa, and Hirpa G Lemu. “Mechanical properties of ULTEM 9085 material processed by fused deposition modeling”. In: *Polymer Testing* 72 (2018), pp. 335–347.
- [40] Albert Forés-Garriga et al. “Role of infill parameters on the mechanical performance and weight reduction of PEI Ultem processed by FFF”. In: *Materials & Design* 193 (2020), p. 108810.
- [41] Walter Castro Smith and Richard W Dean. “Structural characteristics of fused deposition modeling polycarbonate material”. In: *Polymer testing* 32.8 (2013), pp. 1306–1312.
- [42] Volker Schöppner and Kunststofftechnik Paderborn KTP. “Mechanical properties of fused deposition modeling parts manufactured with Ultem* 9085”. In: *Proceedings of the 69th Annual Technical Conference of the Society of Plastics Engineers (ANTEC’11), Boston, MA, USA*. 2011, pp. 1–5.
- [43] Syed H Masood, Kalpeshkumar Mau, and WQ Song. “Tensile properties of processed FDM polycarbonate material”. In: *Materials Science Forum*. Vol. 654. Trans Tech Publ. 2010, pp. 2556–2559.
- [44] Krishna P Motaparti et al. “Effects of build parameters on compression properties for ULTEM 9085 parts by fused deposition modeling”. In: (2016).
- [45] Byoung Hun Lee, Jamaluddin Abdullah, and Zahid A Khan. “Optimization of rapid prototyping parameters for production of flexible ABS object”. In: *Journal of materials processing technology* 169.1 (2005), pp. 54–61.

- [46] Caterina Casavola et al. “Orthotropic mechanical properties of fused deposition modelling parts described by classical laminate theory”. In: *Materials & design* 90 (2016), pp. 453–458.
- [47] Sandeep Rathee et al. “Effect of varying spatial orientations on build time requirements for FDM process: A case study”. In: *Defence technology* 13.2 (2017), pp. 92–100.
- [48] Omar Ahmed Mohamed, Syed Hasan Masood, and Jahar Lal Bhowmik. “Process parameter optimization of viscoelastic properties of FDM manufactured parts using response surface methodology”. In: *Materials Today: Proceedings* 4.8 (2017), pp. 8250–8259.
- [49] Michael Arthur Cuiffo et al. “Impact of the fused deposition (FDM) printing process on polylactic acid (PLA) chemistry and structure”. In: *Applied Sciences* 7.6 (2017), p. 579.
- [50] JM Chacón et al. “Additive manufacturing of PLA structures using fused deposition modelling: Effect of process parameters on mechanical properties and their optimal selection”. In: *Materials & Design* 124 (2017), pp. 143–157.
- [51] Ryosuke Matsuzaki et al. “Three-dimensional printing of continuous-fiber composites by in-nozzle impregnation”. In: *Scientific reports* 6.1 (2016), pp. 1–7.
- [52] S Budhe et al. “An updated review of adhesively bonded joints in composite materials”. In: *International Journal of Adhesion and Adhesives* 72 (2017), pp. 30–42.
- [53] Sun Xiaoyong et al. “Experimental analysis of high temperature PEEK materials on 3D printing test”. In: *2017 9th International conference on measuring technology and mechatronics automation (ICMTMA)*. IEEE. 2017, pp. 13–16.
- [54] Xinhua Liu et al. “Mechanical property parametric appraisal of fused deposition modeling parts based on the gray Taguchi method”. In: *The International Journal of Advanced Manufacturing Technology* 89.5 (2017), pp. 2387–2397.
- [55] Krishna Prasanth Motaparti. *Effect of build parameters on mechanical properties of ultem 9085 parts by fused deposition modeling*. Missouri University of Science and Technology, 2016.
- [56] Jason T Cantrell et al. “Experimental characterization of the mechanical properties of 3D-printed ABS and polycarbonate parts”. In: *Rapid Prototyping Journal* (2017).

- [57] Shahrain Mahmood et al. “Tensile strength of partially filled FFF printed parts: experimental results”. In: *Rapid prototyping journal* (2017).
- [58] Todd Letcher, Behzad Rankouhi, and Sina Javadpour. “Experimental study of mechanical properties of additively manufactured ABS plastic as a function of layer parameters”. In: *ASME International Mechanical Engineering Congress and Exposition*. Vol. 57359. American Society of Mechanical Engineers. 2015, V02AT02A018.
- [59] Jonathan Torres et al. “Mechanical property optimization of FDM PLA in shear with multiple objectives”. In: *Jom* 67.5 (2015), pp. 1183–1193.
- [60] Kyle Raney, Eric Lani, and Devi K Kalla. “Experimental characterization of the tensile strength of ABS parts manufactured by fused deposition modeling process”. In: *Materials Today: Proceedings* 4.8 (2017), pp. 7956–7961.
- [61] RJ Zaldivar et al. “Influence of processing and orientation print effects on the mechanical and thermal behavior of 3D-Printed ULTEM® 9085 Material”. In: *Additive Manufacturing* 13 (2017), pp. 71–80.
- [62] Xiaohu Deng et al. “Mechanical properties optimization of poly-ether-ether-ketone via fused deposition modeling”. In: *Materials* 11.2 (2018), p. 216.
- [63] Vinaykumar S Jatti et al. “A Study On Effect Of Fused Deposition Modeling Process Parameters On Mechanical Properties”. In: *Int. J. Sci. Technol. Res* 8 (2019), pp. 689–693.
- [64] Timothy J Coogan and David Owen Kazmer. “Bond and part strength in fused deposition modeling”. In: *Rapid Prototyping Journal* (2017).
- [65] Fuda Ning et al. “Additive manufacturing of carbon fiber reinforced thermoplastic composites using fused deposition modeling”. In: *Composites Part B: Engineering* 80 (2015), pp. 369–378.
- [66] Sofiane Guessasma, Sofiane Belhabib, and Hedi Nouri. “Thermal cycling, microstructure and tensile performance of pla-pha polymer printed using fused deposition modelling technique”. In: *Rapid Prototyping Journal* (2020).
- [67] Shenglong Jiang et al. “Mechanical properties analysis of polyetherimide parts fabricated by fused deposition modeling”. In: *High Performance Polymers* 31.1 (2019), pp. 97–106.

- [68] Chuncheng Yang et al. “Influence of thermal processing conditions in 3D printing on the crystallinity and mechanical properties of PEEK material”. In: *Journal of Materials Processing Technology* 248 (2017), pp. 1–7.
- [69] Shouling Ding et al. “Effects of nozzle temperature and building orientation on mechanical properties and microstructure of PEEK and PEI printed by 3D-FDM”. In: *Polymer Testing* 78 (2019), p. 105948.
- [70] S Berretta et al. “Fused Deposition Modelling of high temperature polymers: Exploring CNT PEEK composites”. In: *Polymer Testing* 63 (2017), pp. 251–262.
- [71] Mario D Monzón et al. “Process and material behavior modeling for a new design of micro-additive fused deposition”. In: *The International Journal of Advanced Manufacturing Technology* 67.9-12 (2013), pp. 2717–2726.
- [72] Nahal Aliheidari et al. “Fracture resistance measurement of fused deposition modeling 3D printed polymers”. In: *Polymer Testing* 60 (2017), pp. 94–101.
- [73] Q Sun et al. “Effect of processing conditions on the bonding quality of FDM polymer filaments”. In: *Rapid prototyping journal* (2008).
- [74] KG Jaya Christiyan, U Chandrasekhar, and K Venkateswarlu. “A study on the influence of process parameters on the Mechanical Properties of 3D printed ABS composite”. In: *IOP Conference Series: Materials Science and Engineering*. Vol. 114. 1. IOP Publishing. 2016, p. 012109.
- [75] Chamil Abeykoon, Pimpisut Sri-Amphorn, and Anura Fernando. “Optimization of fused deposition modeling parameters for improved PLA and ABS 3D printed structures”. In: *International Journal of Lightweight Materials and Manufacture* 3.3 (2020), pp. 284–297.
- [76] Peng Geng et al. “Effects of extrusion speed and printing speed on the 3D printing stability of extruded PEEK filament”. In: *Journal of Manufacturing Processes* 37 (2019), pp. 266–273.
- [77] Céline Bellehumeur et al. “Modeling of bond formation between polymer filaments in the fused deposition modeling process”. In: *Journal of manufacturing processes* 6.2 (2004), pp. 170–178.
- [78] SF Costa, FM Duarte, and JA Covas. “Towards modelling of Free Form Extrusion: analytical solution of transient heat transfer”. In: *International Journal of Material Forming* 1.1 (2008), pp. 703–706.

- [79] SF Costa, FM Duarte, and JA Covas. “Thermal conditions affecting heat transfer in FDM/FFE: a contribution towards the numerical modelling of the process: This paper investigates convection, conduction and radiation phenomena in the filament deposition process”. In: *Virtual and Physical Prototyping* 10.1 (2015), pp. 35–46.
- [80] JP Thomas and JF Rodriguez. “Modeling the fracture strength between fused-deposition extruded roads 16”. In: *2000 International solid freeform fabrication symposium*. 2000.
- [81] M Atif Yardimci and Selçuk Güçeri. “Conceptual framework for the thermal process modelling of fused deposition”. In: *Rapid Prototyping Journal* (1996).
- [82] M Atif Yardimci et al. “Thermal analysis of fused deposition”. In: *1997 international solid freeform fabrication symposium*. 1997.
- [83] Y Zhang and YK Chou. “Three-dimensional finite element analysis simulations of the fused deposition modelling process”. In: *Proceedings of the Institution of Mechanical Engineers, Part B: Journal of Engineering Manufacture* 220.10 (2006), pp. 1663–1671.
- [84] Liang Bo Ji and Tian Rui Zhou. “Finite element simulation of temperature field in fused deposition modeling”. In: *Advanced Materials Research*. Vol. 97. Trans Tech Publ. 2010, pp. 2585–2588.
- [85] Fang Peng, Bryan D Vogt, and Miko Cakmak. “Complex flow and temperature history during melt extrusion in material extrusion additive manufacturing”. In: *Additive Manufacturing* 22 (2018), pp. 197–206.
- [86] Marcin P Serdeczny et al. “Experimental and analytical study of the polymer melt flow through the hot-end in material extrusion additive manufacturing”. In: *Additive Manufacturing* 32 (2020), p. 100997.
- [87] Dries Vaes et al. “Assessment of crystallinity development during fused filament fabrication through fast scanning chip calorimetry”. In: *Applied Sciences* 9.13 (2019), p. 2676.
- [88] Jonathan E Seppala and Kalman D Migler. “Infrared thermography of welding zones produced by polymer extrusion additive manufacturing”. In: *Additive manufacturing* 12 (2016), pp. 71–76.
- [89] Anthony D’Amico and Amy M Peterson. “An adaptable FEA simulation of material extrusion additive manufacturing heat transfer in 3D”. In: *Additive Manufacturing* 21 (2018), pp. 422–430.

- [90] SF Costa, FM Duarte, and JA Covas. “Estimation of filament temperature and adhesion development in fused deposition techniques”. In: *Journal of Materials Processing Technology* 245 (2017), pp. 167–179.
- [91] Uwe Scheithauer et al. “Thermoplastic 3D printing—an additive manufacturing method for producing dense ceramics”. In: *International journal of applied ceramic technology* 12.1 (2015), pp. 26–31.
- [92] JJ Fitzpatrick et al. “Comparing the caking behaviours of skim milk powder, amorphous maltodextrin and crystalline common salt”. In: *Powder Technology* 204.1 (2010), pp. 131–137.
- [93] M Kasmaee et al. “Effects of different surfactants and physical properties on the coalescence of dimethyl disulfide drops with mother phase at the interface of sodium hydroxide aqueous solutions”. In: *Journal of Molecular Liquids* 263 (2018), pp. 31–39.
- [94] Markus Gross et al. “Viscous coalescence of droplets: A lattice Boltzmann study”. In: *Physics of Fluids* 25.5 (2013), p. 052101.
- [95] Mohammadmahdi Kamyabi et al. “Principles of viscous sintering in amorphous powders: A critical review”. In: *Chemical Engineering Research and Design* 125 (2017), pp. 328–347.
- [96] JJ Frenkel. “Viscous flow of crystalline bodies under the action of surface tension”. In: *J. phys.* 9 (1945), p. 385.
- [97] Ondřej Pokluda, Céline T Bellehumeur, and John Vlachopoulos. “Modification of Frenkel’s model for sintering”. In: *AIChE journal* 43.12 (1997), pp. 3253–3256.
- [98] CT Bellehumeur, MK Bisaria, and J Vlachopoulos. “An experimental study and model assessment of polymer sintering”. In: *Polymer Engineering & Science* 36.17 (1996), pp. 2198–2207.
- [99] Robert W Hopper. “Coalescence of two equal cylinders: exact results for creeping viscous plane flow driven by capillarity”. In: *Journal of the American Ceramic Society* 67.12 (1984), pp. C–262.
- [100] RM Tarafdar and TL Bergman. “Detailed numerical and experimental investigation of non-isothermal sintering of amorphous polymer material”. In: *J. Heat Transfer* 124.3 (2002), pp. 553–563.
- [101] Fabian B Wadsworth et al. “Nonisothermal viscous sintering of volcanic ash”. In: *Journal of Geophysical Research: Solid Earth* 119.12 (2014), pp. 8792–8804.

- [102] Deep Bhalodi, Karan Zalavadiya, and Pavan Kumar Gurrala. “Influence of temperature on polymer parts manufactured by fused deposition modeling process”. In: *Journal of the Brazilian Society of Mechanical Sciences and Engineering* 41.3 (2019), p. 113.
- [103] Nickolas D Polychronopoulos and John Vlachopoulos. “The role of heating and cooling in viscous sintering of pairs of spheres and pairs of cylinders”. In: *Rapid Prototyping Journal* (2020).
- [104] Mukesh K Agarwala et al. “Structural quality of parts processed by fused deposition”. In: *Rapid prototyping journal* (1996).
- [105] Anna Bellini, Selc uk Gu c eri, and Maurizio Bertoldi. “Liquefier dynamics in fused deposition”. In: *J. Manuf. Sci. Eng.* 126.2 (2004), pp. 237–246.
- [106] KPPM Thrimurthulu, Pulak M Pandey, and N Venkata Reddy. “Optimum part deposition orientation in fused deposition modeling”. In: *International Journal of Machine Tools and Manufacture* 44.6 (2004), pp. 585–594.
- [107] Xin Wang et al. “3D printing of polymer matrix composites: A review and prospective”. In: *Composites Part B: Engineering* 110 (2017), pp. 442–458.
- [108] Pedram Parandoush and Dong Lin. “A review on additive manufacturing of polymer-fiber composites”. In: *Composite Structures* 182 (2017), pp. 36–53.
- [109] Jasgurpreet Singh Chohan et al. “Dimensional accuracy analysis of coupled fused deposition modeling and vapour smoothing operations for biomedical applications”. In: *Composites Part B: Engineering* 117 (2017), pp. 138–149.
- [110] Omar A Mohamed, Syed H Masood, and Jahar L Bhowmik. “Optimization of fused deposition modeling process parameters: a review of current research and future prospects”. In: *Advances in Manufacturing* 3.1 (2015), pp. 42–53.
- [111] Achraf Kallel et al. “Study of Bonding Formation between the Filaments of PLA in FFF Process”. In: *International Polymer Processing* 34.4 (2019), pp. 434–444.
- [112] SF Costa, FM Duarte, and JA Covas. “An analytical solution for heat transfer during deposition in extrusion-based 3D printing techniques”. In: *Proceedings of the 15th International Conference Computational and Mathematical Methods in Science and Engineering*. 2015, pp. 1161–1172.

- [113] F Yang and R Pitchumani. “Healing of thermoplastic polymers at an interface under nonisothermal conditions”. In: *Macromolecules* 35.8 (2002), pp. 3213–3224.
- [114] José F Rodriguez, James P Thomas, and John E Renaud. “Mechanical behavior of acrylonitrile butadiene styrene (ABS) fused deposition materials. Experimental investigation”. In: *Rapid Prototyping Journal* (2001).
- [115] Allan D Kraus et al. “Extended surface heat transfer”. In: *Appl. Mech. Rev.* 54.5 (2001), B92–B92.
- [116] Suhas V Patankar and D Brian Spalding. “A calculation procedure for heat, mass and momentum transfer in three-dimensional parabolic flows”. In: *Numerical prediction of flow, heat transfer, turbulence and combustion*. Elsevier, 1983, pp. 54–73.
- [117] Darshan Ravoori et al. “Investigation of process-structure-property relationships in polymer extrusion based additive manufacturing through in situ high speed imaging and thermal conductivity measurements”. In: *Additive Manufacturing* 23 (2018), pp. 132–139.
- [118] Hardikkumar Prajapati et al. “Measurement of anisotropic thermal conductivity and inter-layer thermal contact resistance in polymer fused deposition modeling (FDM)”. In: *Additive Manufacturing* 21 (2018), pp. 84–90.
- [119] Anouar El Magri et al. “Mechanical properties of CF-reinforced PLA parts manufactured by fused deposition modeling”. In: *Journal of Thermoplastic Composite Materials* 34.5 (2021), pp. 581–595.

Appendix : Résumé en français

Appendix A

Introduction générale

Les problèmes de liaison efficace, de résistance réduite et de performances mécaniques des modèles 3D imprimés par fabrication de filaments fondus (FFF) sont des préoccupations majeures dans le domaine de l'impression 3D. La fabrication de filaments fondus - également connue sous le nom d'impression 3D - est largement utilisée afin de produire des prototypes pour des applications aérospatiales, médicales et automobiles. Lors de ce processus, un polymère thermoplastique est introduit dans un liquéfacteur qui extrude un filament tout en se déplaçant dans des plans X-Y successifs le long de la direction Z, pour fabriquer une pièce 3D couche par couche. Par conséquent, au fur et à mesure de l'impression, le filament chaud se dépose sur des filaments précédemment générés et en cours de refroidissement. Ceci provoque une augmentation de la température, qui engendre un temps pendant lequel les interfaces des filaments en contact sont au-dessus de la température de transition vitreuse (T_g), dans le cas des matériaux amorphes, ou de la température de cristallisation (T_c) pour les matériaux semi-cristallins, qui est nécessaire pour une bonne liaison. Par conséquent, chaque filament doit être à une température suffisamment élevée lors du dépôt, sans engendrer de déformations qui pourraient être dues à la gravité et au poids des filaments déposés dans les couches suivantes.

Etant donné que la viscosité dépend de la température, cette dépendance pourrait être corrélée à l'évolution de la température des filaments déposés. A partir de là, il est possible de créer une relation de dépendance entre la viscosité et la température simultanément. On obtient alors un diagramme TTT (Temps, Température, Transformation) du matériau qui permet d'étudier la viscosité et de la température à la fois.

Malgré les avantages du FDM/FFF, il doit être amélioré et optimisé pour répondre aux exigences de l'industrie. Cette optimisation pourrait être obtenue par la maximisation des

caractéristiques mécaniques et de la qualité du collage (objectif : qualité de la pièce), et par la minimisation du coût de la pièce et du temps de fabrication (objectif : optimisation des procédés).

Compte tenu des propos susmentionnées, l'évolution de la température au cours du processus FDM/FFF spécifie la qualité et la résistance mécanique des structures fabriquées. La surveillance expérimentale et les enquêtes analytiques sont toujours difficiles à réaliser lors de la FFF et le manque de connaissances pratiques laisse le problème de la liaison dans ce processus irrésolu. Étant donné que les caractéristiques rhéologiques sont fonction de la température, ainsi que les variables de processus mentionnées, sont largement affectées par l'évolution de la température des filaments pendant l'impression. Pour résumer, l'étude de la viscosité en fonction de la température et de la température des matériaux FFF pendant l'impression en est encore à ses débuts et elle régit la qualité de la liaison elle-même.

La présente thèse se base sur l'étude des variables les plus importantes qui contrôlent la qualité de liaison du produit final comme i) le profil de température et ii) la variation de viscosité en fonction de la température des filaments. La qualité du collage est principalement contrôlée par l'évolution de la température qui gère l'évolution de la viscosité des filaments, et affecte globalement la qualité de la pièce finale.

Par conséquent, deux phénomènes interdépendants seront considérés lors du processus FDM/FFF : le profil de température des filaments et la viscosité en fonction de la température. De plus, les variables du processus seront également considérées à chaque étape de l'étude (figure A.1). L'objectif est d'étudier les caractéristiques rhéologiques à la fois expérimentalement et numériquement (où ces trois phénomènes ainsi que les variables du procédé sont pris en compte et interdépendants), d'évaluer l'influence des paramètres du procédé ou de définir une condition appropriée pour optimiser la liaison et la qualité du produit final.

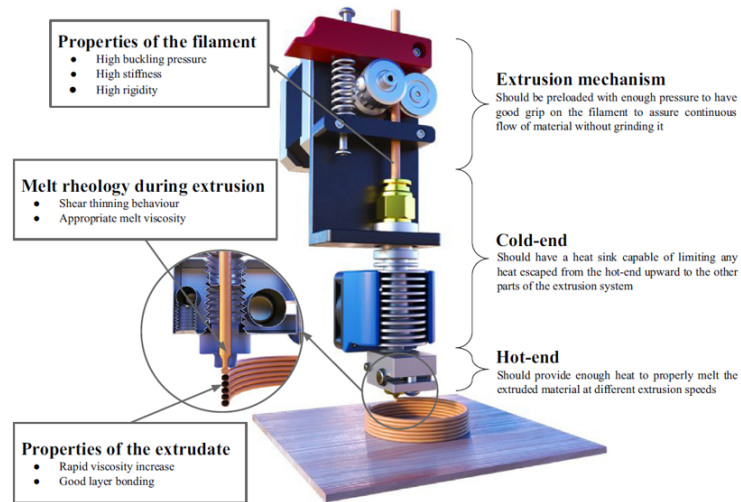


Figure A.1: Schéma des techniques AM [1]

L'objectif principal de cette recherche est d'étudier les caractéristiques rhéologiques des matériaux au cours du processus FDM/FFF. Pour atteindre cet objectif (voir la figure A.2), le profil de température des filaments et la viscosité en fonction de la température doivent être introduits et interconnectés pour être mis en œuvre. D'autre part, il est question d'optimiser le FDM/FFF en utilisant davantage l'interaction des variables du processus avec les phénomènes précédemment mentionnés. Cela permet alors de réaliser une étude paramétrique du procédé.

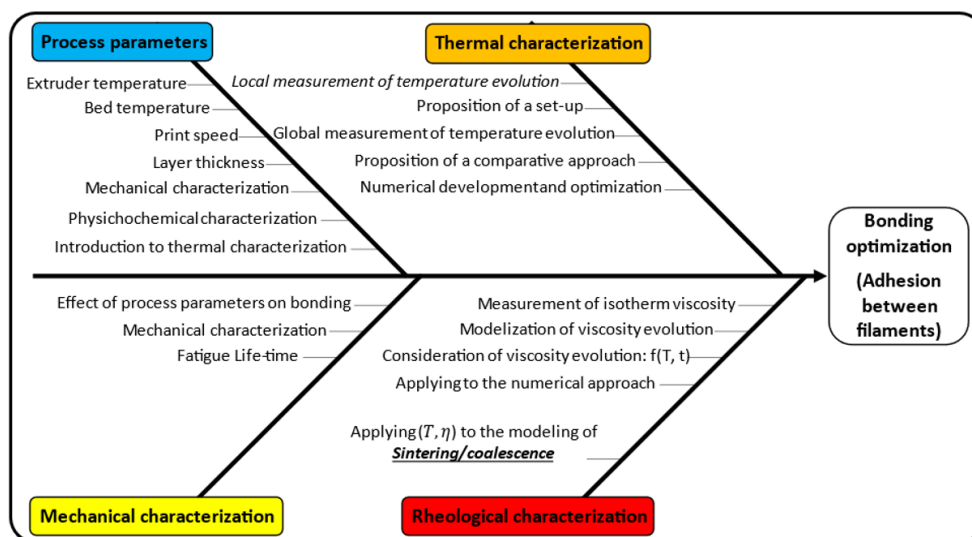


Figure A.2: Principaux éléments/défis existant dans ce processus

Cette thèse comprend 5 chapitres dont cette introduction:

Chapter 1: Étude bibliographique

Chapter 2: Évaluation expérimentale des paramètres de procédé

Chapter 3: Influence de variables de procédé: caractérisations initiale

Chapter 4: Modélisation de transfert thermique de FDM

Chapter 5: Diagramme de Temps-Température-Transformation du filament

En outre, les articles publiés de la présente thèse sont répertoriés comme suit :

Article No. 1: HR Vanaei, M Shirinbayan, M Deligant, K Raissi, S Khelladi, A Tcharkhtchi; Influence of process parameters on thermal and mechanical properties of PLA fabricated by Fused Filament Fabrication; *Polymer Engineering and Science Journal*, 60:1822–1831 (2020). DOI: 10.1002/pen.25419.

Article No. 2: HR Vanaei, K Raissi, M Deligant, M Shirinbayan, J Fitoussi, S Khelladi, A Tcharkhtchi; Towards the Understanding of Temperature Effect on Bonding Strength, Dimensions and Geometry of 3D-printed Parts; *J. of Mat. Sci.*, 55:14677–14689 (2020). DOI: 10.1007/s10853-020-05057-9.

Article No. 3: HR Vanaei, M Shirinbayan, SF Costa, FM Duarte, JA Covas, M Deligant, S Khelladi, A Tcharkhtchi; Experimental study of PLA Thermal Behavior during Fused Filament Fabrication (FFF); *Journal of Applied Polymer Science*, 138(4): 1-7 (2021). DOI: 10.1002/app.49747.

Article No. 4: HR Vanaei, M Deligant, M Shirinbayan, K Raissi, J Fitoussi, S Khelladi, A Tcharkhtchi; A comparative in-process monitoring of temperature profile in fused filament fabrication; *Polymer Engineering and Science Journal*, 61(1): 68-76 (2021). DOI: 10.1002/pen.25555.

Article No. 5: HR Vanaei, M Shirinbayan, S Vanaei, J Fitoussi, S Khelladi, A Tcharkhtchi; Multi-scale damage analysis and fatigue behavior of PLA manufactured by Fused Deposition Modeling (FDM); *Rapid prototyping Journal*, 27(2): 371-378 (2021). DOI: 10.1108/RPJ-11-2019-0300.

Article No. 6: HR Vanaei, S Khelladi, M Deligant, M Shirinbayan, A Tcharkhtchi; Numerical prediction for temperature profile of parts manufactured using fused filament fabrication; Submitted.

Article No. 7: HR Vanaei, M Shirinbayan, M Deligant, S Khelladi, A Tcharkhtchi; In-process monitoring of temperature evolution during Fused Filament Fabrication: A journey from numerical to experimental approaches; Accepted for publication in 2021.

Article No. 8: HR Vanaei, M Shirinbayan, S Khelladi, A Tcharkhtchi; Roadmap: Numerical and experimental characterization toward optimizing the 3D-printed parts – A review; Submitted.

Appendix B

Étude bibliographique

B.1. Fabrication Additive/Prototypage rapide

RP/FA est un terme générique pour un certain nombre de techniques dans lesquelles les composants sont fabriqués sans nécessiter d'outillage conventionnel. L'utilisation de ces techniques permet la construction automatique d'objets physiques à partir de modèles géométriques numériques et permet une production rapide de prototypes. Ces techniques permettent aussi la réduction considérable du temps de développement des produits [11]. Comme le montre la figure B.1, le flux du processus général RP/AM comprend les étapes suivantes du début au produit final : 1) modèle 3D basé sur la CAO, 2) fichier STL, 3) couches tranchées, 4) système RP/AM, 5) Finition de la partie finale. Le processus commence par l'utilisation d'un logiciel de CAO pour obtenir une géométrie 3D numérisée. Ensuite, le modèle est enregistré au format de fichier STL. À l'aide du logiciel des machines d'impression 3D, le modèle de fichier STL est discrétisé en couches individuelles. Enfin, en envoyant le fichier obtenu à la machine, celle-ci commence à imprimer des couches côte à côte (superposées) pour former le produit final. Il est à noter que la pièce finale peut être soumise à un certain post-traitement en fonction de la propriété et de l'application souhaitées de la pièce imprimée.

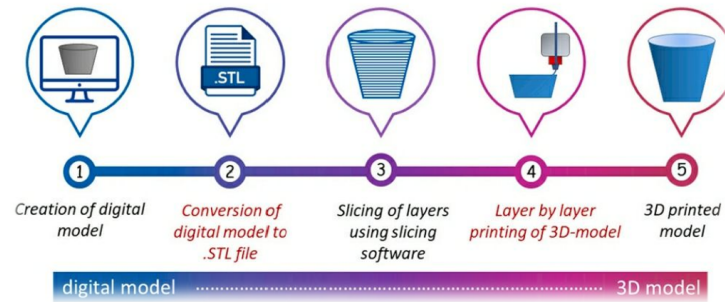


Figure B.1: Prototypage rapide et fabrication additive [12]

Les technologies de FA peuvent être classées en plusieurs catégories. Certains des principaux processus de FA sont classés comme suit :

- **Fused Deposition Modeling (FDM)**

En général, il est également connu sous le nom de fabrication de filaments fondus (FFF). Dans ce processus, le filament thermoplastique est fondu à l'intérieur de la tête d'extrusion (appelée liquéfacteur ou extrudeuse) et déposé sur une plaque de construction (appelée plate-forme/enveloppe/support). Des matériaux tels que les thermoplastiques renforcés et les filaments flexibles peuvent également être utilisés à la place des thermoplastiques.

- **Power Bed Fusion (PBF)**

Ce procédé utilise principalement un liant ou un faisceau laser pour fusionner la poudre en formant une pièce fonctionnelle. Des couches successives de poudre sont ensuite roulées sur la couche précédente et le processus se répète. Enfin, les pièces sont post-traitées si nécessaire. Les systèmes PBF les plus populaires sont le frittage laser sélectif (SLS) et la fusion laser sélective (SLM).

- **Stereolithography (SLA)**

Étant l'une des premières méthodes FA, SLA utilise la lumière ultraviolette (UV) pour polymériser la résine liquide qui se solidifie et, finalement, façonne la pièce. La résine non solidifiée est retirée après le processus d'impression. Alors que SLA peut imprimer avec une faible résolution, il a un choix limité de matériaux, un temps d'impression plus long ainsi que des coûts de matériaux élevés.

- **Laminated Object Manufacturing (LOM)**

est basé sur la découpe couche par couche et, éventuellement, le laminage de feuilles de différents matériaux. Les feuilles sont découpées avec une grande précision puis collées

ensemble ou vice versa. Le matériau non coupé est utilisé comme support et peut être recyclé après le processus d'impression.

B.2. Fused Deposition Modeling (FDM)

La modélisation par dépôt de fusion (FDM), également connue sous le nom de fabrication de filaments fusionnés (FFF), a été développée pour la première fois en 1988 par Scott Crump qui a co-fondé Stratasys Inc, USA et a ensuite été commercialisée en 1992 [13]. Il s'agit d'une fabrication solide de forme libre et forme des objets tridimensionnels à partir de modèles solides ou surfaciques générés par ordinateur. L'évolution et le développement des imprimantes 3D sont illustrés à la figure B.2.

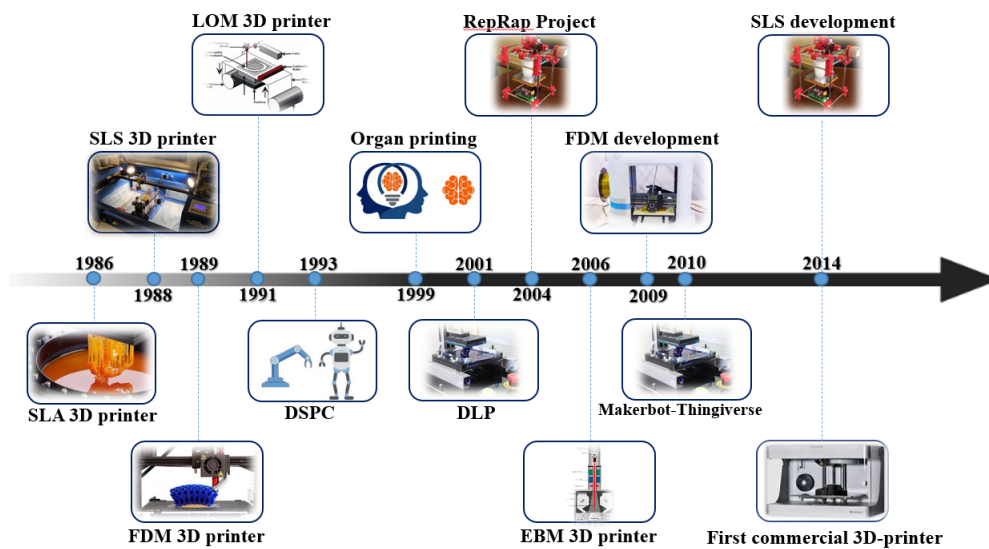


Figure B.2: Évolution des imprimantes 3D

La pièce souhaitée est, dans un premier temps, numérisée par un logiciel de CAO et est convertie en un fichier STL (format de fichier Stéréolithographie). Pendant le processus de fabrication et le dépôt de couche, le filament est chauffé à sa température de fusion pour être extrudé couche par couche à partir d'une pointe de buse dans une tête d'extrusion qui se déplace le long de la direction X-Y. La tête, commandée par un moteur, dépose de fines billes de matériau sur la surface de la plate-forme pour former la première couche qui se solidifie rapidement en raison de la basse température de la plate-forme [14]. La plaque de base est maintenue à une température plus basse pour aider le matériau à refroidir dans un environnement à température contrôlée lorsqu'il est posé dessus.

La plateau s'abaisse ensuite d'une distance spécifiée, c'est-à-dire que le liquéfacteur/buse

y dépose la deuxième couche. Ce processus se poursuit jusqu'à ce que la pièce soit construite conformément aux dimensions données. Avec la pièce, des supports de construction sont conçus pour supporter les sections les plus faibles et les structures suspendues de la pièce. Un diagramme schématique du processus FDM/FFF est fourni à la figure B.3.

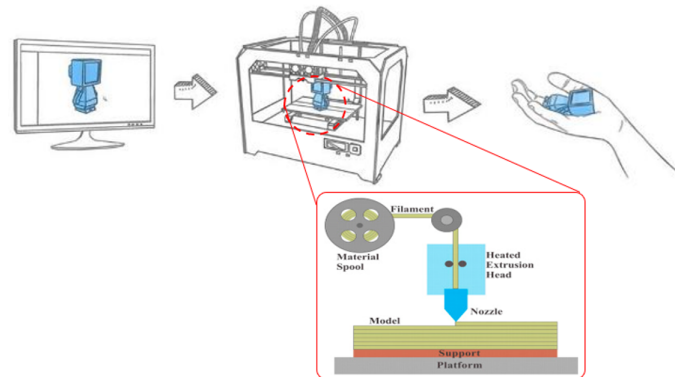


Figure B.3: Schéma du processus FDM/FFF

En comparant le processus FDM/FFF à d'autres processus AM, il existe plusieurs avantages tels que des coûts d'achat initiaux de machine inférieurs, un gaspillage minimal de matériau de construction, un retrait facile du matériau de support, une facilité d'utilisation et un risque réduit de contamination des matériaux et la sécurité des utilisateurs [15]. Certains des inconvénients incluent une faible précision dimensionnelle, une faible résistance des pièces et un temps de construction plus long. Le temps de fabrication et le coût d'une pièce FDM/FFF sont influencés par les paramètres de processus utilisés pour fabriquer les pièces. Par conséquent, il est très crucial de faire le bon choix des paramètres car la qualité de la pièce, y compris la résistance, la précision et la rugosité de surface, dépend principalement des paramètres du processus [16].

Ainsi, une étude approfondie de la littérature montre les limites suivantes :

- Une vue d'ensemble réalisée sur l'influence des paramètres du processus à travers la qualité des pièces fabriquées par le processus FDM/FFF semble avoir des incohérences dans les résultats obtenus. À titre d'exemple, une étude en 2002 a conclu que l'épaisseur de la couche a une influence moins significative sur la résistance à la traction, tandis qu'après 3 ans, d'autres chercheurs ont constaté que la résistance à la traction d'une pièce FDM/FFF diminuait d'abord puis augmentait au fur et à mesure que l'épaisseur de la couche augmentait. Quelques années plus tard, en 2010, une autre recherche a montré que l'épaisseur de la couche possédait un faible impact sur la résistance à la traction. Ces conséquences appellent une investigation globale au travers des paramètres

FDM/FFF.

- Les paramètres FDM/FFF affectent non seulement la qualité de la pièce, mais influencent également le temps de construction impliqué. Cependant, les études trouvées dans la littérature ne se sont pas concentrées sur l'influence des paramètres du processus sur le temps de construction.
- Presque toutes les recherches se sont concentrées sur l'étude d'un matériau à la fois ou même d'un paramètre à la fois, alors qu'il existe en réalité de nombreux paramètres qui jouent un rôle important lors de la production. De plus, sur la base des différentes recherches existantes dans la littérature, il est nécessaire d'étudier l'effet simultané des paramètres importants pour obtenir une meilleure compréhension des paramètres FDM/FFF.
- Une enquête approfondie sur l'effet combiné des paramètres FDM/FFF est nécessaire, ce qui permet de mieux comprendre l'influence de chaque paramètre avec leur interaction sur la qualité de la liaison. Ce point de vue permet d'optimiser le processus FDM/FFF pour atteindre l'objectif final qui est l'amélioration de la qualité des obligations.

B.3. Rôle des paramètres du processus sur la qualité des pièces

La conception pour FDM/FFF exige une grande attention car il est nécessaire de bien prédire les différentes caractéristiques du produit final, par ex. propriétés mécaniques. Par conséquent, l'influence des paramètres du procédé sur les caractéristiques mécaniques, autrement dit la liaison entre les couches déposées doit être prise en compte. Les paramètres FDM/FFF pourraient être principalement classés en 3 groupes différents : paramètres de matériau, paramètres de processus et paramètres de machine (figure B.4).

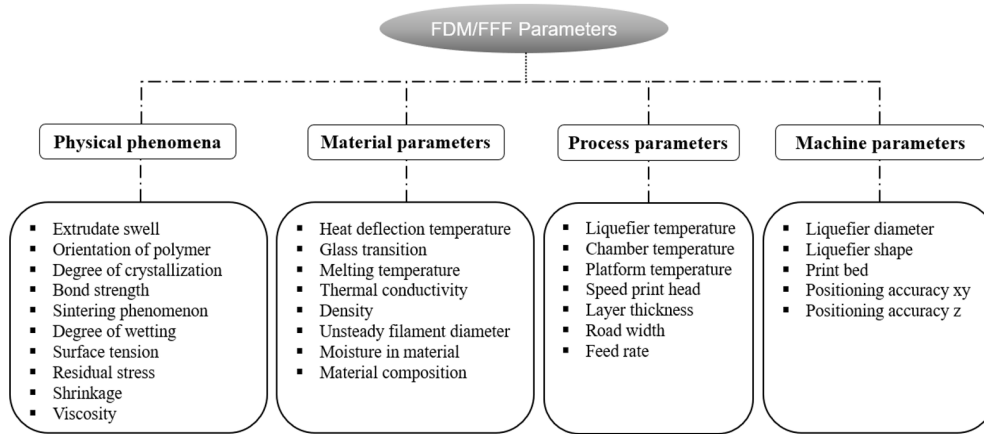


Figure B.4: Représentation des paramètres du processus FDM/FFF [48-52].

B.4. Rôle du transfert de chaleur sur la qualité des pièces

Dans le processus FDM/FFF, un polymère thermoplastique est introduit dans un liquéfacteur qui extrude un filament tout en se déplaçant dans des plans X-Y successifs le long de la direction Z, pour fabriquer une pièce 3D dans un processus couche par couche. Par conséquent, au fur et à mesure du dépôt, le filament chaud se dépose sur les filaments précédemment déposés et qui sont maintenant en cours de refroidissement. Ceci provoque leur réchauffage, définissant un temps pendant lequel les interfaces des filaments en contact sont au-dessus de la température de transition vitreuse (T_g) dans le cas des matériaux amorphes, ou de la température de cristallisation (T_c) pour les matériaux semi-cristallins, ce qui est nécessaire pour qu'une bonne liaison ait lieu. Par conséquent, chaque filament doit être suffisamment chaud pendant le dépôt, mais pas trop chaud pour éviter une déformation due à la gravité et au poids des filaments déposés dans les couches suivantes.

B.5. Rôle de l'évolution de la viscosité et de la coalescence sur la qualité des pièces

Dans FFF/FDM, basé sur la question du chauffage du matériau pendant l'impression, le choix de la température du liquéfacteur est un problème important. Il s'agit d'éviter une surchauffe voire une faible fluidité du matériau lors du dépôt. Par conséquent, la réalisation des caractéristiques rhéologiques est déterminante. Certifier une alimentation optimale du matériau ainsi qu'un changement rapide de la viscosité, le matériau imprimé doit montrer une augmentation suffisante de sa viscosité lors de l'extrusion pour éviter l'instabilité de la

géométrie des pièces finales imprimées en 3D.

B.6. Conclusion

Dans cette étude bibliographique, des paramètres distinctifs qui affectent la qualité de la pièce ont été choisis. Les paramètres de processus sélectionnés sont la température du liquéfacteur, la température de la plate-forme et la vitesse d'impression. Cette étude diffère des études précédentes sur les points suivants :

- L'interaction de paramètres cruciaux tels que la température du liquéfacteur, la température de la plate-forme et la vitesse d'impression (identifiés dans la littérature) sur les propriétés mécaniques a été considérée.
- Le transfert de chaleur et l'évolution de la température des filaments au cours du processus FDM/FFF en proposant un nouveau suivi en cours de la mesure de la température à l'interface des filaments adjacents ont été considérés.
- Une approche numérique utilisant la méthode des volumes finis (FVM) a été utilisée pour la modélisation du transfert de chaleur du profil de température des filaments.
- De plus, en utilisant la valeur de température enregistrée, cette étude traite l'évolution de la viscosité non isotherme des filaments.

Appendix C

Procédure expérimentale

C.1. Matériaux

Commercialement, un filament PLA, acheté auprès de Fillamentum, d'un diamètre de $1,75 \pm 1$ mm a été mis en œuvre. En utilisant ce filament et pour divers objectifs classés dans cette étude, différentes méthodes de caractérisation ont été utilisées afin de corriger les caractéristiques existantes dans ce processus. La fiche technique de ce filament PLA est présentée dans le tableau 3.1 qui provient de la fiche technique du fabricant.

C.2. Méthodologie

C.2.1. Définition de l'étude

Selon la nature du procédé FDM/FFF, chaque dépôt a fortement sa propre influence sur différents aspects des pièces construites. Ce problème signifie clairement que les caractéristiques thermiques, mécaniques et rhéologiques des pièces finales seraient affectées par différents mécanismes de dépôt. Comme expliqué, il existe différents mécanismes de dépôt basés sur le remplissage de couches à savoir contre-remplissage, remplissage raster, contre-remplissage et remplissage raster.

Comme indiqué par Agarwala et al. [107] depuis le tout début, le remplissage raster est le mécanisme de dépôt le plus utile car il offre un meilleur mouvement dans les couches adjacentes. Cependant, les couches déposées pourraient être déposées dans différentes directions considérées en fonction de différents angles de trame (α) [108]. La figure C.1 indique schématiquement les différentes formes de remplissage et les mécanismes possibles de dépôt.

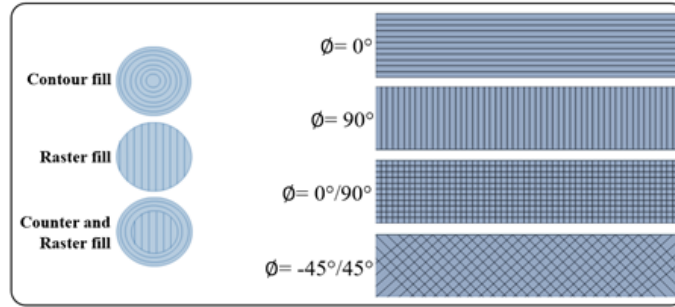


Figure C.1: Vue de dessus de la couche avec différents remplissages et angles de trame

En définissant l'angle raster, relatif à la direction de déplacement, il peut varier d'une couche à une autre. Ainsi, les filaments pourraient être perpendiculaires les uns aux autres ou avoir une direction unidirectionnelle dans laquelle, pour le mode unidirectionnel, ils pourraient être déposés sous forme de filaments asymétriques ou alignés (Figure C.2). Comme les mécanismes de dépôt affectent fortement :

- Inter diffusion des filaments adjacents et donc collage
- Qualité et finition de surface de la pièce finale
- Résistance mécanique de la pièce finale

Elle doit être prise en compte dans différents modes d'analyse et de caractérisation [109].

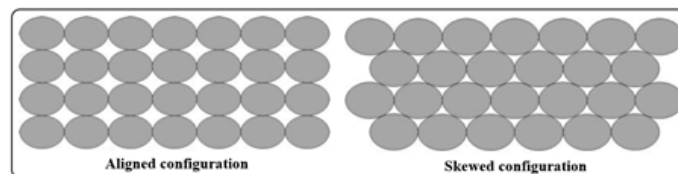


Figure C.2: Différentes configurations de filaments unidirectionnels

Dans cette étude, une tentative a été faite pour concevoir un cas de test qui nous permet de répondre aux exigences. Comme indiqué dans la section B, un filament est confronté à divers mécanismes de transfert de chaleur en raison des différentes sources de chaleur lors de la construction. Par conséquent, les contacts physiques résultant des mécanismes de dépôt jouent également un rôle important dans la caractérisation et l'analyse. Ainsi, une seule technique de dépôt a été modélisée comprenant les caractéristiques suivantes (Figure C.3) :

- Dépôt homogène des filaments les uns sur les autres

- Dépôt unidirectionnel des filaments (Prise en compte du temps de dépôt pour chaque filament)
- Même convection des couches avec l'environnement
- Même conduction entre les couches
- 1^{me} couche: conduction avec support (et avec 2^{me} couche) simultanément (pour la caractérisation thermique)
- 2^{me}, 3^{me}, ..., n^{me} couches : même conduction les unes avec les autres
- Effet symétrique de l'environnement et de la température de la plate-forme sur la solidification du matériau lors du refroidissement.

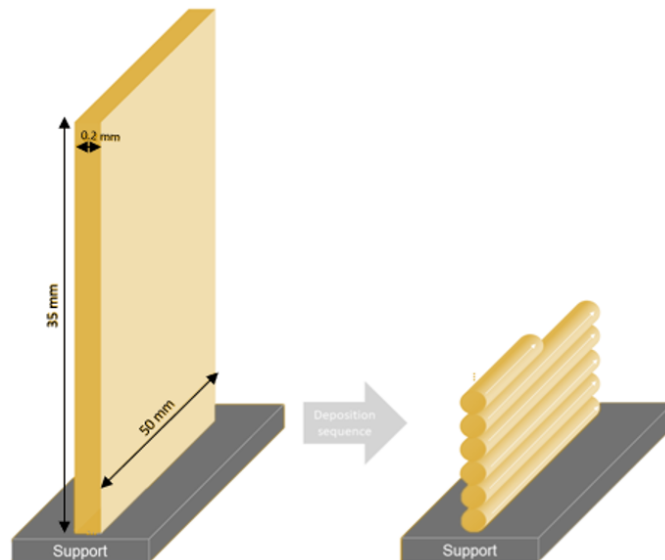


Figure C.3: Schéma du cas d'essai conçu dans le cadre de la présente thèse

C.2.2. Méthodes de caractérisation et disposition des équipements

Suivant l'objectif de cette étude, plusieurs méthodes de caractérisation doivent être envisagées et l'effet de leur interaction est inévitable. Compte tenu des moyens communs de caractérisation, les procédures mises en œuvre sont brièvement présentées dans la figure C.4.

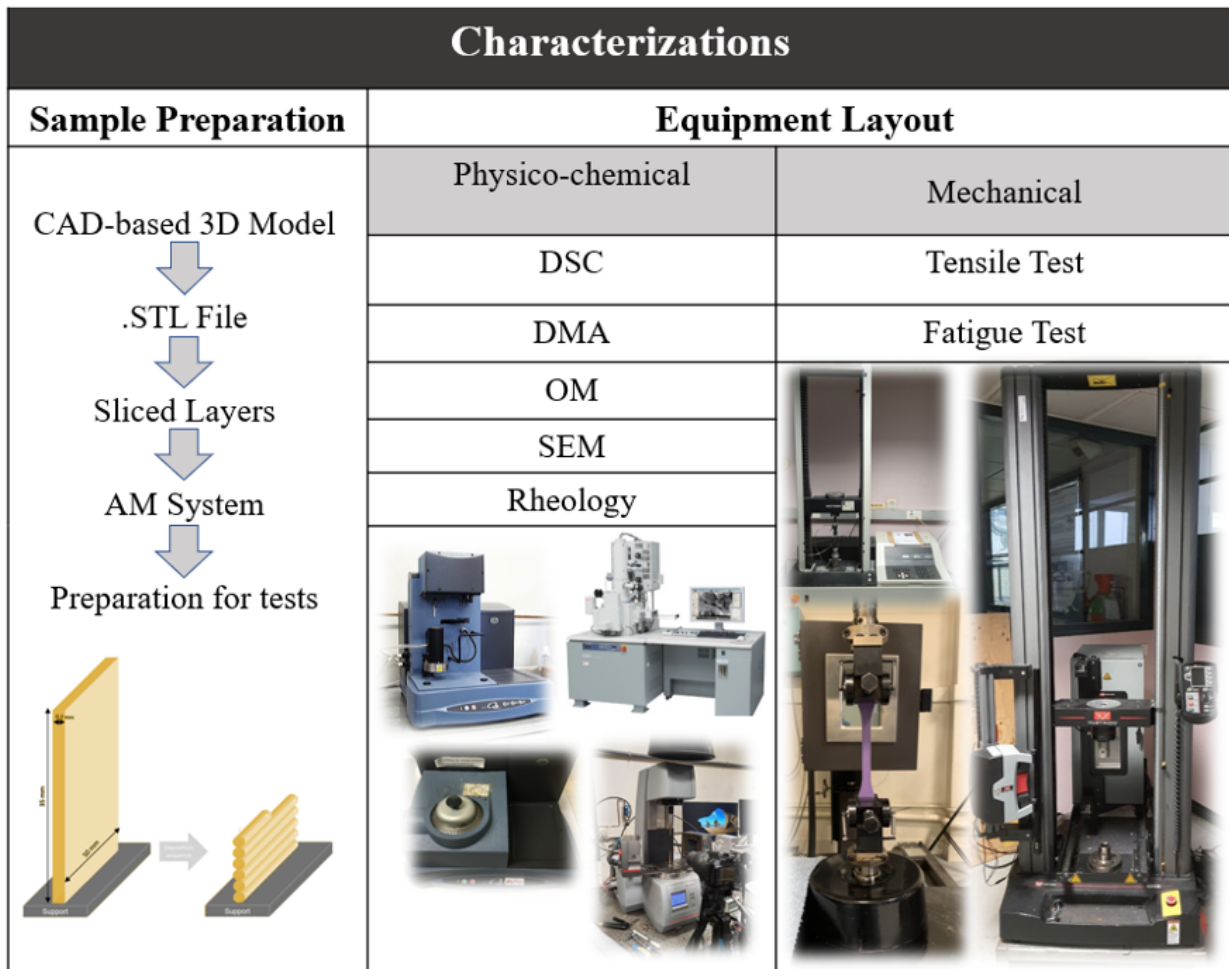


Figure C.4: Un aperçu des méthodes de caractérisation expérimentales

C.2.3. *in situ* surveillance du profil de température des filaments

Dans le cadre de l'optimisation du procédé FDM/FFF, le suivi *in situ* (ou suivi en temps réel) de l'évolution de la température des filaments pendant le dépôt est un enjeu important à des fins de contrôle de qualité. Néanmoins, à la manière de l'investigation expérimentale, les circonstances qui existent dans ce processus font de l'intégration d'outils d'enregistrement *in situ* un problème difficile pour les chercheurs. En ce qui concerne la mise en œuvre expérimentale du contrôle de température *in situ*, le contrôle de température doit être suffisamment précis et rapide pour suivre le refroidissement des filaments et les pics de réchauffage résultant du contact entre les filaments fraîchement déposés et ceux précédemment déposés. De plus, il devrait être possible d'utiliser le capteur localement sans qu'il soit nécessaire d'interrompre le processus. Malgré la variété des travaux effectués par les chercheurs du monde entier, à l'heure actuelle, aucune technique précise et rapide n'a été mise au point.

Pour cette raison, un montage expérimental a été utilisé pour réaliser les profils de température *in situ* et en temps réel lors du dépôt filamentaire d'une pièce. Pour enregistrer la

distribution de température des filaments pendant le dépôt, de très petits thermocouples de type K avec un diamètre de $d=80 \mu\text{m}$ ont été utilisés. Par conséquent, pour l'enregistrement de la température à l'aide des thermocouples de type K, un appareil a été utilisé sous le nom de « *Datapaq* Tracker Telemetry System ». Cet appareil est utilisé comme enregistreur de température lors d'une technique de fabrication : le procédé de Rotational Molding. Le moulage par rotation est un processus qui implique un remplissage de moule creux chauffé avec une charge ou un poids de matériau (normalement en poudre).

Comme le montre la figure C.5, le système de télémétrie *Datapaq* Tracker, se connecte à distance à la machine de moulage par rotation (le LAB40 de type navette construit par STP est disponible au laboratoire PIMM), qui comprend plusieurs ports pour ajouter des thermocouples de type K et ils sont actionnés par son logiciel.

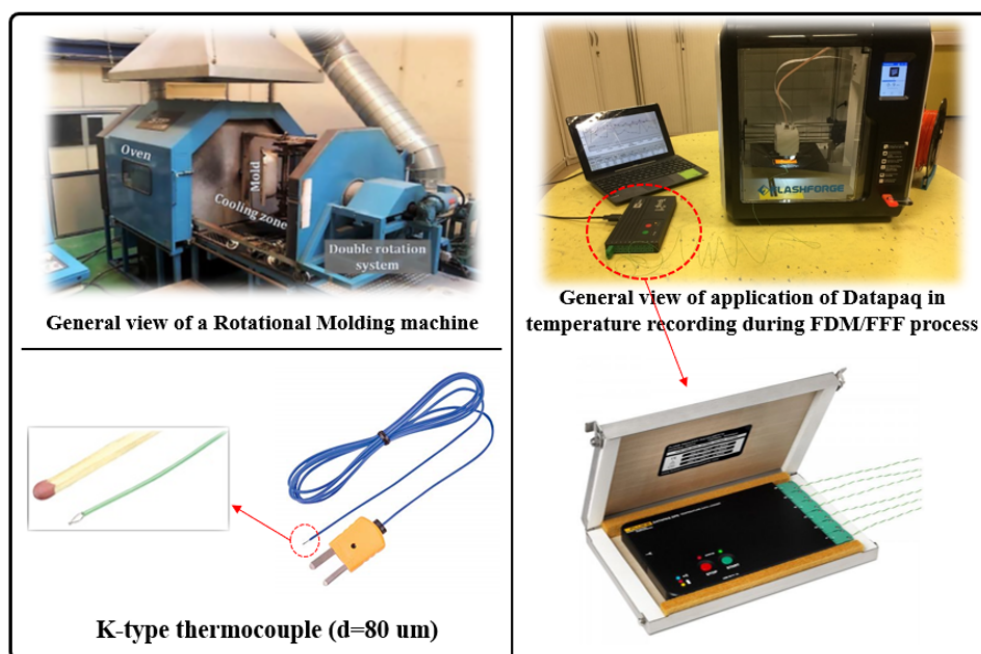


Figure C.5: Vue générale de l'utilisation du système de suivi télémétrique *Datapaq*[®] du moulage par rotation au processus FDM/FFF

Pour atteindre notre objectif, le *Datapaq*[®] a été utilisé pour effectuer le suivi in situ de la température des filaments pendant le dépôt. Ainsi, les thermocouples de type K ont été connectés au *Datapaq* pour procéder à l'enregistrement de la température lors du dépôt du filament. La figure C.6 illustre schématiquement l'utilisation du dispositif mentionné pour conduire l'approche proposée par l'enregistrement de la température des filaments pendant le dépôt. En utilisant le cas de test conçu, plusieurs efforts ont été pris en compte pour placer les thermocouples à différents endroits.

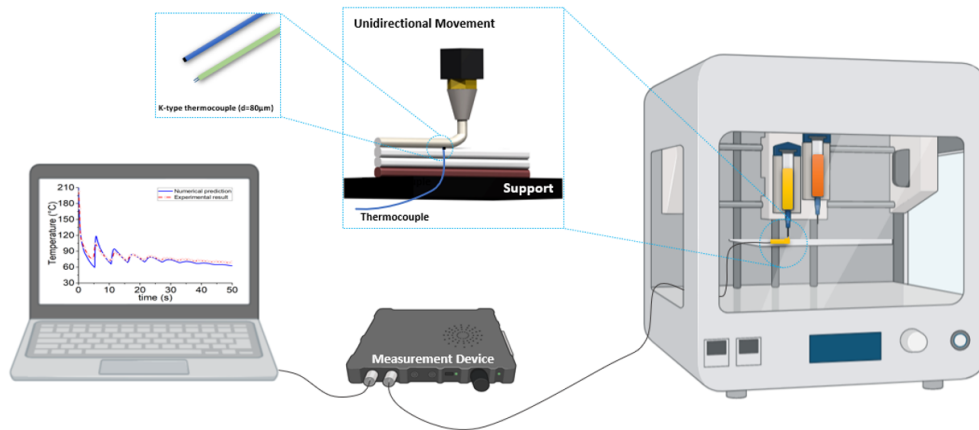


Figure C.6: Mise en place de l'in situ surveillance du profil de température pendant l'étape de dépôt

En considérant la taille des thermocouples, il est important de fixer précisément l'extrémité de la tête de ceux-ci à l'interface des couches déposées. Pour les raisons et déclarations suivantes :

- Le mouvement de l'extrudeuse ainsi que son éloignement du filament préalablement déposé.
- La hauteur de couche (et aussi le diamètre) de la couche déposée est trop petite (environ $200 \mu\text{m}$)
- Le début de l'enregistrement de la température est si important pour pouvoir évaluer la première courbe de refroidissement et donc les courbes de refroidissement et de réchauffage successives.

les raisons ci-dessus mentionnées sont cruciales et doivent être incluses dans le suivi / enregistrement in situ du profil de température.

En se référant à la figure C.7, on peut remarquer que l'enregistrement local de la température à l'interface des filaments adjacents sans interrompre le processus est une technique prometteuse. A titre d'exemple, le point numéro 1 montre l'emplacement d'un thermocouple à l'interface des couches 1 et 2 à un emplacement spécifique. En plaçant les thermocouples, le logiciel montre une augmentation de l'enregistrement de la température qui se réfère à la température de la première couche. Cela signifie que le thermocouple est en train d'enregistrer la variation de température de la première couche qui a déjà été déposée et qui est en cours de

refroidissement (zone I). L'augmentation soudaine représente la température au moment où la deuxième couche est déposée. Il commence alors à se refroidir représentant le refroidissement de la deuxième couche (zone II). Il est à noter qu'en supposant le même gradient de température, la température enregistrée à l'interface des première et deuxième couche représente également leur variation de température. Avant le dépôt de la troisième couche, le même réchauffement et la même augmentation soudaine apparaissent puis commencent à se refroidir et ainsi de suite. Il convient de mentionner que les explications ci-dessus correspondent à l'évolution de la température enregistrée de la deuxième couche par dépôt de 3^{me}, 4^{me}, 5^{me},

La courbe présentée (sur la figure C.7) montre non seulement l'adhérence des filaments, mais représente également la diminution successive de l'évolution de la température d'une couche même par dépôt de filaments plus jeunes. La présence de pics indique bien évidemment l'adhésion des couches et leur diminution successive montre que les couches successives (couches 3, 4, 5, 6, ...) ne suffisent pas à maintenir suffisamment chaude la température de la couche précédemment déposée (couche 1).

Cette affirmation est le pré-requis nécessaire à l'atteinte des objectifs d'optimisation et d'amélioration de l'adhérence des couches successives en reconnaissant l'évolution de la température à l'interface des couches déposées. Pour cette raison, des efforts ont été déployés en considérant l'influence des principales variables du procédé sur l'évolution de la température des filaments. Aussi, en mettant en œuvre plusieurs thermocouples en même temps, l'évolution de la température a été enregistrée à différents endroits depuis le début du dépôt.

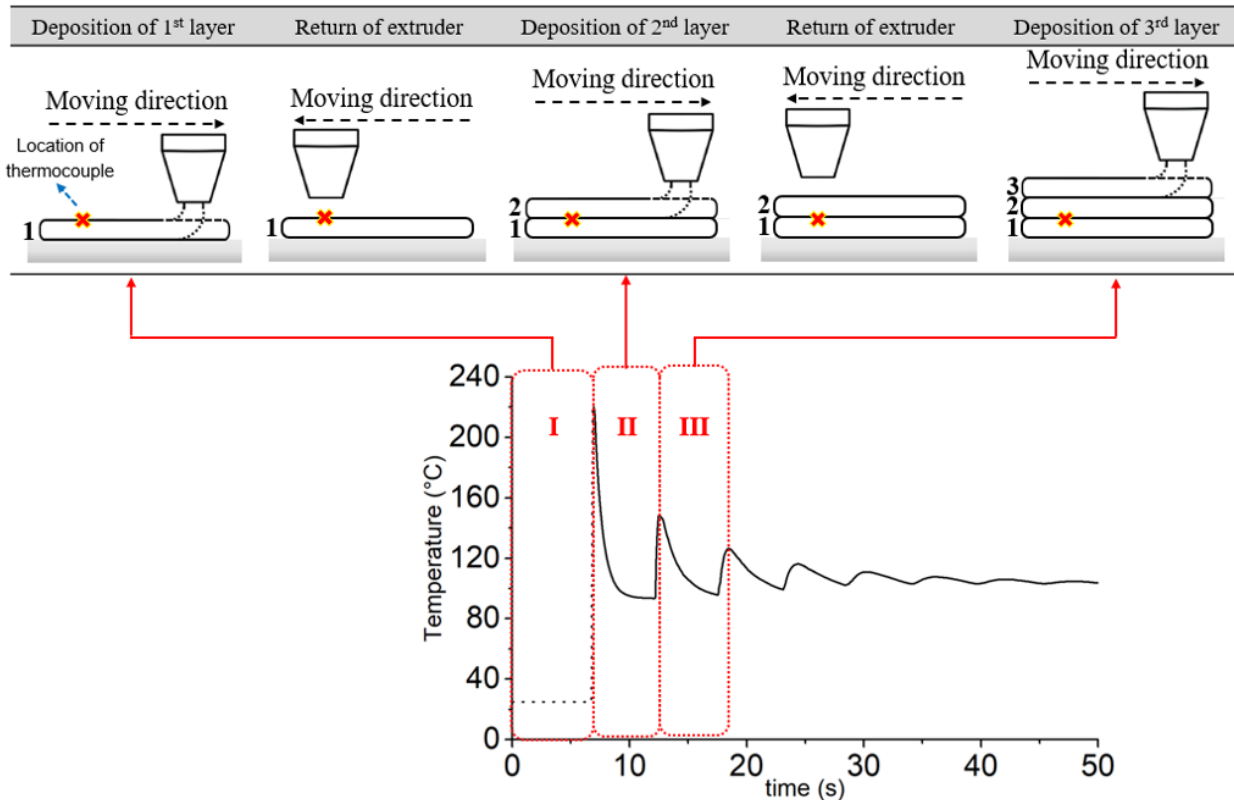


Figure C.7: Évolution de la température de la deuxième couche (à un endroit spécifique) pendant le dépôt de la paroi verticale constituée de filaments uniques déposés les uns sur les autres.

De plus, parallèlement à l'objectif principal des travaux sur l'enregistrement in situ local du profil de température, l'enregistrement in situ global du profil de température. L'objectif est de montrer l'utilité de l'approche proposée (utilisant des thermocouples de type K) et l'importance de l'évolution de la température à l'interface des filaments adjacents ont été réalisés. Comme indiqué dans les sections précédentes, presque tous les chercheurs se sont concentrés sur l'utilisation d'une caméra infrarouge. Bien qu'il semble qu'il s'agisse d'une approche plus facile, pour les raisons et les déclarations suivantes, elle n'est pas aussi utile que l'utilisation de thermocouples :

- Enregistrement de la température sur les surfaces externes des couches déposées.
- Selon le type d'appareil photo, la précision varie.
- L'influence d'autres phénomènes tels que le rayonnement diffusé depuis la plate-forme ou d'autres couches est inévitable.

Par conséquent, une caméra infrarouge Optris a été utilisée pour montrer la différence entre l'approche proposée et les techniques courantes (dans ce cas : la caméra infrarouge) qui

sont populaires. Cependant, il est à noter que les deux approches, l'enregistrement local et global de la température in situ lors du dépôt du filament, ont été appliquées simultanément. Cela signifie qu'au même endroit où les thermocouples sont placés, les données ont été extraites du profil de température enregistré par une caméra infrarouge. Comme le montre la figure C.8 qui représente la configuration pour la surveillance in situ du profil de température et l'assemblage de deux méthodes ainsi que les détails suivants : le thermogramme de la paroi imprimée avec les couches correspondantes et les emplacements mis en évidence pour le profil de température.

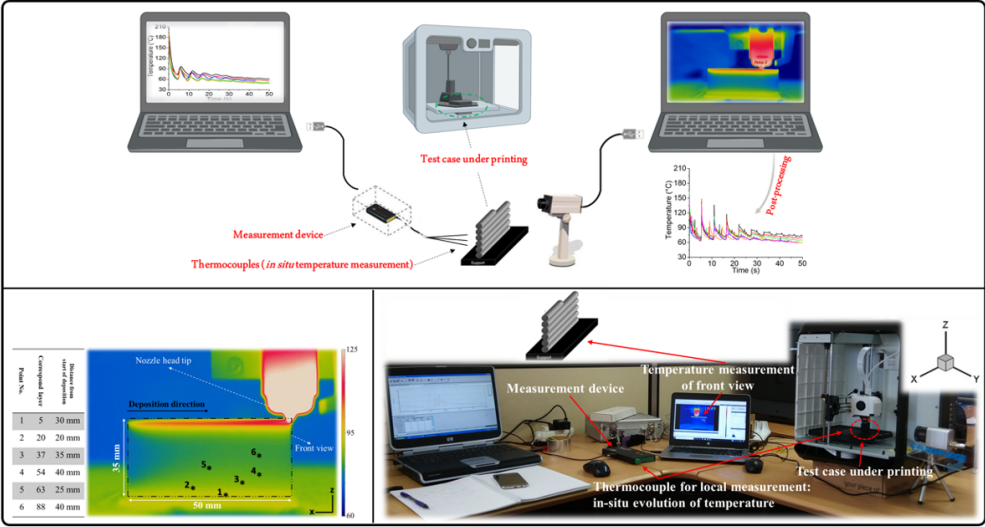


Figure C.8: Représentation de la mesure in situ locale et globale du profil de température en utilisant simultanément des thermocouples de type K et une caméra IR.

Appendix D

Influence des paramètres du processus

L'influence de la variation des principaux paramètres du processus a été étudiée expérimentalement pour reconnaître les différentes caractéristiques des pièces imprimées en 3D en fonction des paramètres du processus. De plus, pour pouvoir atteindre la modélisation analytique du profil de température, l'influence des paramètres du procédé a été expérimentalement enregistrée pour observer leur impact sur l'étape de refroidissement et l'évolution de la température des filaments. L'influence de la température du liquéfacteur, de la température de la plate-forme et de la vitesse d'impression a été prise en compte en définissant trois conditions. Il convient de mentionner que les valeurs nommées ont été considérées sur la base des recherches effectuées dans les littératures. Aussi, pour effectuer une comparaison entre la microstructure et le dépôt de filaments dans différentes conditions, un a été marqué comme référence.

En utilisant des mesures locales, plusieurs expériences ont été réalisées afin d'enregistrer le profil de température des filaments à différents endroits. Le profil de température enregistré pour le premier filament dans une séquence de dépôt à un emplacement de $x = 5$ mm à partir du début du dépôt est indiqué sur la figure D.1.

L'expérimentation a été construite en tenant compte des valeurs des variables de traitement en tant que $T_{Liq} = 210$ °C, $T_{Platform} = 50$ °C, $V = 20$ mm/s et $h = 0,2$ mm qui sont couramment utilisées dans l'imprimante 3D de bureau pour assurer une pièce de bonne qualité en termes de résistance mécanique selon la littérature. Les points A, B, C, D et E correspondent respectivement au dépôt du 2^{me}, 3^{me}, 4^{me}, 5^{me} et 6^{me} filament. Du fait de la nature de la démarche de mesure et après le contact (par nouveau dépôt), la température du filament augmente du fait de l'échauffement apporté par le contact (à l'endroit où était placé le thermocouple) avec un filament plus chaud. À partir de la courbe présentée à la figure D.1,

les observations suivantes peuvent être conclues jusqu'à présent:

- De manière générale, chaque filament fait face à une évolution cyclique de la température lors de son dépôt
- Au moins, le premier pic a un impact considérable sur l'élévation de température égale/supérieure à la température de cristallisation, T_c dans le cas d'un matériau semi-cristallin.
- La reconnaissance du profil de température à l'interface des filaments adjacents lors de l'étape de dépôt est inévitable.

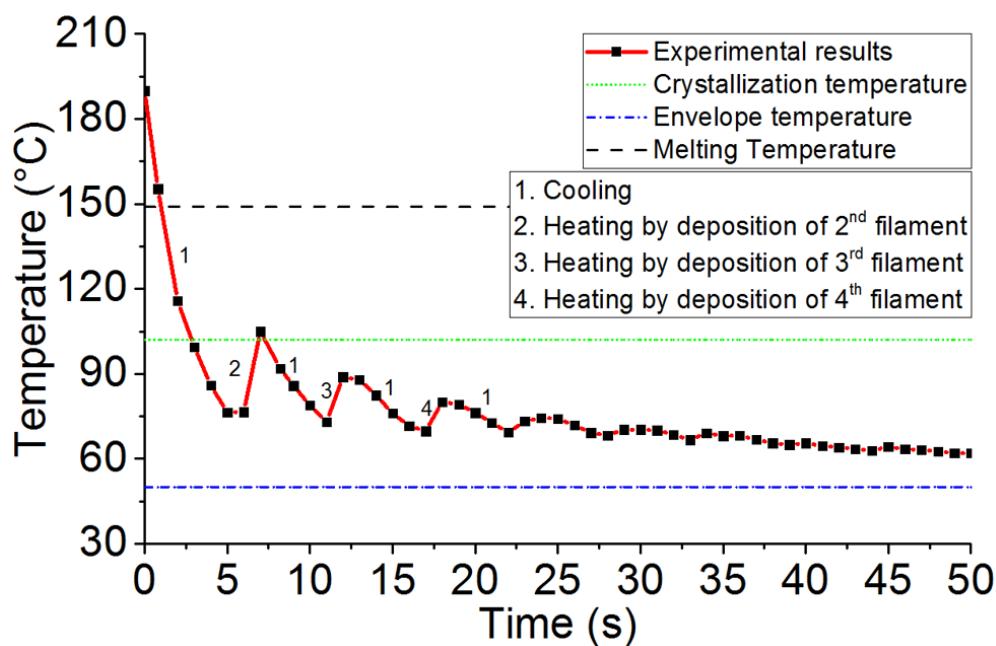


Figure D.1: Évolution de la température pendant le processus FFF ($T_{Liq}=210^{\circ}\text{C}$, $T_{Platform}=50^{\circ}\text{C}$, $V=20\text{ mm/s}$, $h=0.2\text{ mm}$).

D.1. Influence de la température de la plate-forme sur le profil de température

L'étude de l'influence de la température de la plateau l'évolution de la température des filaments a été réalisée au même endroit et dans les mêmes conditions d'impression sur la base de la condition précédente. Comme prévu, plus la température de la plate-forme est basse, plus le refroidissement est rapide (Figure D.2). Pour les pics de réchauffage, ils commencent à la même valeur, mais l'amplitude a tendance à diminuer avec l'augmentation

de la température de la plate-forme. Lorsqu'il atteint 100 °C, le filament étudié se réchauffe de façon répétée au-dessus de sa température de cristallisation (T_c), favorisant le collage.

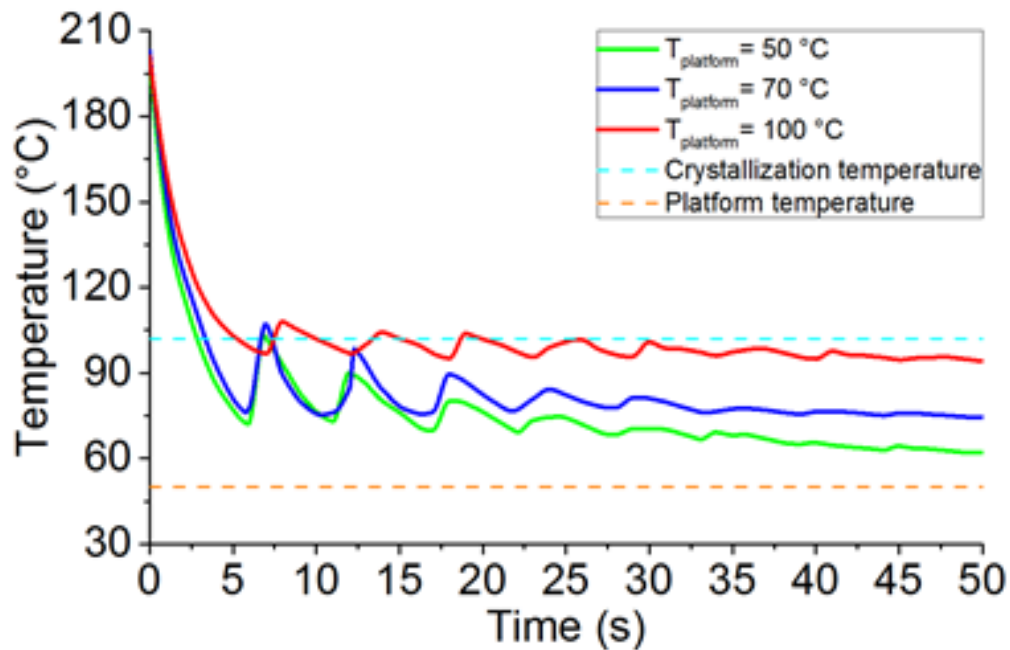


Figure D.2: Évolution de la température des échantillons imprimés à différentes températures de la plate-forme.

D.2. Influence de la vitesse d'impression sur le profil de température

Compte tenu de l'influence de la vitesse d'impression, la figure D.3 montre le profil de température du filament au même emplacement et dans les mêmes conditions d'impression selon trois vitesses comme indiqué. Lorsque la vitesse d'impression augmente, la vitesse de refroidissement diminue. Comme prévu, l'apparition des pics se produit à des moments différents et leur largeur est également altérée. Enfin, l'amplitude des pics obtenus à la vitesse d'impression la plus basse est plus élevée, probablement en raison de la plus grande différence entre les températures des filaments adjacents.

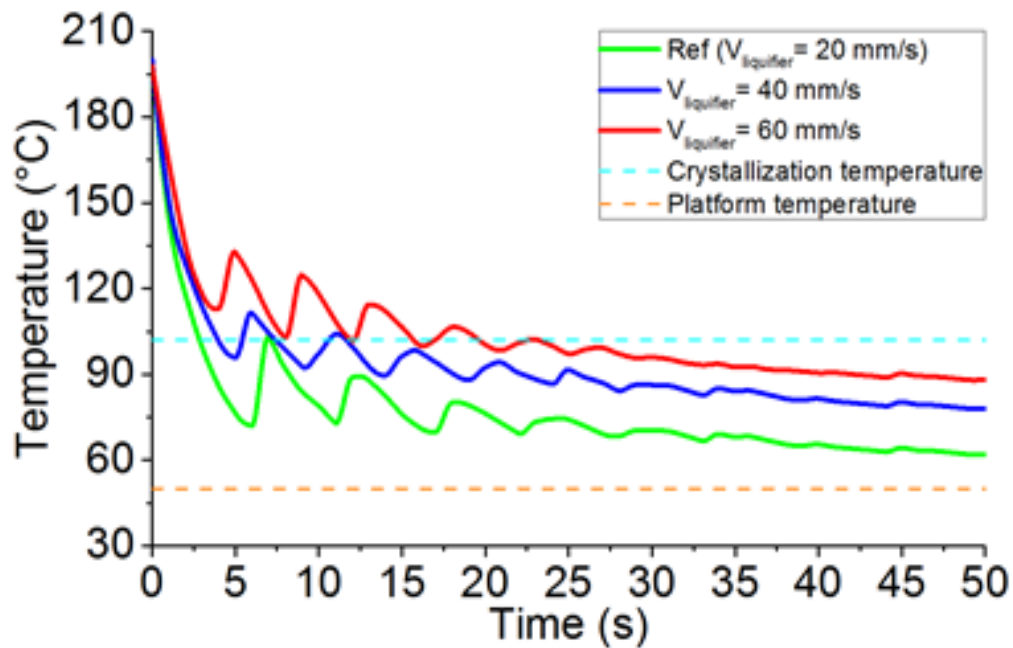


Figure D.3: Évolution de la température pour les échantillons imprimés à différentes vitesses d'impression.

D.3. Conclusion

Cette étude nous a permis de tirer de nombreuses conclusions, à ce jour :

- L'interaction des paramètres joue le rôle le plus important dans la prise en compte de la caractérisation mécanique des pièces imprimées.
- Le module de Young et la déformation à la rupture pourraient être un indicateur pour évaluer les performances mécaniques des pièces imprimées.
- La température des filaments joue un rôle important dans les caractéristiques des pièces imprimées.
- La conséquence du dépôt dans des conditions différentes montre que l'augmentation de la température du liquéfacteur est plus importante sur le contact des filaments, cependant, l'impact de la vitesse d'impression est plus important.
- La température du liquéfacteur et la vitesse d'impression ont un impact plus important sur l'évolution de la température des filaments.

Appendix E

Modélisation du transfert thermique du FDM/FFF

L'amélioration de la qualité des pièces FDM/FFF nécessite des recherches importantes. Afin d'améliorer la stabilité dimensionnelle et les propriétés mécaniques du produit final, de nombreuses études concernant la modélisation analytique et les évaluations expérimentales ont été proposées et étudiées. Dans cette étude, nous nous sommes concentrés sur deux aspects : le transfert de chaleur et la fluidité ; qui doivent être pris en compte à des fins d'optimisation. Comme mentionné, la plupart des approches expérimentales et de modélisation du transfert de chaleur des filaments ne sont valables que pour des conditions spécifiques. Ils ne sont pas considérés pour toutes les géométries, et ne considèrent pas tous les phénomènes possibles dans ce processus. De plus, dans presque toutes les approches expérimentales, le transfert de chaleur a été enregistré à l'aide d'approches globales telles que la mise en œuvre d'une caméra infrarouge. Pour donner suite à nos explications dans la section 3, une nouvelle approche a été proposée permettant la surveillance locale en cours du profil de température à l'interface des filaments adjacents. Pour développer l'approche proposée, l'obtention d'une approche prédictive basée sur les efforts fournis est inévitable.

E.1. Équation de conservation

L'équation de conservation régissant le transfert de chaleur en impression FDM/FFF-3D est donnée par :

$$\frac{\partial}{\partial t}(\rho T) + \text{div}(\rho u T) = \text{div}(\Gamma \text{grad} T) + S_T \quad (\text{E.1})$$

où Γ est le coefficient de diffusion et S est le terme source. La méthode des volumes finis

(FVM) [119] est un bon candidat pour résoudre numériquement l'équation E.1. Ci-dessous est présentée la formulation globale FVM utilisée pour ce problème. Dans ce travail, un code de transfert de chaleur FVM est appliqué afin d'effectuer l'évolution de la température des filaments déposés dans le procédé FDM/FFF.

E.2. Méthode numérique

E.2.1. Méthode des volumes finis

Dans notre cas, la FVM consiste à effectuer un bilan de transfert de chaleur sur un volume donné infinitésimal. En utilisant le théorème de divergence, les intégrales de volume d'une équation aux dérivées partielles sont converties en la surface entière. Ainsi, dans l'approche des volumes finis, les équations gouvernantes sous leur forme conservatrice sont largement utilisées et l'objectif est de s'assurer que toutes les caractéristiques restent similaires dans chaque contrôle cellule/volume. Les principales caractéristiques de FVM pourraient être mentionnées comme suit :

- Subdivision de l'étendue du problème en volumes de contrôle (CV) sans chevauchement.
- Consolidation des équations gouvernantes (dans notre cas : équation de la chaleur) sur les CV.
- Évaluation des intégrales à l'aide de la variation de température entre les points de la grille.
- Représentation du principe de conservation pour le volume de contrôle fini à l'aide de l'équation discrétisée obtenue.

E.2.2. Formulation du problème

Nous envisageons de résoudre le problème de conduction thermique instationnaire bidimensionnel sur une paroi verticale de forme rectangulaire avec la dimension de $50 \times 35 \times 0.2, 2$ mm comme décrit dans la section 3. Ce cas de test a été conçu pour prédire le transfert de chaleur lors du dépôt de filaments sur la base de la hypothèses suivantes : même contact physique entre les filaments et le filament/support, et convection entre le filament et l'air en même temps ; épaisseur supposée être le diamètre d'un filament ; un déplacement unidirectionnel du liquéfacteur ; consistant en plus d'homogénéité dans la distribution de

la température. En maintenant le premier terme de l'équation E.1 dans le processus de discrétisation, l'intégration en volume fini de cette équation sur le CV en remplaçant les termes convectifs et diffusifs par des intégrales de surface obtenues comme suit :

$$\int_{CV} \frac{\partial(\rho T)}{\partial t} dV + \int_{CV} div(\rho T u) dV = \int_{CV} div(\Gamma grad T) dV + \int_{CV} S_T dV \quad (E.2)$$

En utilisant le théorème de divergence de Gauss, on obtient :

$$\int_{\Delta t} \frac{\partial}{\partial t} \left(\int_{CV} (\rho T) dV \right) dt + \int_{\Delta t} \int_A n(\rho T u) dA dt = \int_{\Delta t} \int_A n(\Gamma_T grad T) dA dt + \int_{\Delta t} \int_{CV} S_T dV dt \quad (E.3)$$

E.2.3. Génération du grid

La première étape du lancement de FVM fait référence à la 'grid generation' en divisant la zone applicable en petits CV discrets. Les bordures des CV sont positionnées à mi-chemin entre les nœuds adjacents qui sont eux-mêmes entourés de volume/cellule de contrôle. La figure E.1 indique un domaine rectangulaire divisé en CV sans chevauchement. Ils sont divisés par des lignes discontinues introduisant les limites des CV individuels. Ces modèles sont appelés grilles de calcul. Un point nodal général « P » est spécifié par ses voisins, dans une géométrie 2D, les nœuds au nord, au sud, à l'ouest et à l'est : N, S, W et E, respectivement. Comme le montre la figure E.1, deux ensembles de lignes de quadrillage peuvent être définis comme suit : les lignes de quadrillage définissant l'emplacement des nœuds et celles définissant les faces CV. Ainsi, le point nodal P est toujours placé au centre géométrique de son CV avec les destinations suivantes :

$$y_P - y_s = y_n - y_P = \frac{\Delta y}{2} \quad (E.4)$$

$$x_P - x_w = x_e - x_P = \frac{\Delta x}{2} \quad (E.5)$$

Notamment, les indices minuscules font référence aux emplacements des faces CV ; tandis que les indices majuscules se réfèrent aux emplacements des nœuds. Il est donc important de faire la distinction entre les lettres majuscules et minuscules.

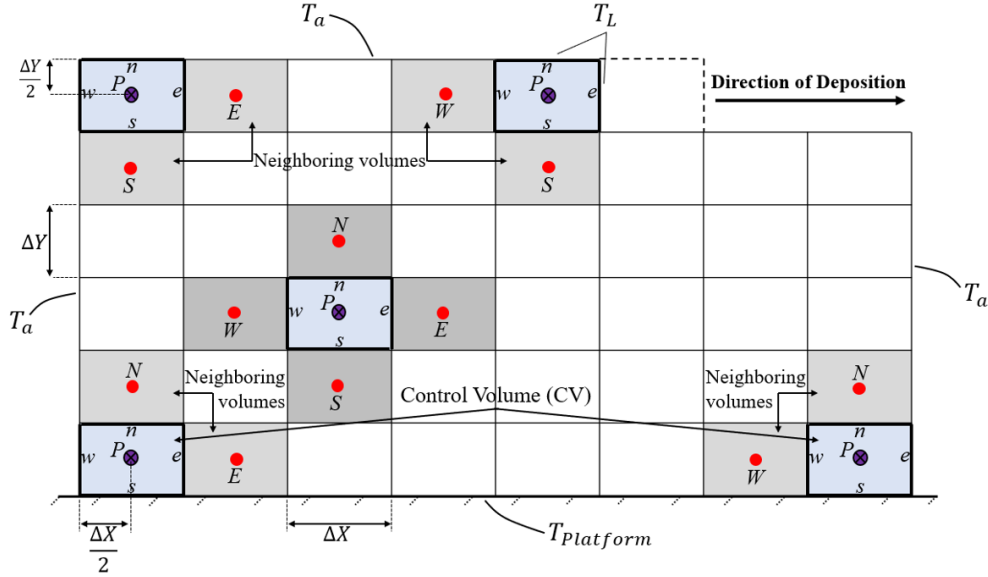


Figure E.1: Schématisation de l'objet en volume fini (T_{Liq} : Température du liquéfacteur, $T_{Platform}$: Température de la plate-forme, T_a : Température ambiante, N: Nord, S: Sud, W: Ouest, E:Est).

E.2.4. Discrétisations

L'intégration de l'équation gouvernante sur un CV est la caractéristique la plus importante de la FVM. L'idée est d'obtenir une équation discrétisée à son point nodal P. L'équation de diffusion bidimensionnelle instationnaire est la suivante :

$$\rho C \frac{\partial T}{\partial t} = \frac{\partial}{\partial X} \left(K \frac{\partial T}{\partial X} \right) + \frac{\partial}{\partial Y} \left(K \frac{\partial T}{\partial Y} \right) + S \quad (\text{E.6})$$

En intégrant l'équation 5.6 sur le CV sur un intervalle de temps de t à $t+\Delta t$, on a :

$$\int_t^{t+\Delta t} \int_{CV} \rho C \frac{\partial T}{\partial t} dV dt = \int_t^{t+\Delta t} \int_{CV} \frac{\partial}{\partial X} \left(K \frac{\partial T}{\partial X} \right) dV dt + \int_t^{t+\Delta t} \int_{CV} \frac{\partial}{\partial Y} \left(K \frac{\partial T}{\partial Y} \right) dV dt + \int_t^{t+\Delta t} \int_{CV} S dV dt \quad (\text{E.7})$$

Cela peut s'écrire comme :

$$\int_t^{t+\Delta t} \int_{CV} \rho C \frac{\partial T}{\partial t} dV dt = \int_t^{t+\Delta t} \int_{CV} \left[\left(K A \frac{\partial T}{\partial X} \right)_e - \left(K A \frac{\partial T}{\partial X} \right)_w \right] + \int_t^{t+\Delta t} \int_{CV} \left[\left(K A \frac{\partial T}{\partial Y} \right)_n - \left(K A \frac{\partial T}{\partial Y} \right)_s \right] + \int_t^{t+\Delta t} \bar{S} dV dt \quad (\text{E.8})$$

où A est la surface faciale du volume de contrôle, ΔV est son volume ($\Delta V = A \Delta X = A \Delta Y$) et \bar{S} est l'intensité moyenne de la source.

E.2.5. Conditions aux limites

Outre les paramètres liés au matériau mis en œuvre, les conditions aux limites sont définies comme suit :

- Limite nord: température fixe égale à la température du liquéfacteur.
 - Cellule devant le liquéfacteur : température fixe égale à la température du la buse
 - Autres cellules : température fixe égale à la température ambiante
- Limite sud: température fixe égale à la température de la plate-forme.
- Limite ouest: température fixe égale à la température ambiante.
- Limite est: température fixe égale à la température ambiante.

Le code étant en 2D, une attention particulière a été prise en compte dans la définition des conditions aux limites. De ce fait, une source thermique a été ajoutée aux frontières avant et arrière pour être implémentée dans l'équation de conservation qui nous permet de considérer la convection avec l'environnement. Cela permet d'avoir un schéma implicite 3D pour notre modélisation.

E.3. Convection avec l'environnement

Le transfert de chaleur par convection qui existe dans le procédé FDM/FFF a été largement étudié dans la littérature. Selon le code numérique développé et afin d'évaluer sa fonctionnalité, l'évolution de la température pendant 50 secondes de refroidissement du dépôt de paroi verticale à différents endroits a été présentée. Pour le post-traitement, tous les signaux sont synchronisés à $t=0$ s en fonction de l'instant de la première température enregistrée (la valeur mesurée la plus élevée considérée comme une valeur à $t=0$ s).

Les résultats obtenus pour les échanges thermiques par convection pour $h=5, 10, 30, 50, 70$ et $88 \text{ W/m}^2 \cdot ^\circ\text{C}$ ont montré que l'effet de ce coefficient est évident, notamment sur la vitesse de refroidissement et les pics de température. Cela peut être clairement vu sur la figure E.2 pour les emplacements aléatoires (comme mis en évidence pour les couches 5, 20

et 88). Une valeur de $h_{conv} = 70 \text{ W/m}^2 \cdot ^\circ\text{C}$ est normalement utilisée et comme elle passe de 5 à $70 \text{ W/m}^2 \cdot ^\circ\text{C}$, la vitesse de refroidissement augmente et son effet est visible sur les pics de température. De plus, en utilisant la corrélation de Churchill pour le refroidissement d'un cylindre par convection naturelle, $h_{conv} = 88 \text{ W/m}^2 \cdot ^\circ\text{C}$ a été obtenu et pris en compte pour le calcul [78, 118].

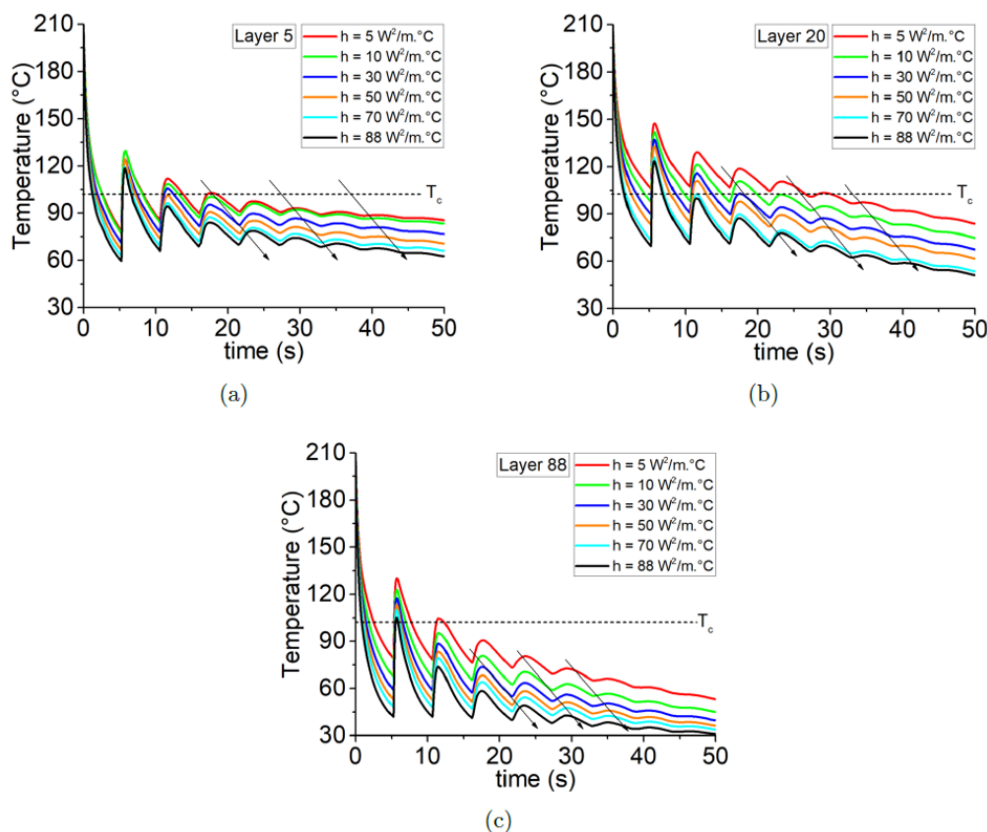


Figure E.2: L'effet de h_{conv} sur le refroidissement des filaments: évolution de la température pour $h_{conv} = 5, 10, 30, 50, 70, 88 \text{ W/m}^2 \cdot ^\circ\text{C}$ pour (a) La couche 5, (b) La couche 20, (c) La couche 88.

La figure E.3 montre l'évolution de la température des filaments à des instants spécifiques lors de la construction de la paroi verticale. Suite aux résultats rapportés ci-dessus, dans ces conditions d'impression, le dépôt d'un nouveau filament provoque le réchauffement de ceux qui ont déjà été refroidis. Présentant un aperçu général des résultats sur la figure E.3 (a), l'évolution de la température sur les CV a été enregistrée pour les couches 5, 10 et 43, respectivement (figure E.3 (b)).

A partir de ces thermogrammes, le réchauffage des filaments préalablement déposés est évidemment fonction de leur localisation. A titre d'exemple, le dépôt de la 43^{me} couche élève la température d'environ 4 à 5 couches, ce qui correspond à environ 8 à 9 couches lorsque la 10^{me} couche est déposée ; ceci est plus évident sur la figure E.3(c) pour le dépôt de la 15^{me}

couche.

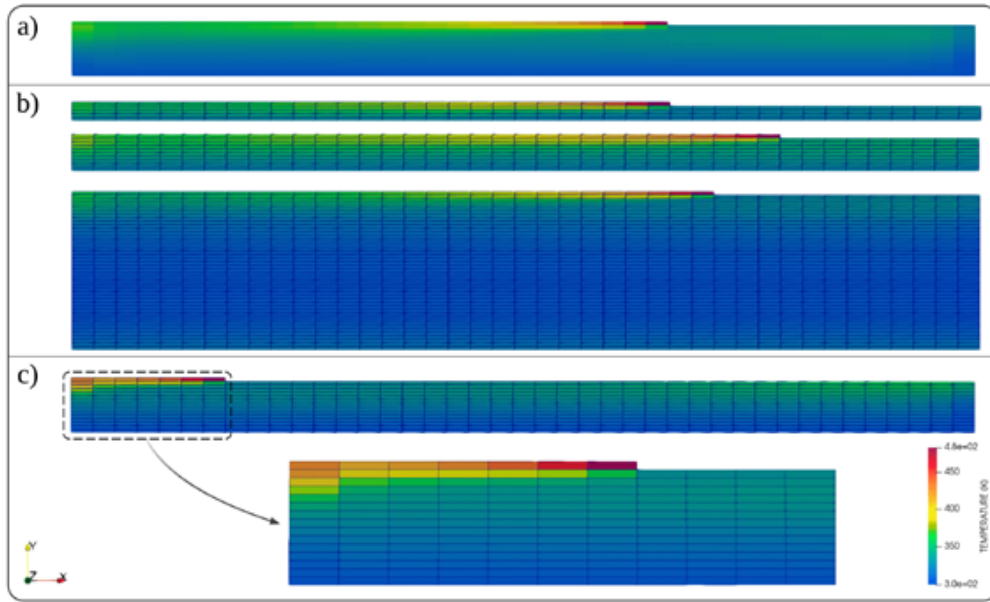


Figure E.3: Température à certains moments du processus de déposition pour la paroi verticale : (a) vue générale, (b) couches 5, 10, 43 ainsi que la présentation des CVs, (c) couche 15 avec haute résolution des CVs.

E.4. Validation expérimentale des résultats obtenus

La surveillance en cours de processus du profil de température permet une mesure locale de la distribution de la température ainsi que des conséquences du dépôt. Ceci est effectué pour une condition définie à côté de différents emplacements du mur vertical proposé. Dans cette série d'expériences, le profil de température du filament est enregistré aléatoirement à certains instants : couche 5 ($x=30$ mm, $y=1$ mm), couche 20 ($x=20$ mm, $y=4$ mm), couche 37 ($x=35$ mm, $y=7,4$ mm), couche 54 ($x=40$ mm, $y=10,8$ mm), couche 63 ($x=25$ mm, $y=12,6$ mm) et couche 88 ($x=40$ mm, $y=17,6$ mm). La température du liquéfacteur a été maintenue à 210 °C ainsi que la température de la plate-forme à 50 °C. La figure 5.4 résume les données enregistrées en traçant l'évolution de la température enregistrée en fonction du temps. Dans chaque cas, comme mentionné dans la section précédente, l'évolution cyclique de la température des filaments varie en fonction de leur emplacement. Un paramètre clé de la courbe de refroidissement de toutes les données extraites est que l'influence du rayonnement thermique du support/plate-forme est observable, ce qui est logique en raison de la nature des moyens de mesure. La figure E.4 représente la distribution de température obtenue par la prédiction du modèle analytique. Sur une large gamme de couches et d'emplacements divers, il existe un bon accord entre le modèle analytique et les données expérimentales.

Indépendamment des courbes de refroidissement, le souffle des pics de température est enregistré et prédit par les deux approches. Cependant, la différence entre le début et l'amplitude relative des pics pourrait être corrélée à la nature de l'approche de mesure. De plus, les pics qui eux-mêmes représentent l'existence d'adhérence et de contact de couches adjacentes, deviennent progressivement plus petits avec le temps. D'autre part, comme aucun changement de phase n'a été pris en compte dans le modèle, l'énergie libérée pourrait être représentative de la différence entre les pics capturés.

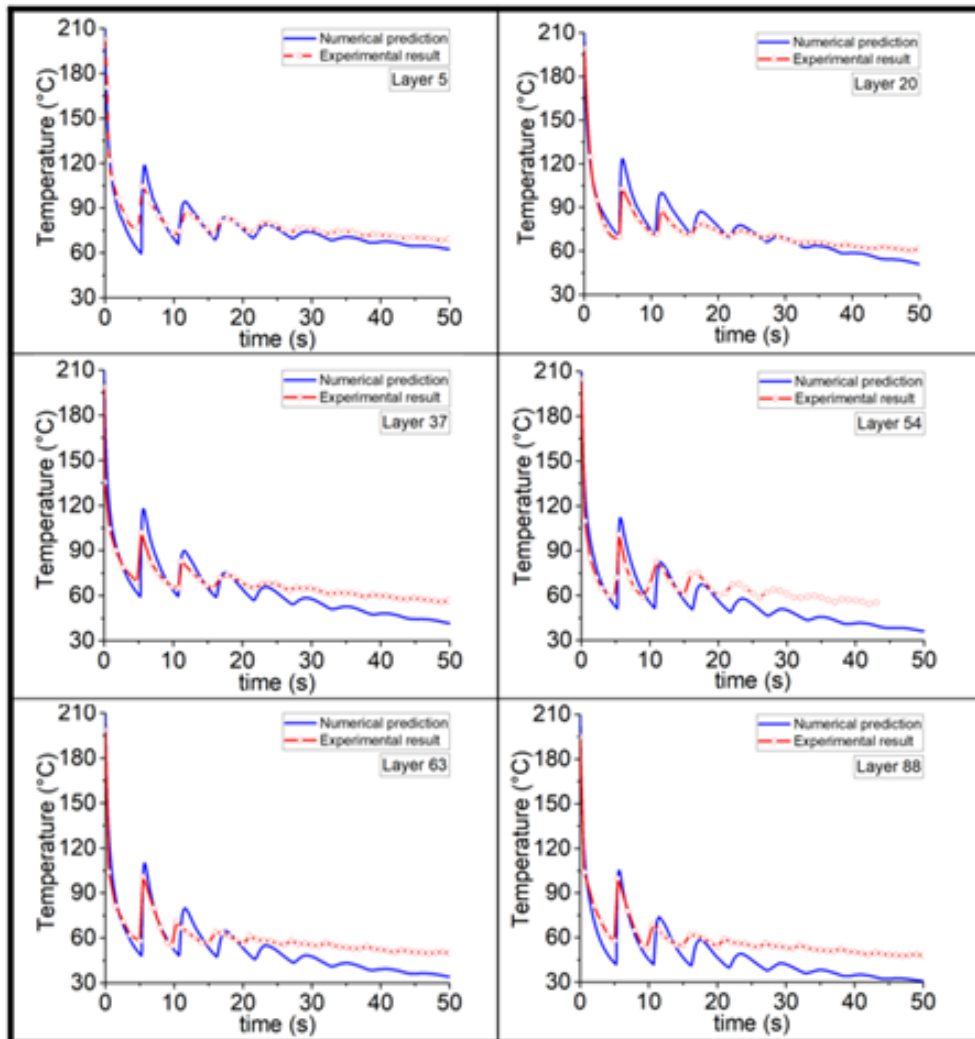


Figure E.4: Comparaison de l'évolution de la température à différents endroits pendant le dépôt d'une paroi verticale constituée de filaments uniques déposés les uns sur les autres avec la prédiction du modèle théorique pour différentes couches avec des emplacements spécifiques.

E.5. Optimisation avec le code développé

Le modèle analytique de transfert de chaleur introduit peut être mis en œuvre à des fins d'optimisation. Le principal avantage du modèle proposé est qu'il est général et qu'il pourrait être mis en œuvre pour divers groupes de matériaux, qu'ils soient amorphes ou semi-cristallins, en considérant une géométrie complexe. Plus précisément, le rôle de divers paramètres de processus peut être pris en compte sur la base du modèle validé expérimentalement.

Dans le cas d'un matériau semi-cristallin (dans notre étude : le PLA), il est largement admis que le temps défini dû au refroidissement et au réchauffage des filaments est crucial pour qu'un bon collage ait lieu. Ainsi, les filaments doivent être suffisamment chauds, mais pas trop, pour éviter la déformation et la dégradation de la qualité de la pièce finale. De plus, l'hypothèse clé du modèle analytique proposé est que le maillage dynamique est considéré par la mise en œuvre de la méthode des volumes finis. Ce problème correspond au transfert de chaleur à l'état instable qui existe dans FDM/FFF.

Pour une meilleure compréhension, les données extraites de la prédiction du code analytique sont présentées en temps réel de dépôt (sans synchronisation du temps à $t=0$). La figure E.5 (a, c) montre le profil de température des couches 1-4 et des couches 20-23. L'optimisation des paramètres à l'aide des valeurs $T_{Liq} = 220$ °C, $T_{Platform} = 70$ °C, $T_{amb} = 30$ °C, $V = 20$ mm/s) est illustrée à la figure E.5(b, d) pour les mêmes couches que celles illustrées à la figure E.5(a, c). La figure E.5(b) montre que la température varie autour de T_c en appliquant les valeurs mentionnées. Ceci conduit à une meilleure cristallisation des couches imprimées et donc une meilleure adhérence, un collage favorable. La figure E.5(d) indique que la température varie pendant un certain temps (environ 20 secondes pour chaque filament) autour de T_c et qu'elle retombe en dessous de T_c et que le refroidissement du matériau ne donne donc pas suffisamment de temps pour la cristallisation et une meilleure adhérence des couches. Ces différences peuvent résulter de l'inhomogénéité des structures imprimées et affecter leur résistance à travers différentes couches.

Les courbes conçues (Figure E.5 (b, d)) montrent la capacité du code analytique présenté ici pour une analyse thermique précise et d'autres objectifs. Cela pourrait être utilisé à des fins d'optimisation en mettant en œuvre tous les paramètres engagés pour avoir la possibilité d'améliorer le processus pour aboutir à des améliorations de la liaison et de l'adhérence. Ces résultats peuvent également être utilisés pour la prise en compte de la viscosité en fonction de la température et de la coalescence des filaments dans les objectifs rhéologiques.

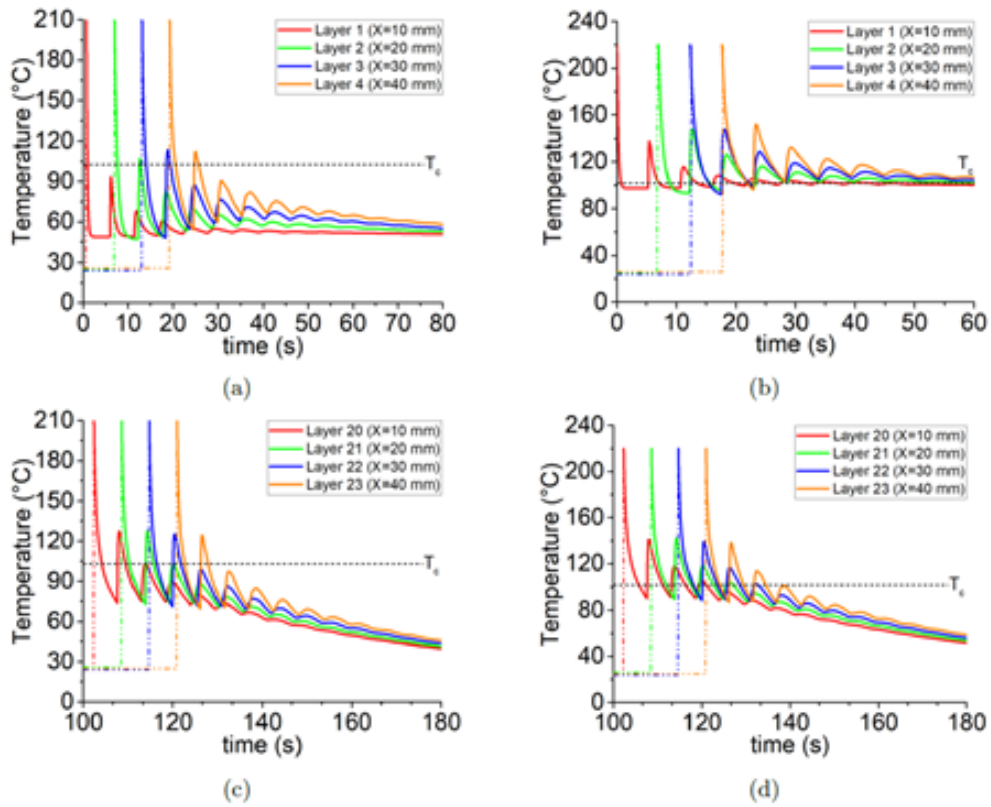


Figure E.5: Évolution de la température pendant le dépôt d'une paroi verticale constituée de filaments uniques déposés les uns sur les autres avec la prédiction obtenue à partir du modèle théorique pour (a) les couches 1-4, (b) la valeur optimisée pour les couches 1-4, (c) les couches 20-23, et (d) la valeur optimisée pour les couches 20-23.

Appendix F

Diagramme

temps-température-transformation des filaments

Connaître l'évolution de la température des polymères thermoplastiques est un enjeu crucial dans l'impression 3D et l'amélioration des caractéristiques finales des pièces fabriquées. Au cours du processus de solidification des thermoplastiques, divers modes de transfert de chaleur (par exemple, convection, conduction et rayonnement) sont engagés. Ce transfert de chaleur a été expliqué dans la section précédente avec les résultats obtenus jusqu'à présent. En fait, ces résultats aident à comprendre le profil de température aux interfaces filament-filament en fonction du temps de dépôt. En simplifiant le modèle général à paramètres Lumpés pour une paire de cylindres (voire une paire de sphères) et selon l'estimation de Holman, on aura :

$$\rho C_P V \frac{dT(t)}{dt} = Q + hA [T(t) - T_\infty(t)] \quad (\text{F.1})$$

où h considère à la fois le coefficient de transfert de chaleur convectif et radiatif, Q la génération de chaleur, C_p la chaleur spécifique, ρ la densité, A la surface, V le volume et k la conductivité thermique. De plus, la viscosité en fonction de la température pour les polymères fondus repose sur la température donnée par une expression d'Arrhenius sous une forme exponentielle [106] :

$$\eta = \eta_0 e^{\left[\frac{E}{R} \left(\frac{1}{T} - \frac{1}{T_0} \right) \right]} \quad (\text{F.2})$$

où E est l'énergie d'activation et R est la constante de gaz. Étant donné que les propriétés rhéologiques telles que la viscosité sont fonction de la température, cette dépendance

pourrait vraisemblablement être corrélée à l'évolution de la température des filaments déposés. Il s'agit d'une idée pour créer une relation entre la viscosité en tant que critère de « Transformation » et la « Température » des filaments pendant le processus par rapport au « Temps » de dépôt pour obtenir le diagramme TTT (Transformation-Température-Temps). Le diagramme TTT permet de comprendre à quelle zone de température et/ou de viscosité, le processus doit être effectué. Dans le cas du FDM/FFF, une meilleure adhérence pourrait être obtenue en connaissant la viscosité. Bien que la diminution de la viscosité entraîne un meilleur écoulement, elle doit être obtenue en augmentant la température qui elle-même entraîne une dégradation. Ainsi, le diagramme TTT permet d'optimiser la viscosité requise par rapport à la température dans un temps de dépôt donné.

En conséquence et en raison de l'évolution cyclique de la température de refroidissement et de réchauffement au cours de FDM/FFF, en considérant les conditions aux limites suivantes :

$$T = T_0 \text{ at } x = 0 \text{ (nozzle head) and } t \geq 0$$

$$T = T_\infty \text{ at } x = \infty \text{ and } t \geq 0$$

Et en résolvant l'équation F.1 en utilisant les conditions aux limites ci-dessus et en tenant compte de la capacité globale pour modéliser le processus de refroidissement du filament cylindrique, nous aurons :

$$T = T_\infty + (T_0 - T_\infty) \exp\left(-\frac{2h}{\rho C_p a_0} t\right) \quad (\text{F.3})$$

où T_0 fait référence à la température de l'extrudeuse. La substitution de l'équation F.3 dans l'équation F.2 donne la relation suivante :

$$\eta = \eta_0 e^{\left[\frac{E}{R} \left(\frac{1}{T_\infty + (T_0 - T_\infty) \exp(-2ht/\rho C_p a_0)} - \frac{1}{T_0} \right)\right]} \quad (\text{F.4})$$

L'équation F.4 est traduit la dépendance à la température de la viscosité pour un filament cylindrique pendant son refroidissement et par conséquent le réchauffage/refroidissement par dépôt de filaments plus jeunes.

La variation de viscosité à l'état fondu en fonction de la température obéit à la loi d'Arrhenius (équation F.2). Pour montrer la validité de cette loi pour le PLA à l'état fondu, nous avons déterminé la viscosité newtonienne du PLA à différentes températures en effectuant des tests isothermes. D'après cette équation, en traçant $\ln \eta$ en fonction de $1/T$, on obtient l'équation suivante qui est une fonction linéaire :

$$\ln \eta = \ln \eta_0 + \left(\frac{E}{R} \right) \times \frac{1}{T} \quad (\text{F.5})$$

La figure F.1 montre clairement la valeur mesurée de la viscosité à différentes températures et états isothermes. Les valeurs pourraient être adaptées à l'équation mentionnée et à la courbe associée, ce qui signifie que les constantes de cette loi, E et η_0 , sont respectivement de 26045 J et 1,7 Pa. S.

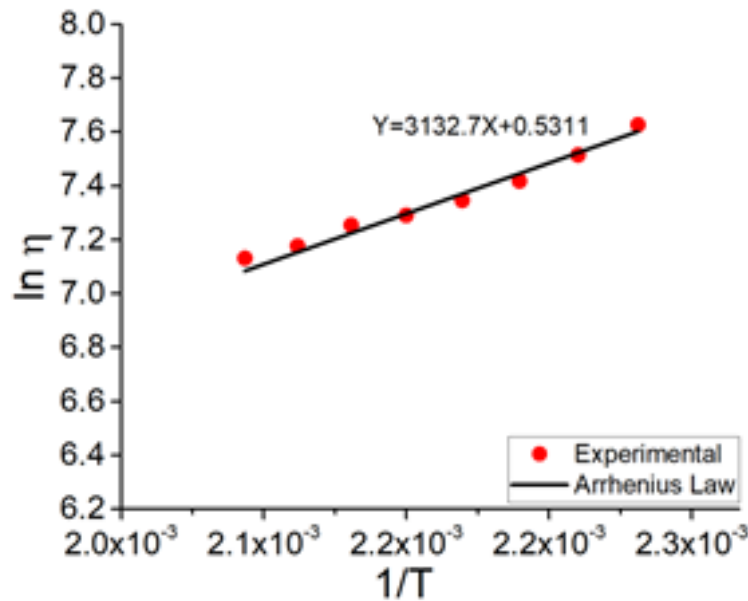


Figure F.1: Évolution de la viscosité dynamique à différentes températures

Comme on peut le voir sur la figure F.2, la viscosité varie pendant la phase de refroidissement d'un filament unique de $T = 210$ °C à la température ambiante dans un temps spécifique. En refroidissant, la viscosité augmente rapidement en régime non linéaire jusqu'au temps ($t \sim 3,5$ s), suit un régime linéaire, et revient à nouveau en régime non linéaire (avec une vitesse plus faible) et atteignant la température ambiante. Apparemment, le $t = 2$ s correspond au $T = 120$ °C, la température à laquelle commence la cristallisation. En revanche, la zone stratégique se situe entre les points de cristallisation et de fusion ($1s < t < 2s$). Sur ce, il est nécessaire de maintenir la température autour ou au-dessus de la température de cristallisation à d'autres fins telles que l'amélioration de la résistance comme expliqué dans les sections précédentes.

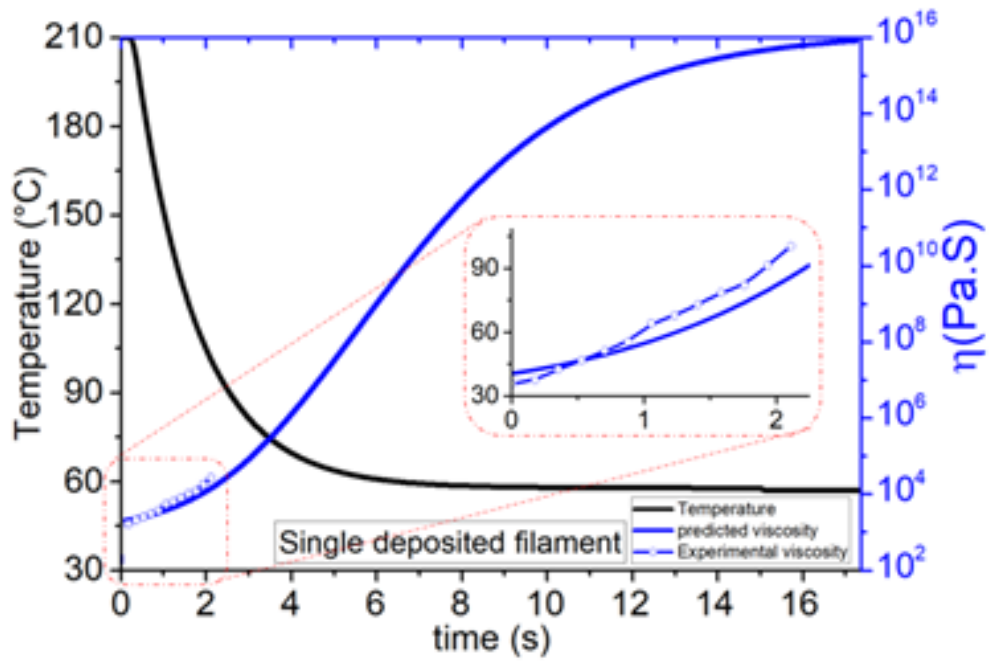


Figure F.2: Diagramme TTT d'un dépôt d'un seul filament

De plus, pour avoir une meilleure vision de la corrélation des trois paramètres mentionnés (Temps-Température-Transformation), leur variation a été présentée dans une courbe 3D comme (voir Figure F.3).

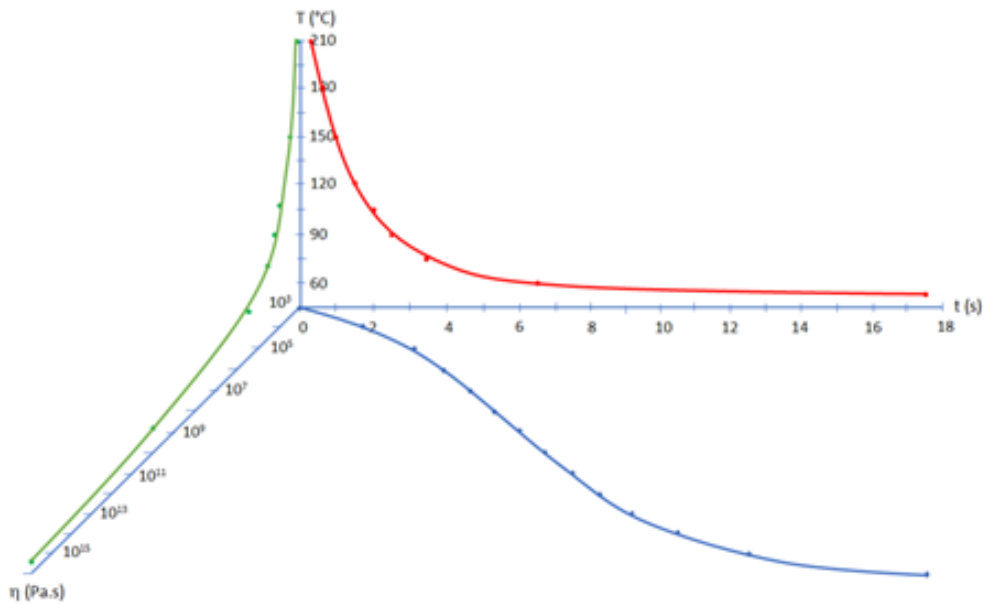


Figure F.3: Diagramme TTT d'un dépôt d'un seul filament

F.1. études de cas : influence des paramètres du processus

Malgré une grande variété d'études essayant d'optimiser le collage des filaments déposés et par conséquent la résistance des pièces finales [36, 120-122], il y a encore un manque de recherches à cet égard. Par conséquent, il est nécessaire de considérer à la fois l'interaction des paramètres et les caractéristiques thermo-rhéologiques des matériaux appliqués pendant le processus FDM/FFF. Cette section montre l'utilité de l'approche proposée en étudiant l'influence des paramètres du procédé sur l'évolution de la viscosité. Jusqu'à présent, nous avons montré l'importance d'étudier la viscosité et la température en même temps et comment elles varient dans les paramètres donnés en FDM/FFF.

L'évolution de la température à différentes vitesses d'impression et températures de plate-forme, identique aux explications précédentes, a été prise en compte comme mentionné dans les sections précédentes. Plus la vitesse d'impression est élevée, plus la vitesse de refroidissement est faible et donc les pics de température se produisent à des moments différents. Apparemment, plus la température de la plate-forme est élevée, plus la vitesse de refroidissement est lente et diminue la période de variation de la viscosité. L'évolution de la viscosité en fonction de la température est illustrée à la figure F.4. Comme mentionné précédemment, la viscosité augmente progressivement à la vitesse d'impression de ($V_{Liq} = 60$ mm/s) par rapport à la condition de référence ($V_{Liq} = 60$ mm/s, $T_{Platform} = 50$ °C). En reliant les observations des graphiques présentés sur la figure F.4, on pourrait conclure que la vitesse d'impression joue un rôle important dans l'évolution de la viscosité plutôt que la température de la plate-forme.

Pour finaliser, l'optimisation de la caractéristique rhéologique et donc du collage des pièces finales a nécessité la prise en compte d'interactions de plusieurs paramètres.

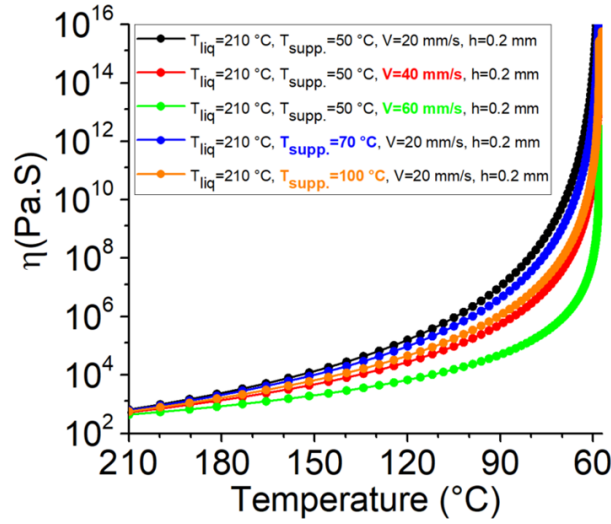


Figure F.4: Évolution de la viscosité de la première couche pendant le dépôt d'une paroi verticale constituée de filaments uniques superposés en fonction de l'évolution de la température du filament déposé.

F.2. Correction de l'évolution de la viscosité

Jusqu'à présent, nous avons considéré l'évolution de la viscosité et de la température simultanément. La viscosité en fonction de la température varie de la température du liquéfacteur à la température ambiante suivant l'équation d'Arrhenius. Cependant, étant donné que le comportement thermomécanique du polymère détermine les diverses transitions et changements d'état physique du polymère, le test DMTA est mis en œuvre en utilisant la configuration de flexion alternée (avec la fréquence de 1 Hz). Le résultat obtenu est montré sur la figure 6.5 comprenant trois états physiques : état vitreux, zone de transition vitreuse et état caoutchouteux. Comme on peut le voir sur la figure 6.5, le matériau présente un état vitreux jusqu'à $\sim 55^\circ\text{C}$ dans lequel il n'y a pas de changement significatif dans E' , E'' , et $\tan \delta$. A l'état vitreux, E' est relativement élevé (>16 GPa). La deuxième zone ($55^\circ\text{C} < T < 85^\circ\text{C}$) correspond à la zone de transition où le phénomène de transition vitreuse s'est produit. E'' diminue drastiquement de 16 GPa à une valeur inférieure à 2 GPa. E'' augmente d'abord puis diminue ; représentant un pic à $\sim 70.2^\circ\text{C}$ appelé température de transition vitreuse du matériau. $\tan \delta$ (E'/E'') indique la même tendance que E'' . L'état caoutchouteux du matériau se situe alors dans la zone de température supérieure à 85°C . Vraisemblablement, la valeur de E' est faible et l'échantillon est relativement mou.

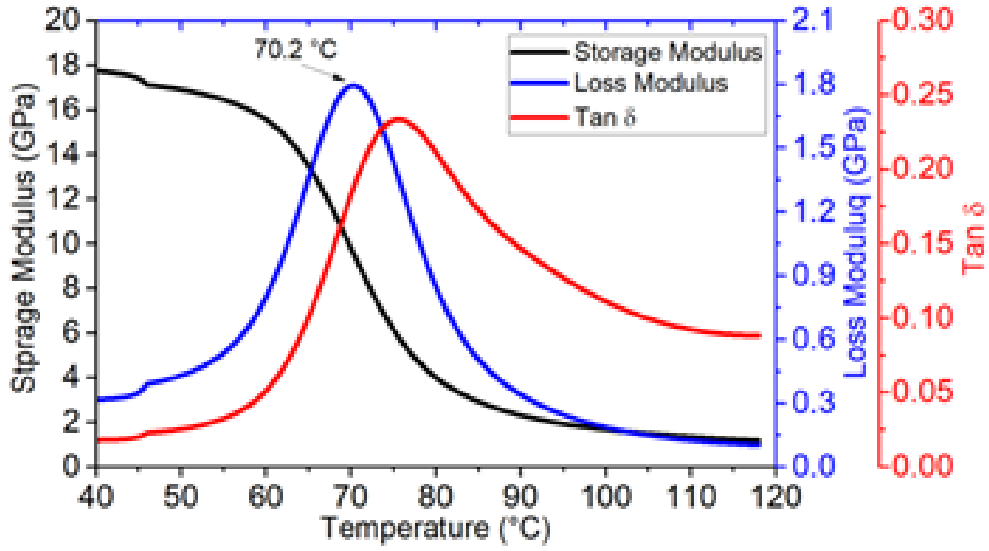


Figure F.5: Résultat du test DMTA pour le PLA

Par conséquent, pour explorer l'influence de la température sur les propriétés viscoélastiques du PLA, un test DMA multi-féquences a été mis en œuvre en mode de flexion en flexion. L'évolution de la viscosité peut être calculée à l'aide de l'équation de Williams-Landel-Ferry (WLF) :

$$\text{Log } a_T = \frac{-C_1(T - T_r)}{C_2 + (T - T_r)} \quad (\text{F.6})$$

où a_T est le facteur de décalage WLF, C_1 et C_2 sont des constantes empiriques ajustées pour s'adapter aux valeurs des paramètres de superposition a_T , T est la température et T_r est la température de référence à la fréquence de référence.

En utilisant la méthode de régression linéaire, l'équation WLF pourrait être transformée comme suit :

$$\frac{1}{\log a_T} = \frac{-C_2}{C_1} \frac{1}{T - T_r} + \frac{1}{C_1} \quad (\text{F.7})$$

Donc, $\frac{1}{\log a_T}$ a été tracé en fonction de $\frac{1}{T - T_r}$. La courbe correspondante est représentée sur la Figure F.6 ($R^2=0.9993$). La valeur de C_1 et C_2 sont alors calculées via les résultats obtenus.

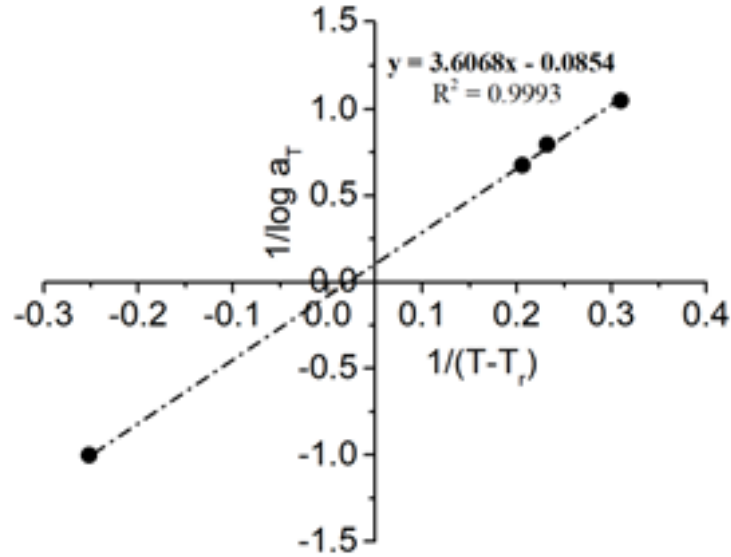


Figure F.6: Régression linéaire de l'équation WLF

Aussi, le coefficient a_T , est défini suivant: $\frac{\eta}{\eta_0}$ qui résulte de l'équation:

$$\eta = \eta_0 \left[10^{\frac{11.7(T-70.2)}{T-28}} \right] \quad (\text{F.8})$$

En substituant l'équation 5.3 dans l'équation F.8, on obtient:

$$\eta = \eta_0 \left[10^{\frac{11.7(T=T_\infty+(T_0-T_\infty)e^{-\frac{2h}{\rho C_p a_0} t} - 70.2)}{T=T_\infty+(T_0-T_\infty)e^{-\frac{2h}{\rho C_p a_0} t} - 28}} \right] \quad (\text{F.9})$$

L'équation F.9 permet de calculer est la viscosité en fonction de la température du polymère à l'état solide (généralement pour $T_{amb} < T < T_g + 50$ °C). Selon les résultats présentés dans la section 6.1, le diagramme TTT d'un filament unique au cours de son dépôt se caractérise par un temps spécifique indiquant la viscosité corrigée obtenue par l'équation WLF. Depuis le début du dépôt ($T = 210$ °C), la viscosité en fonction de la température (équation d'Arrhenius) jusqu'à $t = 1,8$ s ($T=110$ °C) a été déterminée. Ensuite, de $t = 1,8$ s ($T=110$ °C) jusqu'à $t = 17,4$ s ($T = 57$ °C), la viscosité en fonction de la température obtenue par l'équation WLF a été tracée. Le décalage important entre deux courbes montre clairement le comportement viscoélastique du matériau. Comme le montre la figure F.7, les zones 1-3 correspondent respectivement à l'état caoutchouteux, à la zone de transition vitreuse et à l'état vitreux. A l'état caoutchouteux, il y a une augmentation progressive de la viscosité en entrant dans la zone de transition vitreuse, alors que l'évolution de la viscosité reste quasiment constante à l'état vitreux. Bien que le comportement viscoélastique du matériau ait été pris en considération à l'aide de l'équation WLF, il est vraisemblable qu'une augmentation

brutale doit se produire en raison de deux changements de phase, respectivement dans la zone de fusion et la zone de cristallisation. Dans l'approche proposée, ce terme n'est pas inclus car il doit être étudié séparément.

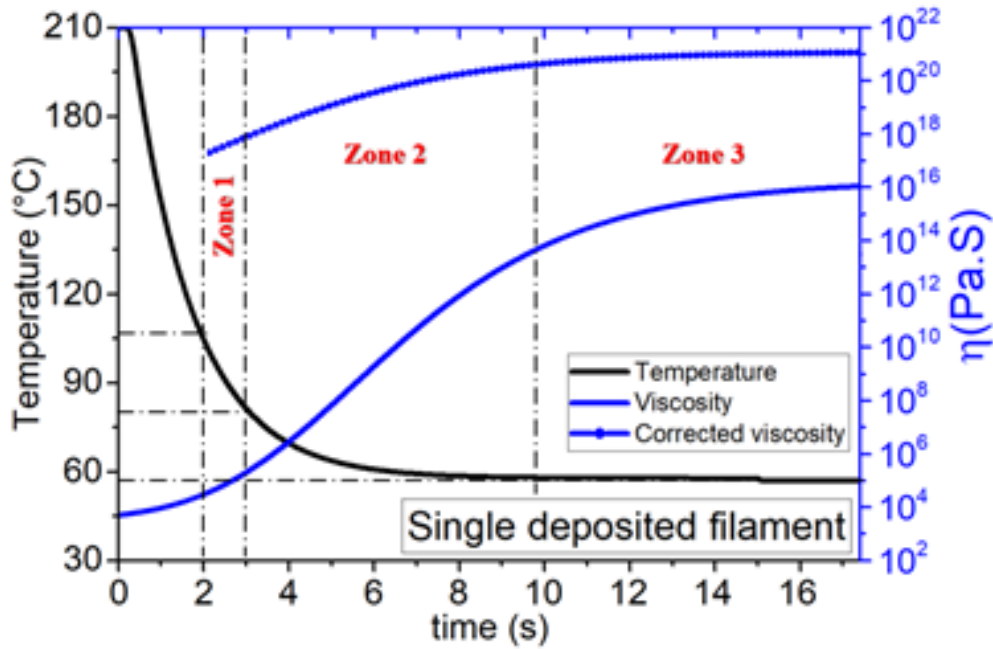


Figure F.7: Diagramme TTT d'un dépôt à filament unique utilisant la prédiction WLF

La principale caractéristique de l'approche présentée est la possibilité d'obtenir le diagramme Temps-Température-Transformation du matériau pendant le dépôt et d'appliquer les résultats dans les procédures d'optimisation. Il a été démontré que la viscosité affectée par le profil de température cyclique pouvait déterminer la caractéristique des produits finaux. Sa variation à travers en fonction de la déposition des couches a été présentée. De plus, une étude de l'évolution de la viscosité paramétrique en fonction des paramètres du procédé a également été réalisée. L'influence de la vitesse d'impression et de la température de la plate-forme sur l'évolution de la viscosité indique que l'effet des paramètres du procédé est inévitable et que l'interaction des paramètres doit être prise en compte.

De plus, l'influence du profil de température cyclique sur le comportement viscoélastique du matériau à l'aide de l'équation WLF a indiqué que la variation de viscosité à l'état solide joue un rôle important dans la caractéristique rhéologique du matériau. Les résultats présentés ici peuvent aider les chercheurs à améliorer la qualité des pièces imprimées en FDM/FFF et par conséquent à améliorer leur résistance.

Appendix G

Conclusion et perspectives

Cette thèse a été réalisée sous la tutelle de deux laboratoires, le LIFSE et le PIMM, à l'École Nationale Supérieure des Arts et Métiers. Il vise à étudier les caractéristiques rhéologiques des matériaux tout au long du procédé FDM/FFF en se basant sur des approches expérimentales et numériques. De plus, une technique in situ de mesure de l'évolution de la température des couches déposées à leurs interfaces a été proposée. Dans un premier temps, une étude bibliographique a été réalisée sur le rôle des variables du procédé et du transfert thermique ainsi que la variation de la viscosité sur la qualité de la pièce. En ce qui concerne les paramètres du processus, le rôle de trois paramètres tels que la température du liquéfacteur, la température de la plate-forme et la vitesse d'impression sur la résistance mécanique et la qualité de la pièce finale a été discutée. Ensuite, l'influence de ces paramètres sur la variation de température des filaments au cours du dépôt a été discutée expérimentalement. Pour ce faire, une technique de mesure locale à l'aide de thermocouples de type K ($d=80\ \mu\text{m}$) a été utilisée permettant de reconnaître la variation de température de chaque couche lors de l'étape de dépôt. Nos observations nous permettent d'avoir un ensemble de conclusions à travers l'influence des paramètres de processus mentionnés :

- L'interaction des paramètres joue le rôle le plus important dans la prise en compte de la caractérisation mécanique des pièces imprimées.
- Le module de Young et la déformation à la rupture pourraient être un indicateur pour évaluer les performances mécaniques des pièces imprimées.) sur les CV.
- La température des filaments joue un rôle important dans les caractéristiques des pièces imprimées.

- La conséquence du dépôt dans des conditions différentes montre que l'augmentation de la température du liquéfacteur est plus importante sur le contact des filaments, cependant, l'impact de la vitesse d'impression est plus important.
- La conséquence du dépôt dans des conditions différentes montre que l'augmentation de la température du liquéfacteur est plus importante sur le contact des filaments, cependant, l'impact de la vitesse d'impression est plus important.

Le profil de température enregistré a ensuite été comparé aux résultats obtenus en utilisant une caméra IR comme approche globale nous permettant d'enregistrer la variation de température à la surface externe des couches déposées. Dans ces deux approches, malgré les avantages et les limites de chacune, les résultats obtenus ont montré qu'il existe une différence remarquable entre la vitesse de refroidissement et les pics de réchauffage. Ce résultat permet de considérer la technique proposée comme une approche prometteuse pour des étapes ultérieures.

La méthode des volumes finis a été appliquée pour modéliser le transfert de chaleur des filaments déposés, puis a été validée par la technique mentionnée pour la mesure de température in situ. L'évolution de la température a été prédite en bon accord avec les résultats expérimentaux enregistrés. Pour montrer l'utilité du code développé, des efforts ont été pris en compte, à des fins d'optimisation, pour considérer l'influence des principales variables du procédé sur la variation de température des filaments lors du dépôt. Classiquement, les paramètres sont déterminés sur la base du fait qu'en diminuant la vitesse de refroidissement du matériau, il maintient sa température suffisamment élevée pour avoir une meilleure adhérence avec le filament préalablement déposé ou celui en cours de dépôt. Les résultats obtenus ont ensuite été intégrés dans la caractéristique rhéologique des filaments en modélisant l'évolution de la viscosité des filaments et l'effet des principales variables de processus sur eux. L'idée est donc d'évaluer l'influence des variables du procédé et de l'évolution de la température des filaments simultanément à mettre en œuvre sur l'évolution de la viscosité non isotherme du filament lors du dépôt. Ainsi, un diagramme « Temps-Température-Transformation » (TTT) des filaments lors du dépôt permettant d'évaluer simultanément la température et la viscosité a été proposé. Le résultat cette étude est alors un code informatique qui permet aux chercheurs d'optimiser le processus pour obtenir de bonnes pièces finales.

En résumé, ce travail a contribué à l'élaboration d'un code permettant de prédire l'évolution de la température des filaments. Elle est basée sur la modélisation des transferts thermiques

et des phénomènes associés. La prochaine étape serait alors la mise en œuvre des caractéristiques rhéologiques avec les paramètres associés à des fins d'optimisation.

Article No. 1:

HR Vanaei, M Shirinbayan, M Deligant, K Raissi, S Khelladi, A Tcharkhtchi; Influence of process parameters on thermal and mechanical properties of PLA fabricated by Fused Filament Fabrication; Polymer Engineering and Science Journal, 60:1822–1831 (2020).

DOI: [10.1002/pen.25419](https://doi.org/10.1002/pen.25419)

Influence of process parameters on thermal and mechanical properties of polylactic acid fabricated by fused filament fabrication

Hamidreza Vanaei^{1,2}  | Mohammadali Shirinbayan² | Michael Deligant¹ | Kaddour Raissi¹ | Joseph Fitoussi² | Sofiane Khelladi¹ | Abbas Tcharkhtchi²

¹Arts et Metiers Institute of Technology, CNAM, LIFSE, HESAM University, Paris, France

²Arts et Metiers Institute of Technology, CNRS, CNAM, PIMM, HESAM University, Paris, France

Correspondence

Hamidreza Vanaei, Arts et Metiers Institute of Technology, CNAM, LIFSE, HESAM University, 75013 Paris, France.
Email: hamidreza.vanaei@ensam.eu

Abstract

Fused filament fabrication is considered one of the most used processes in additive manufacturing rapid prototypes out of polymeric material. Poor strength of the deposited layers is still one of the main critical problems in this process, which affects the mechanical properties of the final parts. To improve the mechanical strength, investigation into various process parameters must be considered. In this article, the influence of different process parameters has been experimentally investigated by means of physicochemical and mechanical characterizations. Special attention was given to the thermal aspect. In that respect, the in situ measurement of temperature profile during deposition indicated that several parameters affect the cooling rate of material and consequently have an influence on the final parts. It was found that the influence of increasing the extruder temperature is more significant in comparison with other process parameters.

KEYWORDS

FFF, in situ temperature measurement, polylactic acid, process parameters

1 | INTRODUCTION

Fused filament fabrication (FFF) is one of the numerous additive manufacturing (AM) processes. In FFF, a three-dimensional (3D) geometry is formed through the deposition of successive layers of extruded thermoplastic filament (eg, polylactic acid [PLA], acrylonitrile butadiene styrene [ABS], polypropylene [PP], polyethylene [PE], Nylon, or polyether ether ketone [PEEK]^[1]). In this process, the filaments are extruded in layers parallel to the X-Y plane and that the layers are built in a successive manner in the Z-direction to create a layer-by-layer 3D part.^[2] Due to the generated heat by extruder, the hot layer deposited onto the previous one. The previous layer is in the progress of cooling and causes cooling

and reheating of substrate layers.^[3,4] It is thought that the bonding of two adjacent filaments would be directly affected by this temperature profile because of the cyclic temperature profile of the polymer during deposition.

The abilities to fabricate complex geometries and lower cost of manufacturing have made research studies motivated into various characterizations and improvements of parts fabricated by FFF.^[5-7] Despite the mentioned advantages, mechanical properties of parts manufactured by FFF process are inherently poor,^[8] which is why it is required to consider the mechanical properties of 3D-printed materials compared with the conventional methods.^[9]

In order to have a better understanding of the features of temperature profile between adjacent filaments,

various mathematical approaches have been proposed. A transient heat transfer has been proposed to analyze the filament deposition with physical contacts between any filament and its neighbors.^[10] Also, a two-dimensional heat transfer model of two filaments was generated to consider the temperature evolution during FFF process using the finite element method.^[11] Furthermore, a one-dimensional transient heat transfer model was developed by Sun et al^[12] and combined with the spherical particle sintering model.^[13] They estimated the FFF temperature profile and the bond formation for a single filament depositing process.

In FFF process, each parameter has its own influence on the microstructure and filaments bonding of the fabricated parts.^[8,14,15] There are three important groups of influencing parameters:

1. Material parameters, such as molecular weight, density, surface tension, thermal conductivity, heat capacity, moisture in polymer, melting temperature, crystallization temperature, and glass transition temperature.
2. Process parameters, such as nozzle temperature, chamber temperature, road width, speed print head, layer thickness, air pocket, and frame angle.
3. Machine parameters, such as nozzle shape, nozzle temperature, print head, positioning accuracy x-y, and positioning accuracy y-z.

Many studies also focused on finding a relationship between the mechanical properties and processing parameters of FFF process in printed parts, such as layer thickness or frame angle.^[16]

In this article, an overview of the process parameters is presented. The experimental procedure is explained. Then, different experimental characterization results are presented. Finally, the temperature evolution of PLA filaments during FFF process was performed as a function of different parameters. The aim of these case studies is to study the effect of each parameter on the mechanical and thermal behavior of fabricated parts. This research is useful for designing and optimizing the process parameters by improving the mechanical properties of products manufactured by FFF.

2 | AN OVERVIEW ON THE PROCESS PARAMETERS IN FFF

Due to the nature of FFF, almost all the 3D-printing machines comprise various process parameters. The temperature of nozzle and chamber, path width, print speed, layer thickness, air pocket, and frame angle could be considered in the characterization of fabricated parts. Almost

all of them affect the filament bonding and consequently the mechanical behavior of 3D-printed parts. However, researchers tried to focus on some key parameters to optimize the experimental procedure and finally get the combination of parameters.^[17] Various research studies considered the influence of process parameters on the parts fabricated using FFF. Build orientation and frame angle and their effect on the mechanical properties of 3D-printed parts have been consequently studied, and the effect of raster angle by consideration of infill patterns has been analyzed.^[8,16]

In addition, another research reported the effect of in-process and postprocess on thermal global state during parts 3D printing and highlighted the importance of environment and support temperatures.^[18] Diffusion and neck growth between two adjacent filaments would be affected by changing of environment or support temperatures, which confirms the importance of heat transfer in this process.

Regarding the applied material and studied parameters, it was found that almost all researchers tried to consider the effect of parameters by different methods of characterization (eg, tensile or bending) with using a unique parameter at different values. A brief representation of research studies on various materials is given in Table 1.

Almost all these studies are based on the consideration of improving the mechanical behavior of materials. Consequently, it is not possible to have a comparison between all the process parameters due to the different material and manufacturing conditions or type of the machine.

Although Ahn et al^[24] studied the effect of layer thickness (height) on ABS specimen, they concluded that mechanical behavior of the material is not affected by the variation of this parameter. Sood et al^[28] showed that the smallest value of layer thickness contributes to better tensile behavior. Besides, other research studies showed that as much as the layer height decreased, mechanical behavior improved.^[25,29] Furthermore, based on the mentioned studies on the effect of process parameters, it was extracted that there are not sufficient research studies on the effect of temperature (namely liquefier, support, and environment temperature) and print speed (that could act as a factor in cooling of the material) on the fabricated parts. Rodríguez et al^[30] concluded that there is no influence of support temperature on the mechanical behavior of the fabricated parts as well as the study performed by Ahn et al.^[24] However, Sun et al^[3] and Xiaoyong et al^[27] showed that the support temperature affects the mechanical behavior of the printed parts.

Eventually, from the above description of the previous research studies and also the fact that each of them considered a portion parameters' values, it would be useful to be noted that the interaction of parameters plays

TABLE 1 Representation of FFF-based research studies in consideration of process parameters

Material	Variable parameters	Mechanical properties	References
PLA	Layer thickness infill density Postprocessing heat treatment at $T = 100^{\circ}\text{C}$	Shear stress	[19]
ABS	Five building orientations on x and y axes	Impact strength	[20]
ABS	Two orientations (at x axis— 0° , 90°) Y axis orientation (0° , 30°)	Tensile strength	[21]
ABS	Raster orientation Number of layers (1-35)	Tensile strength Elastic modulus Elongation at break	[22]
ABS	Five-layer orientation (45/−45, 0, 45, 90, 45/0)	Tensile strength Modulus Impact resistance	[23]
ABS	Raster orientation Air gap Model temperature	Tensile strength Compressive strength Comparison of results with injection molding	[24]
PLA	Effect of process parameters on bonding	Tensile strength	[25]
PLA	Deposition orientation Layer thickness Raster variation	Tensile strength Flexural strength Impact strength	[26]
PEEK ABS	Layer thickness Raster angle	Tensile Compression Bending strength	[16]
PEEK	Temperature variation (bed and environment)	Tensile strength	[27]
ABS	Temperature profile Temperature variation with part building	Three-point bending test Thermal analysis	[3]

Abbreviations: FFF, fused filament fabrication; PLA, polylactic acid; ABS, Acrylonitrile butadiene styrene; PP, Polypropylene; PE, Polyethylene; PEEK, Polyether ether ketone.

the most important role in consideration of mechanical characterization of the fabricated parts. Due to these observations, the effect of a group of process parameters has been studied in the following 3D-printing experimental study.

3 | MATERIALS AND METHODS

3.1 | Material, 3D printer, and sample preparation

A commercially PLA filament with a diameter of 1.75 mm and the density of $\rho = 1.24 \text{ g/cm}^3$ has been used. As shown in Figure 1, a unidirectional moving of the extruder assumed to deposit the filaments once against each other's having a more homogenous shape for temperature measurements. A desktop 3D printer was then used by fixing the temperature of liquefier and support to produce the pieces. One can note that three samples per parameter set were used. The sampling position for all characterizations is shown in Figure 1.

3.2 | Process parameters classification

As mentioned, there are various parameters in 3D printing that affect the mechanical behavior of filaments and the strength of the fabricated parts. Then, it is important to classify these parameters to have a comparison between them (Table 2).

3.3 | Characterization methods

3.3.1 | Physicochemical characterization

Differential scanning calorimetry (DSC) was performed using a TA Instruments Q1000. Samples ($\sim 7 \text{ mg}$) were sealed in aluminum pans and heated from room temperature to 200°C with a heating rate of $10^{\circ}\text{C}/\text{min}$ to determine the crystallization and melting temperature of the filaments. Then, the crystallinity of PLA was calculated using the following equation^[31]:

$$X_c = (\Delta H_m - \Delta H_c) / \Delta H_m^0, \quad (1)$$

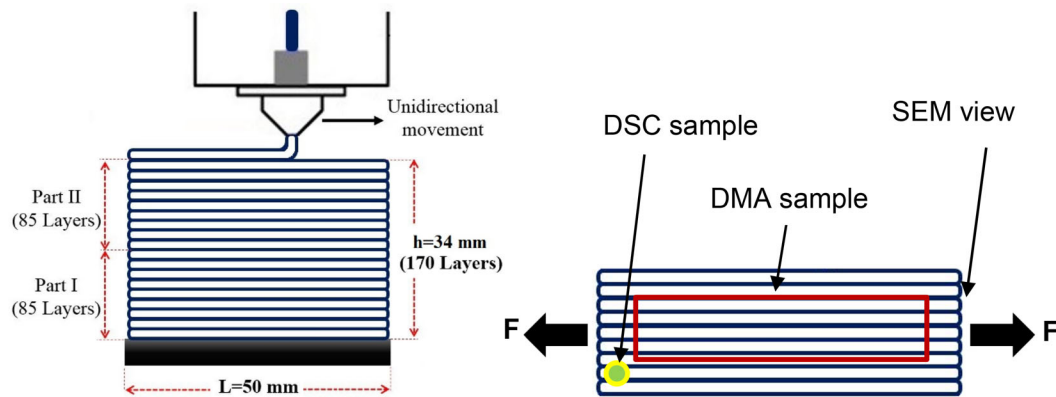


FIGURE 1 Schematic of the test sample: dimension of the applied test sample and deposition mechanism of layers (thickness = 0.2 mm) [Color figure can be viewed at wileyonlinelibrary.com]

TABLE 2 Representation of the groups of process parameters

Condition No.	Liquefier temperature (°C)	Support temperature (°C)	Speed (mm/s)	Layer height (mm)
1	200	50	20	0.2
	210			
	220			
	230			
2	210	50	20	0.2
		70		
		100		
3	210	50	20	0.2
			40	
			60	
4	210	50	20	0.1
				0.2
				0.3

where ΔH_c and ΔH_m are the enthalpies of cold crystallization and melting, respectively. Also, the heat of melting (ΔH_m^0) of 100% crystalline PLA considered equal to $93.7 \text{ J/g}^{[31]}$ according to the literature.

Dynamic mechanical analysis (DMA) was used to measure the glass transition temperature. DMA tests have been performed on the samples using DMA Q800 Instrument from TA Company. The tests have been realized with a sample size of $25 \times 10 \times 4 \text{ mm}^3$ under tensile mode at the following conditions: temperature range 40°C to 100°C , frequency 1 Hz, and temperature rate of $2^\circ\text{C}/\text{min}$.

3.3.2 | Mechanical properties

Tensile tests until failure have been carried out on INSTRON 4301 machine. The specimen geometry used for the quasi-static tensile test was based on a rectangular specimen. The dimension of the specimen defined to be $50 \times 17 \times 0.2 \text{ mm}^3$. However, based on the dimensional change that occurs during the process, a digital caliper was

used to precisely measure the required dimension. All calculations regarding mechanical behavior have been proposed as mentioned. The loading velocity was 1 mm/min.

3.3.3 | Microstructure observation

Microscopic observation, using a scanning electron microscope (SEM; HITACHI 4800 SEM), was performed to investigate the material microstructure and especially the deposition sequence of adjacent filaments. The ImageJ software was also used to evaluate the dimension variation using SEM micrographs.

3.3.4 | Online temperature monitoring of filaments during deposition

Due to multilayer deposition, there is a cyclic temperature profile in FFF process. This is a critical issue to the formation of them and consequently their strength. To

measure this cyclic temperature, it is required to use a device that can measure the temperature of the polymer. A thermocouple type *K* with a diameter of 80 μm , capable of measuring temperature from -75°C to 250°C was used.^[32] To measure the temperature evolutions, a measurement device “Datapaq Tracker Telemetry system” was used (an in situ measurement device using in rotational molding process^[33]).

4 | EXPERIMENTAL RESULTS AND DISCUSSIONS

4.1 | Process parameters effects

4.1.1 | Influence of liquefier temperature

The influence of liquefier temperature has been studied. Four values of liquefier temperature were chosen (200°C , 210°C , 220°C , and 230°C). Based on Figure 2 and the data presented in Table 3, DSC results showed that for each value of liquefier temperature, there is a variation in the crystallization zone, which affects the crystallinity of the material during the process.

Figure 3 shows the tensile behavior at different values of liquefier temperature. Results showed that as much as

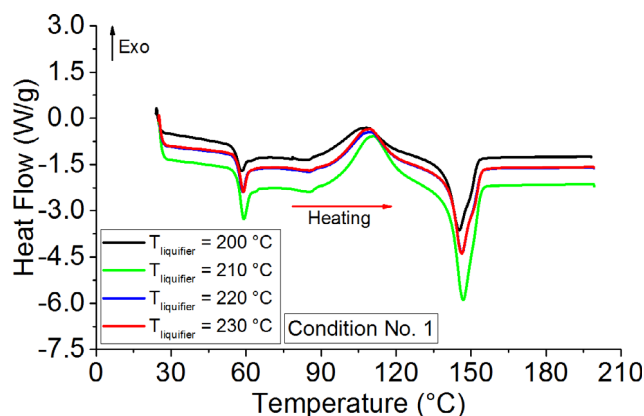


FIGURE 2 Differential scanning calorimetry (DSC) results for samples fabricated at different liquefier temperatures [Color figure can be viewed at wileyonlinelibrary.com]

the crystallinity increased, ultimate strength slightly increased. The highest crystallinity (in condition No. 1) refers to the liquefier temperature $T = 220^\circ\text{C}$. In fact, PLA is a polyester. In the family of polyesters, the crystallization can be slow or rapid. For PLA, the crystallization depends on the crystallization rate or speed. However, it is limited.

Moreover, at $T = 200^\circ\text{C}$, the value of Young's modulus is higher than others. One can note that the results show the same failure strain.

SEM micrographs on two samples under condition No. 1 are shown in Figures 4 and 5. In this regard, for the sample produced by a liquefier temperature of $T = 200^\circ\text{C}$ with the highest Young's modulus, one can note that the brittle failure of samples (Figure 4).

However, for the samples produced by the liquefier temperature of $T = 220^\circ\text{C}$, one can observe that the ductility increased as shown in Figure 5 in which the plastic deformation is observable in the sequence of SEM micrographs.

4.1.2 | Influence of support temperature

Based on the degree of crystallinity and the value of crystallization temperature (see Table 4): (a) the increase of support temperature to $T = 70^\circ\text{C}$ provides more

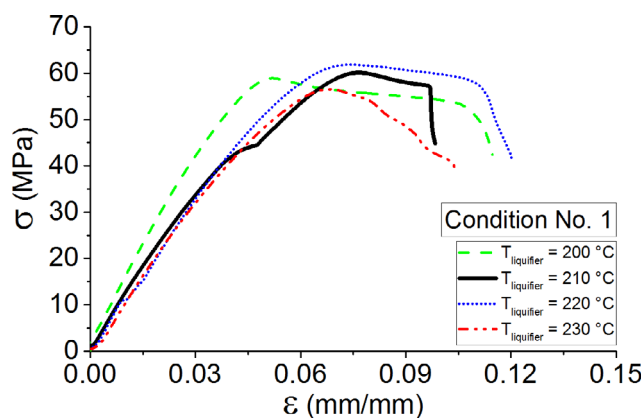


FIGURE 3 Tensile behavior of condition No. 1 for various liquefier temperatures [Color figure can be viewed at wileyonlinelibrary.com]

TABLE 3 Value of different properties obtained from DSC, DMA, and tensile results for condition No. 1

Conditions	T_g ($^\circ\text{C}$)	T_c ($^\circ\text{C}$)	T_m ($^\circ\text{C}$)	% Crystallinity	σ_{max} (MPa)	E (GPa)
No. 1 $T_{\text{Liquefier}} = 200^\circ\text{C}$	62.3	108.4	140.5	6.72	59 ± 2	1.8 ± 0.1
$T_{\text{Liquefier}} = 210^\circ\text{C}$	62.2	109.7	146.9	5.12	60 ± 1.5	1.2 ± 0.1
$T_{\text{Liquefier}} = 220^\circ\text{C}$	62	108.4	146.3	7.25	62 ± 2	1.4 ± 0.1
$T_{\text{Liquefier}} = 230^\circ\text{C}$	62	107.8	146.4	6.83	57 ± 1.5	1.1 ± 0.1

Abbreviations: DMA, dynamic mechanical analysis; DSC, differential scanning calorimetry.

possibilities of polymer chain arrangements and (b) crystallization degree is higher for support temperature of $T = 70^\circ\text{C}$.

Following the tensile behavior and especially the failure strain (Figure 6), the increase of support temperature concluded in higher crystallinity and more ductility in the fabricated sample.

4.1.3 | Influence of print speed

Three values of print speed have been chosen (condition No. 3). Print speed increases the cooling time and let the polymer chains to be rearranged. The DSC results showing that increase in print speed (Table 5) produces a higher degree of crystallinity of the material.

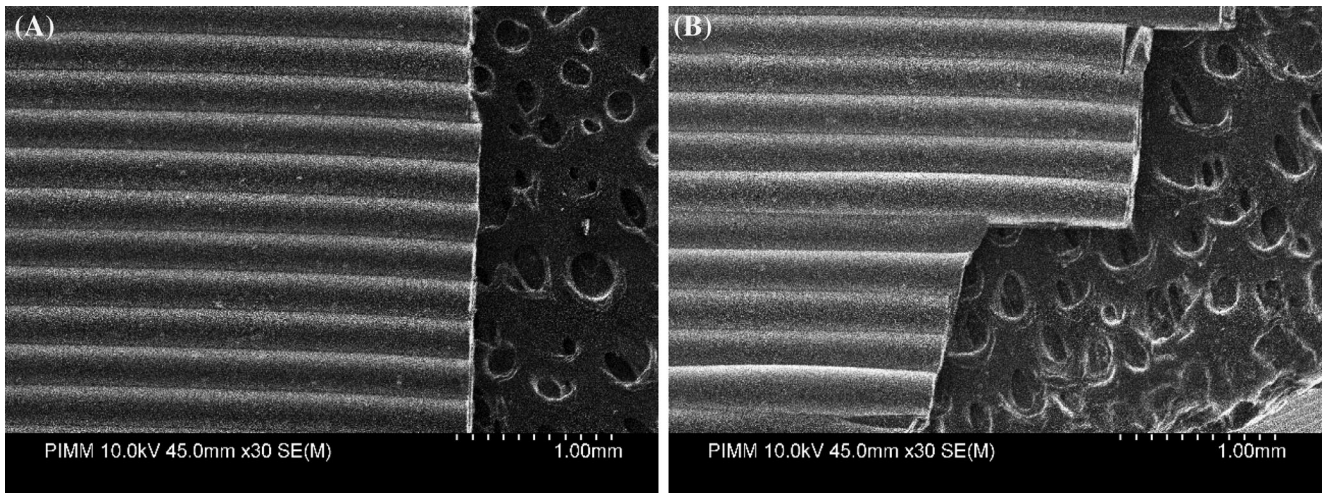


FIGURE 4 Scanning electron microscope (SEM) micrographs for, A, and B, at various location of failure sections for the fabricated sample at $T_{liq} = 200^\circ\text{C}$

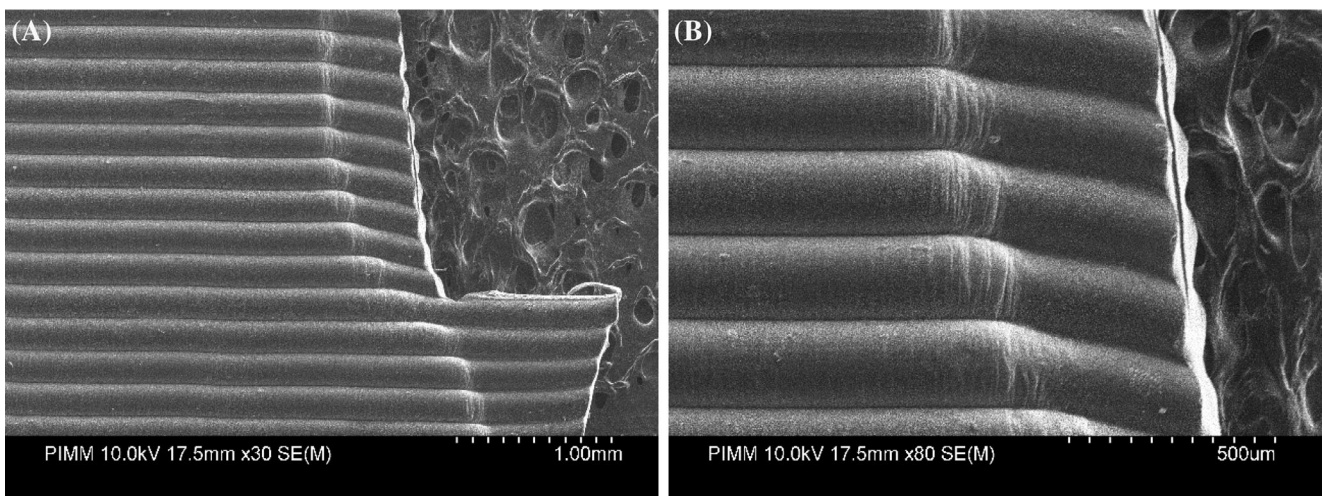


FIGURE 5 Scanning electron microscope (SEM) micrographs for, A-D, at various location of failure sections for the fabricated sample at $T_{liq} = 220^\circ\text{C}$

TABLE 4 Value of different properties obtained from DSC, DMA, and tensile results for condition No. 2

Conditions	T_g ($^\circ\text{C}$)	T_c ($^\circ\text{C}$)	T_m ($^\circ\text{C}$)	% Crystallinity	σ_{max} (MPa)	E (GPa)
No. 2 $T_{Support} = 50^\circ\text{C}$	62.2	109.7	146.9	5.12	60 ± 1.5	1.2 ± 0.1
$T_{Support} = 70^\circ\text{C}$	62	107.8	146.4	6.83	61.5 ± 2	1.3 ± 0.1

Abbreviations: DMA, dynamic mechanical analysis; DSC, differential scanning calorimetry.

However, the results of the tensile test performed for this condition demonstrated that the higher value of crystallinity degree causes higher ductility of the fabricated part. The results showed a similar Young's modulus value for different values of print speed.

4.1.4 | Influence of layer height

The last condition that has been considered is the influence of layer height on formation of adjacent filaments. Degree of crystallinity for each sample has been calculated. Results show that by increasing the layer height, degree of crystallinity is enhanced. Higher thickness can allow the gradient of temperature in each filament and consequent rearrangement of polymer chains (Table 6).

Tensile results present a higher ductility in layer height of $h = 0.3$ mm, while Young's modulus values are the same.

Physicochemical and mechanical characterizations of fabricated parts in various processing conditions are

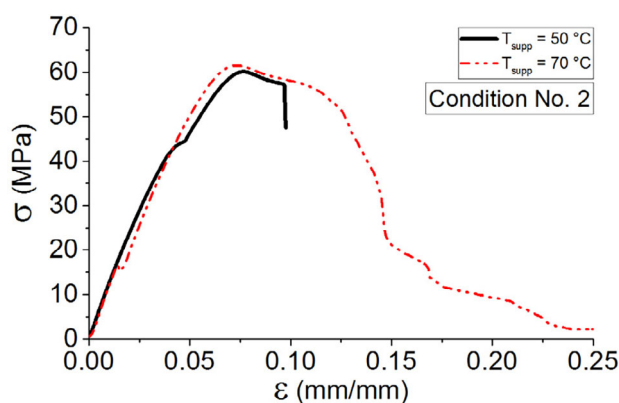


FIGURE 6 Tensile behavior of condition No. 2 for various support temperatures [Color figure can be viewed at wileyonlinelibrary.com]

TABLE 5 Value of different properties obtained from DSC, DMA, and tensile results for condition No. 3

Conditions	T_g (°C)	T_c (°C)	T_m (°C)	% Crystallinity	σ_{max} (MPa)	E (GPa)
No. 3						
$V = 20$ mm/s	62.2	109.7	146.9	5.12	60 ± 1.5	1.2 ± 0.1
$V = 40$ mm/s	62	108.4	146.3	6.83	56.5 ± 2	1.1 ± 0.1
$V = 60$ mm/s	62	107.8	146.4	7.25	56.5 ± 2	1 ± 0.1

Abbreviations: DMA, dynamic mechanical analysis; DSC, differential scanning calorimetry.

TABLE 6 Value of different properties obtained from DSC, DMA, and tensile results for condition No. 4

Conditions	T_g (°C)	T_c (°C)	T_m (°C)	% Crystallinity	σ_{max} (MPa)	E (GPa)
No. 4						
$h = 0.1$ mm	62.3	108.4	140.5	6.72	56 ± 2	1.2 ± 0.1
$h = 0.3$ mm	62	107.8	146.4	6.83	61.5 ± 2	1.3 ± 0.1

Abbreviations: DMA, dynamic mechanical analysis; DSC, differential scanning calorimetry.

performed so far. The results comparison demonstrates that almost in each group of conditions, there might be a best value for a process parameter. However, it is difficult at this stage to have a conclusion related to the optimal values and process configuration. Hereafter, temperature profile of the vertical wall will be discussed.

4.2 | Temperature profile of vertical wall

Several experimental tests have been performed using local measurements in order to record the temperature profile of filaments in different locations. The recorded temperature profile is indicated for the first filament in a sequence of deposition at the location of $x = 5$ mm from the start of deposition (Figure 7). The aim is to recognize the temperature profile of adjacent filaments during deposition using in situ localized measurement.

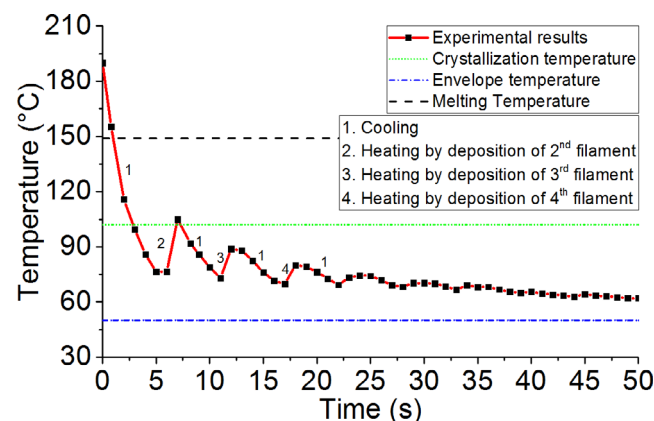


FIGURE 7 Temperature evolution during fused filament fabrication process ($T_{liq} = 210$ °C, $T_{supp} = 50$ °C, $V = 20$ mm/s, and $h = 0.2$ mm) [Color figure can be viewed at wileyonlinelibrary.com]

As a case study (Figure 8), the evolution of temperature for filaments during deposition has been performed at various printing speeds (condition No. 3).

Results show that by increasing the printing speed, the temperature evolution of first deposited filament (at $x = 5$ mm from the deposition) remains above the crystallization temperature. This fact especially occurred at a printing speed of $V = 60$ mm/s. Based on the discussed results, increasing the print speed affects the degree of crystallinity and rearrangement of polymer chains by decreasing the cooling time. This is a preliminary result for measurement of the evolution of temperature during deposition and it is required to be studied numerically.

5 | MICROSTRUCTURE ANALYSIS OF THE FABRICATED PARTS

Figure 9 shows the microstructure analysis of the printed part (10 deposited filaments) for this condition: $T_{liq} = 210^\circ\text{C}$, $T_{supp} = 50^\circ\text{C}$, $V = 20$ mm/s, and $h = 0.2$ mm. The

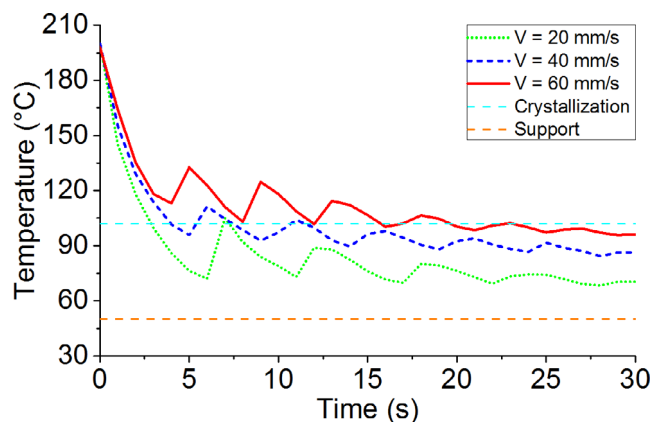
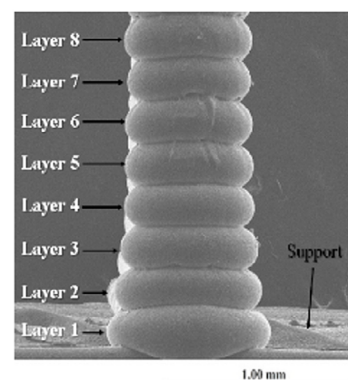
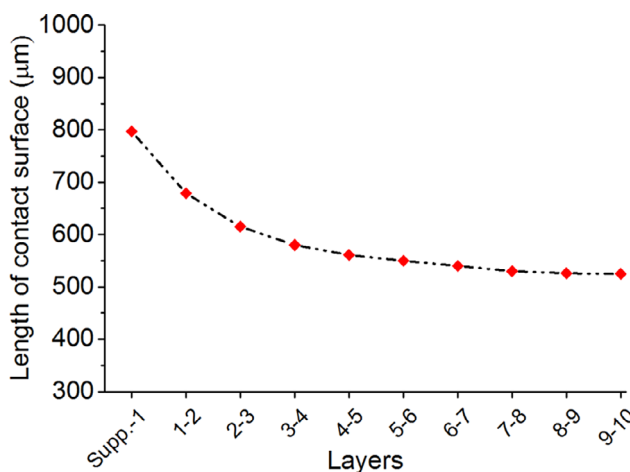


FIGURE 8 Temperature evolution during fused filament fabrication process: effect of print speed [Color figure can be viewed at wileyonlinelibrary.com]

FIGURE 9 Analysis of the length of contact between two adjacent filaments.

($T_{liq} = 210^\circ\text{C}$, $T_{supp} = 50^\circ\text{C}$, $V = 20$ mm/s, and $h = 0.2$ mm) [Color figure can be viewed at wileyonlinelibrary.com]



aim is to show the contact surface of two adjacent filaments. Results show that as much as the distance from support increases, the contact surface of two adjacent filaments decreases. Also based on the temperature evolution of filaments (see Figure 7), one can observe that after two or three sequences of deposition, the temperature decreases below crystallization temperature. This fact contributes to the speed of cooling, solidification of material, lower material diffusion, and then decrease in the contact surface between two adjacent filaments.

This analysis performed on the samples by applying the process parameters. Figures 10 and 11 show the microstructure analysis of condition No. 1 ($T_{liq} = 230^\circ\text{C}$) and condition No. 2 ($T_{supp} = 70^\circ\text{C}$).

Each condition has its influence on the quality and microstructure of the fabricated parts. One can note that in condition No. 2 ($T_{supp} = 70^\circ\text{C}$) after almost 10 deposited layers, perhaps due to high temperature, layers slide on each other as well as for condition No. 4 ($h = 0.3$ mm). However, in condition No. 1 ($T_{liq} = 230^\circ\text{C}$) after 20 deposited layers, filaments remain in a good quality of printing as well as condition No. 3 ($V = 60$ mm/s).

Based on the SEM observations, the same analysis performed on the deposit layers (Figure 12) and the percentages of the contact surface of each two adjacent filaments have been compared. This analysis is a useful summary of the effect of each process parameter. One can note that the influence of increasing the extruder temperature is more significant in comparison with other process parameters. As seen, the higher extruder temperature causes a higher contact surface between two adjacent filaments. However, the influence of print speed is more discussable based on the SEM micrograph performed on the sequence of layers. One can notice that the value of contact length between adjacent filaments is almost constant with increasing the printing speed. Moreover, the quality of the printed part is better.

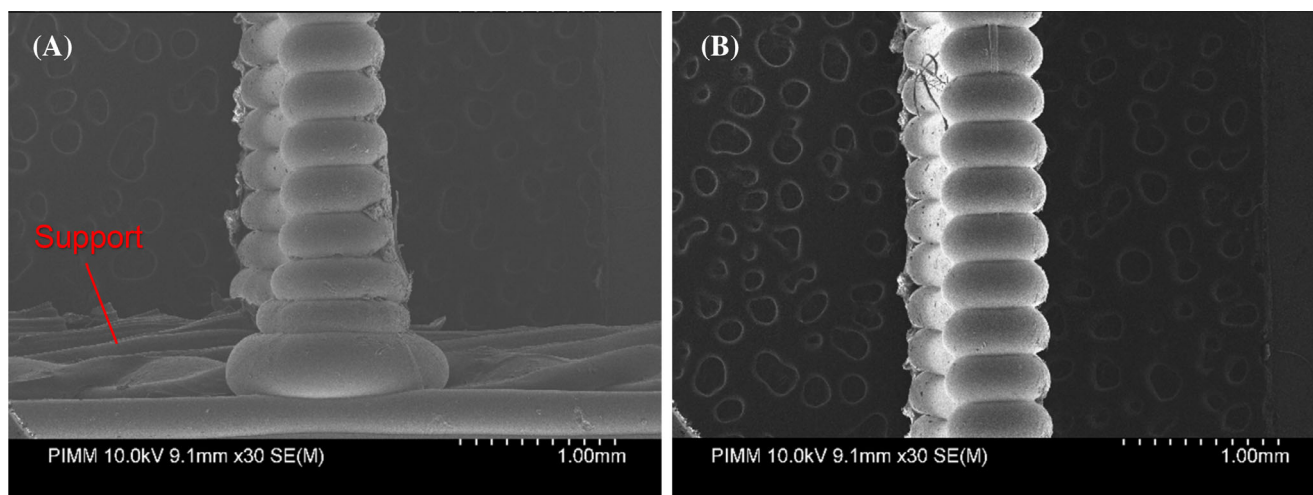


FIGURE 10 Consequence of deposited filaments in condition No. 1 ($T_{liq} = 230^{\circ}\text{C}$) for, A, layers 1 to 8 and, B, layers 9 to 17 [Color figure can be viewed at wileyonlinelibrary.com]

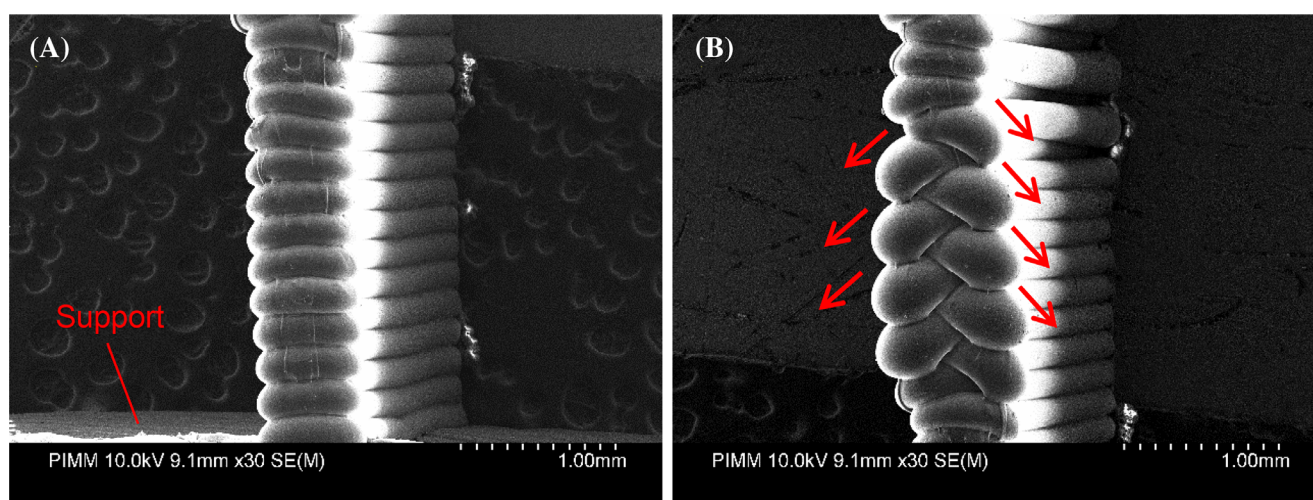


FIGURE 11 Consequence of deposited filaments in condition No. 2 ($T_{supp} = 70^{\circ}\text{C}$) for, A, layers 1 to 12 and, B, layers 13 to 26 [Color figure can be viewed at wileyonlinelibrary.com]

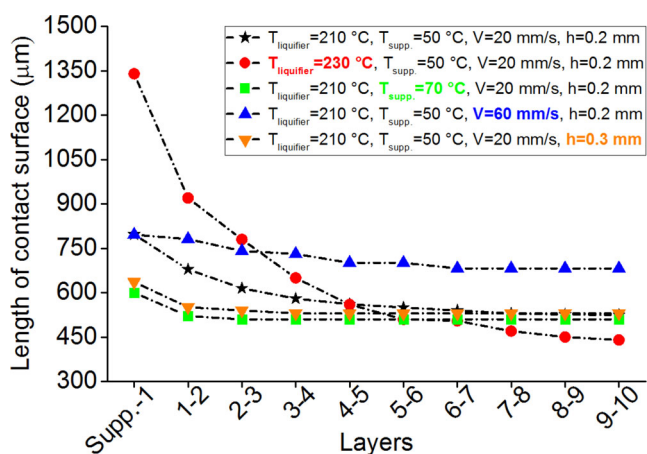


FIGURE 12 Analysis of the length of contact between two adjacent filaments [Color figure can be viewed at wileyonlinelibrary.com]

6 | CONCLUSIONS

This work presents an experimental investigation on the influence of process parameters on thermal and mechanical properties of PLA in FFF process. The preliminary physicochemical and mechanical results showed that there is a difference in the degree of crystallinity during the cooling process and formation of adjacent filaments. Young's modulus and failure strain could be an indicator to evaluate the mechanical properties of FFF fabricated parts. However, the temperature profile measurement of filaments indicates that process parameters have a significant impact on the mechanical strength of the fabricated parts. The results showed that, although it is required to consider the interaction of parameters, the evaluation of each could help to study the strength in FFF process.

One can notice that the effect of different parameters should be investigated at multiscale analysis. The latter can confirm that perhaps we have good mechanical properties of fabricated parts; however, the microstructure of the pieces is not acceptable. Presumably, the influence of increasing the extruder temperature is more significant in comparison with other process parameters: the higher the extruder temperature, the higher the contact surface between two adjacent filaments. However, the influence of print speed is more discussable based on the SEM micrograph performed on the sequence of layers.

CONFLICT OF INTEREST

The authors declare no potential conflicts of interest.

ORCID

Hamidreza Vanaei  <https://orcid.org/0000-0003-1501-0482>

REFERENCES

- [1] S.-S. Yao, F.-L. Jin, K. Y. Rhee, D. Hui, S.-J. Park, *Compos. Part B: Eng.* **2018**, *142*, 241.
- [2] P. Chennakesava, Y. S. Narayan, "Fused deposition modeling-insights," In *Proc. of the Int. Conf. on Advances in Design and Manufacturing ICAD&M*. **2014**; Vol. 14, pp. 1345–1350.
- [3] Q. Sun, G. Rizvi, C. Bellehumeur, P. Gu, *Rapid Prototyp. J.* **2008**, *14*(2), 72.
- [4] C. Bellehumeur, M. Bisaria, J. Vlachopoulos, *Polym. Eng. Sci.* **1996**, *36*(17), 2198.
- [5] H. S. Patanwala, D. Hong, S. R. Vora, B. Bognet, A. W. Ma, *Polym. Compos.* **2018**, *39*(S2), E1060.
- [6] D. Depuydt, M. Balthazar, K. Hendrickx, W. Six, E. Ferraris, F. Desplentere, J. Ivens, A. W. van Vuure, *Polym. Compos.* **2019**, *40*(5), 1951.
- [7] F. Arbeiter, M. Spoerk, J. Wiener, A. Gosch, G. Pinter, *Polym. Test.* **2018**, *66*, 105.
- [8] J. Chacón, M. A. Caminero, E. García-Plaza, P. J. Núñez, *Mater. Des.* **2017**, *124*, 143.
- [9] M. Á. Caminero, J. M. Chacón, E. García-Plaza, P. J. Núñez, J. M. Reverte, J. P. Becar, *Polymers* **2019**, *11*(5), 799.
- [10] S. Costa, F. Duarte, J. A. Covas, Using MATLAB to compute heat transfer in free form extrusion. in *MATLAB-A Ubiquitous Tool for the Practical Engineer* (Ed: C. M. Ionescu), InTech, Rijeka, Croatia **2011**, p. 453.
- [11] A. Bellini, *Ph.D Thesis*, Drexel University (Philadelphia, PA) **2002**.
- [12] L. Li, Q. Sun, C. Bellehumeur, P. Gu, "Investigation of Bond Formation in FDM Process 400," In *2002 Int. Solid Freeform Fabrication Symp.* **2002**.
- [13] O. Pokluda, C. T. Bellehumeur, J. Vlachopoulos, *AIChE J.* **1997**, *43*(12), 3253.
- [14] O. A. Mohamed, S. H. Masood, J. L. Bhowmik, *Mater. Today: Proc.* **2017**, *4*(8), 8250.
- [15] M. A. Cuiffo, J. Snyder, A. M. Elliott, N. Romero, S. Kannan, G. P. Halada, *Appl. Sci.* **2017**, *7*(6), 579.
- [16] W. Wu, P. Geng, G. Li, D. Zhao, H. Zhang, J. Zhao, *Materials* **2015**, *8*(9), 5834.
- [17] B. Huang, S. Meng, H. He, Y. Jia, Y. Xu, H. Huang, *Polym. Eng. Sci.* **2019**, *59*(1), 120.
- [18] M. Harris, J. Potgieter, R. Archer, K. M. Arif, *Mater. Manuf. Process.* **2019**, *34*(6), 701.
- [19] J. Torres, J. Coteló, J. Karl, A. P. Gordon, *JOM* **2015**, *67*(5), 1183.
- [20] F. Górski, W. Kuczko, R. Wichniarek, *Arch. Mech. Technol. Autom.* **2014**, *31*(1), 3.
- [21] F. Górski, R. Wichniarek, W. Kuczko, J. Andrzejewski, *J. Mach. Eng.* **2015**, *15*(4), 121.
- [22] T. Letcher, B. Rankouhi, S. Javadpour, "Experimental study of mechanical properties of additively manufactured ABS plastic as a function of layer parameters," In *ASME 2015 Int. Mechanical Engineering Congress and Exposition*, American Society of Mechanical Engineers Digital Collection, New York, NY. **2015**.
- [23] O. Es-Said, J. Foyos, R. Noorani, M. Mendelson, R. Marloth, B. Pregger, *Mater. Manuf. Process.* **2000**, *15*(1), 107.
- [24] S. H. Ahn, M. Montero, D. Odell, S. Roundy, P. K. Wright, *Rapid Prototyp. J.* **2002**, *8*, 248.
- [25] H. Li, T. Wang, J. Sun, Z. Yu, *Rapid Prototyp. J.* **2018**, *24*, 80.
- [26] X. Liu, M. Zhang, S. Li, L. Si, J. Peng, Y. Hu, *Int. J. Adv. Manuf. Technol.* **2017**, *89*(5–8), 2387.
- [27] S. Xiaoyong, C. Liangcheng, M. Honglin, G. Peng, B. Zhanwei, L. Cheng, "Experimental analysis of high temperature PEEK materials on 3D printing test," In *2017 9th Int. Conf. on Measuring Technology and Mechatronics Automation (ICMTMA)*. IEEE. **2017**, pp. 13–16.
- [28] A. K. Sood, R. K. Ohdar, S. S. Mahapatra, *Mater. Des.* **2010**, *31*(1), 287.
- [29] R. Zaldivar, D. Witkin, T. McLouth, D. Patel, K. Schmitt, J. Nokes, *Addit. Manuf.* **2017**, *13*, 71.
- [30] J. F. Rodríguez, J. P. Thomas, J. E. Renaud, *Rapid Prototyp. J.* **2001**, *7*, 148.
- [31] R. Vadori, A. K. Mohanty, M. Misra, *Macromol. Mater. Eng.* **2013**, *298*(9), 981.
- [32] A. Kallel, I. Koutiri, E. Babaeitorkamani, A. Khavandi, M. Tamizifar, M. Shirinbayan, A. Tcharkhtchi, *Int. Polym. Process.* **2019**, *34*(4), 434.
- [33] A. Lucas, A. Danlos, M. Shirinbayan, V. Motaharnejad, R. Paridaens, K. Benfriha, F. Bakir, A. Tcharkhtchi, *Int. J. Adv. Manuf. Technol.* **2019**, *104*(1–4), 1183.

How to cite this article: Vanaei H, Shirinbayan M, Deligant M, et al. Influence of process parameters on thermal and mechanical properties of polylactic acid fabricated by fused filament fabrication. *Polym Eng Sci.* 2020;60: 1822–1831. <https://doi.org/10.1002/pen.25419>

Article No. 2:

HR Vanaei, K Raissi, M Deligant, M Shirinbayan, J Fitoussi, S Khelladi, A Tcharkhtchi;
Towards the Understanding of Temperature Effect on Bonding Strength, Dimensions and
Geometry of 3D-printed Parts; J. of Mat. Sci., 55:14677–14689 (2020).

DOI: [10.1007/s10853-020-05057-9](https://doi.org/10.1007/s10853-020-05057-9)



Toward the understanding of temperature effect on bonding strength, dimensions and geometry of 3D-printed parts

H. R. Vanaei^{1,2,*} , K. Raissi¹, M. Deligant¹, M. Shirinbayan², J. Fitoussi², S. Khelladi¹, and A. Tcharkhtchi²

¹Arts et Metiers Institute of Technology, CNAM, LIFSE, HESAM University, 75013 Paris, France

²Arts et Metiers Institute of Technology, CNRS, CNAM, PIMM, HESAM University, 75013 Paris, France

Received: 20 May 2020

Accepted: 5 July 2020

© Springer Science+Business Media, LLC, part of Springer Nature 2020

ABSTRACT

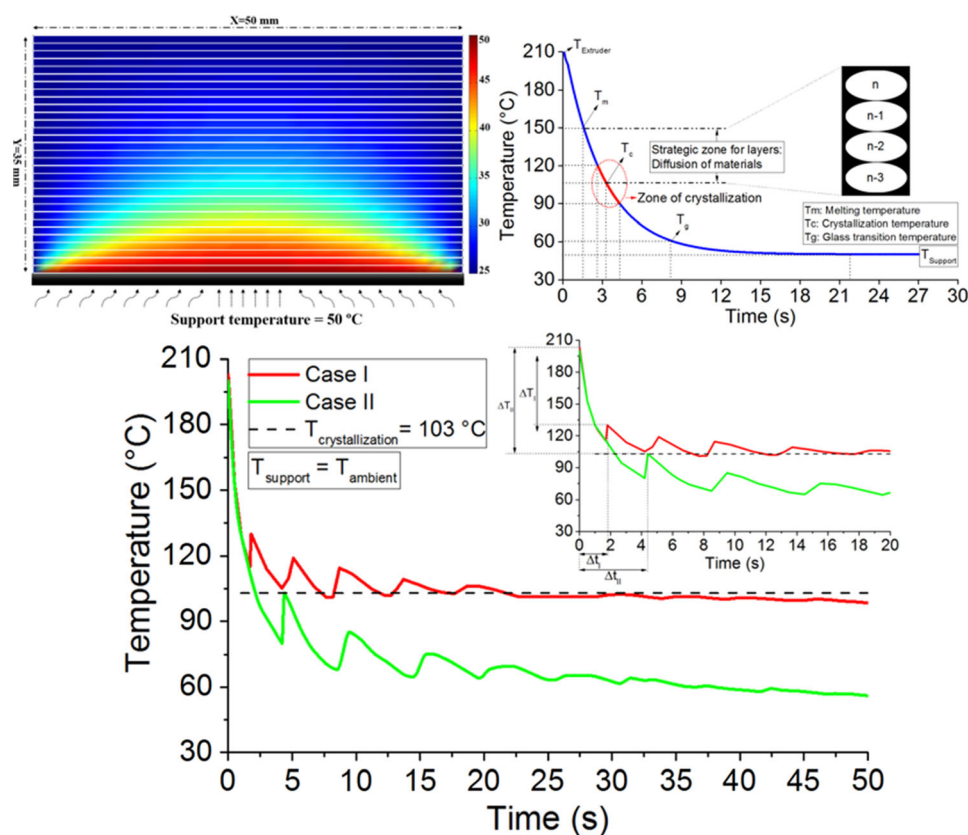
Fused filament fabrication (FFF), which is an additive manufacturing technique, opens alternative possibilities for complex geometries fabrication. However, its use in functional products is limited due to anisotropic strength issues. Indeed, the strength of FFF fabricated parts across successive layers in the build direction (Z direction) can be significantly lower than the strength in X–Y directions. This strength weakness has been attributed to poor bonding between printed layers. This bonding depends on the temperature of the current layer being deposited—at melting temperature (T_m)—and the temperature of the previously deposited layer. It is assumed that depositing a layer at T_m on a layer at temperature around crystallization temperature (T_c) would enable higher material crystallinity and thus better bonding between previous and present layers. On the contrary, if the previous layer temperature is below T_c , material crystallinity will be low and bonding strength weak. This paper aims at studying the significant effect of temperature difference (ΔT) between previous and current deposited layers temperatures on (1) inter-layers bonding strength improvement and (2) part dimensions, geometry and structure stability. A 23% increase in the inter-layers bonding strength for previous layer temperature slightly higher than T_c reported here confirms the above assumption and offers a first solution toward the increase in inter-layers bonding strength in FFF.

Address correspondence to E-mail: hamidreza.vanaei@ensam.eu

<https://doi.org/10.1007/s10853-020-05057-9>

Published online: 13 July 2020

GRAPHICAL ABSTRACT



Introduction

Additive manufacturing (AM) process comprises various techniques allowing the construction of three-dimensional parts of complex geometry, difficult or impossible to manufacture using traditional manufacturing processes [1, 2]. Fused filament fabrication (FFF), also known as 3D printing, is one of those AM processes used to produce prototypes in different industrial sectors such as aerospace, medical and automotive [3, 4]. In FFF, the most important materials for parts manufacturing are thermoplastic polymers [5]. Accordingly, several parameters affect the manufactured part quality [6, 7], like the temperature profile of the polymer and consequently the inter-layers bonding [8–10]. It is therefore important

to understand how the process parameters affect the evolution of filaments temperature as mentioned [11–14].

The problems of effective bonding, reduced strength and mechanical performance are a major concern of manufactured 3D-printed structures. In the process of parts fabrication, as the deposition progresses, the hot filament is deposited onto filaments that were previously deposited and which are in the process of cooling. The contact between the hot filament and the previous deposited filaments causes re-heating of the latter. At the interface of adjacent filaments, temperature rises above the crystallization temperature (T_c) and proper bonding take place.

Therefore, in order to foster material crystallization at the interface between filaments and allow better

molecular chain re-arrangement during the deposition of the melted filament, the previously deposited filaments should be sufficiently hot, probably around crystallization temperature. Higher temperature of previously deposited filament could cause molten material flows and deformation of subsequent deposited layers. In case of lower previously deposited filament temperature, the molecular chain of the deposited material does not have enough time to be re-arranged, causing lower bonding of the two adjacent filaments [15].

Nowadays, one of the challenging features in order to improve the bonding of 3D-printed parts is to optimize the temperature at the interface between previous and current deposited filaments. In fact, control of previous filament cooling speed is a crucial factor for interface bonding for the following reasons:

- High cooling rate causes poor interface bonding.
- Low cooling rate causes deformation of fabricated parts due to the effect of gravity, etc.

Therefore, controlling the cooling speed or temperature profile of deposited filaments acts as an important criterion in the strengthening of 3D-printed parts [8]. Numerous numerical- and experimental-based researches investigated this criterion for different polymers in order to characterize thermal behavior of the filaments. Costa et al. [16] developed a model based on the heat transfer between filaments during deposition and predicted temperature and adhesion quality of the 3D-printed parts. This model showed a good agreement with experimental data. Sun et al. [15] studied the mechanisms controlling the bond formation for ABS filaments in FFF process. They showed that temperature and variation in the convective conditions have a strong effect on thermal distribution and overall quality of the bond strength. In another study, they focused on the thermal behavior for PLA polymer filaments [17]. They tried to understand both numerically and experimentally the effect of nozzle and platform temperatures, extrusion speed and layer thickness on bond formation. However, recent researches demonstrated that cyclic cooling and re-heating of filaments during FFF have an impact on the sintering by considering the effect of temperature on viscosity [18, 19]. Beside this, inter-layer adhesion has been widely investigated. Yin et al. [20] investigated both numerically and experimentally the effect of process parameters on the bonding strength of multi-material, and they

found that the variation of temperature profile has an impact on mechanical behavior of the printed parts. Consequently, they later focused on the improvement of inter-layer bonding by addition of bimodal blends to the polymeric parts and found that low molecular weight (LMW) additives reinforce interfaces and reduce anisotropy [21, 22]. These efforts led to the application of novel materials, using acrylonitrile–butadiene–styrene (ABS) as a matrix thermoplastic polyurethane (TPU) as an additive, allowing 3D-printing without platform heating [23].

One of the most important key factors that researchers are working on is “pre-heating of the previously deposited filaments”. Partain [24] used a nozzle to blow hot air onto the fabricated part to decrease the cooling rate of deposited filaments, while Kishore et al. [25] exerted infrared ray to evaluate the strength of fabricated parts. Despite the interesting results they obtained, surface exposure was observed because of the radiation of infrared ray. However, a local pre-heating laser was also applied to the layered zone near the extruder to increase the interface temperature. The pre-heated sample had more strength, elasticity and toughness, but surface re-flow causes damage and affects the quality of printed parts [26].

To sum up, in the case of FFF process, the thermal aspect seems to play a key role as for inter-filaments bonding and dimensions of 3D-printed parts. The temperature of previously deposited filament (T_{previous}) strongly affects the material crystallinity occurring at the interface during the deposition of the current filament at T_m . In order to investigate the influence of T_{previous} on bonding and other dimensional aspects, an experimental study is conducted. For the purpose of this study, T_{previous} ranges between the room temperature (T_r) and the crystallization temperature (T_c).

Experimental study

Preliminary observations

During FFF part printing, the polymer filament undergoes several successive cooling and re-heating due to the presence of two neighboring thermal sources: (1) the extruder and (2) the heating bed (support). On leaving the extruder, the filament cools down from a temperature of 210 °C to the room

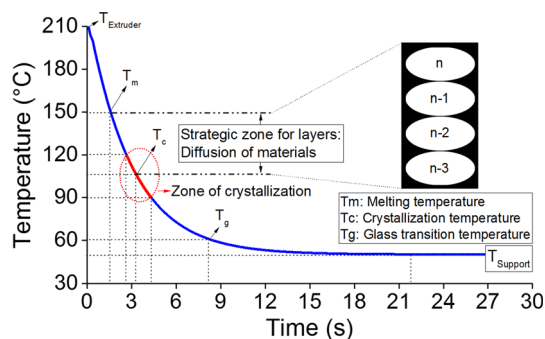


Figure 1 Cooling of a single deposited filament.

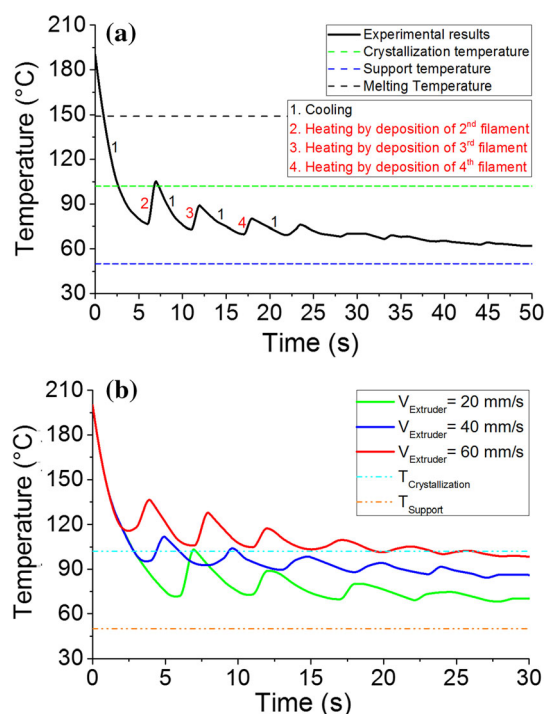


Figure 2 Results of the in situ measurement for the temperature evolution of **a** a sample with process parameters: $T_{ext} = 210\text{ }^\circ\text{C}$, $T_{supp.} = 50\text{ }^\circ\text{C}$, $V_{ext} = 20\text{ mm s}^{-1}$, $h = 0.2\text{ mm}$ and **b** samples in various print speed.

temperature, passing through the melting temperature and later the crystallization temperature (Fig. 1).

Once deposited, this filament will transfer part of its heat to the neighboring filaments previously deposited. The latter will undergo every new filament deposition, successive heating/cooling cycles which could affect the mechanical and dimensional results. Figure 2a shows the cooling profile of first deposited filament at $X = 5\text{ mm}$ from the start of deposition at the following conditions: extruder temperature ($T_{Ext} = 210\text{ }^\circ\text{C}$), support temperature ($T_{Supp} = 50\text{ }^\circ\text{C}$), print speed of 20 mm s^{-1} and layer

height of 0.2 mm . A cyclic evolution of the temperature of the first deposited filament, due to the deposition of the following filaments, could be noted. Each peak refers to a new filament deposition and proves that two adjacent filaments contact occurred. Figure 2b shows the cooling profile of first deposited filament for different printing speeds. We note that increasing the printing speed avoids filaments cooling down before new filament deposition.

Finally, in addition to the heat transfer from the extruder, these filaments also undergo heat transfer originated by the heating bed. This heat transfer from the heating bed to the filaments will increase the anisotropy of the sample. Heat diffusion equation was applied by replacing the objective to a set of nodes at steady state. Then, derivative of temperature with respect to X and Y directions was calculated using the following equation and taking into account the grid generation:

$$\frac{\partial^2 T}{\partial x^2} + \frac{\partial^2 T}{\partial y^2} = 0 \tag{1}$$

$$\left[\left(\frac{T_{i-1,j}^k - 2T_{i,j}^k + T_{i+1,j}^k}{\Delta x^2} \right) + \left(\frac{T_{i,j-1}^k - 2T_{i,j}^k + T_{i,j+1}^k}{\Delta y^2} \right) \right] = 0 \tag{2}$$

The temperature of node (i, j) was obtained as follows:

$$T_{i,j} = \frac{1}{4} (T_{i,j-1} + T_{i-1,j} + T_{i+1,j} + T_{i,j+1}) \tag{3}$$

Concerning the dimensions of the object (Fig. 3a, b), these are applied to a source of heat and injected in MATLAB® based on the following boundary conditions:

- $\Delta x = \Delta y$ (Consideration of Gauss–Seidel iterative)
- $dt = 0$ (Consideration of steady state)

Based on the obtained results in Fig. 3c, it is observable that the source of heat contributes to the anisotropy of the fabricated parts and demonstrates the effect of the heating bed on the temperature distribution in the printed part.

Test design and samples printing

Heat transfers from the extruder and the heating bed have a significant influence on the printed part. Our study considers only heat generated by the extruder

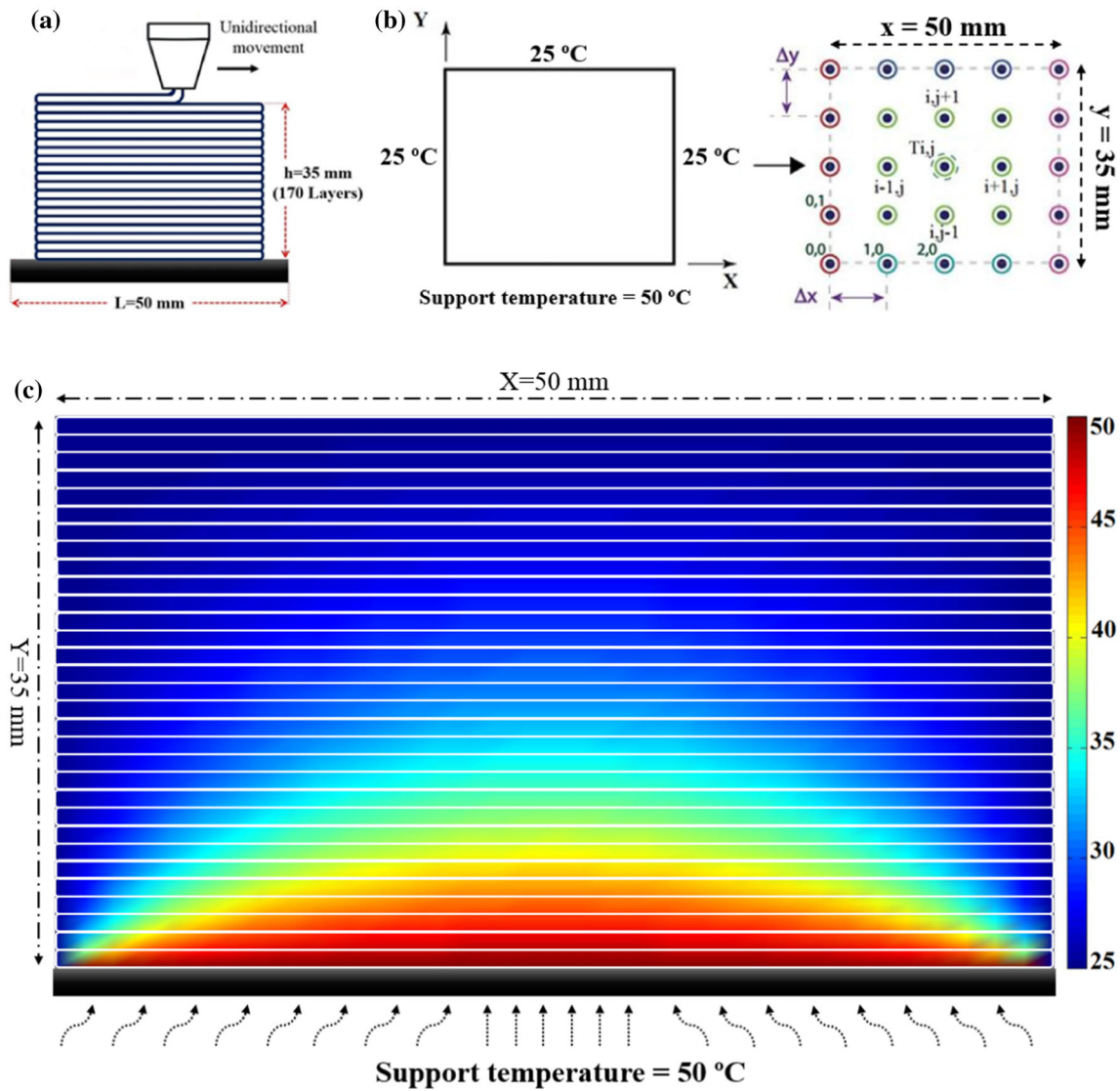
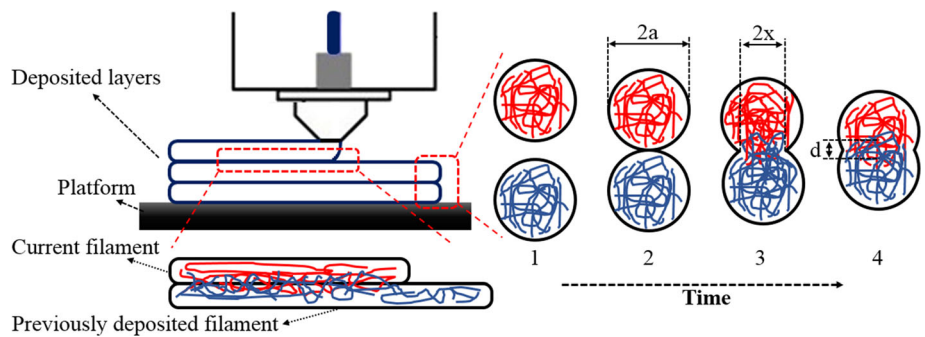


Figure 3 Representation of **a** schematic of the test case, **b** nodes for finite difference method, **c** obtained results at steady state.

Figure 4 Typical image representing the inter-filaments bonding.



and transferred to the printed part through the filaments. The heating bed effect, as presented in Fig. 3, is cancelled by setting its temperature to $0\text{ }^\circ\text{C}$ (turn off the heating bed and let it at ambient temperature).

In this context, we paid particular attention to the temperature difference, ΔT , between the temperature of the current filament (T_{extruder}) and the temperature of the previously deposited filament, T_{previous} (Fig. 4).

This experimental study aims at investigating and understanding precisely how ΔT affects material crystallinity at the interface between previous and current deposited filaments, and consequently the inter-filaments bonding and dimensional results.

The temperature difference (ΔT) can be expressed as follows:

$$\Delta T = T_{\text{Extruder}} - T_{\text{Previous}} = 210^{\circ}\text{C} - T_{\text{Previous}} \quad (4)$$

where T_{extruder} is the temperature of current filament and T_{previous} is the temperature of the previously deposited filament.

The ΔT depends on the extruder speed, V_{extruder} , and the distance travelled by the extruder before redepositing the melting filament in the same point. According to the filament's cooling curve presented in Fig. 1, the longer the distance travelled by the extruder, the higher the cooling time (Δt) and consequently ΔT . For example, based on Fig. 1, if T_{previous} is set equal to T_c ($\sim 103^{\circ}\text{C}$), then ΔT is around 107°C and the corresponding cooling time is $\Delta t = 3.3$ s. These values mean that if the cooling time between two successive filaments in a given point (P) equals 3.3 s, then the current filament at temperature T_{extruder} (210°C) will be deposited onto a previously deposited filament at temperature T_c (103°C).

For the purpose of this experimental study, the temperature of the previously deposited filament ranges around the crystallization temperature. Indeed, the zone around crystallization temperature is considered as a strategic zone. The extruder speed is kept constant in order to avoid any influence driven by this speed on the printing result. Three solid blocks per each case are printed following the designed path with constant extruder speeds (V_{extruder} and V_{return}) as presented in Fig. 5.

Finally, according to the ISO 37-3 standard (Fig. 6c, d), the quasi-static tensile specimens were cut from the printed solid blocks using a proper standard mold and a press machine as shown in Fig. 6a, b: three samples for case I and nine samples for case II (three for each location).

According to Fig. 5, the cooling time of the filament can be expressed as follows:

$$\Delta t = L/V_{\text{extruder}} + L/V_{\text{reverse}} \quad (5)$$

where L is the length of test piece, V_{extruder} is the speed of the extruder (material deposition), and V_{reverse} is the reverse speed of the extruder (no material deposition).

Based on the printer capabilities, reverse speed was set to a maximum speed of 40 mm s^{-1} and extruder speed (deposition) was set to 12 mm s^{-1} .

The length of the test piece was chosen in such a way as to reduce the cooling time, Δt , for case study I and to increase Δt for case study II (Fig. 6). In that respect, these lengths were set equal to 15 mm for case I and 40 mm for case II. Thanks to Eq. 5, Δt is calculated for each case:

- Case I: cooling time is $\Delta t_{\text{I}} = 1.625$ s
- Case II: cooling time is $\Delta t_{\text{II}} = 4.333$ s

Based on Fig. 1:

- $\Delta t_{\text{I}} = 1.625$ s corresponds to $T_{\text{previous}} = 140^{\circ}\text{C}$ and $\Delta T_{\text{I}} = 210^{\circ}\text{C} - 140^{\circ}\text{C} = 70^{\circ}\text{C}$
- $\Delta t_{\text{II}} = 4.333$ s corresponds to $T_{\text{previous}} = 90^{\circ}\text{C}$ and $\Delta T_{\text{II}} = 210^{\circ}\text{C} - 90^{\circ}\text{C} = 120^{\circ}\text{C}$

Table 1 summarizes the two case studies conditions as follows:

A commercially available orange PLA filament with diameter 1.75 mm ($\pm 0.01\text{ mm}$) and density $\rho = 1.24\text{ gr cm}^{-3}$ was used for test parts printing.

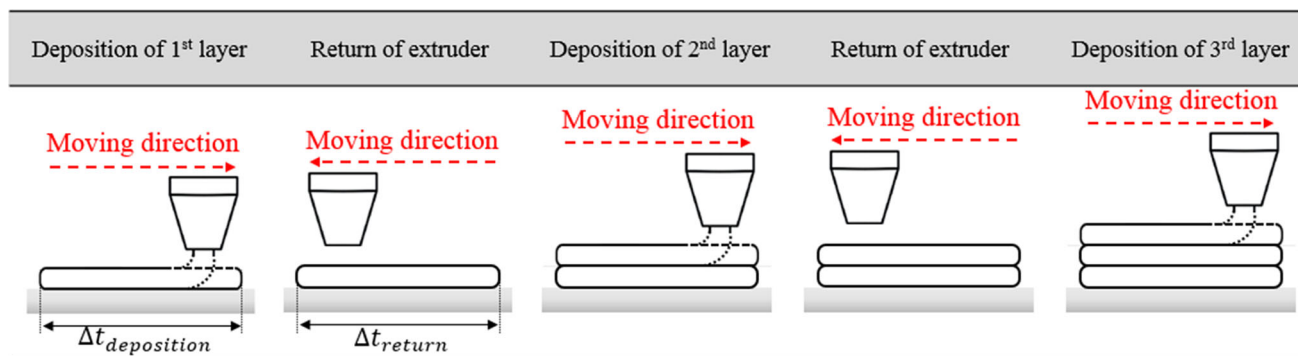


Figure 5 Typical image showing the deposition mechanism.

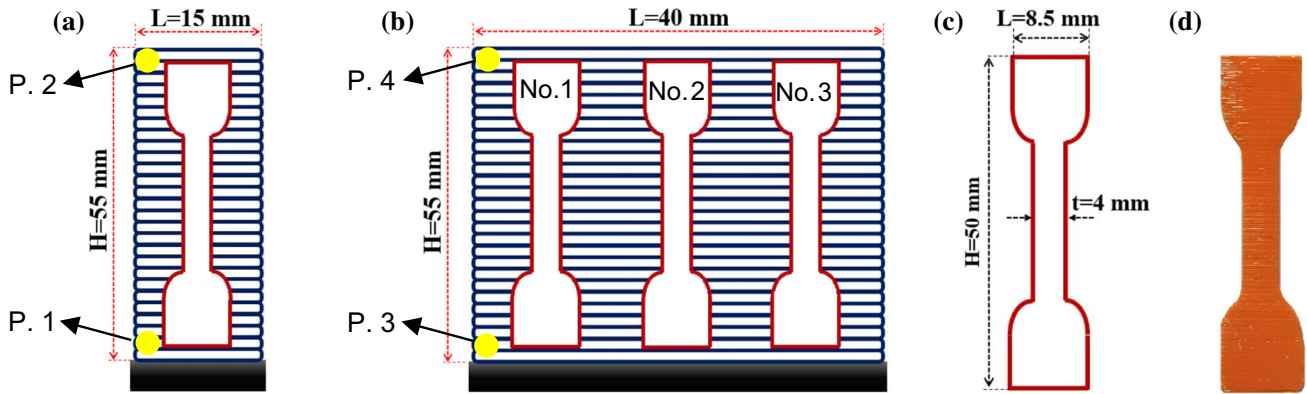


Figure 6 Typical image of **a** case I with representation of selected locations (points 1 and 2) for DSC characterization, **b** case II with representation of selected locations (points 3 and 4) for DSC

characterization and classification of tensile sample in consideration of the distance from start of deposition, **c** designed samples based on ISO 37-3 standard, **d** fabricated samples.

Table 1 Calculated values for both cases

	ΔT (°C)	Δt (s)	V_{extruder} (mm s ⁻¹)	V_{reverse} (mm s ⁻¹)	L (mm)	H (mm)
Case I	70	1.625	12	40	15	55
Case II	120	4.333	12	40	40	55

Characterization methods

Differential scanning calorimetry (DSC)

Differential scanning calorimetry (DSC) was accomplished using a TA instruments Q1000 (New Castle, USA). Four points located on the test parts have been selected to be characterized (see Fig. 6). Samples (~ 5.5 mg) were sealed in aluminum pans and heated from ambient temperature to 200 °C with heating rate of 10 °C min⁻¹ to determine crystallization and melting temperatures of the filaments. Then, the crystallinity of PLA was calculated using the following equation [27]:

$$X_c = (\Delta H_m - \Delta H_c) / \Delta H_m^0 \tag{6}$$

where ΔH_c and ΔH_m are cold crystallization and melting enthalpies, respectively, and the melting heat (ΔH_m^0) of 100% crystalline PLA is considered equal to 93.7 J g⁻¹ according to the literature [27].

Quasi-static tensile test

Tensile tests until failure have been performed on INSTRON 4301 machine. The specimen geometry used for quasi-static tensile tests is presented in “Test design and samples printing” section. However, based on the dimensional change that occurs during

the process and specimen preparation, a digital caliper has been implemented to precisely measure the required dimension. All calculations regarding mechanical behavior have been proposed as mentioned. The loading velocity was 1 mm min⁻¹.

Microstructure characterization

Microscopic observations, using scanning electronic microscope (HITACHI 4800 SEM), have been performed in order to qualitatively investigate the material microstructure and particularly bonding of adjacent filaments. ImageJ software was also utilized to evaluate the dimension variation using SEM micrographs.

Online temperature measurement of filaments

To track filaments cooling and the re-heating peaks of deposition of successive layers, a very small ($d = 80 \mu\text{m}$) K-type thermocouple was used (see [28, 29] for method description).

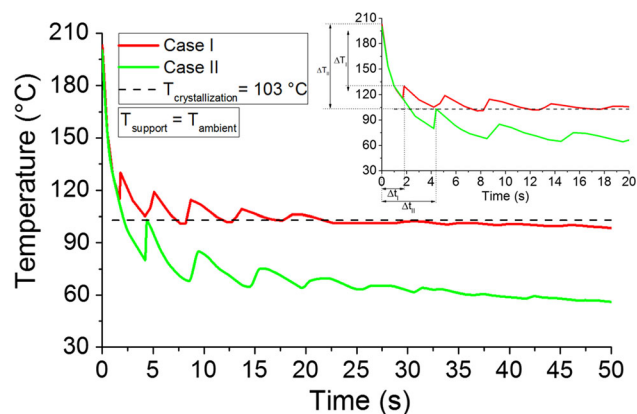


Figure 7 Results of the in situ measurement for the temperature evolution for both cases.

Results and discussion

Temperature profile of the fabricated parts

During test parts printing, temperature measurements were taken using in situ localized measurement device. The aim was to follow the temperature profile in a given location L (X , H) (Fig. 7). The measured temperature profiles showed at their first part the cooling curve for the filament located in L ($X = 5$ mm, $H = 0.2$ mm) followed by several peaks corresponding to the successive filaments' depositions. Indeed, the filament located in L ($X = 5$ mm, $H = 0.2$ mm) undergoes a series of heating and cooling effects.

The red curve (Fig. 7), related to case I, shows that the depositions of filaments (2) (3) (4) and (5) bring the temperature of filament (1) higher than the crystallization temperature T_c , while for the green curve, related to case II, only the deposition of filament (2) gets filament (1) temperature reaching T_c . The depositions of the other filaments leave filament (1) temperature below T_c . It is known that when the deposition of the current filament occurs at previously deposited filament temperatures greater or equal to the polymer crystallization temperature T_c , the degree of crystallinity across the interface will be higher, which will have great influence on the bonding strength development. Based on the latter, case I should present higher bonding strength (to be confirmed by tensile behavior tests).

Characterization results

Material crystallinity

DSC results for both test parts I and II are shown in Fig. 8. Using Eq. 6, the crystallinity in points 1, 2, 3 and 4 has been calculated, and the results are presented in Table 2. It appears from these results that crystallinity is higher in case I than in case II, thereby allowing to confirm the lower the cooling rate, the higher the possibility of crystallization.

The difference between point 1 and point 2 and between point 3 and point 4 could be explained by the series of heating and cooling effects generated during the deposition of the following filaments at point 1 and at point 3, while at point 2 and 4 the heating and cooling effects are weak.

Tensile behavior

Moreover, tensile behaviors of both cases are illustrated in Fig. 9. Results indicate that the ultimate strength increases when the cooling rate decreases. It is worth mentioning that in the case of filaments deposition occurring at temperature greater or equal to T_c , the degree of crystallinity is higher than in the 'high cooling rate case'. However, a detailed study is required in order to get precise information about material crystallinity and polymer re-arrangement.

Given the above-mentioned results and following the discussion performed on the mechanical behavior, tensile tests have been realized to illustrate the effect of the cooling rate (T_{previous}) on the tensile behavior. The results presented in Fig. 9 and data collected in Table 3, are summarized as follows:

- Influence of T_{previous} on Young's modulus is limited. When T_{previous} is increased, young's modulus roughly changed from 0.5 GPa in case I to 0.6 GPa in case II.
- Average failure strain occurs around 3.9%, and average failure stress occurs around 21 MPa.
- Finally, these results show 23% increase in the bonding strength for case I, confirming the influence and importance of the temperature of previously deposited filament, T_{previous} .

SEM micrographs for fractured samples (Fig. 10) show no local damage for case I as there might be a concentrated local damage at the failure zone. The

Figure 8 DSC results of **a** case I and **b** case II.

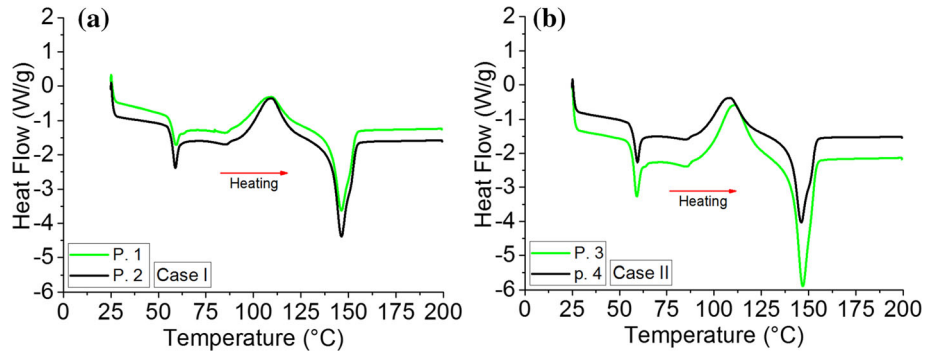


Table 2 Value of degree of crystallinity obtained from DSC

Conditions	% Crystallinity
Case I	
Point 1	8.3 ± 0.2
Point 2	6.2 ± 0.1
Case II	
Point 3	7.1 ± 0.1
Point 4	6.0 ± 0.2

Microstructure characterization

Figure 11 presents the deposition sequence of filaments in both cases I and II. First observations show a significant difference between both cases, and an analysis on the SEM micrographs was performed for better understanding. In the context of this analysis, we carry out measures of the cross section of deposited filaments in both cases.

The results of the analysis performed on the cross section of deposited filaments for case I and II are presented in Fig. 12. The measurements show that when varying the previously deposited filament temperature ($T_{previous}$), we observe 35% difference in filament deformation and slight structural subsidence

sample failure happens suddenly, reflecting the higher mechanical strength in the inter-filament regions. However, SEM micrographs for case II show a series of local damage in the inter-filament region, which could explain its lower mechanical strength.

Figure 9 Representation of samples for tensile test for **a** case I and **b** case II with tensile behavior of **c** case I and **d** case II.

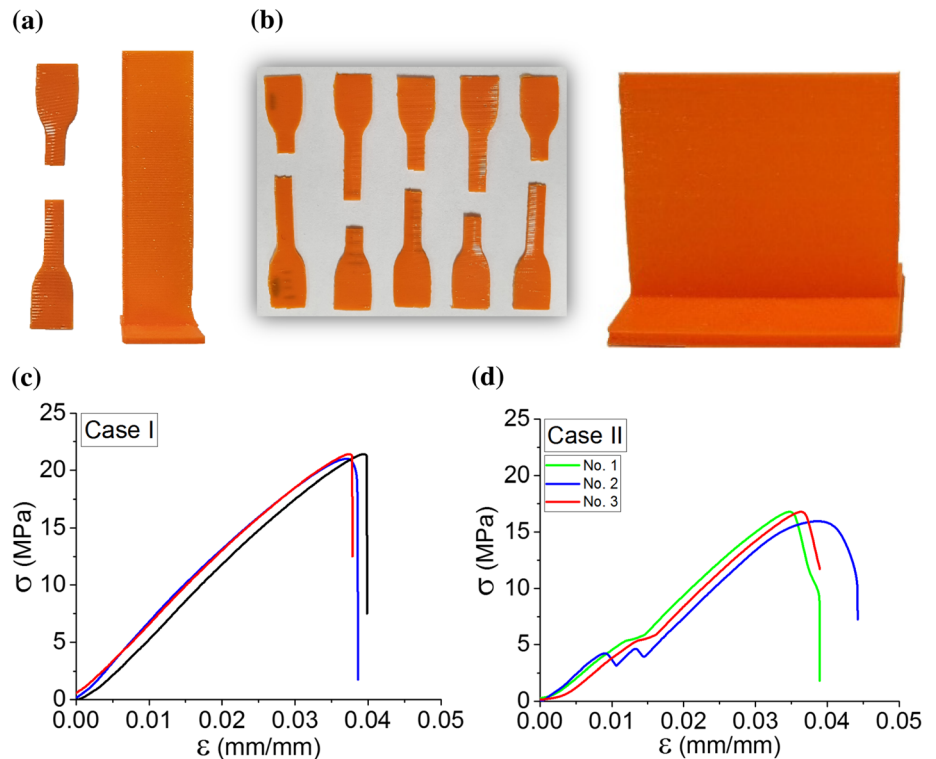
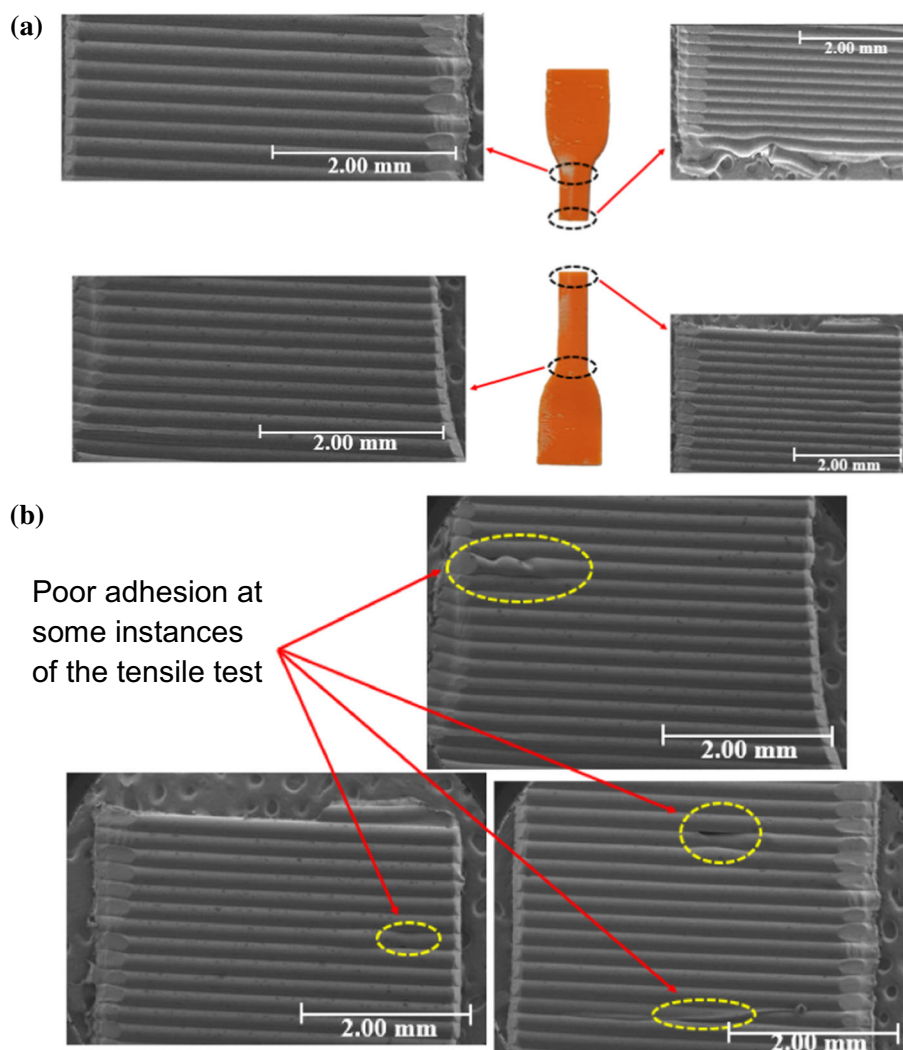


Table 3 Results of tensile behavior of printed PLA samples from cases I and II

Samples	Location	E (GPa)	σ_{\max} (MPa)	ε at σ_{\max} (%)
Case I	N/a	0.6 ± 0.05	21 ± 2	3.9 ± 0.1
Case II	No. 1	0.51 ± 0.01	17 ± 1.5	3.5 ± 0.2
	No. 2	0.5 ± 0.01	16 ± 1.5	3.9 ± 0.3
	No. 3	0.5 ± 0.01	17 ± 0.2	3.6 ± 0.2

of the wall (Fig. 12a–c). These results validate the effect of temperature evolution during fabrication on the geometry of both cases.

Figure 10 SEM micrographs for **a** case I and **b** case II of the fractured sample.

Concluding remarks

This work presents an experimental investigation on the effect of temperature difference (ΔT) between previous and current deposited layers temperatures on: (1) material crystallization and thus inter-layers bonding strength improvement and (2) dimensional and geometrical results of 3D-printed PLA. Two test cases were designed for having different temperatures of previously deposited filaments (T_{previous}) which were proposed and studied. The main results are summarized as follows:

- The in situ measurements of filament temperature for case I indicate that the evolution of its filaments temperature remains above crystallization temperature T_c , which allows better material crystallization.

Figure 11 Consequence of deposited filaments in **a** case I for layers 1–11, in case II for **b** layers 1–6, **c** layers 6–12 and **d** schematic representation of calculating the aspect ratio.

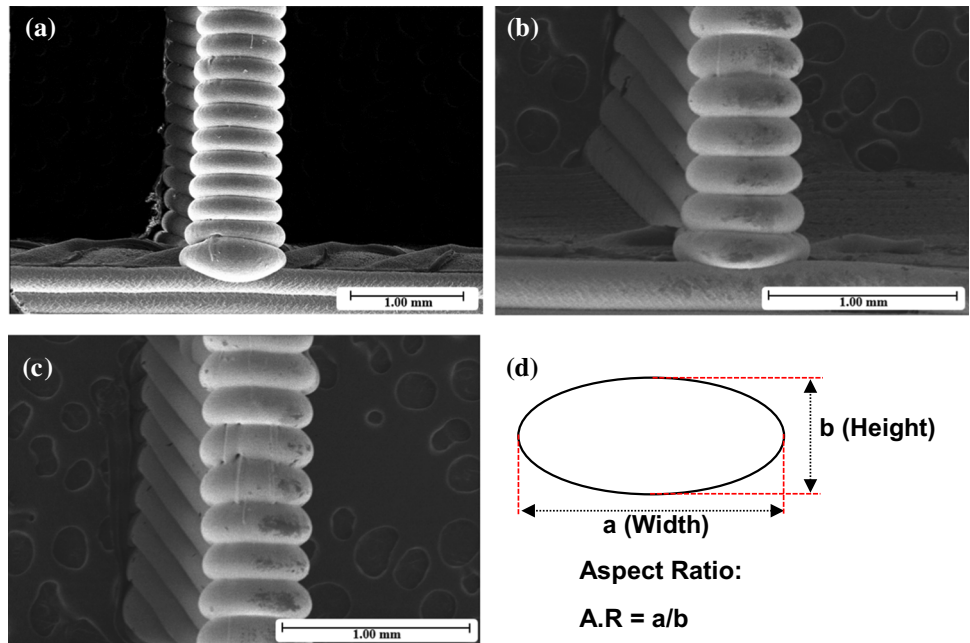
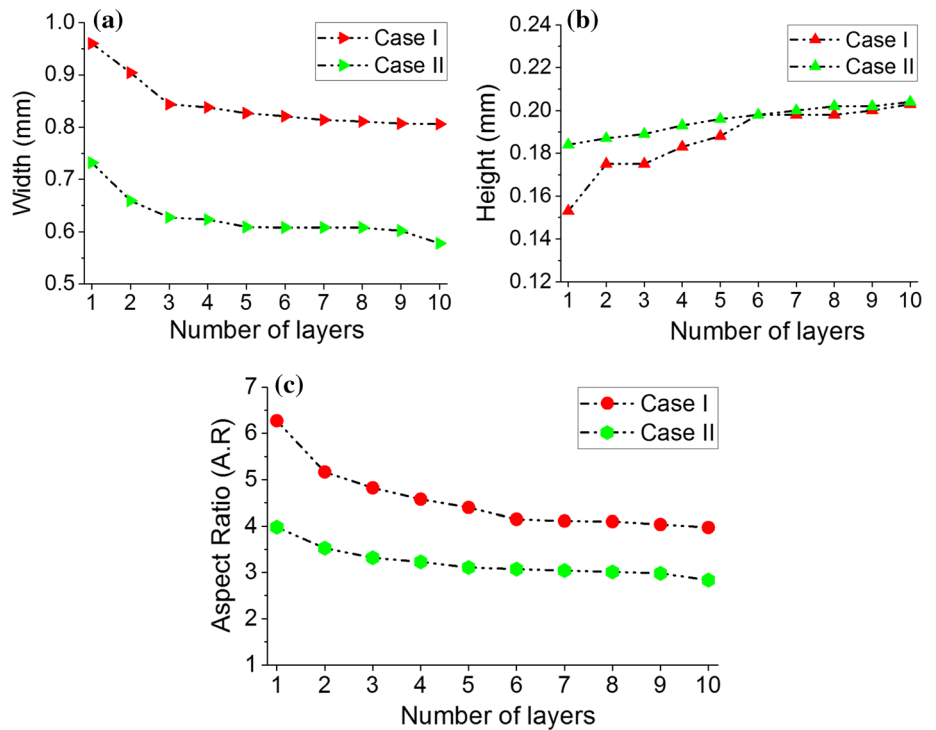


Figure 12 Analysis of cross section of microstructure in both cases: **a** width of filaments, **b** height of filaments and **c** aspect ratio (A.R) of cross section.



- The preliminary physicochemical and mechanical results showed higher values of crystallinity for case I ($T_{\text{previous}} = T_c$) leading to a better material crystallinity.
 - Tensile experiments showed that there is almost 23% increase in the inter-layer bond strength for case I.
 - Measurements of the cross-section variation of the deposited filaments show almost 35% difference between both cases, showing the effect of temperature evolution on the geometry of both cases.
- The results of our experiments confirm that when the deposition of the current filament (1) occurs at

previously deposited filament (2) temperatures greater or equal to the polymer crystallization temperature T_c (case I), the inter-filaments bonding strength will be higher. Likewise, when the depositions of filaments (3), (4), (5)... bring the temperature of filament (1) to a temperature greater or equal to the crystallization temperature T_c , the inter-filaments bonding strength will undergo an additional improvement.

This research is a preliminary study into understanding and improving temperature aspects and inter-layers bonding. In future developments, we will focus our attention on defining a solution about local pre-heating helping to control previously deposited layer temperature close to crystallization temperature during the printing. When implemented on 3D printers, this solution should ensure higher mechanical strength of printed parts.

Compliance with ethical standards

Conflict of interest The authors certify that they have NO affiliations with or involvement in any organization or entity with any financial interest, or non-financial interest in the subject matter or materials discussed in this manuscript.

References

- [1] Mohamed OA, Masood SH, Bhowmik JL (2015) Optimization of fused deposition modeling process parameters: a review of current research and future prospects. *Adv Manuf* 3(1):42–53. <https://doi.org/10.1007/s40436-014-0097-7>
- [2] Holmström J, Partanen J, Tuomi J, Walter M (2010) Rapid manufacturing in the spare parts supply chain: alternative approaches to capacity deployment. *J Manuf Technol Manag* 21(6):687–697. <https://doi.org/10.1108/17410381011063996>
- [3] Iftikhar A et al (2013) Turbine blade manufacturing through rapid tooling (RT) process and its quality inspection. *Mater Manuf Process* 28(5):534–538. <https://doi.org/10.1080/10426914.2012.746698>
- [4] Yagnik D (2014) Fused deposition modeling—a rapid prototyping technique for product cycle time reduction cost effectively in aerospace applications. *IOSR J Mech Civ Eng* 5:62–68
- [5] Chennakesava P, Narayan YS (2014) Fused deposition modeling—insights. In: *Proceedings of the international conference on advances in design and manufacturing ICAD&M*, vol 14, pp 1345–1350
- [6] Turner BN, Strong R, Gold SA (2014) A review of melt extrusion additive manufacturing processes: I. Process design and modeling. *Rapid Prototyp J* 20(3):192–204. <https://doi.org/10.1108/RPJ-01-2013-0012>
- [7] Abbott A, Tandon G, Bradford R, Koerner H, Baur J (2018) Process-structure-property effects on ABS bond strength in fused filament fabrication. *Addit Manuf* 19:29–38. [https://doi.org/10.1016/S1526-6125\(04\)70071-7](https://doi.org/10.1016/S1526-6125(04)70071-7)
- [8] Bellehumeur C, Li L, Sun Q, Gu P (2004) Modeling of bond formation between polymer filaments in the fused deposition modeling process. *J Manuf Process* 6(2):170–178. [https://doi.org/10.1016/S1526-6125\(04\)70071-7](https://doi.org/10.1016/S1526-6125(04)70071-7)
- [9] Oladapo BI, Obisesan OB, Oluwole B, Adebisi VA, Usman H, Khan A (2020) Mechanical characterization of a polymeric scaffold for bone implant. *J Mater Sci*. <https://doi.org/10.1007/s10853-020-04638-y>
- [10] Vanaei H et al (2020) Influence of process parameters on thermal and mechanical properties of polylactic acid fabricated by fused filament fabrication. *Polym Eng Sci*. <https://doi.org/10.1002/pen.25419>
- [11] Sweeney M, Campbell LL, Hanson J, Pantoya ML, Christopher GF (2017) Characterizing the feasibility of processing wet granular materials to improve rheology for 3D printing. *J Mater Sci* 52(22):13040–13053. <https://doi.org/10.1007/s10853-017-1404-z>
- [12] Naghieh S, Ravari MK, Badrossamay M, Foroozmehr E, Kadkhodaei M (2016) Numerical investigation of the mechanical properties of the additive manufactured bone scaffolds fabricated by FDM: the effect of layer penetration and post-heating. *J Mech Behav Biomed Mater* 59:241–250. <https://doi.org/10.1016/j.jmbbm.2016.01.031>
- [13] Widden M, Gunn K (2010) Design–build–test of model aerofoils for engineering education using FDM. *Virtual Phys Prototyp* 5(4):189–194. <https://doi.org/10.1080/17452759.2010.528841>
- [14] Pandey PM, Venkata Reddy N, Dhande SG (2006) Virtual hybrid-FDM system to enhance surface finish. *Virtual Phys Prototyp* 1(2):101–116. <https://doi.org/10.1080/17452750600763905>
- [15] Sun Q, Rizvi G, Bellehumeur C, Gu P (2008) Effect of processing conditions on the bonding quality of FDM polymer filaments. *Rapid Prototyp J* 14(2):72–80. <https://doi.org/10.1108/13552540810862028>
- [16] Costa S, Duarte F, Covas J (2017) Estimation of filament temperature and adhesion development in fused deposition techniques. *J Mater Process Technol* 245:167–179. <https://doi.org/10.1016/j.jmatprotec.2017.02.026>
- [17] Zhou X, Hsieh S-J, Sun Y (2017) Experimental and numerical investigation of the thermal behaviour of polylactic acid during the fused deposition process. *Virtual Phys*

- Prototyp 12(3):221–233. <https://doi.org/10.1080/17452759.2017.1317214>
- [18] Polychronopoulos ND, Vlachopoulos J (2020) The role of heating and cooling in viscous sintering of pairs of spheres and pairs of cylinders. *Rapid Prototyp J*. <https://doi.org/10.1108/RPJ-06-2019-0162>
- [19] Kamyabi M, Sotudeh-Gharebagh R, Zarghami R, Saleh K (2019) Analysis of non-isothermal viscous flow coalescence at micro scale. *Can J Chem Eng* 97(9):2565–2572. <https://doi.org/10.1002/cjce.23499>
- [20] Yin J, Lu C, Fu J, Huang Y, Zheng Y (2018) Interfacial bonding during multi-material fused deposition modeling (FDM) process due to inter-molecular diffusion. *Mater Des* 150:104–112. <https://doi.org/10.1016/j.matdes.2018.04.029>
- [21] Levenhagen NP, Dadmun MD (2017) Bimodal molecular weight samples improve the isotropy of 3D printed polymeric samples. *Polymer* 122:232–241. <https://doi.org/10.1016/j.polymer.2017.06.057>
- [22] Levenhagen NP, Dadmun MD (2018) Interlayer diffusion of surface segregating additives to improve the isotropy of fused deposition modeling products. *Polymer* 152:35–41. <https://doi.org/10.1016/j.polymer.2018.01.031>
- [23] de León A, Domínguez-Calvo A, Molina S (2019) Materials with enhanced adhesive properties based on acrylonitrile-butadiene-styrene (ABS)/thermoplastic polyurethane (TPU) blends for fused filament fabrication (FFF). *Mater Des* 182:108044. <https://doi.org/10.1016/j.matdes.2019.108044>
- [24] Partain SC (2007) Fused deposition modeling with localized pre-deposition heating using forced air, Montana State University-Bozeman, College of Engineering
- [25] Kishore V et al (2017) Infrared preheating to improve interlayer strength of big area additive manufacturing (BAAM) components. *Addit Manuf* 14:7–12. <https://doi.org/10.1016/j.addma.2016.11.008>
- [26] Ravi AK, Deshpande A, Hsu KH (2016) An in-process laser localized pre-deposition heating approach to inter-layer bond strengthening in extrusion based polymer additive manufacturing. *J Manuf Process* 24:179–185. <https://doi.org/10.1016/j.jmapro.2016.08.007>
- [27] Vadori R, Mohanty AK, Misra M (2013) The effect of mold temperature on the performance of injection molded poly (lactic acid)-based bioplastic. *Macromol Mater Eng* 298(9):981–990. <https://doi.org/10.1002/mame.201200274>
- [28] Vanaei HR et al (2020) Experimental study of PLA thermal behavior during fused filament fabrication (FFF). *J Appl Polym Sci*. <https://doi.org/10.1002/app.49747>
- [29] Lucas A et al (2019) Conventional rotational molding process and aerodynamic characteristics of an axial-flow hollow blades rotor. *Int J Adv Manuf Technol* 104(1–4):1183–1194. <https://doi.org/10.1007/s00170-019-03962-1>

Publisher's Note Springer Nature remains neutral with regard to jurisdictional claims in published maps and institutional affiliations.

Article No. 3:

HR Vanaei, M Shirinbayan, SF Costa, FM Duarte, JA Covas, M Deligant, S Khelladi, A Tcharkhtchi; Experimental study of PLA Thermal Behavior during Fused Filament Fabrication (FFF); Journal of Applied Polymer Science, 138(4): 1-7 (2021).

DOI: [10.1002/app.49747](https://doi.org/10.1002/app.49747)



ARTICLE

Experimental study of PLA thermal behavior during fused filament fabrication

Hamid Reza Vanaei^{1,2} | Mohammadali Shirinbayan² |
Sidonie Fernandes Costa³ | Fernando Moura Duarte⁴ | José António Covas⁴ |
Michael Deligant¹ | Sofiane Khelladi¹ | Abbas Tcharkhtchi²

¹Arts et Metiers Institute of Technology, CNAM, LIFSE, HESAM University, Paris, France

²Arts et Metiers Institute of Technology, CNRS, CNAM, PIMM, HESAM University, Paris, France

³School of Technology and Management of Porto Polytechnic Institute, CIICESI - Center for Research and Innovation in Business Sciences and Information Systems, Felgueiras, Portugal

⁴IPC - Institute for Polymers and Composites, Department of Polymer Engineering, University of Minho, Guimarães, Portugal

Correspondence

Hamid Reza Vanaei, Arts et Metiers Institute of Technology, CNAM, LIFSE, HESAM University, F-75013 Paris, France.

Email: hamidreza.vanaei@ensam.eu

Abstract

Fused filament fabrication (FFF) is an additive manufacturing technique that is used to produce prototypes and a gradually more important processing route to obtain final products. Due to the layer-by-layer deposition mechanism involved, bonding between adjacent layers is controlled by the thermal energy of the material being printed, which strongly depends on the temperature development of the filaments during the deposition sequence. This study reports experimental measurements of filament temperature during deposition. These temperature profiles were compared to the predictions made by a previously developed model. The two sets of data showed good agreement, particularly concerning the occurrence of reheating peaks when new filaments are deposited onto previously deposited ones. The developed experimental technique is shown to demonstrate its sensitivity to changing operating conditions, namely platform temperature and deposition velocity. The data generated can be valuable to predict more accurately the bond quality achieved in FFF parts.

KEYWORDS

manufacturing, thermal properties, thermoplastics

1 | INTRODUCTION

Additive manufacturing (AM) denotes a group of innovative technologies that enable the rapid fabrication of three dimensional (3D) physical objects directly from computer-aided design (CAD) data without the use of tooling. Parts with complex geometry that are difficult to produce using traditional manufacturing processes can be obtained by AM.^{1,2} A large array of AM techniques is currently used to process thermoplastic polymers, polymer composites, metals, and ceramics.³⁻⁶

Fused filament fabrication (FFF) is extensively used to produce prototypes for applications in, for example, the aerospace, medical, and automotive industries.^{7,8} In this process, a thermoplastic polymer is fed into a

liquefier that extrudes a filament while moving in successive X-Y planes along the Z direction, to fabricate a 3D part layer-by-layer.⁹ Consequently, as the deposition progresses, the hot filament is deposited onto filaments that were previously deposited and that are now in the process of cooling. This causes their reheating, defining a time during which the interfaces of contacting filaments are above the glass transition temperature (T_g) in the case of amorphous materials, or of the crystallization temperature (T_c) for semicrystalline materials, which is necessary for proper bonding to take place.^{10,11} Therefore, each filament should be sufficiently hot during deposition, but not too hot, to avert deformation due to gravity and to the weight of the filaments deposited in subsequent layers.

Given the above, the evolution of the temperature profile of the filaments during deposition is a key parameter affecting the bonding quality.¹² Both experimental and theoretical approaches have been proposed to obtain data on the temperature profile of a printed structure.¹³ Generally, temperature measurements are limited to a single location. Also, the deposition may be interrupted to fix a thermocouple to the part being fabricated.¹⁴ To circumvent this limitation, infrared (IR) thermography has been used. This approach yields the surface temperature, but it cannot read the temperature at the interface of adjacent layers, both due to the camera measurement accuracy and the small filament dimensions.¹⁵ Ferraris et al.¹⁶ used IR thermography to measure the temperature profile of a vertical wall, but the comparison with theoretical predictions showed poor agreement. Kousiatza et al.¹⁷ applied local measurement of the temperature profile in a specific case on acrylonitrile butadiene styrene (ABS) using *K*-type thermocouples ($d = 250 \mu\text{m}$) by pausing the process manually to add them. Although they have concluded that there is a good agreement between experimental and theoretical results, the sudden drop of temperature at the head tip of the extruder clearly shows that there is still a gap between the monitored and numerically derived temperature peak values.

Theoretical efforts to model the temperature profile have focused on 1D or 2D approaches. Sun et al.¹⁸ and Zhang et al.¹⁹ investigated both numerically and experimentally the effect of numerous parameters that exist in the nature of the process. Yardimci and Güçeri²⁰ developed a 1D numerical model to predict the cooling/bonding in fused deposition of ceramics, considering exclusively convection with the environment. Bellehumeur et al.²¹ also developed a 1D model with the same assumption of taking into account the temperature profile along the length of the deposited filament. More recently, Costa et al.²² developed a computer code that takes into account the heat transfer between adjacent filaments during deposition and predicts temperature and adhesion quality for most 3D-printed parts. The model was shown to be in good agreement with experimental data.²³

Despite the above developments, there is still a lack of practical knowledge on the temperature development of filaments during the deposition stage in FFF. To address this limitation, A. Tcharkhtchi et al.²⁴ added thermocouples to the build simultaneously with the fabrication without damaging or pausing the process. However, a drop of approximately 50°C was observed on the experimental data. This work presents an improved measurement setup enabling to record the temperature evolution in various locations of the part during deposition, including the interface between two adjacent filaments. The data collected is

compared with the predictions provided by the model of Costa et al.²² that have been already developed.

The paper is organized as follows. The experimental procedure is presented in detail and the used heat transfer model is introduced. The temperature evolutions of a single PLA filament and a vertical wall are measured experimentally and the data are compared with the theoretical predictions for validation purposes. Finally, the usefulness of the new experimental method is illustrated by studying the influence of the platform temperature and deposition velocity on the heat transfer during cooling.

2 | EXPERIMENTS

2.1 | Materials

A commercial PLA filament with a diameter of 1.75 mm (± 0.01 mm) and a density of $\rho = 1.24 \text{ g/cm}^3$ have been used. Differential scanning calorimetry (DSC Q10 from TA Company) determined the crystallization and the melting temperature of the material before and after printing. The test was performed by subjecting a 6.8 mg sample from room temperature to 210°C at a heating rate of 5°C/min under nitrogen atmosphere. To measure the main transition temperatures, dynamic mechanical analysis tests were performed (DMA Q800 from TA Company) under tensile mode from 40 to 100°C at a temperature rate of 2°C/min and a frequency of 1 Hz. The rectangular sample with a dimension of $25 \times 10 \text{ mm}^2$ was used. For both DSC and DMA characterization, 'TA instrument' software was applied in measurement of the T_g , the T_c , the melting temperature (T_m) and the enthalpy at these temperatures (ΔH) of both materials.

2.2 | 3D printing

The printed parts were manufactured by a desktop 3D printer fitted with a single nozzle ($d = 0.4$ mm) printing head and a temperature-controlled atmosphere (build platform). The solid model file corresponding to the part illustrated in Figure 1 was designed using the FreeCad software and then exported as stereolithography (STL) format to be loaded into the FlashPrint software, which generates the printing path.

The test case was built considering the values for the processing variables (Table 1) that are commonly used in the desktop 3D printer to ensure a good quality part in terms of bonding between filaments and mechanical strength.^{21,25–28}

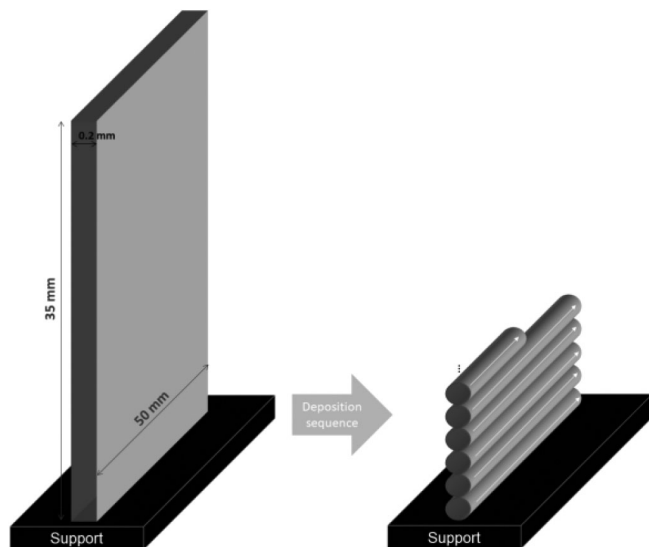


FIGURE 1 Schematic of the test case representing the deposition mechanism of each layer

TABLE 1 Process parameters used for printing

Parameter	Value
Liquefier temperature (°C)	210
Platform temperature (°C)	60
Printing speed (mm/s)	20
Layer height (mm)	0.2
Infill (%)	100
Filament cross-section	Circular

2.3 | In situ temperature measurements

In situ temperature measurement methods should be sufficiently precise and quick to track filament cooling and the reheating peaks arising from contact between freshly and previously deposited filaments. In addition, it should be possible to apply the sensor locally without the need to pause the process. A very small *K*-type thermocouple ($d = 80 \mu\text{m}$), capable of measuring temperatures between -75°C and 250°C , was used. By taking advantage of this size, it is possible to squeeze the device between two adjacent filaments. The thermocouple is connected to a Datapaq® Tracker Telemetry system (previously employed for the in situ temperature measurement in rotational molding process²⁹) for temperature recording and connection to a polycarbonate (PC). As shown in Figure 2 (setup of the work), when the print was started by fabrication of the support (by opening the door) thermocouple placed at the location of 5 mm from the starting point of the deposition and then the door closed in order to have a stabilized temperature of the environment.

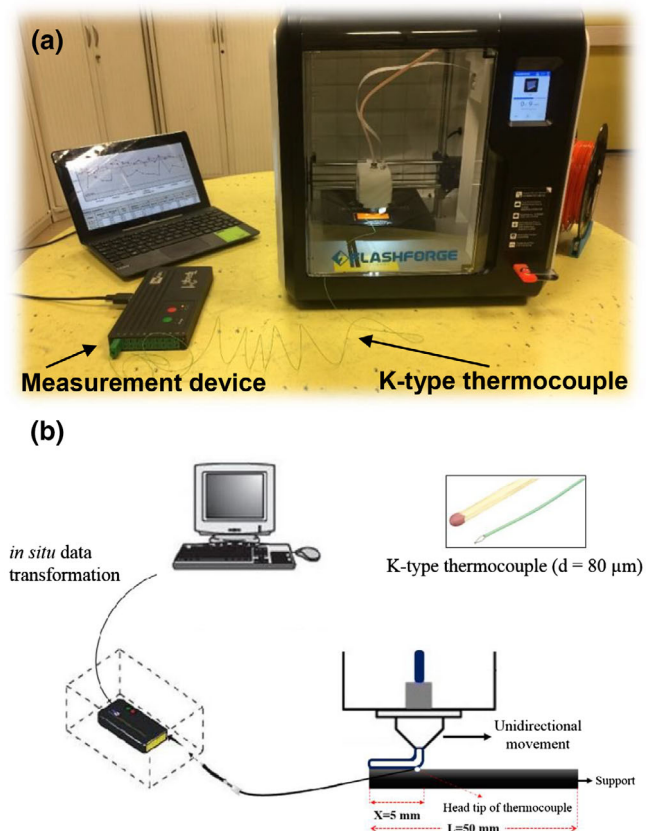


FIGURE 2 (a) Setup and (b) schematic used for the in situ measurement of temperature during the deposition stage in FFF [Color figure can be viewed at wileyonlinelibrary.com]

3 | MODELLING OF FILAMENT COOLING DURING DEPOSITION

Heat transfer during deposition is complex, with contributions from radiation, convection, and conduction. However, it has been demonstrated that (a) the heat losses by convection with the environment (b) the thermal contacts with the support and with adjacent filaments are the main contributors to the filament temperature evolution.²² A computer code that has been already developed, was applied assuming the gradual deposition of small axial filament segments, an analytical solution for the energy equation³⁰ whilst updating the local thermal conditions, and a healing criterion proposed by Yang and Pitchumani.³¹ This gave rise to a useful tool that allows us to predict the temperature evolution and the degree of bonding between filaments for 3D parts including the usage of two distinct materials (e.g., the material of the part plus support material).

Figure 3 shows the evolution of the temperature of the filaments at specific instants upon building the first ten layers of a vertical wall. As in the experiments

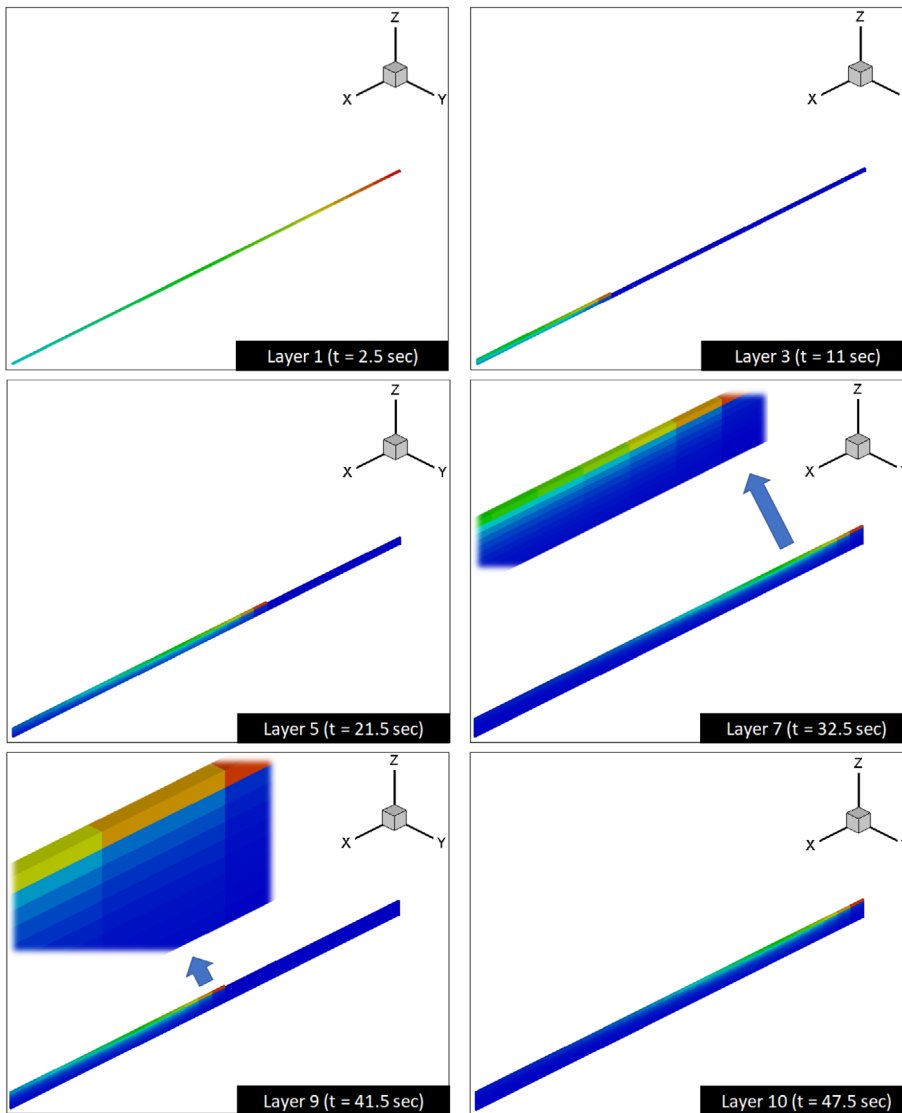


FIGURE 3 Temperatures of the ten first layers of the vertical wall at some instants of the deposition process [Color figure can be viewed at wileyonlinelibrary.com]

reported in this work, the liquefier deposits one filament, then stops and returns to the initial point to deposit the next filament. Under these printing conditions, when a new filament is deposited, the previous one has already significantly cooled down. Nevertheless, the deposition of a new hot filament prompts the reheating of filaments of the previous layers (as seen at 32.5 and 41.5 s), thus demonstrating the importance of considering the thermal contacts in the calculations.

4 | RESULTS AND DISCUSSION

4.1 | Polymer characterization

Figure 4(a) shows the DSC traces for the PLA filament and the printed part. The T_g , the T_c , the T_m , and the

enthalpy at these temperatures (ΔH) of both materials are measured and summarized in Table 2. The temperature range between the crystallization and melting temperatures (102 to 148 °C) is paramount for FFF, as it determines the extent of diffusion for bonding purposes. Moreover, from DMA result (Figure 4(b)) the T_g was detected to be around 57°C.

4.2 | Validation of the measurement methodology

For validation purposes, the temperature evolution of PLA during the deposition of a single filament and of a vertical wall as measured using the applied methodology was compared with the predictions of the thermal model.

FIGURE 4 (a) DSC and (b) DMA traces for PLA filaments. DSC, differential scanning calorimetry; DSC, differential scanning calorimetry [Color figure can be viewed at wileyonlinelibrary.com]

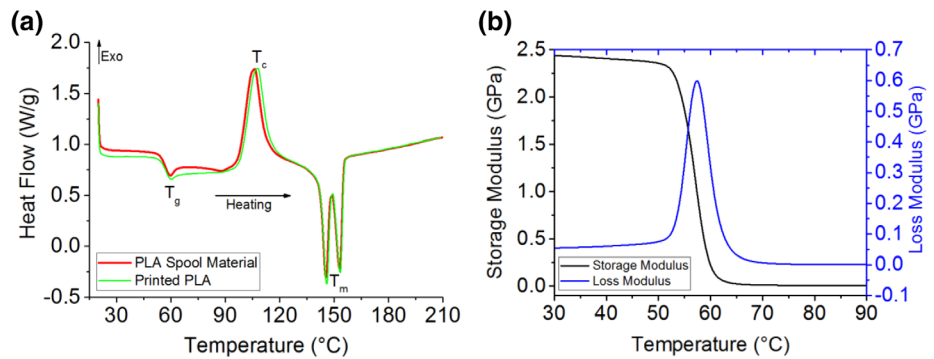


TABLE 2 Thermal properties of PLA (before and after printing as obtained from DSC and DMA)

Properties	PLA spool material	Printed PLA
T_g (°C)	56.6	54.6
T_c (°C)	102	107
ΔH at T_c (j/gr)	19.23	22.36
T_m (°C)	148	149
ΔH at T_m (j/gr)	3.8	8.2

Abbreviations: DMA, dynamic mechanical analysis; DSC, differential scanning calorimetry.

4.2.1 | Deposition of a single filament

The temperature evolution during the deposition of a single filament is presented in Figure 5 for the first deposited filament. Both experimental measurements and theoretical curves for two values of the heat transfer coefficient are shown. Practice revealed that opening/closing the door of the environmental chamber to add/remove thermocouples would slightly disturb the platform temperature. This is why an interval in the range 50–60°C (approximated using thermocouples to see the temperature variation of the platform) and not the value of 60°C (see Table 1) is shown in the mentioned figure (Figure 5). The value of 70 W/m² °C for the heat transfer coefficient (h_{conv}) is commonly used (e.g.,³²). A value of 88 W/m² °C is obtained when using the Churchill correlation for the cooling down of a cylinder by natural convection³³:

$$h_{\text{conv}} = \frac{Nu_d \cdot k}{d} \quad (1)$$

where d is the diameter (m), k is the thermal conductivity (W/m °C) and Nu_d is the Nusselt number defined by:

$$Nu_d = \left\{ 0.60 + \frac{0.387 Ra_d^{1/6}}{\left[1 + \left(\frac{0.559}{Pr} \right)^{9/16} \right]^{8/27}} \right\}^2 \quad (2)$$

where the Rayleigh Ra_d number and P_r are expressed as:

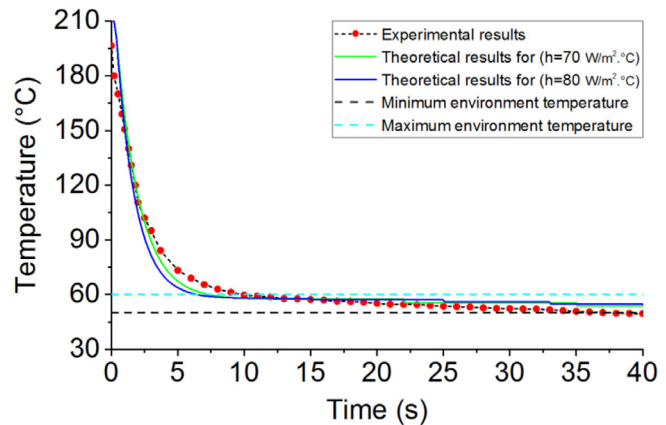


FIGURE 5 Experimental ($\pm 2^\circ\text{C}$) and theoretical temperature evolution during the deposition of a single filament (at $x = 5$ mm) [Color figure can be viewed at wileyonlinelibrary.com]

$$\begin{cases} Ra_d = Gr_d Pr \\ Pr = \frac{\nu_k}{\alpha} \end{cases} \quad (3)$$

In the above expressions, ν_k is the kinematic viscosity (m²/s), α is the thermal diffusivity (m²/s), and Gr_d is the Grashof number:

$$Gr_d = \frac{g\beta(T_s - T_E)d^3}{\nu_k^2} \quad (4)$$

Here g is the gravity acceleration (9.8 m/s²), β is the volumetric thermal expansion coefficient, T_s is the cylinder temperature (°C) and T_E is the environment temperature (°C).

Figure 5 shows a good agreement between the theoretical and the experimental values. The difference between the two sets of data occurs mostly between 3 and 8 s, when the predicted cooling rate is higher than the one measured. This is probably due to the fact that the theoretical model does not consider the change in state and crystalline growth, and thus forecasts faster cooling.

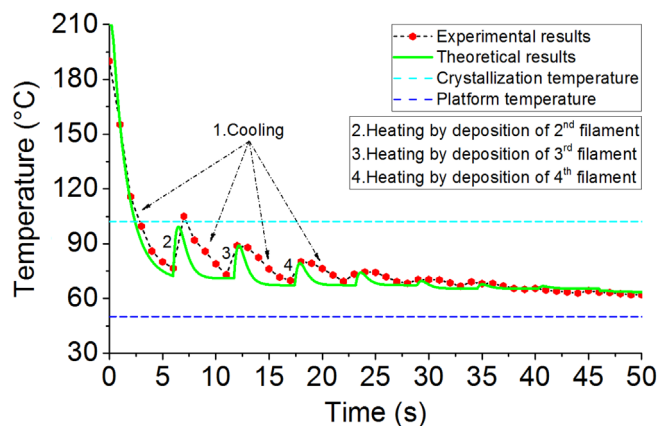


FIGURE 6 Experimental ($\pm 2^\circ\text{C}$) and theoretical temperature evolution of the first filament (at $x = 5$ mm) during the deposition of a vertical wall consisting of single filaments deposited on top of each other. The numbers identify regions of the data: 1- cooling of the first filament, 2-4 reheating of the filament due to the deposition of filaments 2-4 [Color figure can be viewed at wileyonlinelibrary.com]

4.2.2 | Deposition of a vertical wall

Figure 6 depicts the evolution of the temperature of the first filament (at a location distant 5 mm from the edge) during the building of a vertical wall consisting of single filaments deposited on top of each other. It is clear that cooling of this first filament is significantly affected by the successive deposition of younger filaments, which may cause important reheating. The numbers identify regions of the data (1: cooling of the first filament; 2-4: reheating of the filament due to the deposition of filaments 2 to 4). The crystallization and platform temperatures are also identified.

For computational purposes, it is important to define the thermal contact conductance (h) between adjacent filaments. This is difficult, as it depends on pressure, surface roughness, and other conditions that are difficult to quantify.³⁴ Apparently, there are no theoretical or empirical correlations providing an exact value for h . Using a value of $h = 800 \text{ W/m}^2 \text{ }^\circ\text{C}$, the magnitude of the experimental and theoretical reheating peaks became virtually coincident.

Regardless of this approximation, the onset, relative magnitude, and breadth of the various temperature peaks are similarly captured by the two approaches. As expected, the peaks become gradually smaller with time, as the new filament being deposited is separated from the first filament by more filaments. As before, the predictions seem to overestimate the cooling rate, as no phase change and crystallization were built in the model. On the other hand, a delay in receiving the experimental data can exist and contribute to the differences.

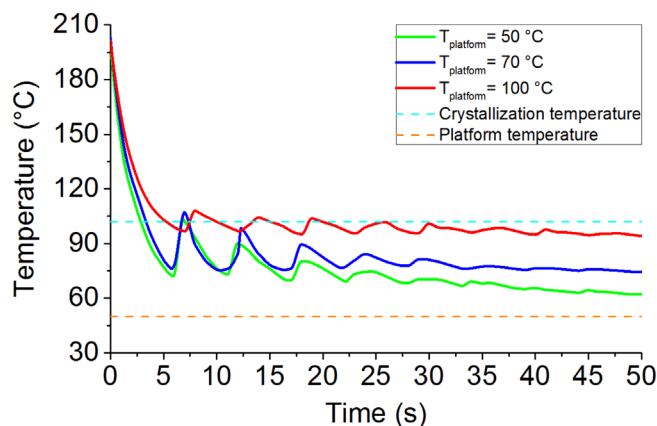


FIGURE 7 Temperature profile ($\pm 2^\circ\text{C}$) of vertical wall at $x = 5$ mm from the start of deposition at different platform temperatures [Color figure can be viewed at wileyonlinelibrary.com]

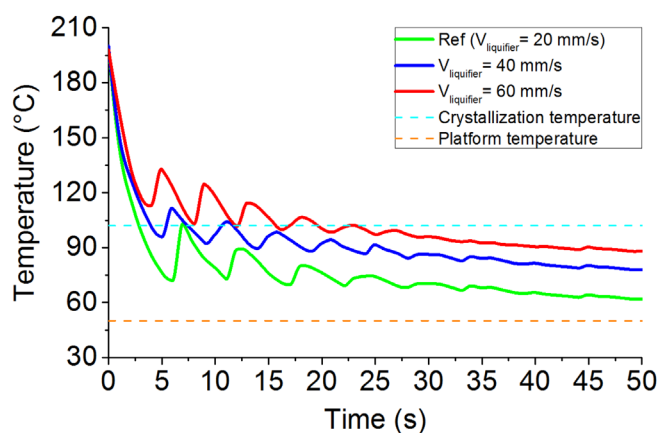


FIGURE 8 Temperature profile ($\pm 2^\circ\text{C}$) of vertical wall at ($x = 5$ mm) from the start of deposition at different print speed [Color figure can be viewed at wileyonlinelibrary.com]

4.3 | Case studies

This section demonstrates the usefulness of the proposed in situ temperature measurement technique, by studying the effect of the platform temperature and deposition velocity on the heat transfer during cooling.

Figure 7 shows the temperature evolution of three different temperature of the platform, at location distance 5 mm from the edge. As expected, the lower the platform temperature the faster the cooling. As for the reheating peaks, they have identical onsets, but the magnitude tends to decrease with increasing platform temperature. When the platform temperature is set to 100°C , the filament being monitored reheats repeatedly above its T_c , favoring bonding.

When the deposition velocity increases (Figure 8), the rate of cooling decreases. Also, and as expected, the onset of

the peaks occurs at different times and their breadth is also altered. Finally, the magnitude of the peaks for the lowest deposition velocity is higher, probably due to the higher difference between the temperatures of adjacent filaments.

5 | CONCLUSIONS

This work presents a 'localized measurement' setup enabling to record temperature profile of two adjacent filaments (or a sequence of deposition) during the FFF process. The main characteristic of the proposed method is the accurate measurements of polymer material temperature using 80 μm thermocouples. It has been shown that the experimental results are in good agreement with the utilized numerical method. It correctly measures the temperature profile of a single filament and filaments embedded in multilayer parts by taking into account the effect of the variant temperature of the environment and thermal contact conductance between adjacent filaments. A parametric study on the effect of the bed temperature and the printing speed indicated the influence on reheating of the previously deposited filament during additional layer deposition.

These results are important for the understanding of filament bonding. The main outcome of this study is to apply the incoming results for prediction of bonding and consequently to optimize the strength of successively deposited layers. Future work will focus on the improvement of the proposed setup to show its capacity in complex geometry. Accordingly, it could help the optimization of bonding quality by correlating the thermal and mechanical characteristic results.

ORCID

Hamid Reza Vanaei  <https://orcid.org/0000-0003-1501-0482>

REFERENCES

- [1] O. A. Mohamed, S. H. Masood, J. L. Bhowmik, *Adv. Manuf.* **2015**, 3, 42.
- [2] J. Holmström, J. Partanen, J. Tuomi, M. Walter, *J. Manuf. Technol Manage.* **2010**, 21, 687.
- [3] J. F. Rodríguez, J. P. Thomas, J. E. Renaud, *J. Mech. Design* **2003**, 125, 545.
- [4] P. Kulkarni, A. Marsan, D. Dutta, *Rapid prototyping j.* **2000**, 6, 18.
- [5] S. Saeidlou, *Cinétique de Cristallisation, Structure Et Applications Des Stéréocomplexes de PLA*, Université de Sherbrooke, Québec, Canada **2014**.
- [6] E. C. Santos, M. Shiomi, K. Osakada, T. Laoui, *Int. J. Mach. Tools Manuf* **2006**, 46, 1459.
- [7] A. Iftikhar, M. Khan, K. Alam, S. H. Imran Jaffery, L. Ali, Y. Ayaz, A. Khan, *Mater. Manuf. Processes* **2013**, 28, 534.
- [8] D. Yagnik, *IOSR J. Mech. Civil Eng* **2014**, 5, 62.
- [9] P. Chennakesava, Y. S. Narayan, Fused deposition modeling-insights. in *Proceedings of the International Conference on Advances in Design and Manufacturing ICAD&M*, Vol. 14, Hyderabad, India **2014**, p. 1345.
- [10] R. W. Hopper, *J. Am. Ceram. Soc.* **1984**, 67, C262.
- [11] N. Rosenzweig, M. Narkis, *Polym. Eng. Sci.* **1981**, 21, 1167.
- [12] H. R. Vanaei, K. Raissi, M. Deligant, M. Shirinbayan, J. Fitoussi, S. Khelladi, A. Tcharkhtchi, *J Mater Sci* **2020**, <https://doi.org/10.1007/s10853-020-05057-9>
- [13] A. D'Amico, A. M. Peterson, *Addit. Manuf* **2018**, 21, 422.
- [14] C. Kousiatza, D. Karalekas, *Mater. Des.* **2016**, 97, 400.
- [15] J. E. Seppala, K. D. Migler, *Addit. manuf.* **2016**, 12, 71.
- [16] E. Ferraris, J. Zhang, B. Van Hooreweder, *CIRP Annals* **2019**, 68, 213.
- [17] C. Kousiatza, N. Chatzidai, D. Karalekas, *Sensors* **2017**, 17, 456.
- [18] Q. Sun, G. Rizvi, C. Bellehumeur, P. Gu, *Rapid Prototyping J.* **2008**, 14, 72.
- [19] J. Zhang, X. Z. Wang, W. W. Yu, Y. H. Deng, *Mater. Des.* **2017**, 130, 59.
- [20] M. Atif Yardimci, S. Güçeri, *Rapid Prototyping J.* **1996**, 2, 26.
- [21] C. Bellehumeur, L. Li, Q. Sun, P. Gu, *J. Manuf. Processes* **2004**, 6, 170.
- [22] S. Costa, F. Duarte, J. Covas, *Virtual.Phys. Prototyping* **2015**, 10, 35.
- [23] S. Costa, F. Duarte, J. Covas, *J. Mater. Process. Technol.* **2017**, 245, 167.
- [24] A. Kallel, I. Koutiri, E. Babaeitorkamani, A. Khavandi, M. Tamizifar, M. Shirinbayan, A. Tcharkhtchi, *Int. Polym. Process.* **2019**, 34, 434.
- [25] W. Han, M. A. Jafari, K. Seyed, *Rapid Prototyping J.* **2003**, 9, 212.
- [26] H. Vanaei, M. Shirinbayan, M. Deligant, K. Raissi, J. Fitoussi, S. Khelladi, A. Tcharkhtchi, *Polym. Eng. Sci.* **2020**, <http://dx.doi.org/10.1002/pen.25419>.
- [27] S.-H. Ahn, M. Montero, D. Odell, S. Roundy, P. K. Wright, *Rapid prototyping j.* **2002**, 8, 248.
- [28] M. Spoerk, F. Arbeiter, H. Cajner, J. Sapkota, C. Holzer, *J. Appl. Polym. Sci.* **2017**, 134, 45401.
- [29] A. Lucas, A. Danlos, M. Shirinbayan, V. Motaharnejad, R. Paridaens, K. Benfriha, F. Bakir, A. Tcharkhtchi, *Int. J. Adv. Manuf. Technol.* **2019**, 104, 1183.
- [30] S. F. Costa, F. M. Duarte, J. A. Covas, *J. Mater. Form.* **2008**, 1, 703. <http://dx.doi.org/10.1007/s12289-008-0312-9>
- [31] F. Yang, R. Pitchumani, *Macromolecules* **2002**, 35, 3213.
- [32] J. F. Rodríguez, J. P. Thomas, J. E. Renaud, *Rapid prototyping j.* **2001**, 7, 148.
- [33] A. D. Kraus, A. Aziz, J. Welty, D. Sekulic, *Appl. Mech. Rev.* **2001**, 54, B92.
- [34] J. P. Holman, *Transferência de Calor. São Paul o*, McGraw-Hill do Brasil, São Paulo **1983**.

How to cite this article: Vanaei HR, Shirinbayan M, Costa SF, et al. Experimental study of PLA thermal behavior during fused filament fabrication. *J Appl Polym Sci.* 2021;138:e49747. <https://doi.org/10.1002/app.49747>

Article No. 4:

HR Vanaei, M Deligant, M Shirinbayan, K Raissi, J Fitoussi, S Khelladi, A Tcharkhtchi; A comparative in-process monitoring of temperature profile in fused filament fabrication; Polymer Engineering and Science Journal, 61(1): 68-76 (2021).

DOI: [10.1002/pen.25555](https://doi.org/10.1002/pen.25555)

RESEARCH ARTICLE

A comparative in-process monitoring of temperature profile in fused filament fabrication

H.R. Vanaei^{1,2}  | M. Deligant¹ | M. Shirinbayan²  | K. Raissi¹ |
J. Fitoussi² | S. Khelladi¹ | A. Tcharkhtchi²

¹Arts et Metiers Institute of Technology, CNAM, LIFSE, HESAM University, Paris, France

²Arts et Metiers Institute of Technology, CNRS, CNAM, PIMM, HESAM University, Paris, France

Correspondence

H.R. Vanaei, Arts et Metiers Institute of Technology, CNAM, LIFSE, HESAM University, F-75013 Paris, France.
Email: hamidreza.vanaei@ensam.eu

Abstract

Fused filament fabrication (FFF), an additive manufacturing technique, is used to produce prototypes and a gradually more important processing route to get final products. Due to the layer-by-layer deposition mechanism involved, bonding between adjacent layers is controlled by the thermal energy of the material being printed. Thus, it is strongly in conjunction with the temperature development of the filaments during the deposition sequence. This study gives out an in-process set-up enabling to record temperature profile of two adjacent filaments or a sequence of deposition in various locations during FFF process. The main characteristic of the presented procedure is the possibility of obtaining a global temperature profile resulted from an IR-camera; parallel to those recorded using a K-type thermocouple. Needless to say that a K-type thermocouple accurately records the local temperature at the interface of adjacent filaments. Conversely, an IR-camera signifies the temperature profile on the captured surface. The obtained results showed that there is a remarkable difference between the cooling rate and re-heating peaks. The primary outcome of this study is the consideration of results accuracy and the possibility of working on optimization of the obtained temperature profile. Altogether it helps optimize inter-layer strength while assessing the temperature evolution.

KEYWORDS

fused filament fabrication, in-process measurement, IR-camera, local-global approach, thermocouple

1 | INTRODUCTION

Fused Filament Fabrication (FFF), an extensively Additive Manufacturing (AM) process,^[1] involves extrusion of thermoplastic filaments while moving in successive X-Y planes along the Z direction using the mechanism of layer-by-layer deposition.^[2,3]

As deposited filaments are facing with deposition of new filaments during the process, there is always a cyclic temperature profile resulting in the cooling and re-heating of each one. The evolution of the temperature

profile of filaments during deposition controls the inter-layer bonding. In literature, many works have mentioned the FFF process a thermally driven procedure in which neck growth is stemmed from thermal diffusion of adjacent filaments above the crystallization temperature (for semi-crystalline materials) and the glass transition temperature (for amorphous materials).^[4-6]

Variety of studies have been performed to investigate the mechanical strength of 3D-printed parts,^[7-10] and it have been pointed out that the evolution of the temperature profile is a key parameter that affects the bonding

quality.^[11,12] More specifically, cyclic cooling and re-heating exists during layer deposition of the filaments. The criterion of effective bonding and consequently the mechanical properties are a major concern in FFF.^[13,14] In the process of parts fabrication, as the deposition progresses, the hot filament is deposited onto filaments that were previously deposited and/or are being cooled. The contact between the hot filament and the previously deposited filaments causes re-heating of the latter. At the interface of adjacent filaments, temperature rises above the crystallization temperature (T_c) and proper bonding takes place. The evolution of temperature profile could be obtained by employing thermocouples to have local measurements. The deposition; however, might be interrupted while fixing the thermocouple.^[15]

Kousiatza et al.^[16] locally measured the temperature profile. Although they have had an adequate agreement between experimental and theoretical results, the sudden drop of temperature at the head tip of the extruder showed a gap between the recorded and numerically derived temperature peak values. To wipe out this limitation, infrared thermography has been widely used. Albeit it deals with the surface temperature, it still does not record the interface temperature of adjacent layers.^[17] Ferraris et al.^[18] used IR thermography in determination of the temperature profile of a vertical wall and they observed poor agreement with theoretical predictions. Furthermore, 1D or 2D models have been developed to evaluate the temperature profile of deposited filaments during fabricating a structure. Sun et al.^[5] and Jie Zhang et al.,^[19] tried to evaluate, both numerically and experimentally, the influence of process parameters on the temperature evolution. In another study, Bellini and Güçerli^[20] used FEM to model extrusion and cooling rate of FFF process. Rodriguez et al.^[21] computed the cooling rate numerically as a criterion for the bonding. In addition, Bellehumer et al.^[4] developed a 1D model by taking into account the temperature profile. More recently, Costa et al.^[22] developed an analytical approach to predict temperature profile and adhesion quality of 3D-printed parts.

For the above-mentioned reasons, experimental monitoring of temperature is still challenging in FFF and lack of practical knowledge corresponds to the problem of bonding in this process. To address this limitation, K-type thermocouples ($d = 80 \mu\text{m}$) were added in parallel with deposition without pausing the process or causing damage.^[23] The experimental data were then compared with the predictions obtained by Costa et al.^[24] and it was found that there is a sufficient agreement between the experimental and analytical results.

To conclude, research on in process monitoring of temperature profile is still in its infancy. This work

presents a comparison between the local and global assessment of temperature profile using both contact and non-contact approach. The aim is to evaluate the nature of both methods, the IR thermography, and small thermocouples ($d = 80 \mu\text{m}$) in parallel.

2 | MATERIALS AND METHODS

To track the cooling of filaments and the re-heating peaks of deposition of successive layers during deposition, very small ($d = 80 \mu\text{m}$) K-type thermocouples were used (see^[23] for method description). The schematic of the experiment is presented in Figure 1 containing: the set-up for in-process measurement of temperature profile during the deposition, assembling of two methods together, and thermogram of the printed vertical wall with corresponding layers and locations highlighted for temperature profile. In parallel to the deposition and temperature recording using K-type thermocouples, an Optris PI450 infrared camera was used (at the same points 1-6) with the technical data presented in Table 1. Material emissivity (ϵ) was obtained by calibrating the absolute difference of the tracks obtained by IR-camera and a thermocouple.

The camera was placed with a specific distance from the extruder to have the plain field of view (FOV) of all the deposited layers. Experiments have been carried out while the camera inspecting (a) the X-Z planes and (b) the Y-Z planes. In the first case (X-Z planes), the printed part is stationary on FOV. It was then recorded temporal temperature variations in the object front plane. Therefore, temperature changes at every location are the consequence of several re-heating that stem from new depositions. In-process monitoring was performed on a designed vertical wall sample with geometry of $50 \times 0.2 \times 35 \text{ mm}^3$ using the one-way direction of deposition. Process parameters and related settings to the process are indicated in Table 2.

In the second case (Y-Z planes), the nozzle was fixed and the part was printed by moving the built plate in Y direction. Four points specified as shown in Figure 2 with the following descriptions. Point a stays on extruder during printing (verifying the extruder temperature and the accuracy of measurement). Point b specifies the variation of temperature when material exits from the extruder (diffusion zone of material between two adjacent layers). Point c indicates the temperature of same layer. In other word, it is located on the same layer as that of point b, but with a specific distance from extruder (out of diffusion zone). Point d represents the effect of extruder temperature (or material when exits from extruder) on the previous layer (end of diffusion zone).

Temperature difference (ΔT) between point b and d is an indicator of temperature profile between two

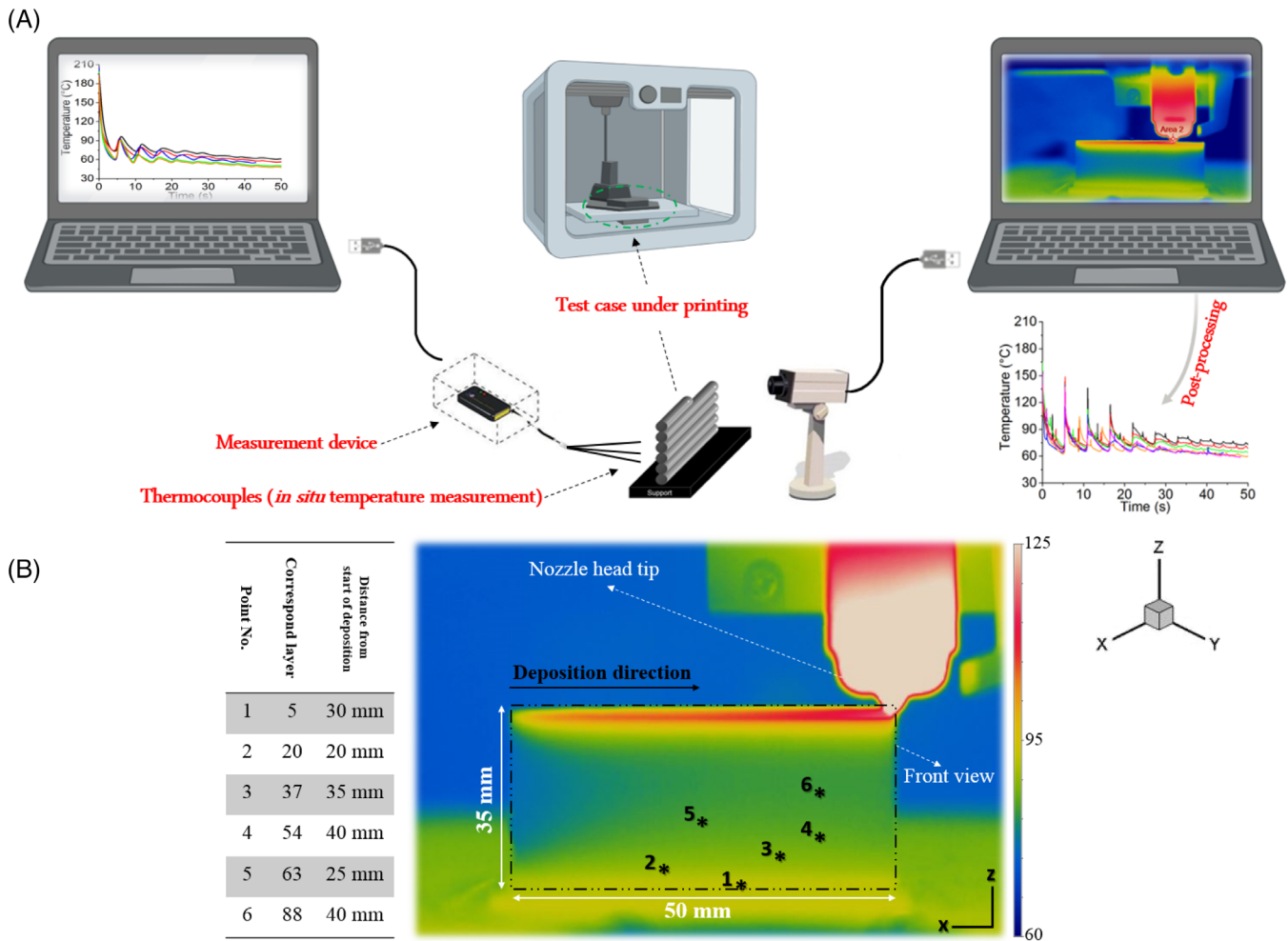


FIGURE 1 Representation of (A) in situ measurement of temperature profile during the deposition stage in FFF process, (B) thermogram of a vertical wall and points representing the location of the thermocouples with corresponding layers highlighted for temperature profile [Color figure can be viewed at wileyonlinelibrary.com]

TABLE 1 Technical data of Optris PI 450 camera

Technical data	Value
Wavelength range (μm)	8-14
Frequency (Hz)	32
Frame rate (Hz)	80
Optical resolution (pixels)	382*288
Material emissivity	0.89
Accuracy (%)	± 2

TABLE 2 Process parameters used for printing

Parameter	Value
Liquefier temperature ($^{\circ}\text{C}$)	210
Support temperature ($^{\circ}\text{C}$)	50
Printing speed (mm/s)	20
Layer height (mm)	0.2
Infill (%)	100

adjacent layers. It could be compared with point c for complementary assessment of the inter-layer temperature evolution. Two cases have been shown as (a) deposition from first layer-to-layer 5 and (b) deposition from layer 15 to layer 20 to show the influence of distance from the heat flux of support.

To perform the experimental procedure, polylactic acid (PLA) filament ($d = 1.75 \pm 0.01$ mm) with the density of $\rho = 1.24$ g/cm³ has been used (fillamentum supplier). Differential scanning calorimetry (DSC) was done using DSC Q1000 from TA instrument. Sample (~ 6 mg), cut from the printed part, was sealed in an aluminum pan and heated from room temperature to 200 $^{\circ}\text{C}$ with heating rate of 5 $^{\circ}\text{C}/\text{min}$ to determine crystallization and melting temperature, T_c and T_m , respectively. The related curve and the gathered data are presented in Table 3. The temperature range between $T_c = 103^{\circ}\text{C}$ and $T_m = 148^{\circ}\text{C}$ is an important temperature range in the FFF process in semi-crystalline materials.

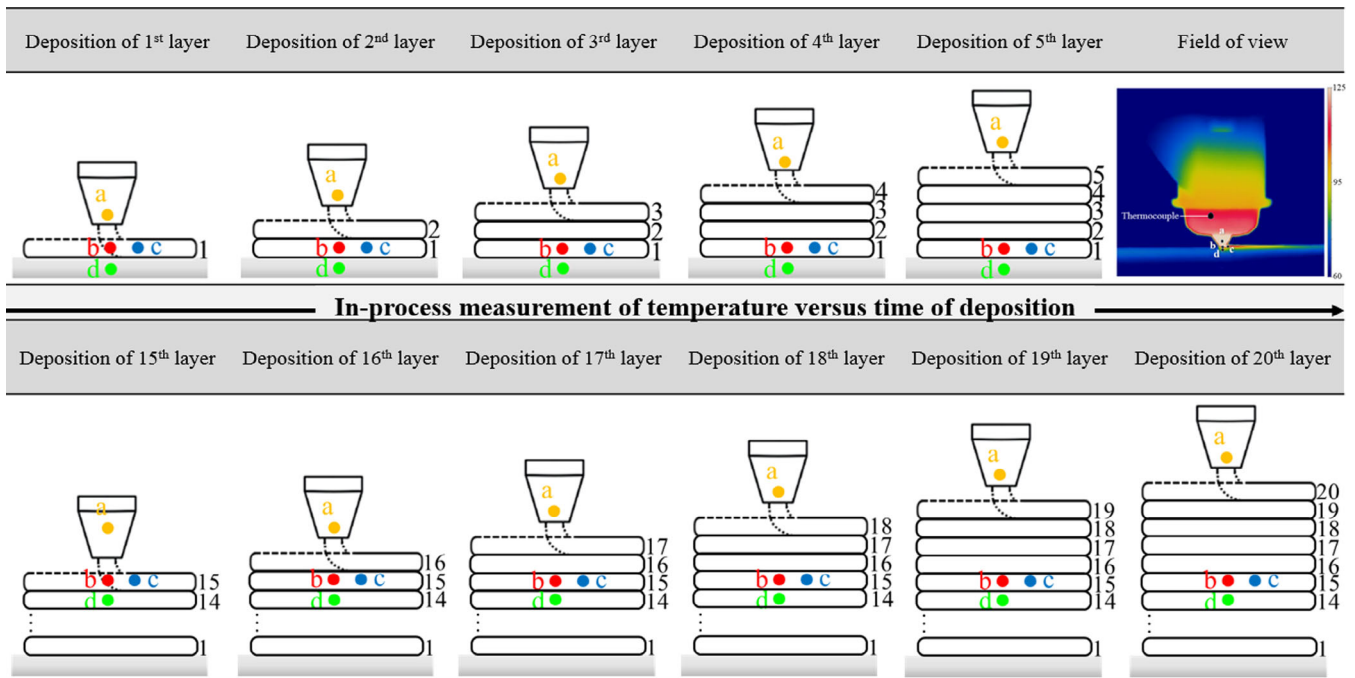
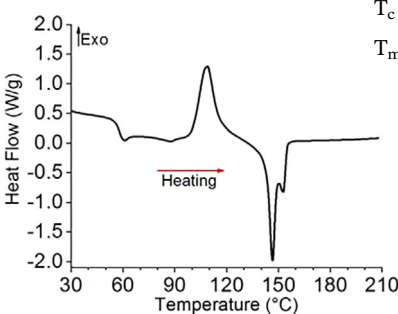


FIGURE 2 Schematic representation of temperature variation of point a-d at instance of deposition for (A) layer 1 to 5 and (B) layer 15 to 20 [Color figure can be viewed at wileyonlinelibrary.com]

TABLE 3 Differential scanning calorimetry curve and thermal properties of PLA

DSC curve	Properties	PLA material
	T_c (°C)	103
	T_m (°C)	148

3 | RESULTS AND DISCUSSION

3.1 | Local and global temperature profile

The accompanying graphs presented in Figure 3 provide the experimental results (temperature profile) of both IR-camera and K-type thermocouple. They comprise six points in different locations (in different layers) of the sample (see Figure 1). As described, the reported

experiments are based on the layer-by-layer deposition of filaments. Under the 3D printing conditions, when a new filament is deposited, the previous one has significantly cooled down. Although there is a notable variance in starting point (when the filament exists from the nozzle) of deposition for each layer, the temperature evolves in the same cooling rate. For post processing, the two signals are synchronized at $t = 0$, based on the instant of the first peak of temperature (the highest measured value considered as a value at $t = 0$).

As illustrated in Figure 4, the temperature peaks recorded by both methods is described as following. Peak 1 is the re-heating of fifth filament by deposition of sixth filament; peak 2 is the re-heating of fifth filament by deposition of seventh filament; peak 3 is the re-heating of fifth filament by deposition of eighth filament; peak 4 is the re-heating of fifth filament by deposition of ninth filament. Peaks on cooling curves are the return of the extruder to the point of next deposition without feeding of material (not important).

Owing to the nature of thermocouple and the local measurement of temperature at the inter-layer bonding, the temperature peaks recorded by IR-camera are highly overestimated comparing with those recorded by the K-type thermocouple. On the other hand, the sequences of temperature peaks concluded by K-type thermocouple has an acceptable evolution in comparison with those derived from IR-camera. In almost all the conditions, by increasing the distance

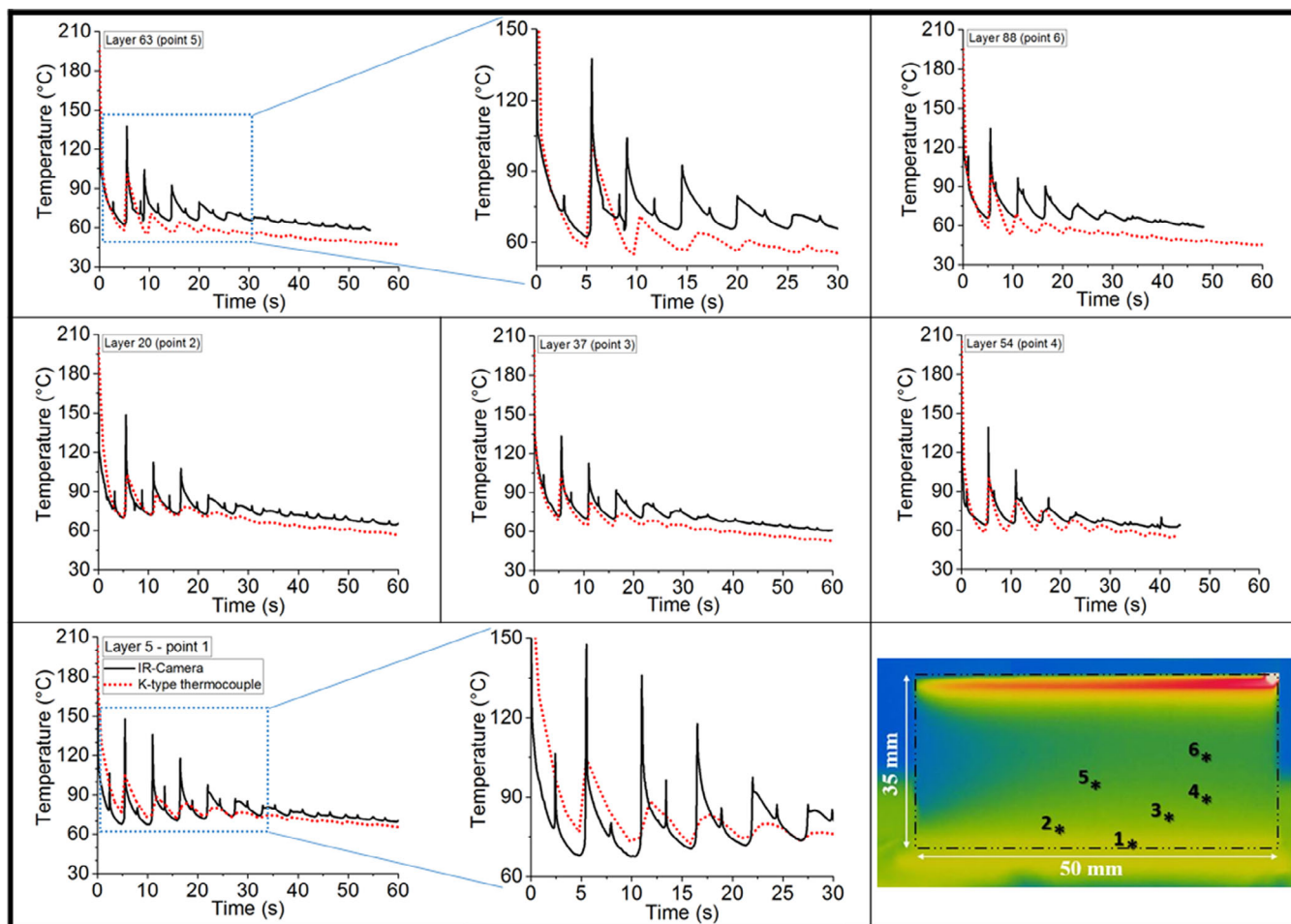


FIGURE 3 Temperature evolution at six locations during the deposition of a vertical wall consisting of single filaments deposited on top of each other. Point 1–6 corresponds to the fifth, 20th, 37th, 54th, 63rd, and 88th while indicating 30, 20, 35, 40, 25, and 40 mm from start of deposition, respectively [Color figure can be viewed at wileyonlinelibrary.com]

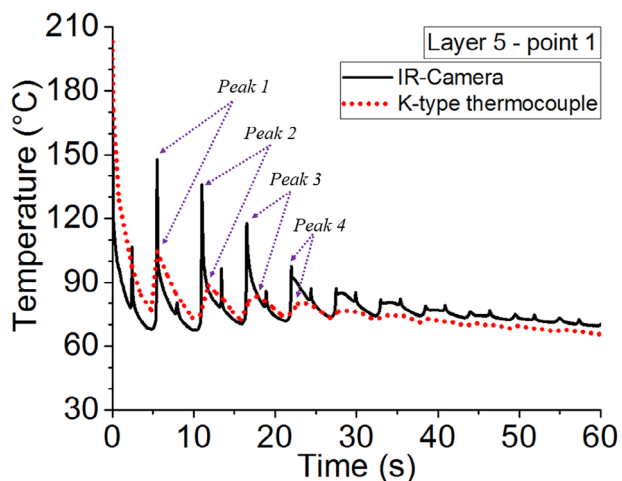


FIGURE 4 Experimental temperature evolution of layer 5 (at $x = 30$ mm) during the deposition of a vertical wall consisting of single filaments deposited on top of each other [Color figure can be viewed at wileyonlinelibrary.com]

from the support, the temperature profile remains above 50°C . The secondary re-heating (and consequently third, fourth, fifth, and other re-heatings) are increasingly weak enough to enhance and keep the temperature of the previously printed parts. Accordingly, the inter-layer diffusion is limited to adjacent filaments as the secondary re-heating peak is at almost $T = 103 (\pm 2)^{\circ}\text{C}$.

Presented results in Figure 3 showed that there is a notable difference between the monitored temperature profiles. Despite the acceptable precision of the IR-camera, peak values (particularly in the first 20 seconds) are overestimated. This could be deduced from the radiation of extruder, previously deposited filaments under cooling, or even the heat radiation from support for the first layers. Believable, the precision of the IR-camera is lower than a thermocouple based on the nature of each measurement method. It has some

advantages such as straightforwardness of the test and overfilling of data. In future work, numerical validation of both methods will be done for further discussions.

3.2 | Upper-limit and peaks evolution

Re-heating peaks decrease with progressively deposition of filaments. As mentioned in section 2, the temperature above T_c and below T_m is important for inter-diffusion of successive layers. Cyclic evolution of temperature plays an important role in the overall incident. In Figure 5, upper-limit of peak consequences indicates two different observations. Seemingly, the first data recorded by the IR-camera (refer to Figure 5(A) decreases about 23% with a distance increase from support, whereas, those captured by the K-type thermocouple (refer to Figure 5(B) stay around 5%. Apparently, on behalf of the extruder temperature, the thermocouple hands over $\sim 4\%$ deviation from real data ($T_{ext} = 210^\circ\text{C}$) while $\sim 19\%$ by the IR-camera. As an example, the first data recorded by K-type thermocouple and IR-camera for layer 54 at $x = 40$ mm from deposition are 202°C and 155°C , respectively.

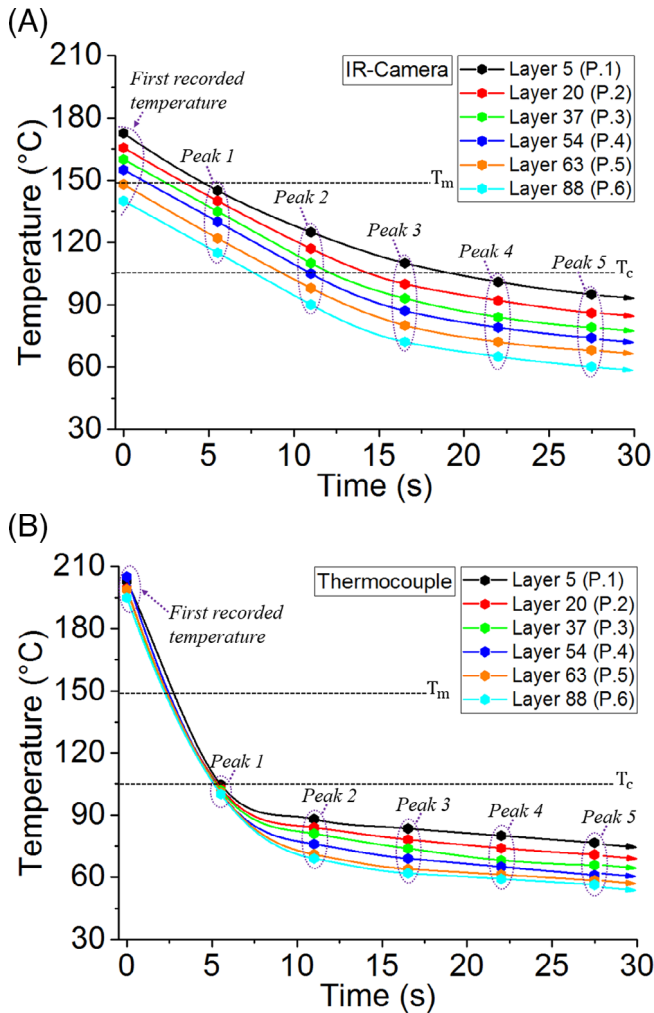


FIGURE 5 Upper-limit and peaks evolution of data recorded at each layer by (A) IR-camera and (B) type K thermocouple [Color figure can be viewed at wileyonlinelibrary.com]

3.3 | Interval of peaks between two approaches

Following observations obtained so far: layers near support are more affected by T_{supp} (higher peaks in IR-camera); layers in the middle distance are less affected by T_{supp} . Whereas T_{supp} does not affect layers far from the support (Recorded peaks by IR-camera are near those recorded by thermocouple).

Table 4 shows the “ $\Delta T = T_{IR-camera} - T_{thermocouple}$ ” at each peak. Worth mentioning that based on described features, such as, support radiation, there is a small difference in correspond peaks at layers far from the support.

The graphs in Figure 6 reveal the difference of upper-limit obtained by both methods as a function of building time. The specified contour for each layer expresses the nature of each measurement method. Apparently, temperature varies between T_c and T_m in first layers, whereas, the contour drops below T_c as the

IR-camera and thermocouple temperature difference at each peak ($^\circ\text{C}$)					
Layer	1	2	3	4	5
5	44.9	31.5	34.2	21	18.4
20	43	29	26.8	18	15.1
37	37.3	27	21.2	15.8	13.2
54	36.5	25.3	13.7	12.1	9.9
63	33.5	24.3	11.1	10.8	9.6
88	33.2	21	8.1	5.8	3.6

TABLE 4 Data collected from the difference in peak values (Calculated using “ $\Delta T = T_{IR-camera} - T_{thermocouple}$ ” at each peak)

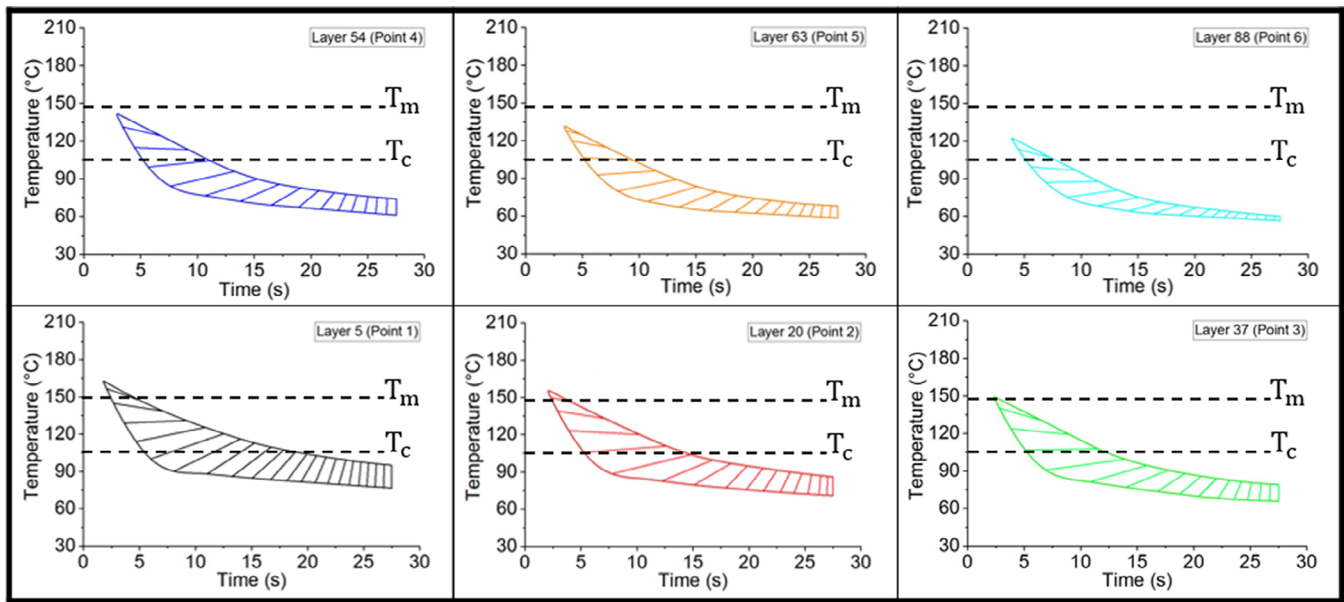


FIGURE 6 Temperature contour at six locations during the deposition of a vertical wall consisting of single filaments deposited on top of each other. Point 1-6 corresponds to the fifth, 20th, 37th, 54th, 63rd, and 88th while indicating 30, 20, 35, 40, 25, and 40 mm from start of deposition, respectively [Color figure can be viewed at wileyonlinelibrary.com]

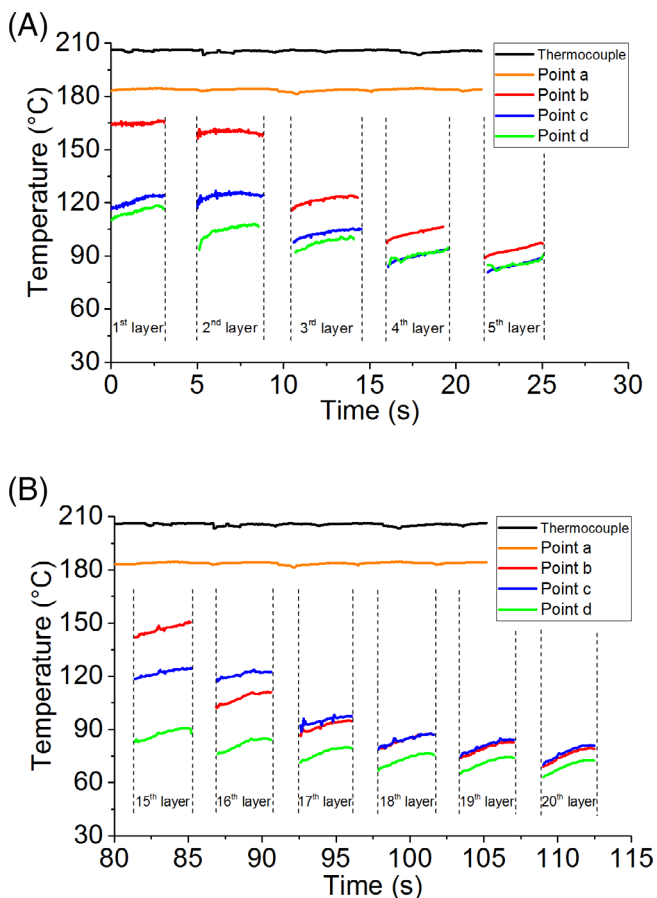


FIGURE 7 Temperature variation of point a-d at instance of deposition for (A) layer 1 to 5 and (B) layer 15 to 20 [Color figure can be viewed at wileyonlinelibrary.com]

distance from the support is increasing. Their relative change is an important concern in the problem of inter-layers bonding and it should be taken into consideration.

3.4 | Four points on IR-camera (second experiment with stationary nozzle)

To have better comprehension, four points have been chosen around the extruder based on Figure 2 (in section 2). The temperature was recorded with the deposition. The mechanism of recording could be explained: the location of points a-d are fixed while the support is moving and it means that at any instance of deposition, the temperature variation of each point is recording. This partially clarifies the temperature of points a-d from beginning of the deposition of a layer and progressively the successive layers.

Figure 7 shows the obtained results. They cover the previous assumptions displaying the effect of distance from support. Presumably from Figure 7(A) and by deposition from layer one to layer five, the temperature of point b shifts between 165°C and 90°C. This is also valid for point c while temperature shifts between 120°C and 80°C. Figure 7(B) could explain the general statement by observing the evolution of point b shifts from 150°C and 70°C by progressive deposition of further layers. In fact, one can note that after a specific deposition of layers (in this case after layer 15) points b and c have almost the

TABLE 5 Strengths and limitations of approaches introduced in this study

Approach	Strengths	Limitations
K-type thermocouple (Local approach)	In situ Temperature profile at interface of adjacent filaments Using obtained results in bonding studying Using obtained results in neck-growth and welding of filaments	Incapable of temperature recording in complex geometry
IR-camera (Global approach)	In situ Capable of temperature recording in complex geometry	Temperature profile on surface of adjacent filaments Incapable of recording temperature of adjacent filaments Over-estimation of recorded peaks Sudden drop of the recorded value

same temperature. Worth mentioning to say, point d remains constant after third layer. For instance, the distance across point b and d during deposition of the first layer expresses the inter-layer diffusion zone. It varies from 165°C to 100°C that is approximately between T_c and T_m . This issue thoroughly explains the cyclic temperature profile discussed before.

3.5 | Comparison of two applied approaches

A vertical wall of a single filament thickness is considered for the analysis of thermal interaction by employing two methods: IR-camera as a global and applying K-type thermocouples as a local approach. As can be seen from the obtained results and depending on the nature of measurement methods, both local and global in-process monitoring of temperature profile have their own strengths and limitations (see Table 5).

As listed in Table 5, regarding the nature of measurement approach and the obtained experimental results, one can note that the capability of each approach as well as their strengths and limitations has a determinative role in the evaluation of temperature profile. Nevertheless, an entire optimization between two approaches could precisely result in characterization of thermal behavior during fabrication of 3D printed parts.

4 | CONCLUSIONS AND PERSPECTIVES

This work presents an in-process set-up enabling the record of temperature profile of two adjacent filaments

(and/or a sequence of deposition) in various locations during the FFF process. The main characteristic of the presented procedure is the possibility of obtaining a global temperature profile resulted from the IR-camera; parallel to those recorded using a K-type thermocouple (local temperature at interface). Accurate acquisition via local measurement revealed by putting K-type thermocouples in different successive layers. However, IR-camera showed that there is a considerable difference by increasing the distance from support. A comparison through the upper-limit and interval of peaks validated the mentioned difference. The obtained experimental results showed that the optimization of the results obtained with the IR-camera by those achieved using the K-type thermocouples are necessary for the bonding optimization.

Additional experiments with a numerical validation are necessary to the set-up and its usefulness. Future work will focus on applying the results in complex geometry with a controlled-environment (Chamber) temperature and developing a predictive approach. This study is useful in inter-layer bonding optimization of adjacent layers by implementing the temperature evolution of filaments.

ORCID

H.R. Vanaei  <https://orcid.org/0000-0003-1501-0482>

M. Shirinbayan  <https://orcid.org/0000-0002-2757-8529>

REFERENCES

- [1] J. Holmström, J. Partanen, J. Tuomi, M. Walter, *J. Manuf. Technol. Manage.* **2010**, *21*(6), 687.
- [2] P. Chennakesava, Y. S. Narayan, Fused deposition modeling-insights. in *Proceedings of the International Conference on Advances in Design and Manufacturing ICAD&M*, Vol. 14 **2014**, p. 1345.

- [3] T. Ambone, A. Torris, K. Shanmuganathan, *Polym. Eng. Sci.*
- [4] C. Bellehumeur, L. Li, Q. Sun, P. Gu, *J. Manuf. Processes* **2004**, 6(2), 170.
- [5] Q. Sun, G. Rizvi, C. Bellehumeur, P. Gu, *Rapid Prototyping J.* **2008**, 14(2), 72.
- [6] A. K. Ravi, A. Deshpande, K. H. Hsu, *J. Manuf. Processes* **2016**, 24, 179.
- [7] W. Wu, P. Geng, G. Li, D. Zhao, H. Zhang, J. Zhao, *Materials* **2015**, 8(9), 5834.
- [8] R. Zaldivar, D. Witkin, T. McLouth, D. Patel, K. Schmitt, J. Nokes, *Addit. Manuf.* **2017**, 13, 71.
- [9] H. R. Vanaei, M. Shirinbayan, M. Deligant, K. Raissi, J. Fitoussi, S. Khelladi, A. Tcharkhtchi, *Polym. Eng. Sci.* **2020**, 60, 1822. <https://doi.org/10.1002/pen.25419>.
- [10] B. Huang, S. Meng, H. He, Y. Jia, Y. Xu, H. Huang, *Polym. Eng. Sci.* **2019**, 59(1), 120.
- [11] A. D'Amico, A. M. Peterson, *Addit. Manuf.* **2018**, 21, 422.
- [12] H. R. Vanaei, K. Raissi, M. Deligant, M. Shirinbayan, J. Fitoussi, S. Khelladi, A. Tcharkhtchi, *J. Mater. Sci.* **2020**, 55 (29), 14677. <https://doi.org/10.1007/s10853-020-05057-9>.
- [13] E. Brandl, U. Heckenberger, V. Holzinger, D. Buchbinder, *Mater. Des.* **2012**, 34, 159.
- [14] F. Wang, *Int. J. of Adv. Manuf. Technol.* **2012**, 58(5–8), 545.
- [15] C. Kousiatza, D. Karalekas, *Mater. Des.* **2016**, 97, 400.
- [16] C. Kousiatza, N. Chatzidai, D. Karalekas, *Sensors* **2017**, 17(3), 456.
- [17] J. E. Seppala, K. D. Migler, *Addit. Manuf.* **2016**, 12, 71.
- [18] E. Ferraris, J. Zhang, B. Van Hooreweder, *CIRP Annals* **2019**, 68, 213.
- [19] J. Zhang, X. Z. Wang, W. W. Yu, Y. H. Deng, *Mater. Des.* **2017**, 130, 59.
- [20] A. Bellini, S. Güçeri, *Rapid Prototyping J.* **2003**, 9, 252.
- [21] J. F. M. A. T. A. S. RODRIGUEZ, J. P. Thomas, J. E. Renaud, *J. Mech. Des.* **2003**.
- [22] S. Costa, F. Duarte, J. Covas, *J. Mater. Process. Technol.* **2017**, 245, 167.
- [23] H. R. Vanaei, M. Shirinbayan, S. F. Costa, F. M. Duarte, J. A. Covas, M. Deligant, S. Khelladi, A. Tcharkhtchi, *J. Appl. Polym. Sci.* **2020**, 1. <https://doi.org/10.1002/app.49747>.
- [24] S. Costa, F. Duarte, J. Covas, *Virtual Phys. Prototyping* **2015**, 10 (1), 35.

How to cite this article: Vanaei HR, Deligant M, Shirinbayan M, et al. A comparative in-process monitoring of temperature profile in fused filament fabrication. *Polym Eng Sci.* 2020;1–9. <https://doi.org/10.1002/pen.25555>

Article No. 5:

HR Vanaei, M Shirinbayan, S Vanaei, J Fitoussi, S Khelladi, A Tcharkhtchi; Multi-scale damage analysis and fatigue behavior of PLA manufactured by Fused Deposition Modeling (FDM); Rapid prototyping Journal, 27(2): 371-378 (2021).

DOI: [10.1108/RPJ-11-2019-0300](https://doi.org/10.1108/RPJ-11-2019-0300)

Multi-scale damage analysis and fatigue behavior of PLA manufactured by fused deposition modeling (FDM)

Hamid Reza Vanaei

Arts et Metiers Institute of Technology, CNAM, LIFSE, HESAM University, Paris, France and Arts et Metiers Institute of Technology, CNRS, CNAM, PIMM, HESAM University, Paris, France

Mohammadali Shirinbayan

Arts et Metiers Institute of Technology, CNRS, CNAM, PIMM, HESAM University, Paris, France

Saeedeh Vanaei

INSA Centre Val de Loire, Blois, France

Joseph Fitoussi

Arts et Metiers Institute of Technology, CNRS, CNAM, PIMM, HESAM University, Paris, France

Sofiane Khelladi

Arts et Metiers Institute of Technology, CNAM, LIFSE, HESAM University, Paris, France, and

Abbas Tcharkhtchi

Arts et Metiers Institute of Technology, CNRS, CNAM, PIMM, HESAM University, Paris, France

Abstract

Purpose – Fused deposition modeling (FDM) draws particular attention due to its ability to fabricate components directly from a CAD data; however, the mechanical properties of the produced pieces are limited. This paper aims to present the experimental aspect of multi-scale damage analysis and fatigue behavior of polylactic acid (PLA) manufactured by FDM. The main purpose of this paper is to analyze the effect of extruder temperature during the process, loading amplitude, and frequency on fatigue behavior.

Design/methodology/approach – Three specific case studies were analyzed and compared with spool material for understanding the effect of bonding formation: single printed filament, two printed filaments and three printed filaments. Specific experiments of quasi-static tensile tests coupled with microstructure observations are performed to multi-scale damage analysis. A strong variation of fatigue strength as a function of the loading amplitude, frequency and extruder temperature is also presented.

Findings – The obtained experimental results show the first observed damage phenomenon corresponds to the inter-layer bonding of the filament interface at the stress value of 40 MPa. For instance, fatigue lifetime clearly depends on the extruder temperature and the loading frequency. Moreover, when the frequency is 80 Hz, the coupling effect of thermal and mechanical fatigue causes self-heating which decreases the fatigue lifetime.

Originality/value – This paper comprises useful data regarding the mechanical behavior and fatigue lifetime of FDM made PLA specimens. In fact, it evaluates the effect of process parameters (extruder temperature) based on the nature of FDM that is classified as a thermally-driven process.

Keywords FDM, Damage, PLA, Fatigue, Inter-layer bonding

Paper type Research paper

1. Introduction

Fused deposition modeling (FDM), an additive manufacturing (AM) process, was patented (Crump, 1991) and developed for modeling and prototyping to produce complex geometries, low cost and easy operation parts (Mohamed *et al.*, 2015; Macdonald *et al.*, 2014; Vanaei *et al.*, 2020). Owing to its specific characteristic by allowing fabrication of complex geometries, it

became a well-known and most commonly used technology in recent years (Chua *et al.*, 2010). In FDM, based on the sliced CAD model and the fact that the sequence of deposited layers occurs successively once upon each other's, the mechanism of layer-by-layer deposition takes place by extruding semi-molten thermoplastic materials through a liquefier over a platform (Yagnik, 2014; Chennakesava and Narayan, 2014).

Three-dimensional-printed structures fabricated by FDM process possessed entirely different mechanical properties from those manufactured by other methods. It is widely mentioned

The current issue and full text archive of this journal is available on Emerald Insight at: <https://www.emerald.com/insight/1355-2546.htm>



Rapid Prototyping Journal
© Emerald Publishing Limited [ISSN 1355-2546]
[DOI 10.1108/RPJ-11-2019-0300]

Received 26 November 2019
Revised 24 April 2020
5 June 2020
31 October 2020
Accepted 29 November 2020

that the mechanical properties of plastic parts are extensively influenced by the mechanism of layer-by-layer deposition (Vanaei et al., 2020b). This particularly exists in FDM that offers a wide range of process parameters affecting the mechanical behavior of manufactured parts (Vanaei et al., 2020c). Although in recent years the knowledge of mechanical characterization of FDM components is barely significant, most studies concentrated on enhancing the strength of materials by preserving the ability to fabricate complex geometry through AM. Consequently, it is stated that there is still a requirement for updating the mechanical strength of these parts.

Meanwhile, there are various studies on thermoplastics such as acrylonitrile butadiene styrene (ABS), polylactic acid (PLA) and polycarbonate (PC) to estimate and analyze their mechanical properties and especially fatigue analysis. They showed that the more density of the parts resulted in more correlation to the traditionally manufactured of the same material. This requires an acceptable orientation to avoid delamination.

According to the above-mentioned point, AM parts offer improvement in fatigue lifetime rather than traditional manufacturing processes (Blattmeier et al., 2012). However, (Van Hooreweder et al., 2013) indicated that fatigue properties of Nylon specimens remained similar in both injection molding and selective laser sintering. It is well-noted that these materials have significantly lower fatigue lifetime compared with others (Brandl et al., 2012; Santos et al., 2002). In fact, there are some parameters that have impact on the mentioned fatigue lifetime; including lack and/or weakness of bonding through the lamination resulted particularly during layer-by-layer deposition mechanism and also the presence of voids (Brandl et al., 2012; Santos et al., 2002; Wang, 2012).

Furthermore, Lee and Huang (2013) investigated on ABS and ABS-plus materials fabricated by FDM process to study the effect of print orientations on fatigue lifetime. On the other hand, another work was performed on ABS-M30i by optimizing process parameters of FDM and applying Taguchi method to determine the tensile strength and surface roughness of the material (Alhubail et al., 2013). A similar work fabricated PC specimens, which was based on the analysis of tensile strength for FDM parts, and they obtained a 75% enhancement in tensile strength comparing to that of the extruded PC parts (Masood et al., 2010). In comparison to others and on the same level to ABS, PLA is a common material in 3D printing. It is stronger than ABS, whereas the ductility is lower. It is a biodegradable thermoplastic made of recyclable sources that do not have a health risk (Stephens et al., 2013). Its high mechanical strength and convincing barrier properties make it important to extend the application of this material. Although several researchers considered the mechanical properties of PLA as a composite comprising many fibers (Dong et al., 2014; Kasuga et al., 2000), other tried to work on the mechanical behavior of PLA by changing the most useful parameters in FDM process (Jerez-Mesa et al., 2017; Averett et al., 2011; Letcher and Waytashek, 2014; Afrose et al., 2016; Susmel, 2014). Despite the variety of published work in the fatigue properties of FDM-processed PLA, it is imperative to have a deeper and more detailed investigation.

Worth mentioning that analyzing the mechanical properties and especially damage mechanism of FDM parts is an important issue. In literature, there are a limited number of works on the damage phenomenon of polymeric parts and exclusively PLA. Moreover, the temperature evolution of deposited filaments is a key parameter and has impact on the bonding quality.

The presented work concentrates on the fatigue properties of PLA by putting through dog-bone samples under cyclic loading. The aim is to analyze the influence of extruder temperature on the mechanical properties of the final sample and also multi-scale damage mechanisms under quasi-static loading-unloading tensile test.

2. Material and experimental methodology

2.1 Polylactic acid filament

A commercially available Pearl Violet PLA filament with a diameter of 1.75 mm has been analyzed, which is manufactured by Fillamentum® (Czech Republic). Some physicochemical properties are presented in Table 1.

2.2 Three-dimensional-printer device

The dog bone specimen was produced using a desktop 3D printer. The pattern for each layer was selected to be printed in 45° to the axis X and Y (90° to each other's), to make sure that each successive layer has enough support on it. Presumably, at 45°, the 3D model is printed properly because every layer is in about 50% contact with the previous layer. The printer fixed in a temperature-controlled atmosphere of the envelope and built the rapid-prototyped (RP) model based on ASTM D638 type IV in layers by using a single nozzle print head. In the experiments reported here, the solid model file exported as a STL format to be loaded into the FlashPrint software which generates the print path. The designed model is demonstrated in Figure 1.

2.3 Methods

2.3.1 Preliminary characterization methods

Microscopic observations were performed using a scanning electronic microscope (HITACHI 4800 SEM) to investigate qualitatively the material microstructure.

To measure the main transition temperatures, thermo-mechanical (DMTA) tests were applied to the samples using DMA Q800 instrument from TA Company. The tests were realized using a standard sample size of $25 \times 10 \times 4 \text{ mm}^3$ at the following condition: temperature range of 40°C to 100°C; frequency 1 Hz; temperature rate 2°C/min.

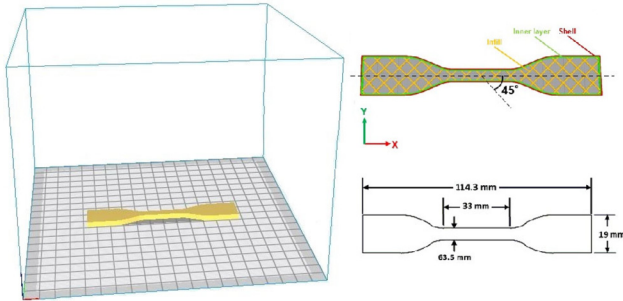
2.3.2 Mechanical characterization: tensile and fatigue tests

Tensile tests until failure have been carried out at room temperature on MTS 830 hydraulic machine. The printed

Table 1 Physio-chemical properties of PLA filament

Properties	Typical Value
Material density	1.24 g/cm ³
Diameter (Tolerance)	1.75 mm (± 0.01 mm)
Glass transition temperature	72°C
Melting temperature	158°C

Figure 1 Test case printed using FlashForge 3D printer (based on ASTM D638 type IV)



sample (based on ASTM D638 type IV) were used for tensile test with velocity of 1 mm/min. A contactless technique is used to measure the local deformation using a camera. The strain measurement procedure consists of analyzing the images of the filmed surface during deformation.

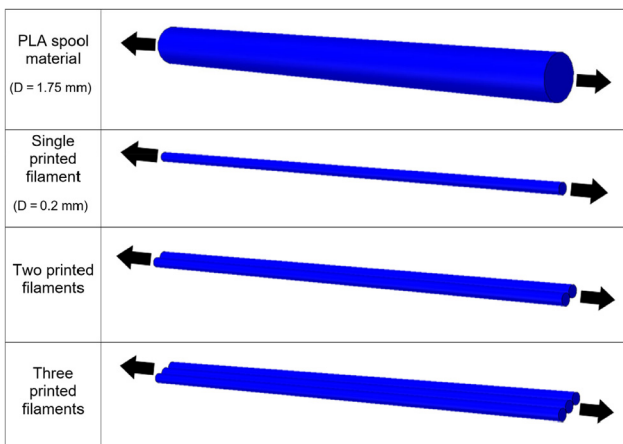
To understand the effect of bonding formation on the tensile behavior of printed PLA, tensile facts on these filaments are proposed (Figure 2):

- Spool material
- Single printed filament
- Two printed filaments
- Three printed filaments

Tension-tension fatigue tests were carried out at different applied maximum stress on MTS 830 hydraulic fatigue machine using the same standard (ASTM D638 type IV). The minimum applied stress was chosen to be equal to 10% of the maximum applied stress. In this paper, results of the experimental procedure performed at different frequencies of 1, 10 and 80 Hz are presented.

During cyclic loading, the temperature rise (due to self-heating) has been measured using an infrared camera (Raynger-MX4) in a specific area (maximum temperature). The evolution of Young's modulus was also determined.

Figure 2 Proposed printed filaments to perform tensile tests



2.4 Conditions of printing

The influence of extruder temperature was taken into account by defining three conditions as displayed in Table 2. Five samples were tested for each condition of tensile tests.

3. Results and discussion

The objective of this study is to analyze the effects of extruder temperature on the mechanical properties and fatigue lifetime of parts produced by FDM process.

3.1 Thermo-mechanical properties

In the presented work, all mechanical tests were performed at room temperature. To measure the main transition temperatures due to molecular mobility as a function of temperature, DMTA tests were used. The graph presented in Figure 3 clearly displays the evolution of the storage and loss modulus versus temperature obtained by the DMTA test. Apparently, PLA filament presents at least three distinct zones in the temperature range of 40°C-100°C. The first zone, extended until 60°C, is the glassy state. The second zone is related to the glass transition zone. From 80°C the rubbery state appeared.

According to the mentioned graph and data extracted by monitoring the temperature during the fatigue test, the temperature growth (self-heating) during the test will not exceed 50°C. Otherwise, the thermal fatigue will be intervened.

3.2 Tensile behavior

3.2.1 Polylactic acid filaments

Figure 4 depicts the results of tensile tests at room temperature for the set of specimens investigated in this study. These results have surprisingly referenced the nature of FDM process. Regardless of the variation in failure strain for the four specimens (PLA spool material, one printed filament, two printed filaments and three printed filaments), no significant difference observed in Young's modulus. Apparently, the

Table 2 Various conditions of printing

Condition no.	Extruder Temperature (°C)	Bed Temperature (°C)	Speed (mm/s)	Layer height (mm)
1	210	70	40	0.2
2	220	70	40	0.2
3	230	70	40	0.2

Figure 3 DMTA test result

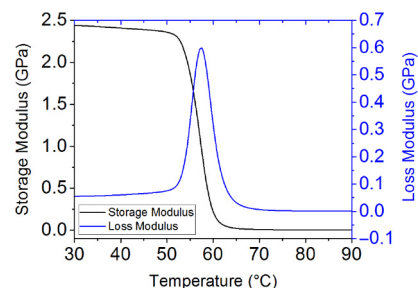
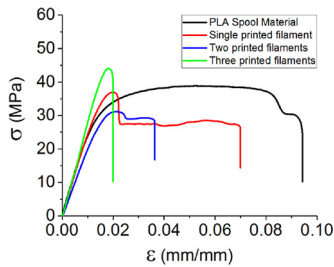


Figure 4 Tensile curves of different formed filaments

remarkable failure strain in the case of raw material is a notable issue in the assessment of the mechanical behavior of 3D-printed parts.

It seems barely incredible that by increasing the printed layer, the failure strain was decreased about 70%. Conversely, there was a significant increase in the maximum stress up to 20%. It could be argued that the mentioned observations well confirms the brittle behavior of PLA filament after printing. As an example, the failure strain of PLA spool ($\sim 9.5\%$) is almost 4.75 times greater than that of three printed filaments ($\sim 2\%$).

This approach could be a confirmation to the underlying assumption that in the additively manufactured polymer being tested, the mechanical behavior (and in particular the elongation) in the incipient failure condition was markedly affected by the mechanism of layer-by-layer deposition.

3.2.2 Effect of extruder temperature on the tensile behavior

Contrary to the tensile behavior of the progressively printed filaments (Section 3.2.1), different behavior was detected in the samples printed according to the conditions presented in Table 2. To have a more clear precision on the characterization of the fabricated samples, tensile tests were applied at least five times on the samples per each condition. Figure 5 presents the tensile behavior for the set of five specimens assessed according to condition No. 1 ($T_{\text{ext}} = 210^\circ\text{C}$). One explanation might be the fact that rupture occurred at the center of the specimens (activate zone of tensile loading). Another convincing point was the repeatability of the set of specimens by the occurrence of rupture at the center of them, as well as the fact that the failure mode was due to the material departure in a plane almost normal to the tensile stress.

Given the above-mentioned results and following the discussion performed on the mechanical behavior, tensile tests have been realized to illustrate the effect of extruder temperature on the tensile behavior. The graph presented in

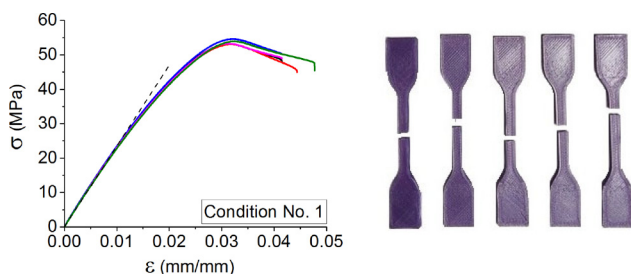
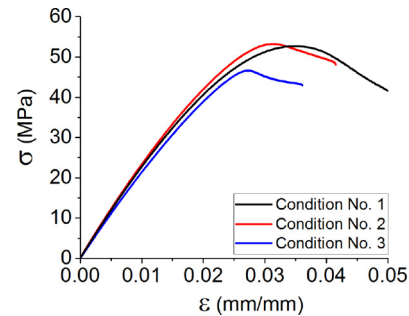
Figure 5 Tensile behavior for the set of five sample according to the condition No. 1 at $T_{\text{ext}} = 210^\circ\text{C}$ **Figure 6** Tensile behavior of printed PLA samples from condition No. 1 to 3

Figure 6 and data collected in Table 3, clearly display and compare the overall results as follows:

- Influence of the extruder temperature on Young's modulus is limited. It roughly changed from 2.3 GPa to 2.5 GPa as the extruder temperature increased from 210°C to 220°C .
- By variation of T_{ext} from 220°C to 230°C , a sudden drop observed below to that of the $T_{\text{ext}} = 210^\circ\text{C}$.
- Failure stress changed periodically from 52 MPa to 53 MPa and then 47 MPa by the increase in T_{ext} based on the conditions No. 1-3.
- Failure strain stayed around 3.5% as the T_{ext} decreased from 230°C to 220°C , at $T_{\text{ext}} = 210^\circ\text{C}$.
- By comparing the tensile results obtained on filaments and those observed on the set of samples in three conditions, both failure stress and strain dramatically increased.

SEM micrographs of a fractured sample of condition No. 2 are presented in Figure 7. Logically, by increasing the distance from the envelope, the temperature gradient decreases and causes inhomogeneity of the cooling rate of successively deposited filaments. It is probably true to say that based on Figure 7(a), a deformed zone was observed. There is convincing evidence since the surface fracture depicted in Figure 7(b) with the void sequences of upper layers. Presumably, the fracture path proceeded over weak inter-layers bonding.

3.3 Multi-scale damage investigation

Experimental stress-strain curves for quasi-static tensile tests coupled with microstructure observations are shown in Figure 8. The same representative observation zone was microscopically analyzed at consecutive increasing value of applied stress level. The local investigation was assumed as a statistical representative of the damage accumulation in the studied material. Furthermore, microscopic observations have confirmed that this zone is statistically representative of the

Table 3 Results of tensile behavior of printed PLA samples from condition No. 1 to 3

Samples	E (GPa)	σ_{max} (MPa)	ε at σ_{max} (%)
Condition no. 1	2.3 ± 0.1	52 ± 2	3.5 ± 0.3
Condition no. 2	2.5 ± 0.1	53 ± 1.5	3.5 ± 0.2
Condition no. 3	2.2 ± 0.1	47 ± 2	2.7 ± 0.2

Figure 7 SEM micrograph for a) external surface and b) surface fracture of the specimen in condition No. 2

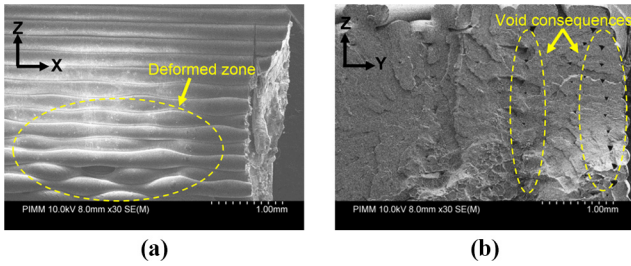
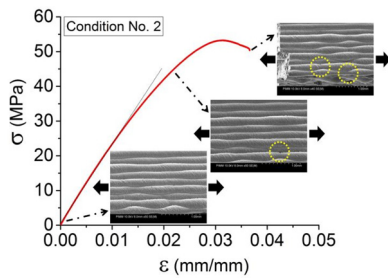


Figure 8 Damage mechanisms under quasi-static loading



damage accumulation. The first observed damage phenomenon corresponds to the inter-layer failure of the filament interface at the stress value of 40 MPa. This phenomenon is the predominant damage mechanism for quasi-static loading.

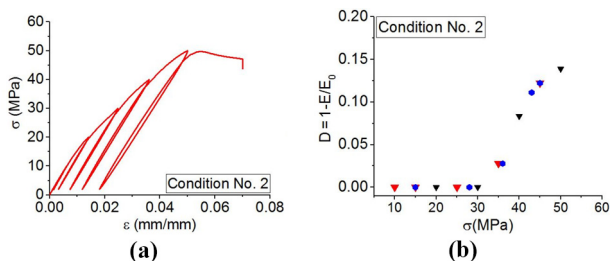
Filaments oriented perpendicularly to the principal stress direction are submitted to a high local normal stress at the interface.

To clarify the mentioned issue, a “quantitative multi-scale analysis” of damage effect was performed in this section. At the macroscopic scale, the evolution of stiffness reduction is determined for PLA samples printed from condition No. 2 under quasi-static loading. Stiffness reduction is an appropriate macroscopic damage indicator to express the damage development in materials. In the case of tensile loading, one can define a macroscopic damage variable as:

$$D = 1 - E_D/E_0, \quad (1)$$

where E_0 and E_D are Young’s modulus of virgin and the damaged material, respectively. The graph shown in Figure 9

Figure 9 a) Applied stress for PLA printed from condition No. 2 and b) macroscopic damage evolution



provides the evolution of the macroscopic damage parameter, D , under quasi-static loading-unloading tensile test as a function of applied stress. It should be indicated that for each microstructure, several tests (at least 3) were performed and the results have been reported in this figure in such a way that at least 15 points have been measured until the very last stages just before failure. Figure 9 shows the damage threshold in the term of stress is almost about 35 MPa. Seemingly, an altered slope of the curve (from $D = 0.12$) signifying the saturation of the filaments interface failure occurring together, with the beginning of the propagation of transverse cracks.

3.4 Fatigue behavior analysis

3.4.1 Effect of the extruder temperature

Figure 10 shows the Wöhler curve obtained in tension-tension fatigue tests for a frequency of

1 Hz in the case of the samples tested from conditions No. 1, 2 and 3. The diagram shows that for the three cases at high applied stresses, the same fatigue lifetime was observed. However, at low amplitudes, there is a significant difference in fatigue lifetime. In the case of samples printed according to condition No. 3, the fatigue lifetime is about 7×10^3 cycles for applied stress (30 MPa), while the fatigue lifetime is about 2×10^4 cycles for sample printed according to condition No. 2. So, a variation of 10°C on extruder temperature leads to a fatigue lifetime three times greater. Figure 10 confirms that the samples printed according to condition No. 2 represented acceptable fatigue properties.

Thus, the fatigue lifetime at low amplitudes is strongly influenced by the temperature of extruder. Regarding fatigue results at a frequency of 1 Hz, Figure 10 shows a linear curve. In this case, the high loading amplitude zone corresponds to loading amplitude up to 35 MPa. This upper zone corresponds to fatigue lifetime less than 2,000 cycles. Fatigue behavior and specialty S-N curve of PLA printed using FDM process could be modeled by a logarithmic linear expression:

$$\sigma_{max} = A \cdot \ln(N) + B, \quad (2)$$

where A and B are the material parameters corresponding to the slope of the curve and the Y-intercept, respectively. The slope A defines the sensitivity of the fatigue resistance and intercept B represents the apparent tensile strength. Data gathered in Table 4 shows the value of A and B for three conditions of printing related to high and low-stress domains.

Figure 10 Wöhler curves for PLA printed at the three conditions mentioned in Table 2 at 1 Hz

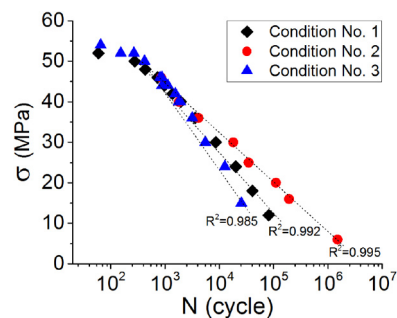


Table 4 Values of a and B

Samples	Low stress domain		High stress domain	
	A (MPa)	B (MPa)	A (MPa)	B (MPa)
Condition no. 1	-6.19	91.66	-0.86	55.95
Condition no. 2	-5.22	79.95		
Condition no. 3	-8.67	104.78		

The evolution of the relative Young's modulus is followed to describe quantitatively the degree of fatigue damage. It may be used in a stiffness-based fatigue failure criterion. Figure 11 shows the evolution of the relative Young's modulus for two applied maximum stresses equal to 18 MPa and 46 MPa corresponding to low and high amplitudes, respectively. These results confirm that for three conditions of printing, the same evolution of relative Young's modulus could be observed at high amplitudes [Figure 11(b)]. It can confirm the same damage mechanism. Believable, the extruder temperature has no effect on the relative Young's modulus evolution while it can affect the fatigue lifetime [Figure 11(a)]. In addition, the graph highlighted the fact that there is no significant damage at low amplitudes just before the failure of the samples while it is more significant at high fatigue amplitudes.

SEM fractography after fatigue tests has been performed to understand the difference between low loading amplitudes (Figure 12). SEM analysis, in the case of a sample printed according to condition No. 2, highlighted that there is a remarkable bonding formation associated with condition No. 3.

Figure 11 Evolutions of the relative Young's modulus (E/E_0) during fatigue tests of three conditions: (a) $\sigma_{\max} = 18$ MPa and (b) $\sigma_{\max} = 46$ MPa

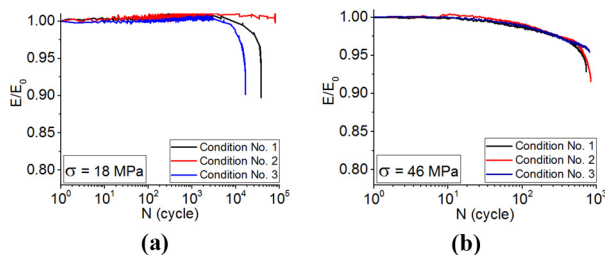
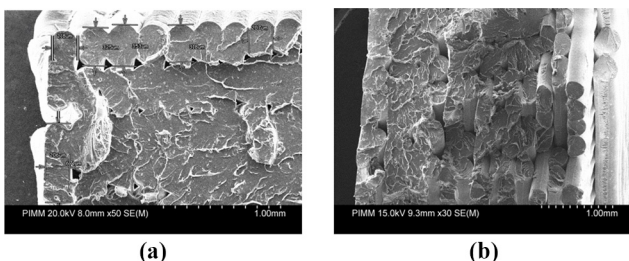


Figure 12 SEM micrographs after fatigue tests at 1 Hz and $\sigma_{\max} = 18$ MPa for PLA samples printed according to (a) condition No. 2 and (b) condition No. 3



3.4.2 Effect of frequency

For different applied stresses (or amplitudes), the Wöhler curve obtained from fatigue tests in the case of PLA samples printed according to condition No. 3 in the frequencies of 1, 10 and 80 Hz as shown in Figure 13. Obviously, there is a small difference between the fatigue lifetime at mentioning frequencies at low amplitude while by increasing frequency, the curves shifted to low fatigue lifetime at high loading amplitude. According to Figure 13, one can note that the effect of frequency is more significant at loading stress from 35 MPa, which is corresponding to the damage threshold relating to Figure 9.

As an example, for applied stress of 40 MPa, the fatigue lifetime of the sample tested at 80 Hz is three times smaller than that of 1 Hz (respectively $\sim 1,000$ and $\sim 3,000$ cycles). This difference becomes more significant when the fatigue stress increases. It can be concluded that independent of the loading amplitudes, for values up to 1 Hz, frequency has a determinant role in the fatigue lifetime: increasing frequency decreases the fatigue lifetime. This phenomenon, in fact, is owing to the self-heating during the fatigue tests. Figure 14 shows the evolution of temperature as a function of time during fatigue test. One can observe the increase of about 3°C , at a loading amplitude of 31 MPa at the initial time of the test.

For the fatigue test at 1 Hz, self-heating is not significant while there is a slight increase in temperature at the frequency of 80 Hz (Figure 14). In this case, E/E_0 decreases by increasing the self-heating temperature. The slope of decreasing is increased by frequency augmentation. This phenomenon can be observed at low and high fatigue amplitudes. For high-frequency tests, the failure of the sample is because of both thermal fatigue and mechanical fatigue (Figure 15).

Figure 13 Wohler curves at different frequencies in tension-tension tests for PLA samples printed according to condition No. 3

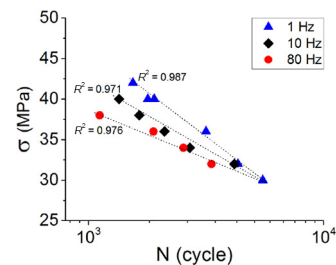


Figure 14 Self-heating curve during fatigue test of PLA samples printed according to condition No. 3

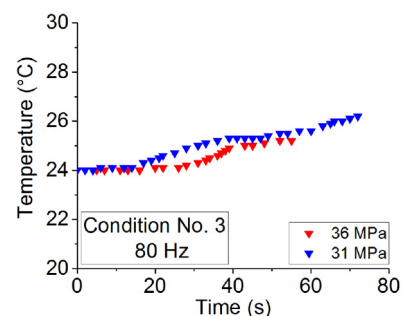
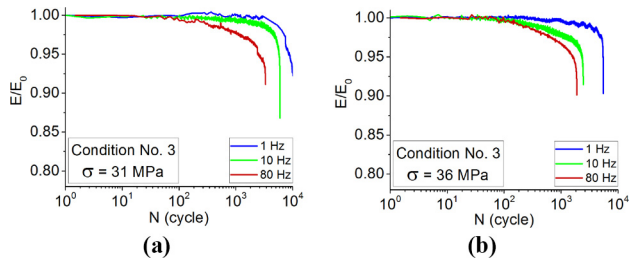


Figure 15 Evolution of the relative Young's modulus (E/E_0) during fatigue tests at different frequencies at (a) $\sigma_{\max} = 31$ MPa (b) $\sigma_{\max} = 36$ MPa



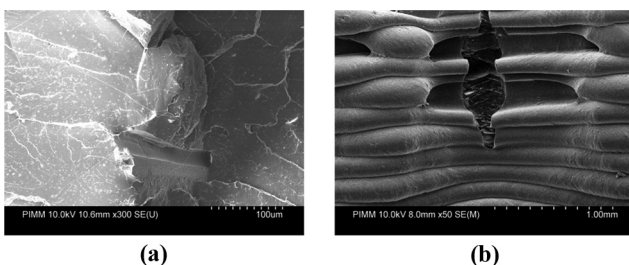
In fact, SEM analysis of the samples tested at 80 Hz, highlights ductile behavior during loading. During the test at 10 Hz, the matrix remains brittle. The self-heating phenomenon causes the molecular motion to increase, the modulus decreases, and the polymer becomes softer. Moreover, one can observe from Figure 16(b) the change in rupture mode of PLA produced by FDM process. As indicated, inter-layer failure of the filaments and the transverse cracks exist.

4. Concluding remarks

The mechanical behavior of PLA specimens using FDM under both static and fatigue loadings is influenced mainly by the following parameters: filling temperature, filling rate, filling pattern, layer thickness, infill percentage, nozzle size and manufacturing orientation. According to the previous works (Vanaei et al., 2020d), the temperature of extruder is the main parameter which influences the mechanical properties of PLA sample manufactured using FDM process.

In this paper, the mechanical properties of PLA specimens were tested to investigate the effect of extruder temperature. From this work, the obtained experimental results show the first observed damage phenomenon corresponds to the inter-layer bonding of the filament interface at the stress value of 40 MPa at the microscopic scale. A strong variation of fatigue lifetime as a function of the loading amplitude, frequency and extruder temperature is presented. For instance, fatigue lifetime is clearly dependent on the extruder temperature. Moreover, when the frequency is 80 Hz, self-heating decreased the fatigue lifetime which also depends on the coupling effect of thermal and mechanical fatigue. SEM observations demonstrated that the samples tested at 80 Hz, exhibited

Figure 16 SEM micrographs after fatigue tests at 80 Hz and $\sigma_{\max} = 36$ MPa for PLA samples printed according to condition No. 3: (a) and (b) show two views of observation



ductile behavior, whereas, the polymer remains brittle during the fatigue tests achieved at 1 Hz.

As mentioned in this work during sample preparation, the pattern for each layer was selected to be printed in 45° to the axis X and Y (90° to each other's). This was to make sure that each successive layer has enough support on it. It means the best structural pattern. Nevertheless, the mechanical properties of the PLA samples printed by FDM process are limited. There are other process parameters to improve. Moreover, one can note that temperature analysis and control during FDM process should be performed (Vanaei et al., 2020a).

References

- Afrose, M.F., Masood, S., Iovenitti, P., Nikzad, M. and Sbarski, I. (2016), "Effects of part build orientations on fatigue behaviour of FDM-processed PLA material", *Progress in Additive Manufacturing*, Vol. 1 Nos 1/2, pp. 21-28.
- Alhubail, M., Alenezi, D. and Aldousiri, B. (2013), "Taguchi-based optimisation of process parameters of fused deposition modelling for improved part quality", *International Journal of Engineering Research and Technology*, Vol. 2, p. 2519.
- Averett, R.D., Realf, M.L., Jacob, K., Cakmak, M. and Yalcin, B. (2011), "The mechanical behavior of poly (lactic acid) unreinforced and nanocomposite films subjected to monotonic and fatigue loading conditions", *Journal of Composite Materials*, Vol. 45 No. 26, pp. 2717-2726.
- Blattmeier, M., Witt, G., Wortberg, J., Eggert, J. and Toepker, J. (2012), "Influence of surface characteristics on fatigue behaviour of laser sintered plastics", *Rapid Prototyping Journal*, Vol. 18 No. 2, pp. 161-171.
- Brandl, E., Heckenberger, U., Holzinger, V. and Buchbinder, D. (2012), "Additive manufactured AlSi10Mg samples using selective laser melting (SLM): microstructure, high cycle fatigue, and fracture behavior", *Materials & Design*, Vol. 34, pp. 159-169.
- Chennakesava, P. and Narayan, Y.S. (2014), "Fused deposition modeling-insights", *Proceedings of the International Conference on Advances in Design and Manufacturing ICAD&M*, pp. 1345-1350.
- Chua, C.K., Leong, K.F. and Lim, C.S. (2010), *Rapid Prototyping: principles and Applications (with Companion CD-ROM)*, World Scientific Publishing Company.
- Crump, S.S. (1991), "Fast, precise, safe prototypes with FDM", *ASME annual winter conference, Atlanta*, 53-60.
- Dong, Y., Ghataura, A., Takagi, H., Haroosh, H.J., Nakagaito, A.N. and Lau, K.-T. (2014), "Poly(lactic acid) (PLA) biocomposites reinforced with coir fibres: evaluation of mechanical performance and multifunctional properties", *Composites Part A: Applied Science and Manufacturing*, Vol. 63, pp. 76-84.
- Jerez-Mesa, R., Travieso-Rodriguez, J.A., Llumà-Fuentes, J., Gomez-Gras, G. and Puig, D. (2017), "Fatigue lifespan study of PLA parts obtained by additive manufacturing", *Procedia Manufacturing*, Vol. 13, pp. 872-879.
- Kasuga, T., Ota, Y., Nogami, M. and Abe, Y. (2000), "Preparation and mechanical properties of polylactic acid composites containing hydroxyapatite fibers", *Biomaterials*, Vol. 22 No. 1, pp. 19-23.

- Lee, J. and Huang, A. (2013), "Fatigue analysis of FDM materials", *Rapid Prototyping Journal*, Vol. 19 No. 4, pp. 291-299.
- Letcher, T. and Waytashek, M. (2014), "Material property testing of 3D-printed specimen in PLA on an entry-level 3D printer", *ASME 2014 international mechanical engineering congress and exposition*, American Society of Mechanical Engineers, pp. V02AT02A014-V02AT02A014.
- Macdonald, E., Salas, R., Espalin, D., Perez, M., Aguilera, E., Muse, D. and Wicker, R.B. (2014), "3D printing for the rapid prototyping of structural electronics", *IEEE Access*, Vol. 2, pp. 234-242.
- Masood, S.H., Mau, K. and Song, W. (2010), "Tensile properties of processed FDM polycarbonate material", *Materials Science Forum*, Vols 654/656, pp. 2556-2559, Trans Tech Publ.
- Mohamed, O.A., Masood, S.H. and Bhowmik, J.L. (2015), "Optimization of fused deposition modeling process parameters: a review of current research and future prospects", *Advances in Manufacturing*, Vol. 3 No. 1, pp. 42-53.
- Santos, E., Abe, F., Kitamura, Y., Osakada, K. and Shiomi, M. (2002), "Mechanical properties of pure titanium models processed by selective laser melting", *Proceedings of the Solid Freeform Fabrication Symposium*, pp. 180-186.
- Stephens, B., Azimi, P., EL Orch, Z. and Ramos, T. (2013), "Ultrafine particle emissions from desktop 3D printers", *Atmospheric Environment*, Vol. 79, pp. 334-339.
- Susmel, L. (2014), "A unifying methodology to design un-notched plain and short-fibre/particle reinforced concretes against fatigue", *International Journal of Fatigue*, Vol. 61, pp. 226-243.
- VAN Hooreweder, B., Moens, D., Boonen, R., Kruth, J.-P. and Sas, P. (2013), "On the difference in material structure and fatigue properties of nylon specimens produced by injection molding and selective laser sintering", *Polymer Testing*, Vol. 32 No. 5, pp. 972-981.
- Vanaei, S., Parizi, M.S., Vanaei, S., Saleemizadehparizi, F. and Vanaei, H.R. (2020), *An Overview on Materials and*

- Techniques in 3D Bioprinting Toward Biomedical Application, Engineered Regeneration Journal*, available at: <https://doi.org/10.1016/j.engreg.2020.12.001>
- Vanaei, H.R., Deligant, M., Shirinbayan, M., Raissi, K., Fitoussi, J., Khelladi, S. and Tcharkhtchi, A. (2020a), "A comparative in-process monitoring of temperature profile in fused filament fabrication", *Polymer Engineering & Science*, p. 9.
- Vanaei, H.R., Raissi, K., Deligant, M., Shirinbayan, M., Fitoussi, J., Khelladi, S. and Tcharkhtchi, A. (2020b), "Toward the understanding of temperature effect on bonding strength, dimensions and geometry of 3D-printed parts", *Journal of Materials Science*, Vol. 55 No. 29, pp. 14677-14689.
- Vanaei, H., Shirinbayan, M., Deligant, M., Raissi, K., Fitoussi, J., Khelladi, S. and Tcharkhtchi, A. (2020c), "Influence of process parameters on thermal and mechanical properties of polylactic acid fabricated by fused filament fabrication", *Polymer Engineering & Science*, Vol. 60, p. 10.
- Vanaei, H.R., Shirinbayan, M., Costa, S.F., Duarte, F.M., Covas, J.A., Deligant, M., Khelladi, S. and Tcharkhtchi, A. (2020d), "Experimental study of PLA thermal behavior during fused filament fabrication", *Journal of Applied Polymer Science*, Vol. 138, p. 7.
- Wang, F. (2012), "Mechanical property study on rapid additive layer manufacture Hastelloy® X alloy by selective laser melting technology", *The International Journal of Advanced Manufacturing Technology*, Vol. 58 Nos 5/8, pp. 545-551.
- Yagnik, D. (2014), "Fused deposition modeling—a rapid prototyping technique for product cycle time reduction cost effectively in aerospace applications", *IOSR Journal of Mechanical and Civil Engineering*, Vol. 5, pp. 62-68.

Corresponding author

Hamid Reza Vanaei can be contacted at: hamidreza.vanaei@ensam.eu

Etude et Modélisation de la rhéologie des polymères au cours du procédé FDM (Fabrication additive)

Résumé:

L'étude a pour objet de modéliser les caractéristiques rhéologiques des pièces imprimées en 3D. Pour atteindre cet objectif, une étude bibliographique a été réalisée sur les effets des principales variables du processus de l'évolution de la température et leur impact sur les caractéristiques rhéologiques. Puisque les caractéristiques rhéologiques telles que la viscosité dépendent de la température, elles pourraient être corrélées à l'évolution de la température des filaments déposés. Par ailleurs, pour reconnaître la liaison des filaments adjacents, il est important de prendre en considération l'évolution de la température à leurs interfaces.

Au début, le rôle de la température de la buse, la température du plateau et la vitesse d'impression sur la résistance mécanique et la qualité de la pièce finale a été discuté. Il a été constaté que l'interaction des paramètres joue un rôle important en ce qui concerne la caractérisation mécanique des pièces imprimées et le module de Young. De plus la déformation à la rupture pourraient être un indicateur pour évaluer les performances mécaniques des pièces imprimées. Ensuite, la méthode des volumes finis a été appliquée pour modéliser le transfert de chaleur des filaments déposés puis a été validé par une nouvelle approche expérimentale dans laquelle de très petits thermocouples de type K ont été utilisés pour surveiller la température du profil à l'interface des filaments déposés. L'évolution de la température a été prédite en concordance avec les résultats expérimentaux enregistrés.

Les résultats obtenus ont ensuite été intégrés dans la caractéristique rhéologique des filaments en modélisant l'évolution de leur viscosité et l'effet des principales variables du processus. De plus, un diagramme « Temps-Température-Transformation » (TTT) des filaments pendant le dépôt qui permet d'évaluer simultanément la température et la viscosité a été mis en place. Cette étude a permis d'aboutir à un code informatique regroupant les résultats obtenus qui peut permettre aux chercheurs d'optimiser le processus d'obtention de pièces possédant un bon état de surface.

Mots clés : Impression 3D, Rhéologie, Evolution de la température, Liaison des couches, Résistance mécanique.

Studying and Modelization of Polymer Rheology during the FDM Process (Additive Manufacturing)

Abstract:

The aim of this study is to model the rheological characteristics of 3D-printed parts. To achieve this goal, a bibliographic study was carried out on the effects of major process variables on temperature evolution and their impact on rheological characteristics. Since the rheological characteristics such as viscosity are a function of temperature, they could be correlated to the temperature evolution of deposited filaments. Besides, to acknowledge the bonding of adjacent filaments, it is important to consider the temperature evolution at their interfaces.

At the early stage, the role of three parameters, liquefier temperature, platform temperature, and print speed on the mechanical strength and the quality of final part has been discussed. It was found that interaction of parameters plays the most important role in consideration of mechanical characterization of printed parts and also Young's modulus and failure strain could be an indicator to evaluate the mechanical performance of printed parts. Then, finite volume method was applied to model the heat transfer of deposited filaments and then was validated by a novel experimental approach in which very small K-type thermocouples were employed to perform the in-process monitoring of temperature profile at the interface of deposited filaments. The temperature evolution was predicted in good agreement with the recorded experimental results.

The obtained results were then embedded into the rheological characteristic of filaments by modeling the viscosity evolution of filaments and the effect of major process variables on them. Moreover, efforts have been made to propose a 'Time-Temperature-Transformation' (TTT) diagram of filaments during deposition that enables the evaluation of temperature and viscosity simultaneously. The consequence of this study is then a computer code that considers the obtained results and predictions, with the potential of letting researchers in optimizing the process to obtain good final parts.

Keywords : 3D printing, Rheology, Temperature evolution, Inter-layer bonding, Mechanical strength

